

Università degli Studi di Torino

PhD Programme in Biological Sciences
and Applied Biotechnologies

Decoding Kiwifruit Vine Decline Syndrome (KVDS): from microbial ecology to molecular diagnostics and host stress responses

Tutor:
Davide Spadaro

Candidate:
Micol Guaschino

XXXVII° Cycle: 2021 /2024

Table of Contents

Chapter 1 – Introduction and state of the art 1

1. Introduction to the Genus *Actinidia*: Biology, Ecology, and Economic Importance **..... 1**

1.1 The genus *Actinidia* 1

1.2 Root anatomy and soil–water interactions 3

1.3 Domestication and market of the genus *Actinidia* 4

2. Phytosanitary issues of *Actinidia deliciosa* in Europe 5

2.1. Field diseases and pests 5

2.2 Postharvest diseases 7

3. Kiwifruit Vine Decline Syndrome (KVDS) 9

3.1. Overview and symptomatology 9

3.2. Abiotic stress factors involved in KVDS onset 12

3.3. Biotic factors involved in KVDS onset 15

3.4. Microbiome and dysbiosis hypotheses 20

3.5. Approaches for diagnosis and disease modelling 22

4. Aims of the work 25

References 27

Chapter 2 - Soil, rhizosphere, and root microbiome in kiwifruit vine decline, an emerging multifactorial disease 40

Abstract 42

1. Introduction 43

2. Materials and methods 46

3. Results 50

4. Discussion 58

5. Conclusions 64

Acknowledgments 65

References 66

Tables 84

Figures 89

Supplementary material 98

Chapter 3 - Development of a qPCR assay for early detection and quantification of *Phytopythium vexans* in kiwifruit plant and soil affected by Vine Decline Syndrome ... 107

Abstract 109

1. Introduction 110

2. Materials and methods 112

3. Results 116

4. Discussion 118

Acknowledgements 120

References 121

Tables 126

Figures 131

Supplementary material 134

Chapter 4 - Transcriptional dynamics of kiwifruit roots under combined biotic and abiotic stressors: insights into multifactorial stress responses 148

Abstract 150

1. Introduction 151

2. Materials and Methods 153

3. Results 158

4. Discussion 173

5. Conclusion 181

Acknowledgements 182
References 182
Tables 196
Figures 203
Supplementary material 212
Chapter 5 - General discussion and outlooks 221
References 226

Chapter 1 – Introduction and state of the art

1. Introduction to the Genus *Actinidia*: Biology, Ecology, and Economic Importance

1.1 The genus *Actinidia*

The genus *Actinidia*, commonly known as kiwifruit, belongs to the order Ericales and to the family Actinidiaceae and it is a group of plants characterized as perennial, functional dioecious, deciduous, or semi-deciduous or evergreen woody vines (Huang, 2016). *Actinidia chinensis* var. *deliciosa* was long accepted as the botanical name, but it was later reclassified as *Actinidia deliciosa* because the differences between *A. chinensis* var. *chinensis* and *A. chinensis* var. *deliciosa* were sufficient to justify two distinct species (Chou-Fen & Ferguson, 1986).

The genus *Actinidia* includes 66 species e 118 taxa, most are native to China. Notable exception are four species: *Actinidia strigosa* from Nepal, *Actinidia petelotii* from Vietnam, and *Actinidia hypoleuca* and *Actinidia rufa* from Japan (Huang et al., 2003). Despite the wide variety of the genus, only *Actinidia deliciosa* and *Actinidia chinensis* are of significant economic interest (Huang & Ferguson, 2001). Specifically, *Actinidia deliciosa* cv. 'Hayward', selected in New Zealand in the late 1920s, has become the most widely cultivated and internationally recognized kiwifruit variety.

The genus *Actinidia* spans a broad latitudinal range in eastern Asia, from tropical to temperate zones, which contributes to its remarkable biological diversity. Naturally, kiwifruit thrives in humid, shaded habitats such as forests and gullies, while it is rarely found in arid or elevated environments (Huang, 2016).

Reflecting these natural preferences, successful cultivation requires high humidity, distributed rainfall, cold winters, long frost-free periods, moderate sunlight, and shelter from wind for cultivation (Bardi, 2020).

Under suitable conditions, kiwifruit vines can live for over a century, supported by a short juvenile phase, long productive lifespan, and a vigorous regenerative capacity (Huang, 2016). This

remarkable adaptivity is supported by distinct anatomical and morphological features that characterize the genus.

Plants of the *Actinidia* genus exhibit a shallow, fibrous root system with well-developed lateral roots. Their shoots are typically covered in fine hairs, with older stems becoming glabrous and dark brown, often showing exfoliating epidermis and prominent xylem rays (Figure 1). Leaves are large, simple, and alternate, while the vascular system features large xylem vessels and a thin phloem cortex (Huang, 2016).

Actinidia species are dioecious, with pistillate and staminate flowers on separate plants. Although the flowers are morphologically hermaphroditic, functional unisexuality arises from either pollen or ovary abortion (Figure 2). Pollination is primarily entomophilous but can also occur *via* wind (anemophilous). The fruit is a hairy berry, highly variable in size, colour, and shape across species, and valued for its nutritional properties, particularly vitamin C, dietary fibre, and antioxidant content (Figure 3) (Huang, 2016).

Traditionally propagated by seed, *Actinidia* is now more commonly propagated via grafting, cuttings, or tissue culture, depending on regional horticultural practices (Huang, 2016).



Figure 1 – Stem, emerging shoot, and leaves of A. deliciosa (Huang, 2016)



Figure 2 (on the top) and Figure 3 (on the bottom) – Flowers (pistillate, staminate) and fruit of A. deliciosa (Huang, 2016)

1.2 Root anatomy and soil–water interactions

Actinidia deliciosa exhibits a shallow yet highly branched root system, which reaches a depth of approximately 40–50 cm by the third year of growth and then expands laterally (Huang, 2016). Around 95% of the total root length is composed of fine, fleshy fibrous roots that emerge in bunches from structural roots and have a high moisture content (84–89%) (Bardi, 2020; Smith et al., 1989). The taproot is underdeveloped, and structural roots tend to slow down after early lateral expansion. Fibrous roots endure across multiple seasons, alternating between dormancy and growth. New roots arise from older fibrous or structural roots and change in appearance as they mature—from milky white to reddish, and eventually dark brown (Bardi, 2020).

The vascular anatomy of *Actinidia* is adapted for efficient transport under optimal conditions but remains vulnerable under stress. The secondary phloem primarily consists of parenchyma, with additional sieve tube elements, companion cells, and idioblasts containing mucilage or raphides (Bardi, 2020). The xylem includes tracheids and a limited number of large-diameter vessels (150–200 μm), with perforated transverse walls that facilitate water flow. Conductivity is highest in the

outer growth rings, where vessels tend to be larger, but this system is highly susceptible to embolism when exposed to water stress (Xiloyannis & Montanaro, 2004).

Due to its anatomical traits, *Actinidia* requires carefully managed soil and water conditions. Optimal soils should be deep, well-aerated, sub-acidic (pH ~6.2), rich in organic matter (around 4%), and non-compacted to prevent water accumulation, which the plant does not tolerate well (De Leo, 2014). Uniform hydration of the root zone is essential, and irrigation strategies should ensure even moisture distribution, with the wetting radius tailored to plant age (Xiloyannis & Montanaro, 2004; Huang, 2016).

Environmental factors, particularly temperature and oxygen availability, greatly influence root performance. Root growth peaks at around 20 °C, while temperatures exceeding 25 °C or dropping below 10 °C significantly reduce both root and shoot development (Buwalda & Hutton, 1988; Smith et al., 1989). Furthermore, kiwifruit roots are highly sensitive to anoxic conditions due to their limited intercellular air spaces—less than 5% of total root volume—combined with high oxygen demand (Jackson & Drew, 1984; Smith et al., 1989; Donati et al., 2020).

1.3 Domestication and market of the genus *Actinidia*

Despite China being the native land, kiwifruit was not intensively grown in the native country, and the interest in this species was quite low. By 1917, New Zealand nurseries began to offer seedlings of *A. deliciosa* to the public and a few years later interest in this new plant was growing. However, large-scale kiwifruit production in New Zealand, the United States and Europe did not begin until the late 1960s (Huang and Ferguson, 2001).

For over 70 years, commercial kiwifruit production was dominated by early selected cultivars of *A. deliciosa*, such as ‘Hayward’.

Nowadays it is a very important fruit crop in several countries, such as Italy, China, New Zealand, Iran, Greece, USA and France, totalling more than 4 million tons of fruits produced annually world-wide (Bardi, 2020; Save & Serrano, 1986; Savian et al., 2020). In 2023, it is estimated that total kiwifruit plantings in China were 198,809 ha, whereas Italy had 23,850 ha and New Zealand 14,686 ha (FAOSTAT, accessed on 16 April 2025).

Kiwifruit (both *A. deliciosa* and *A. chinensis*) is one of the most important fruit crops in Italy and is cultivated in northern (Emilia-Romagna, Veneto, Piedmont, Friuli, Lombardy), central (Latium), and southern (Campania, Basilicata, Calabria) regions (Spigaglia et al., 2020). In Italy,

the cultivation of *Actinidia* as a fruit crop began in the early 1970s and its expansion has reached almost 420,000 tonnes of fruit produced annually. In fact, according to FAO data from 2025, Italy is the third largest producer of kiwifruit in the world (391,100 t), preceded only by China (2,362,658.11 t) and New Zealand (662,743.61 t) and followed by Greece (317,080 t) and Iran (295,142.37 t; FAOSTAT, accessed on 16 April 2025). However, this remarkable growth has been increasingly challenged by the emergence of serious phytosanitary threats.

2. Phytosanitary issues of *Actinidia deliciosa* in Europe

The Italian kiwifruit industry has faced increasing challenges in recent decades. The major adversities affecting the kiwifruit crop are bacterial canker caused by *Pseudomonas syringae* pv. *actinidiae* (Psa; Donati et al., 2014) and the brown marmorated stink bug: *Halyomorpha halys* (Cesari et al., 2015*).* In 2012, a new and particularly destructive issue emerged: Kiwifruit Vine Decline Syndrome (KVDS). This syndrome was initially observed in flood-irrigated areas such as the province of Verona and has since spread rapidly throughout northern and central Italy (Spigaglia et al., 2020; Tacconi et al., 2015). Affected soils have shown no signs of recovery so far, forcing many farmers to abandon kiwifruit production and switch to alternative crops (Tacconi et al., 2019).On the other hand, critical issues concerning postharvest fruit rots are caused by fungal pathogens such as *Botrytis cinerea*, *Cadophora luteo-olivacea* and *Penicillium expansum* (Bardi et al., 2020).

2.1. Field diseases and pests

Since 2008, Italian kiwifruit orchards have been heavily affected by bacterial canker caused by *Pseudomonas syringae* pv. *actinidiae* (PSA), an occlusive disease that invades the xylem and leads to cankers on trunks and shoots, often resulting in whole-plant death. The bacterium enters through natural openings or wounds and progresses endophytically with a long latency period. Symptoms typically emerge in late winter marked by white or red exudates during early vegetative growth (Figure 4) (Scortichini et al., 2012; Bardi, 2020; Savian et al., 2020).

The development and spread of PSA are strongly influenced by climatic conditions, particularly temperature. The pathogen is most active around 18 °C, with disease severity decreasing above 20 °C and significantly limited above 25 °C. Seasonal variations also affect infection routes:

systemic spread occurs in spring, colonization is minimal in summer, and lenticels and buds become primary entry points in autumn. Additionally, wind and rainfall contribute to the epidemics by causing plant wounds and facilitating bacterial dispersal (Scortichini et al., 2012).

Infected branches produce stunted buds, withering young fruits, and wilting leaves throughout the season. Leaves develop small, angular necrotic spots with a yellow halo during the growing season, these lesions can be circular or irregular and sunken or raised (Prencipe et al., 2019).

Copper-based compounds are used to manage bacterial blight in kiwifruit. In a recent study, several formulations were tested under both greenhouse and field conditions (Monchiero et al., 2015). Among them, copper hydroxide and copper oxychloride proved effective, reducing foliar symptoms by up to 80%; however, their application during low temperatures can induce phytotoxicity. Similar results were observed with acibenzolar-S-methyl, while other products showed inconsistent or limited efficacy. The study also highlighted the potential of integrated strategies combining copper compounds with organic soil amendments to enhance disease control. Nonetheless, prolonged use of copper-based products may lead to the development of copper-resistant pathogen strains (Rinaldi & Leite, 2000) and the accumulation of metallic copper in the soil, posing environmental risks (Alva et al., 1995).

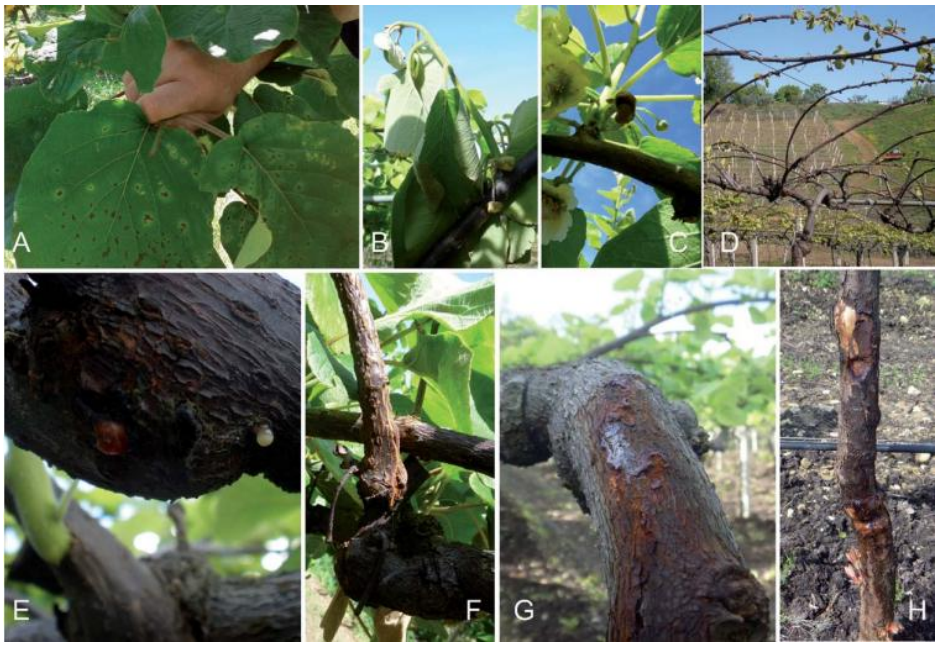


Figure 4 – Symptoms of P. syringae pv. actinidiae *on A. deliciosa cv. 'Hayward' (A) Leaf spots by yellow haloes on A. deliciosa plants, (B) Twig dieback, (C) Flower necrosis, (D) Lack of bud break, (E) Red and*

white exudates from a cane, (F) Reddening of the lenticels, (G) Bacterial canker with exudation, (H) Reddish-brown discoloration under the bark below a canker on the trunk and rootstock (Donati et al., 2014)

Serious damages to Italian kiwifruit orchards also arose from *Halyomorpha halys*, known as brown marmorated stink bug, an invasive species of insect in the family Pentatomidae native to East Asia (Figure 5). This species is present in many parts of North America and has recently become established in Europe and South America (Sparks et al., 2020).

This insect is highly polyphagous, with 170 known host plants, including fruit, horticultural, and ornamental crops (Haye et al., 2015). Crop damage is mainly due to trophic activity on various plant organs, as stink bugs pierce plant tissue with their stylets to extract fluids. In most cases, it can cause a reduction in the fruit's storage life and the signs of stink bug damage makes fruits unsuitable for sale in the market (Bariselli et al., 2016).



Figure 5 – H. halys (B) H. halys nymphs, first instar, cluster around a mass of newly-hatched eggs on the underside of a leaf, (C) adult (top) and fifth-instar nymph (bottom) (Sparks et al., 2020)

2.2 Postharvest diseases

Postharvest diseases of kiwifruit are commonly caused by three fungi: *Botrytis cinerea*, *Cadophora luteo-olivacea* and *Penicillium expansum*. The first one is a necrotrophic fungus that can cause severe disruption to flowers, fruits, leaves, and shoots of many crops, including kiwifruit. Conidia are spread by wind and rain, and infections can occur whenever favourable climatic conditions, such as prolonged humidity and temperature between 16°C and 25°C (Williamson et al., 2007).

If the flowering stage is preceded by repeated rainfall, *Botrytis cinerea* infections can occur in the field, potentially leading to brownish rot symptoms (Figure 6), excessive drooping, and disruption of normal fruit set (Wurms et al., 1999). In contrast, during postharvest storage at 0 °C, *B. cinerea* is primarily responsible for apical (stem-end) rot, which often originates from latent infections entering through harvest wounds (peduncle detachment). These infections typically remain dormant until fruit ripening during cold storage or shelf life. Defence is accomplished primarily by using curing, a process in which kiwifruit are kept at room temperature for 48 hours to promote stalk healing processes so as to block the main entry of the pathogen (Wurms et al., 1999).

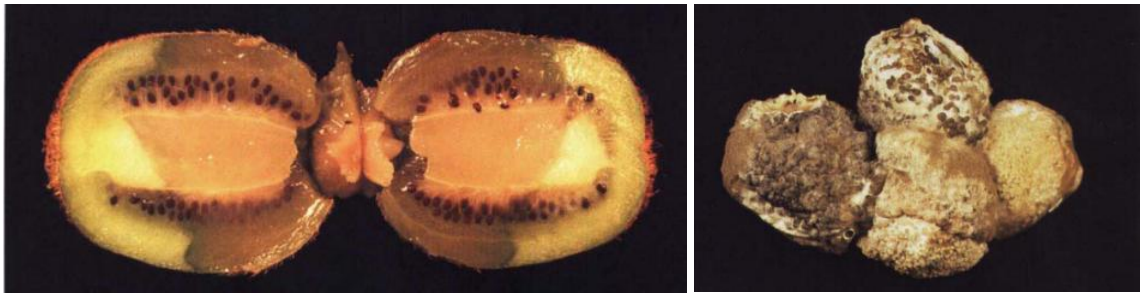


Figure 6 – Cross-sectioned fruit with stem-end rot shows water-soaked tissues, a sign of decay by B. cinerea (left); a cluster of fruit with grey mould, white (immature) and black (mature) sclerotia structures of B. cinerea are present (right) (Michailides & Elmer, 2000)

A postharvest disease of kiwifruit caused by *Cadophora luteo-olivacea*, has been reported in most Italian packinghouses in recent years, characterised by the appearance of skin pitting after 3 or more months of storage (Spadaro et al., 2010; 2011). The incidence of the disease was initially low but increased through the years, reaching 65% in 2006 (Piano et al., 2001; Spadaro et al., 2010). The causal agent was originally identified as *Phialophora* sp. (Gorini, 1991; Piano et al., 2001), or *Phialophora luteo-olivacea* van Beyma (Gams, 2000). Typically, the first symptoms of the disease appear as minor lesions after 100-120 days of storage. The economic concern around kiwifruit skin pitting is mainly due to the lack of effective postharvest fungicides so far (Directive 2009/128 EC on sustainable use of pesticides).

Penicillium expansum, the causal agent of blue mould, is one of the most important postharvest pathogen in many fruits, and can infect also kiwifruit. Initial infection most often occurs at sites

of fruit injury, such as bruises, puncture wounds or stem lesions that form at harvest or during postharvest processing.

Symptoms observed on the surface of infected fruit consist of soft, watery lesions, pale yellow to light brown in colour and the presence of blue-green mould (Rosenberger et al., 2006).

The lesions are soft due to maceration of the tissue by the enzyme polygalacturonase, which plays a significant role in the virulence of *P. expansum*. Spore masses later appear on the surfaces of infected fruit, initially appearing as white mycelium, then turning blue to blue-green in colour as the asexual spores mature.

Infection by *P. expansum* leads to significant economic losses during storage and also affect fruit destined for processing due to the production of the carcinogenic mycotoxin patulin (Rosenberger et al., 2006).

3. Kiwifruit Vine Decline Syndrome (KVDS)

3.1. Overview and symptomatology

Reported for the first time in the Veneto region in 2012 (Tacconi et al., 2019), kiwifruit vine decline syndrome (KVDS), also known locally as ‘’*Moria del kiwi’’*, has since spread to Piedmont in 2015 and to central (Lazio) and southern (Calabria) production areas in 2017 (Savian et al., 2022). The syndrome affects both green- and yellow-fleshed cultivars, regardless of plant age (Spigaglia et al., 2020). Initially affecting over 10% (around 2,900 hectares) of Italian kiwifruit orchards across northern (Veneto, Piedmont, Friuli Venezia Giulia), central (Lazio, Emilia Romagna), and southern regions (Calabria) (Sorrenti et al., 2016), more recent estimates suggest that over 25% of Italian kiwifruit orchards are now affected (Savian et al., 2020).

In kiwifruit vines affected by decline, the root system shows clear morphological and anatomical abnormalities. A significant reduction in fibrous roots is observed, with structural roots exhibiting brown discoloration of the stele and fibrous roots showing cortical decay (Figure 7). The cortical tissue loses its rigidity and detaches from the central stele due to the dissolution of an entire layer of cortical cells surrounding the endodermis; these cells often appear distorted, with missing intercellular material (Bardi, 2020). In many cases, the white feeding roots—crucial for water and nutrient uptake—undergo almost complete decay, and when present, are typically confined to the top 5–10 cm of soil (Tacconi et al., 2015). A distinctive symptom is the presence of a viscous

mucilage on the root surface, which traps rhizospheric soil and forms clumps containing rod-shaped crystals (Bardi et al., 2020). Such root deterioration is often latent, with feeder root dysfunction or death—potentially triggered by flooding—causing vascular symptoms such as stem discoloration (Reid et al., 1991). Kiwifruit vines have large xylem vessels that enable rapid water uptake and transport, allowing them to tolerate reductions in root system size (Dichio et al., 2013). However, this efficient water absorption can mask underlying root deterioration. As a result, vines may develop a vigorous canopy in spring, then suddenly wilt during heat waves when high transpiration rates exceed the compromised root system's ability to supply water (Black et al., 2011).

Leaf symptoms typically appear only after significant root damage has occurred, making early diagnosis challenging. Initially, the canopy may seem vigorous in spring, masking the compromised root system. As the disease progresses and root water uptake becomes insufficient, especially during periods of high heat and transpiration demand, above-ground symptoms become apparent. The peak of symptomatology generally occurs in mid to late summer, when high temperatures drive the vine transpiration rate to its maximum, leading to leaf epinasty, chlorosis, marginal deformation, progressive desiccation from the leaf edges inward, and sprout desiccation, especially in 1- to 2-year-old vines (Donati et al., 2020). Necrotic leaf patches tend to develop suddenly during mid to late summer, when ambient temperatures peak and humidity drops (Smith et al., 1989). Eventually, widespread leaf margin desiccation and extensive phylloptosis occur, leading to canopy collapse and severely affecting plant growth, fruit production, and quality (Bardi, 2020; Bardi et al., 2020; Spigaglia et al., 2020; Donati et al., 2020).



Figure 7 – A. deliciosa cv. 'Hayward' roots showing symptoms related to Kiwifruit Vine Decline Syndrome (a) Extensive reduction of capillary roots, (b) Reddish discoloration of main root (Spigaglia et al., 2020)

In symptomatic vines, a diffuse fruit drop may take place, while remaining berries are impaired in their development, showing a stunted growth often associated to skin wrinkling at harvest (Figure 8) (Donati et al., 2020).



Figure 8 – Symptoms of Kiwifruit Vine Decline Syndrome on A. deliciosa cv. 'Hayward' (Spigaglia et al., 2020)

3.2. Abiotic stress factors involved in KVDS onset

Several abiotic stress factors have been taken in account for their effect on the occurrence of decline symptoms in plants, especially in the context of climate change. Agronomical practices such as over pruning and overcropping (Black et al., 2012) and pathogenic microorganisms (Tacconi et al., 2015) have been found to contribute to decline symptoms.

Soil waterlogging, which often occurs due to traditional surface irrigation practices or heavy rainfall, is a significant abiotic factor associated with this syndrome (Spigaglia et al., 2020). Excessive irrigation can cause soil compaction and reduction in soil porosity, especially in soils with a low organic matter fraction content (Donati et al., 2020).

Kiwifruit is highly sensitive to root anoxia, elevated transpiration demand, and high soil temperatures (Save and Serrano, 1986; Smith et al., 1989). Research indicates that kiwifruit vines are poorly adapted to low oxygen levels in the root zone due to the small intercellular spaces between adjacent cells, which restrict internal gas exchange and worsen symptoms of root asphyxia (Donati et al., 2020; Smith et al., 1989).

Symptoms of waterlogging damage typically appear within 3–7 days after rainfall ceases (Reid et al., 1991). Flooding has been shown to suppress dry weight accumulation in both shoots and roots, while also limiting the formation of adventitious roots on submerged stem sections (Save & Serrano, 1986). The severity of growth reduction is directly related to the number of hours per day the root zone remains unaerated (Smith et al., 1989). Notably, once aeration is restored, growth recovery is generally absent—except for the emergence of new roots at the stem base in vines waterlogged for less than five days (Bardi, 2020).

Flooding also causes stomatal closure and decreases in transpiration rate, xylem water potential, osmotic potential, turgor potential, and photosynthesis (Save & Serrano, 1986). The decrease in stomatal conductance leads to an increase in the maximum daily temperature of the leaves, suppressing root-to-canopy water flow and causing leaves and shoots to suffer from water scarcity (Smith et al., 1989). Additionally, leaves cannot enact thermoregulation mechanisms against sun burn damages (Donati et al., 2020).

Beyond waterlogging, other factors may also contribute to root damage in declining kiwifruit vines. Studies from several orchards in Northern Italy have revealed that such damage can also occur in the absence of excess soil moisture (Tacconi et al., 2019). This suggests that other factors,

such as elevated soil temperatures, may contribute to root decline. High soil temperatures can indirectly affect root health by altering soil properties—for instance, by reducing the concentration of oxygen in the soil solution and further limiting root respiration (Smith et al., 1989). Soil temperatures above 20°C can strongly reduce root growth in kiwifruit and increase shoot/root ratio (Smith et al., 1989), hindering growth and starch accumulation in the roots, which may cause a severe reduction of growth and flowering in the following season (Richardson et al., 2004).

Another critical effect of high soil temperatures, causing the induction of hypoxic conditions, is on meristematic tissues. These tissues due to the high cell density and metabolic activity, are especially sensitive to oxygen depletion. Under hypoxia, these tissues shift from aerobic respiration to anaerobic fermentation (Bailey-Serres & Voesenek, 2008), leading to increased alcohol dehydrogenase (ADH) activity and elevated ethanol accumulation (Liao & Lin, 2001). Because fermentation produces less energy than respiration, the demand for sugars rises sharply. At the same time, reduced phloem transport and the buildup of photosynthates in the leaves lead to a rapid depletion of soluble sugars, followed by the mobilization of stored carbohydrates such as starch (Liao & Lin, 2001). If hypoxic conditions persist, these metabolic disruptions ultimately result in cell death (Bailey-Serres & Voesenek, 2008). Consequently, high summer soil temperatures may significantly contribute to the decline in root growth and function, accelerating overall plant weakening (Bardi et al., 2020).

Supporting this hypothesis, scanning electron microscopy (SEM) of severely KVDS-affected vines revealed anatomical alterations in the root phloem (Figure 9) (Bardi et al., 2020). These included numerous canals likely corresponding to lysogenic aerenchyma—air-filled spaces formed in response to hypoxia to facilitate oxygen diffusion from leaves to roots (Bailey-Serres & Voesenek, 2008). Aerenchyma formation is hormonally regulated, with ethylene and abscisic acid playing key roles; low oxygen conditions stimulate ethylene synthesis, triggering programmed cell death via calcium signaling (Liao & Lin, 2001; Bouranis et al., 2006; Pegg et al., 2020). SEM also showed tissue detachment in root meristems, narrower xylem vessels, disorganized phloem with areas of cell collapse, and abundant calcium oxalate crystals (raphides; Figure 10), often associated with mucilage—likely a byproduct of cell wall degradation (Bardi et al., 2020; Kostman et al., 2001). These structural changes further highlight the damaging effects of hypoxia on kiwifruit root systems.

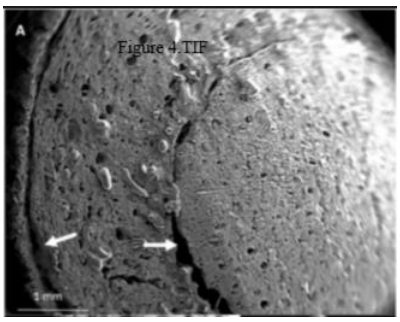


Figure 9 – SEM micrographs showing modifications of the root anatomy in kiwifruit plants grown under different soil management conditions. Arrows are showing detachment in correspondence of the meristematic layers between xylem-phloem and phloem-cortex (Bardi et al., 2020)

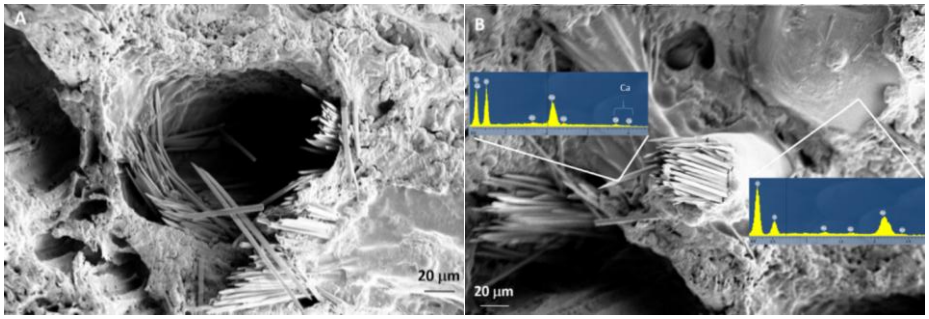


Figure 10 – SEM micrographs showing canals formed in phloem layers of KVDS symptomatic plants with raphides in the inner lumen without (A) or with mucilage (B). Results of the EDS analysis of both raphides and mucilage are presented in (B). (Bardi et al., 2020)

3.3. Biotic factors involved in KVDS onset

While these SEM analyses emphasize the contribution of abiotic stressors such as high soil temperatures and hypoxia, the etiology of KVDS has not been fully elucidated. Previous studies have suggested that no single abiotic factor alone accounts for the syndrome (Sorrenti et al., 2016; Tacconi et al., 2019). This has led to increasing interest in the potential role of soil-borne microorganisms, as distinct bacterial, fungal, and oomycete communities have been identified in KVDS-affected orchards using various approaches. Significant differences were observed in the dry weight of roots and leaves collected from plants grown in sterilised and non-sterilised soil, indicating that microorganisms in the soil caused severe damage to the kiwifruit root system (Savian et al., 2020).

Further supporting a multifactorial origin, transmission electron microscopy (TEM) analyses revealed additional structural responses indicative of both abiotic and biotic interactions. In a study by Savian et al. (2020), a higher number of tyloses and fibrils were observed in the xylem vessels of flooded, unsterilised plants (FU) compared to not flooded unsterilised (NU) and flooded sterilised (FS) ones (Figure 11). These features—considered non-specific plant responses to stress—have been associated with both flooding and pathogen infection (Davison, 2014; De Micco et al., 2016). Although no clear pathogen structures such as hyphae or conidia were detected, the presence of gums adhering to cell walls in FU plants further suggests a stress-induced physiological response, reinforcing the hypothesis of a synergistic interaction between waterlogging and soil-borne pathogens in KVDS development.

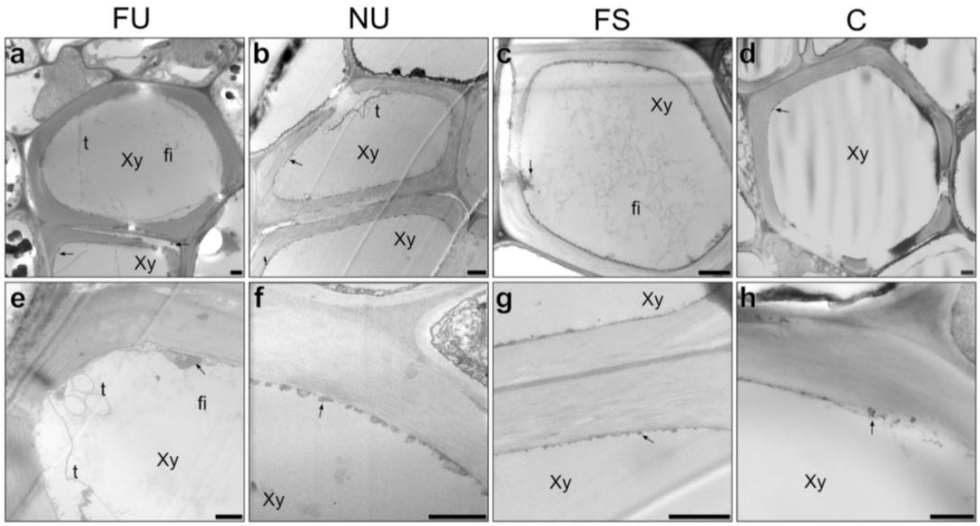


Figure 11– TEM micrographs of xylem vessels of A. deliciosa cv. 'Hayward' subjected to different combinations of water supply and soil sterilization conditions. Whole cells (a-d) and details (e-f) of xylem vessels (Xy). Sections of plants grown in non-sterile (FU; a, e) and sterile soil (FS; e, g) and subjected to flooding; not subjected to flooding and growing in non-sterile soil (NU; b, f) and sterile peat (c, d, h): Tyloses (t) are visible in (a, b and e), fibrils (fi) in (a, c and e). Scale bar = 2 µm (Savian et al., 2020)

However, these structural changes alone do not fully explain the progression and spatial dynamics of the syndrome. An additional consequence of excessive soil water content may be the proliferation of pathogenic organisms on root surfaces and inner tissues. High load of pathogens identified as *Ph. infestans*, *Ph. megasperma*, *P. helicoides* and *D. tabescens* – up to 10^5 CFU g^{-1} fresh weight – was detected on the root surface, potentially serving as inoculum sources for neighbouring vines and helping to explain the observed pattern of symptoms spread in the orchard (Donati et al., 2020). In fact, it has been observed that infected plants are initially localised in a limited area of the orchard and that symptoms apparently spread from infected vines to surrounding ones (Tacconi et al., 2015).

Additionally, transplantation experiments using soil from affected vines reproduced KVDS symptoms after repeated flooding cycles. Notably, soil sterilization prevented symptom development, while improvement of soil conditions—such as increasing aeration and drainage—was not sufficient to stop the syndrome. These findings suggest that biotic factors play a significant role in the onset of KVDS (Donati et al., 2020).

Pathogenic agents can act as primary or secondary factors when plants are weakened by environmental, climatic, or agricultural stresses (Bettenfeld et al., 2020).

Monitoring soil conditions and studying the temporal dynamics of different fungal and bacterial populations associated with kiwifruit roots could help distinguish between populations that act as drivers of KVDS and those that are modified as a result of KVDS or that colonize weakened tissues (Donati et al., 2020; Reid et al., 1991).

Different species of pathogenic organisms have been suggested to be involved, in particular, oomycetes (genera *Phytopythium*, *Pythium* and *Phytophthora*) seem to play a major role in KVDS onset (Bardi, 2020; Donati et al., 2020; Prencipe et al., 2020; Savian et al., 2021); however, fungi (genera *Desarmillaria*, *Cylindrocarpon*, *Fusarium*, *Pyrenochaeta*, *Armillaria* and *Erwinia*) and bacteria (genus *Clostridium*) have also been associated with the disease (Bardi, 2020; Donati et al., 2020; Savian et al., 2021; Spigaglia et al., 2020).

Phytophthora represents an important genus of oomycetes causing root diseases that are also intensified by waterlogging as it promotes the formation and dispersion of zoospores, the exudation from the roots of more chemical attractors for zoospores, thus predisposing the roots to infection (Reid et al., 1991). *Phytophthora* species, including *P. megasperma*, *P. citrophthora*, *P. cryptogea*, *P. cactorum* and *P. infestans* were isolated from roots and soil samples of affected kiwifruit (Donati et al., 2020; Reid et al., 1991; Tacconi et al., 2015).

The genus *Phytophythium*, defined form the clade K of *Pythium* spp., which showed combined features of both *Pythium* and *Phytophthora* (de Cock et al., 2015), is reported to have an important role in the onset of KVDS (Donati et al., 2020). The symptoms produced by these pathogens at the root level partially overlap with those observed in KVDS-affected vines (Donati et al., 2020). This genus also requires free water for zoospore movement and initiation of infection (de Cock et al., 2015). Most species of the *Phytopythium* genus produce papillate and internally proliferating sporangia except for *P. vexans* (Figure 12). *Phytopythium* species typically have subglobose to ovoid sporangia, like those of *Phytophthora*, and cylindrical or lobed antheridia (Figure 13). However, *Phytophthora* never shows a papillate sporangium with internal proliferation, nor does it have a discharge tube, formed by growing sporangia, which is formed from growing sporangia and is typical of both *Pythium* and *Phytopythium*. Zoospores develop outside the sporangium and are released after the rupture of the vesicular membrane outside the sporangium (de Cock et al., 2015).



Figure 12 – Subglobose and non-papillate sporangia of P. vexans (de Cock et al., 2015)

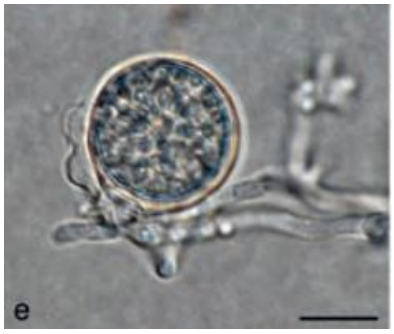


Figure 13 – Elongate antheridium with distinct constrictions of P. vexans (de Cock et al., 2015)

Based on isolation techniques performed on diseased kiwifruit plants, Donati et al. (2020) reported a higher frequency of *Phytophthora* spp. and *Phytopythium* spp. in symptomatic plants (58.6%) compared to asymptomatic ones (19%). In the same paper, the inoculation of *Phytopythium* spp., *Phytophthora* spp., *Desarmillaria tabescens*, and oomycete reference strains was performed together with the waterlogging of pots. The results showed the reproduction of symptoms by all the isolates, regardless of the irrigation strategy, suggesting a crucial role of both oomycetes and other soilborne pathogens, such as *Desarmillaria tabescens*, in the disease.

Building on these findings, Savian et al. (2020) further investigated the interplay between waterlogging, soil pathogens, and KVDS through a combination of historical rainfall analysis in Northeastern Italy and controlled greenhouse trials. When kiwi plantlets were exposed to both waterlogging and natural pathogen inocula, symptoms of KVDS were successfully reproduced. Pathogen isolation from symptomatic plants revealed frequent presence of *P. vexans*, *Phytopythium chamaehyphon*, and *Fusarium solani*. The pathogenicity of *P. vexans* and *P. chamaehyphon* was later confirmed in independent studies (Polat et al., 2017; Savian et al., 2021;

Prencipe et al., 2020). This hypothesis is further confirmed by the well-known root rot activity of oomycetes on kiwifruit vines in different areas (Akilli et al., 2011; Çiftçi et al., 2016; Kurbetli & Ozan, 2013; Savian et al., 2020), In contrast, *F. solani* was shown in earlier studies to cause crown rot on kiwifruit only when forcefully introduced into the collar through wounding, while it was unable to induce fine root decay when applied via root submersion in hyphal and conidial suspensions (Porta-Puglia and Corazza, 1985).

Further surveys in Northwestern Italy between 2016 and 2019 also isolated oomycetes such as *P. vexans*, *P. chamaehyphon*, *Phytopythium helicoides*, and *Phytopythium litorale* from KVDS-affected plants, whose pathogenic potential was validated under waterlogged conditions, thus fulfilling Koch's postulates (Prencipe et al., 2023). These combined findings strengthen the hypothesis that both pathogenic infections and environmental stressors like excess soil moisture contribute synergistically to the onset and progression of KVDS.

The pathogenicity of these oomycetes is increased by waterlogging since their lifestyle require water for zoospore production and spreading (Savian et al., 2020). The high plant mortality rate before waterlogging and the rapid symptom onset afterward suggest that KVDS can develop under near-field capacity conditions and that infections may already be present prior to flooding (Savian et al., 2021). Waterlogging may therefore have a dual effect on plants by causing temporary anoxia stress while also promoting the release of infective zoospores by oomycetes.

Fungal genera like *Fusarium*, *Desarmillaria* and *Armillaria* are also reported in literature as associated to KVDS, according to previous work, *F. solani* was found to cause crown rot on kiwifruit only when it was forcefully introduced into the collar by wounding. It appeared to be unable to cause fine root decay when inoculated by submerging kiwifruit roots in a suspension of hyphae and conidia (Savian et al., 2020). However, it was reported as a secondary invader that could accelerate fine root decay when associated with oomycetes, since it was unable to cause root rot by itself (Savian et al., 2020).

D. tabescens and *Armillaria mellea* are known to cause severe root rot on many horticultural crop plants (Mihail et al., 2002). *D. tabescens* was found exclusively in the roots of symptomatic plants, and its infection is reported to be exacerbated by climate change and waterlogging (Sturrock et al., 2011; Klopfenstein et al., 2009).

Armillaria also causes root rot and death in kiwifruit vines, and orchard epidemics may start from infected wood remaining in the soil (Donati et al., 2020).

Fungi belonging to the *Cylindrocarpon*/*Ilyonectria* complex could be isolated or detected from roots showing symptoms (Tacconi et al., 2015), in particular the species *Cylindrocarpon paucisepticum* were identified by Tosi et al. (2015).

A recent study suggested that soil bacteria may have a role in kiwifruit decline, with Clostridia being identified as a potential contributor, despite not being typically considered as phytopathogens (Bardi, 2020). In Italian kiwifruit orchards affected by the syndrome, *Clostridium* spp. were isolated from both rotten roots and soils, suggesting a role in causing damage to woody crops (Spigaglia et al., 2020).

3.4. Microbiome and dysbiosis hypotheses

While traditional isolation techniques have played a crucial role in identifying key microbial groups associated with KVDS, they only reveal a limited fraction of the microbial diversity present in plant-associated environments (Abdelfattah et al., 2018). To overcome this limitation, recent studies have adopted culture-independent approaches such as metabarcoding, which allows for a comprehensive profiling of the entire microbial community, including unculturable and low-abundance taxa.

In Central Italy, Manici et al. (2022) explored the biotic components of KVDS by integrating fungal endophyte isolation with quantitative PCR to measure fungal and bacterial DNA, alongside next-generation sequencing (NGS) to assess soil bacterial diversity. Their findings showed a significant reduction in bacterial communities in diseased samples, potentially contributing to impaired plant growth.

In Northeastern Italy, Savian et al. (2022) applied a metabarcoding approach to profile oomycete and fungal communities in the root endosphere and rhizosphere of healthy versus symptomatic kiwifruit plants. The study identified *Phytophthora sojae* as the most abundant taxon in diseased samples and detected several *Phytopythium* species — including *P. chamaehyphon* and *P. citrinum* (the latter not previously associated with KVDS) — along with fungi related to the *Ilyonectria* genus, such as *Dactylonectria pauciseptata*, *D. macrodidyma*, and *I. robusta*. Interestingly, *P. vexans* was also found in the roots of healthy plants, supporting the idea that this species may persist asymptomatically but become pathogenic under stress conditions such as waterlogging or plant debilitation (Savian et al., 2020; Tacconi et al., 2015). Savian et al. (2022) proposed that KVDS etiology could be initiated by the early action of one or a few aggressive pathogens, notably

P. sojae, and later aggravated by opportunistic species such as *Phytopythium* spp.. However, this hypothesis remains to be fully validated, as the pathogenicity of *P. sojae* in kiwifruit has yet to be experimentally confirmed, whereas that of *P. vexans* has already been demonstrated (Prencipe et al., 2020; 2023).

Building on efforts to clarify the microbial dynamics underlying KVDS, Mian et al. (2023) employed a targeted metabarcoding approach to investigate oomycete communities in relation to different *Actinidia* genotypes. Genotypes exhibiting resistance to KVDS, such as *A. macrosperma* accessions Ma176 and Ma183 and *A. arguta* cv. Miss Green, harbored distinct oomycete profiles compared to susceptible genotypes like *A. polygama* and *A. chinensis* var. *deliciosa* cv. Hayward. *Phytophthora* spp. were predominantly detected in sensitive genotypes, while *Globisporangium intermedium* was more abundant in asymptomatic plants, suggesting a potential antagonistic or competitive interaction between these taxa. Notably, across diverse host genotypes, the oomycete community was consistently dominated by operational taxonomic units (OTUs) affiliated with *Phytophthora* and *Globisporangium* (formerly *Pythium* clade F), indicating a stable core community structure despite host variation. Most of the other oomycetes highly frequent in the dataset were Pythiaceae, particularly members of the genus *Phytopythium* and *Pythium*. This structure was observed across both rhizosphere and endosphere compartments, underscoring the prevalence of a few dominant taxa.

Bergamaschi et al. (2024) investigated the impact of KVDS on soil microbial communities and health indicators in Central Italy, using bacterial and fungal amplicon sequencing. Their results revealed clear differences in microbial community composition between symptomatic and asymptomatic soils, with NMDS analyses confirming significant shifts associated with both disease status and orchard location. Seasonal dynamics played a major role, while symptomatic soils showed a depletion of beneficial fungal groups such as Glomeromycota and Basidiomycota and an increase in potential pathogens like *Ilyonectria* spp.. Although *Phytopythium vexans* was not directly analyzed, the authors discussed its relevance as a known root pathogen contributing to microbial imbalances. The study also highlighted the potential of β-glucosidase activity in symptomatic rhizospheres as a biomarker for disrupted plant–soil interactions, supporting the idea that KVDS is a multifactorial condition linked to microbiome dysbiosis.

Further insights into the microbial dynamics of KVDS were provided by Mosca et al. (2024), who used a combination of metabarcoding and targeted isolation to investigate the microbiomes

associated with symptomatic and asymptomatic kiwifruit plants in Southern Italy. While their results did not indicate strong shifts in overall microbial diversity or clear evidence of community-wide dysbiosis, they confirmed a consistent association of *Phytopythium vexans* with KVDS symptoms. This species was significantly enriched in both root and soil samples from symptomatic plants, matching sequences of the isolates obtained during their baiting assays. *Phytopythium vexans* was the most abundant oomycete isolated.

At the community level, the root oomycete community of symptomatic plants was dominated by *Phytopythium*, *Pythium*, and *Apodachlya*. In the soil, *Phytopythium* was again prominent in symptomatic samples, contrasting with more taxonomically diverse oomycete communities in healthy soils.

The fungal community also showed distinct patterns between compartments. In the roots, symptomatic samples were predominantly colonized by *Dactylonectria*, *Fusarium*, and *Acrocalymma*.

Despite these compositional changes, Mosca et al. (2024) did not observe significant differences in bacterial or fungal alpha diversity between symptomatic and asymptomatic plants. Additionally, only weak signals of deterministic processes, tested by applying the Anna Karenina Principle (AKP; Arnault et al., 2023), were observed in the assembly of the oomycete community, suggesting limited evidence for strong community restructuring. This discrepancy in the results might be driven by different factors, including sampling timepoint, geographic variation and environmental conditions.

3.5. Approaches for diagnosis and disease modelling

Effective management of KVDS remains a significant challenge due to the complex etiologyf the disease, primarily involving soilborne oomycetes, particularly *Phytopythium vexans*. With chemical fumigation no longer a viable option under current European Union regulations (Regulation EC No. 1107/2009), the development of alternative strategies is essential. One of the most promising approaches is the use of resistant *Actinidia* species as rootstocks or in breeding programs. Genotypes such as *A. macrosperma* have shown high levels of tolerance to KVDS when grown in disease-promoting soils, suggesting their potential for rootstock development. Grafting susceptible cultivars like *A. deliciosa* or *A. chinensis* onto resistant genotypes has demonstrated the ability to reduce disease symptoms and alter the structure of the oomycete community within

the rhizo- and endosphere (Mian et al., 2023). However, the long-term agronomic compatibility of such grafts—including effects on fruit yield, quality, and graft union stability—requires further evaluation.

Beyond breeding efforts, early and reliable detection of *P. vexans* is critical for managing inoculum sources and modeling disease risk. Advances in molecular diagnostics have led to the development of several DNA-based assays, including qPCR, TaqMan probes, and LAMP, targeting conserved regions such as the ITS (Spies et al., 2011; Yano et al., 2011; Yang et al., 2012; Wang et al., 2021) and a putative inositol polyphosphate 5-phosphatase region (Moein et al., 2019a). This is particularly relevant considering that inoculum sources may not only reside in soil but can also originate from nursery stock and irrigation water (Moein et al., 2019b).

Discrepancies in observed microbiome shifts across studies suggest that KVDS may not always trigger classical dysbiosis, and differences may stem from variations in sampling timepoints, environmental conditions, or stress interactions (Mosca et al., 2024). This complexity underscores the importance of adopting disease models that incorporate both biotic and abiotic stress factors, particularly as kiwifruit orchards become increasingly vulnerable to multifactorial stress combinations (MFSC) due to climate change.

Future disease modeling efforts must therefore integrate host genotype susceptibility, microbiome dynamics, and environmental stressors (Zandalinas et al., 2023). To better understand the impact of multifactorial stress conditions (MFSC) on plant health and microbiome interactions, it is essential to study the molecular responses of plants, such as through transcriptomic analyses; although some progress has been made in other crops (Reeksting et al., 2016; Sinha et al., 2024), such studies are still lacking in kiwifruit and represent an important avenue for future research.

In an alternative approach to understanding the dynamics of KVDS, Manici et al. (2025) integrated soil physico-chemical and biochemical analyses with plant tissue enzymatic profiling and microbial quantification using qPCR. Their study revealed that the main changes associated with KVDS occurred in the root-explored soil, where a decline in functional microbial populations pointed to reduced soil suppressiveness—potentially facilitating the establishment of pathogenic fungi. Enzymatic markers such as catalase (CAT), phenylalanine ammonia-lyase (PAL), and proline (PRO) were significantly elevated in plants from symptomatic orchards, indicating heightened physiological stress. Moreover, canonical correlation analysis linked 14 soil variables with these enzymatic stress markers, offering a novel diagnostic perspective for assessing soil

health and plant decline in KVDS-affected systems. New strategies should also explore how microbiomes can be harnessed or engineered to improve resilience. Introducing microbial consortia pre-adapted to MFSC during planting could complement traditional breeding efforts, contributing to more holistic and sustainable disease mitigation frameworks for KVDS and other emerging plant health challenges.

4. Aims of the work

Kiwifruit vine decline syndrome (KVDS) is an emerging threat to *Actinidia deliciosa* production, marked by rapid canopy wilting and severe root system degradation. Since its first detection in 2012, KVDS has become a major concern in Italy—the leading kiwifruit-producing country in Europe—due to its unclear etiology and devastating impact on crop yield.

A comprehensive microbiome characterization of kiwifruit orchards in Northwestern Italy was lacking, particularly one that simultaneously investigated oomycetes, fungi, and bacteria across belowground compartments. Moreover, it was also included testing for microbial dysbiosis or integrated microbial co-occurrence networks with physicochemical soil parameters to better understand how these factors might collectively contribute to disease onset. On the diagnostic front, a validated molecular tool specifically designed for detecting *Phytopythium vexans* in kiwifruit systems was missing—especially one that accounted for host cross-reactivity and could be used to screen propagation materials and quantify pathogen loads in roots and soil. At the host level, molecular responses of *Actinidia deliciosa* to multifactorial stressors, such as those brought on by climate change, represent a largely unexplored frontier. In the context of KVDS, the plant transcriptional responses to biotic, abiotic, and combined stress conditions have never been experimentally tested. Understanding how these stressors interact to weaken the host could open new avenues for deciphering the underlying mechanisms of the syndrome. Importantly, such insights could support the identification of candidate genes linked to stress resilience, potentially informing breeding strategies or biotechnological applications aimed at improving plant stress tolerance.

This work addresses this knowledge gap through three integrated research chapters, each targeting a distinct but complementary aspect of KVDS:

Chapter 2 presents a comprehensive characterize of the belowground microbial communities - bacteria, fungi, and oomycetes - associated with healthy and KVDS-affected kiwifruit plants in three distinct compartments: bulk soil, rhizosphere, and roots. This was achieved through amplicon sequencing (metabarcoding) of samples collected from orchards in Northwestern Italy (Piedmont region). The study further aimed to both assess microbial interactions (e.g., co-occurrence networks) and to examine evidence of microbial dysbiosis (through AKP testing) in symptomatic

plants. Investigation of how soil physicochemical parameters may shape microbial community assembly was also considered. By integrating both biotic and abiotic datasets, this chapter elucidates the complex community and ecological networks potentially contributing to KVDS.

Chapter 3 focuses on the development and validation of a sensitive, specific diagnostic tool for early detection of *Phytopythium vexans* which is reported to be strongly implicated in KVDS. The assay targets the mitochondrial cytochrome oxidase subunit I (COI) gene, a more discriminating marker than commonly used nuclear ITS regions. Primer specificity was evaluated against closely related oomycetes and common soil fungi, while validation was performed on both symptomatic *Actinidia deliciosa* tissues and soils, following EPPO guidelines. The tool broader applicability was assessed in apple replant disease (ARD) affected soils sampled in the United States. This diagnostic assay offers a practical means to monitor infection sources in nurseries and orchards, potentially mitigating the spread and impact of *P. vexans* in woody perennials.

Chapter 4 investigates the molecular responses of *Actinidia deliciosa* roots to biotic stress (pathogen inoculation), abiotic stress (root flooding), and their combination to mimic KVDS-like conditions under controlled environments. Using RNA-seq, differentially expressed genes (DEGs) were identified over a time course to reveal pathways involved in stress perception, signaling, and adaptation. Selected DEGs were validated via qPCR to confirm expression patterns. This chapter explores the molecular crosstalk between biotic and abiotic stress pathways, providing the first comprehensive insight into *Actinidia*'s transcriptional plasticity under multifactorial stress conditions.

Overall, this thesis aims to advance our understanding of KVDS by integrating microbial ecology, diagnostic innovation, and plant molecular biology, ultimately contributing to the development of effective management strategies for this complex disease.

References

Abdelfattah, A., Malacrinò, A., Wisniewski, M., Cacciola, S. O., & Schena, L. (2018). Metabarcoding: A powerful tool to investigate microbial communities and shape future plant protection strategies. *Biological Control*, 120, 1–10. https://doi.org/10.1016/j.biocontrol.2017.07.009.

Alva, A. K., Graham, J. H., & Anderson, C. A. (1995). Soil pH and Copper Effects on Young 'Hamlin' Orange Trees. *Soil Science Society of America Journal*, 59(2), 481–487. https://doi.org/10.2136/sssaj1995.03615995005900020031x.

Akilli, S., Serçe, Çi. U., Zekaİ Katircioğlu, Y., Karakaya, A., & Maden, S. (2011). Involvement of Phytophthora citrophthora in Kiwifruit Decline in Turkey: Involvement of Phytophthora citrophthora on Kiwifruit. *Journal of Phytopathology*, 159(7–8), 579–581. https://doi.org/10.1111/j.1439-0434.2011.01798.x.

Arnault, G., Mony, C., and Vandenkoornhuyse, P. (2023). Plant microbiota dysbiosis and the Anna Karenina principle. *Trends Plant Science*, 28, 18–30. doi: 10.1016/j.tplants.2022.08.012.

Bailey-Serres, J., & Voesenek, L. A. C. J. (2008). Flooding Stress: Acclimations and Genetic Diversity. *Annual Review of Plant Biology*, 59(1), 313–339. https://doi.org/10.1146/annurev.arplant.59.032607.092752.

Bardi, L., Nari, L., Morone, C., Faga, M. G., & Malusà, E. (2020). Possible Role of High Temperature and Soil Biological Fertility on Kiwifruit Early Decline Syndrome. *Frontiers in Agronomy,* 2, 580659. https://doi.org/10.3389/fagro.2020.580659.

Bariselli, M., Bugiani, R., & Maistrello, L. (2016). Distribution and damage caused by Halyomorpha halys in Italy. EPPO Bulletin, 46(2), 332–334. https://doi.org/10.1111/epp.12289.

Bergamaschi, V., Vera, A., Pirone, L., Siles, J. A., López-Mondéjar, R., Luongo, L., Vitale, S., Reverberi, M., Infantino, A., & Bastida, F. (2024). Kiwifruit Vine Decline Syndrome (KVDS) Alters Soil Enzyme Activity and Microbial Community. *Microorganisms*, 12(11), 2347. https://doi.org/10.3390/microorganisms12112347.

Bettenfeld, P., Fontaine, F., Trouvelot, S., Fernandez, O., & Courty, P.-E. (2020). Woody Plant Declines. What's Wrong with the Microbiome? *Trends in Plant Science*, 25(4), 381–394. https://doi.org/10.1016/j.tplants.2019.12.024.

Buwalda, J. G., & Hutton, R. C. (1988). Seasonal changes in root growth of kiwifruit. *Scientia Horticulturae*, 36(3–4), 251–260. https://doi.org/10.1016/0304-4238(88)90059-3.

Black, M. Z., Patterson, K. J., Minchin, P. E. H., Gould, K. S., & Clearwater, M. J. (2011). Hydraulic responses of whole vines and individual roots of kiwifruit (Actinidia chinensis) following root severance. *Tree Physiology*, 31(5), 508–518. https://doi.org/10.1093/treephys/tpr045.

Bardi, L. (2020). Early kiwifruit decline: A soil-borne disease syndrome or a climate change effect on plant–soil relations?. *Frontiers in Agronomy*, *2*, 3. https://doi.org/10.3389/fagro.2020.00003.

Black, M., Patterson, K., Gould, K., & Clearwater, M. (2012). Physiological responses of kiwifruit vines (Actinidia chinensis Planch. Var. Chinensis) to trunk girdling and root pruning. *New Zealand Journal of Crop and Horticultural Science*, 40(1), 31–41. https://doi.org/10.1080/01140671.2011.603343.

Bouranis, D. L., Chorianopoulou, S. N., Kollias, C., Maniou, P., Protonotarios, V. E., Siyiannis, V. F., & Hawkesford, M. J. (2006). Dynamics of Aerenchyma Distribution in the Cortex

of Sulfate-deprived Adventitious Roots of Maize. *Annals of Botany*, 97(5), 695–704. https://doi.org/10.1093/aob/mcl024.

Cesari, M., Maistrello, L., Ganzerli, F., Dioli, P., Rebecchi, L., & Guidetti, R. (2015). A pest alien invasion in progress: Potential pathways of origin of the brown marmorated stink bug Halyomorpha halys populations in Italy. *Journal of Pest Science*, 88(1), 1–7. https://doi.org/10.1007/s10340-014-0634-y.

Çiftçi, O., Serçe, Ç. U., Türkölmez, Ş., & Derviş, S. (2016). First Report of Phytophthora palmivora Causing Crown and Root Rot of Kiwifruit (Actinidia deliciosa) in Turkey. *Plant Disease*, 100(1), 210. https://doi.org/10.1094/PDIS-04-15-0394-PDN.

Chou-Fen, L., & Ferguson, A. R. (1986). The botanical nomenclature of the kiwifruit and related taxa. *New Zealand Journal of Botany*, 24(1), 183–184. https://doi.org/10.1080/0028825X.1986.10409728.

Davison, E. M. (2014). Resolving confusions about jarrah dieback—Don't forget the plants. *Australasian Plant Pathology*, 43(6), 691–701. https://doi.org/10.1007/s13313-014-0302-y.

de Cock, A. W. A. M., Lodhi, A. M., Rintoul, T. L., Bala, K., Robideau, G. P., Abad, Z. G., Coffey, M. D., Shahzad, S., & Lévesque, C. A. (2015). Phytopythium: Molecular phylogeny and systematics. Persoonia - *Molecular Phylogeny and Evolution of Fungi*, 34(1), 25–39. https://doi.org/10.3767/003158515X685382.

De Leo. (2014). L'actinidia (kiwi) e la sua coltivazione in Calabria. A.R.S.A.C., Gioia Tauro, 94 pp.

De Micco, V., Balzano, A., Wheeler, E. A., & Baas, P. (2016). Tyloses and gums: a review of structure, function and occurrence of vessel occlusions. *IAWA Journal*, 37(2), 186–205. https://doi.org/10.1163/22941932-20160130.

Dichio, B., Montanaro, G., Sofo, A., & Xiloyannis, C. (2013). Stem and whole-plant hydraulics in olive (Olea europaea) and kiwifruit (Actinidia deliciosa). *Trees*, 27(1), 183–191. https://doi.org/10.1007/s00468-012-0787-3.

Donati, I., Buriani, G., Cellini, A., Mauri, S., Costa, G., & Spinelli, F. (2014). New insights on the bacterial canker of kiwifruit (Pseudomonas syringae pv. Actinidiae). *Journal of Berry Research*, 4(2), 53–67. https://doi.org/10.3233/JBR-140073.

Donati, I., Cellini, A., Sangiorgio, D., Caldera, E., Sorrenti, G., & Spinelli, F. (2020). Pathogens Associated to Kiwifruit Vine Decline in Italy. *Agriculture*, 10(4), 119. https://doi.org/10.3390/agriculture10040119.

FAOSTAT. FAO Statistical Database. Available online: https://www.fao.org/faostat/ (accessed on 16 April 2025).

Gams W. (2000). Phialophora and some similar morphologically little-differentiated anamorphs of divergent ascomycetes. *Studies in Mycology* 45: 187-199.

Gorini F. (1991). Skin pitting of kiwifruit during storage. *Acta Horticulturae* 297: 595-598.

Grant, J. J., & Loake, G. J. (2000). Role of Reactive Oxygen Intermediates and Cognate Redox Signaling in Disease Resistance. *Plant Physiology*, 124(1), 21–30. https://doi.org/10.1104/pp.124.1.21.

Haye, T., Gariepy, T., Hoelmer, K., Rossi, J.-P., Streito, J.-C., Tassus, X., & Desneux, N. (2015). Range expansion of the invasive brown marmorated stinkbug, Halyomorpha halys: An

increasing threat to field, fruit and vegetable crops worldwide. *Journal of Pest Science*, 88(4), 665–673. https://doi.org/10.1007/s10340-015-0670-2.

Huang, H., & Ferguson, A. R. (2001). Review: Kiwifruit in China. *New Zealand Journal of Crop and Horticultural Science*, 29(1), 1–14. https://doi.org/10.1080/01140671.2001.9514154.

Huang, H., Wang, S., Jiang, Z., Zhang, Z., & Gong, J. (2003). Exploration of Actinidia genetic resources and development of kiwifruit industry in China. *Acta Horticulturae*, 610, 29–43. https://doi.org/10.17660/ActaHortic.2003.610.2.

Huang, H. (2016). Kiwifruit: The genus Actinidia. Elsevier/AP, Academic Press is an imprint of Elsevier ; Science Press.

Jackson, M. B., & Drew, M. C. (1984). Effects of Flooding on Growth and Metabolism of Herbaceous Plants. *In Flooding and Plant Growth* (pp. 47–128). Elsevier. https://doi.org/10.1016/B978-0-12-424120-6.50008-0.

Klopfenstein, N.B.; Kim, M.-S.; Hanna, J.W.; Richardson, B.A.; Lundquist, J.W. (2009). Approaches to Predicting Potential Impacts of Climate Change on Forest Disease: An Example with Armillaria Root Disease. In Research Paper RMRS-RP-76. U.S. Department of Agriculture, Forest Service; Rocky Mountain Research Station: FortCollins, CO, USA, p. 10.

Kostman, T. A., Tarlyn, N. M., Loewus, F. A., & Franceschi, V. R. (2001). Biosynthesis of l -Ascorbic Acid and Conversion of Carbons 1 and 2 of l -Ascorbic Acid to Oxalic Acid Occurs within Individual Calcium Oxalate Crystal Idioblasts. Plant Physiology, 125(2), 634–640. https://doi.org/10.1104/pp.125.2.634.

Kurbetli, İ., & Ozan, S. (2013). Occurrence of Phytophthora Root and Stem Rot of Kiwifruit in Turkey. *Journal of Phytopathology*, 161(11–12), 887–889. https://doi.org/10.1111/jph.12145.

Liao, C. T., & Lin, C. H. (2001). Physiological adaptation of crop plants to flooding stress. Proceedings of the National Science Council, Republic of China. Part B, Life Sciences, 25(3), 148-157.

Manici, L. M., Maisto, G., Abbate, C., Caputo, F., Memoli, V., Santorufo, L., Morello, B., Zizolfi, M., Santini, G., Vitale, S., & Infantino, A. (2025). Quantitative soil indicators for identifying primary stressors in fruit tree decline: a case study on kiwifruit vine decline syndrome. *Applied Soil Ecology*, 206, 105887. https://doi.org/10.1016/j.apsoil.2025.105887.

Manici, L. M., Saccà, M. L., Scotti, C., and Caputo, F. (2022). Quantitative reduction of soil bacteria and qualitative microbial changes: biotic components associated to kiwifruit decline. *Plant Soil*, 477, 613–628. doi: 10.1007/s11104-022-05470-w.

Mian, G., Cipriani, G., Firrao, G., Martini, M., & Ermacora, P. (2023). Genetic diversity of Actinidia spp. shapes the oomycete pattern associated with Kiwifruit Vine Decline Syndrome (KVDS). *Scientific Reports*, 13(1), 16449. https://doi.org/10.1038/s41598-023-43754-y.

Mihail, J. D., Bruhn, J. N., & Leininger, T. D. (2002). The effects of moisture and oxygen availability on rhizomorph generation by Armillaria tabescens in comparison with A. gallica and A. mellea. *Mycological Research*, *106*(6), 697-704. https://doi.org/10.1017/S0953756202005920.

Moein, S., Mazzola, M., Spies, C. F. J., & McLeod, A. (2019a). Evaluating different approaches for the quantification of oomycete apple replant pathogens, and their relationship with seedling growth reductions. European Journal of Plant Pathology, 154:243-257. doi: 10.1007/s10658-018-01652-4.

Moein, S., Mazzola, M., Ntushelo, N. S., & McLeod, A. (2019b). Apple nursery trees and irrigation water as potential external inoculum sources of apple replant disease in South Africa. *European Journal of Plant Pathology*, *153*, 1131-1147. doi: 10.1007/s10658-018-01631-9.

Monchiero, M., Gullino, M. L., Pugliese, M., Spadaro, D., & Garibaldi, A. (2015). Efficacy of different chemical and biological products in the control of Pseudomonas syringae pv. Actinidiae on kiwifruit. *Australasian Plant Pathology*, 44(1), 13–23. https://doi.org/10.1007/s13313-014-0328-1.

Mosca, S., Aci, M. M., Procopio, G., Vadalà, V., Vizzari, G., Francomano, E., Mohamed, N., Z., Li Destri Nicosia, M., G., Agosteo, G., E., Spadaro, D., Schena,L., & Malacrinò, A. (2024). Integrated analyses of the plant and soil microbiome identify Phytopythium vexans as agent of the Kiwifruit Vine Decline Syndrome. *Plant and Soil*, 1-14. https://doi.org/10.1007/s11104-024-06891-5.

Pegg, T., Edelmann, R. R., & Gladish, D. K. (2020). Immunoprofiling of Cell Wall Carbohydrate Modifications During Flooding-Induced Aerenchyma Formation in Fabaceae Roots. *Frontiers in Plant Science*, 10, 1805. https://doi.org/10.3389/fpls.2019.01805.

Piano S., Gilardi G., Galliano A., Gullino M.L., (2001). Gravi attacchi di Phialophora sp. su frutti di actinidia. *Informatore Fitopatologico – La Difesa delle Piante* 51: 76.

Polat, Z., Awan, Q. N., Hussain, M., & Akgül, D. S. (2017). First report of Phytopythium vexans causing root and collar rot of kiwifruit in Turkey. *Plant Disease*, 101(6), 1058.doi.org/10.1094/PDIS-11-16-1554-PDN.

Porta-Puglia, A., & Corazza, L. (1985). Fusarium solani (Mart.) Sacc. associato ad un marciume del colletto dell'Actinidia. *Rivista di ortoflorofrutticoltura italiana*, 81-83.

Prencipe, S., Nari, L., Vittone, G., Gullino, M.L., Garibaldi, A. and Spadaro, D. (2019). Postharvest quality and health of kiwifruit 'Hayward' affected by Pseudomonas syringae pv. actinidiae. *Acta Horticolturae*. 1243, 91-96 doi: 10.17660/ActaHortic.2019.1243.15 https://doi.org/10.17660/ActaHortic.2019.1243.15.

Prencipe, S., Savian, F., Nari, L., Ermacora, P., Spadaro, D., & Martini, M. (2020). First Report of Phytopythium vexans Causing Decline Syndrome of Actinidia deliciosa 'Hayward' in Italy. *Plant Disease*, 104(7), 2032. https://doi.org/10.1094/PDIS-10-19-2101-PDN.

Prencipe, S., Schiavon, G., Rosati, M., Nari, L., Schena, L., & Spadaro, D. (2023). Characterization of Phytopythium Species Involved in the Establishment and Development of Kiwifruit Vine Decline Syndrome. *Microorganisms*, 11(1), 216. https://doi.org/10.3390/microorganisms11010216.

Reeksting, B. J., Olivier, N. A., & Van Den Berg, N. (2016). Transcriptome responses of an ungrafted Phytophthora root rot tolerant avocado (Persea americana) rootstock to flooding and Phytophthora cinnamomi. *BMC plant biology*, 16, 1-19. doi: 10.1186/s12870-016-0893-2.

Reid, J. B., Tate, K. G., Brown, N. S., & Cheah, L. H. (1991). Effects of flooding and alluvium deposition on kiwifruit (Actinidia deliciosa): 1. Early vine decline. *New Zealand Journal*

of Crop and Horticultural Science, 19(3), 247–257. https://doi.org/10.1080/01140671.1991.10421808.

Richardson, A. C., Marsh, K. B., Boldingh, H. L., Pickering, A. H., Bulley, S. M., Frearson, N. J., Ferguson, A. R., Thornber, S. E., Bolitho, K. M., & Macrae, E. A. (2004). High growing temperatures reduce fruit carbohydrate and vitamin C in kiwifruit. *Plant, Cell and Environment*, 27(4), 423–435. https://doi.org/10.1111/j.1365-3040.2003.01161.x.

Rinaldi, D. A. M. F., Leite, R.P., Jr. (2000). Adaptation of Xanthomonas axonopodis pv. citri population to the presence of copper compounds in nature. Proceedings of the International Society of Citriculture 2:1064.

Rosenberger, D. A., Engle, C. A., Meyer, F. W., & Watkins, C. B. (2006). Penicillium expansum Invades Apples Through Stems during Controlled Atmosphere Storage. *Plant Health Progress*, 7(1), 1. https://doi.org/10.1094/PHP-2006-1213-01-RS.

Save, R., & Serrano, L. (1986). Some physiological and growth responses of kiwi fruit (Actinidia chinensis) to flooding. *Physiologia Plantarum*, 66(1), 75–78. https://doi.org/10.1111/j.1399-3054.1986.tb01236.x.

Savian, F., Ginaldi, F., Musetti, R., Sandrin, N., Tarquini, G., Pagliari, L., Firrao, G., Martini, M., & Ermacora, P. (2020). Studies on the aetiology of kiwifruit decline: Interaction between soil-borne pathogens and waterlogging. *Plant and Soil*, 456(1–2), 113–128. https://doi.org/10.1007/s11104-020-04671-5.

Savian, F., Prencipe, S., Filippini, N., Nari, L., Martini, M., Ermacora, P., & Spadaro, D. (2021). Pathogenicity of Phytopythium chamaehyphon: A New Player in Kiwifruit Vine Decline Syndrome of Actinidia chinensis var. deliciosa 'Hayward' in Italy. *Plant Disease*, 105(10), 2781–2784. https://doi.org/10.1094/PDIS-01-21-0143-SC.

Savian, F., Marroni, F., Ermacora, P., Firrao, G., & Martini, M. (2022). A Metabarcoding Approach to Investigate Fungal and Oomycete Communities Associated with Kiwifruit Vine Decline Syndrome in Italy. *Phytobiomes Journal*, 6(4), 290–304. https://doi.org/10.1094/PBIOMES-03-22-0019-R.

Scortichini, M., Marcelletti, S., Ferrante, P., Petriccione, M., & Firrao, G. (2012). Pseudomonas syringae pv. actinidiae: A re-emerging, multi-faceted, pandemic pathogen: Pseudomonas actinidiae. *Molecular Plant Pathology*, 13(7), 631–640. https://doi.org/10.1111/j.1364-3703.2012.00788.x.

Sinha, R., Peláez-Vico, M. Á., Shostak, B., Nguyen, T. T., Pascual, L. S., Ogden, A. M., Lyu, Z., Zandalinas, S. I., Joshi, T., Fritschi, F. B., & Mittler, R. (2024). The effects of multifactorial stress combination on rice and maize. *Plant Physiology*, 194(3), 1358-1369. doi: 10.1093/plphys/kiad557.

Smith, G. S., Buwalda, J. G., Green, T. G. A., & Clark, C. J. (1989). Effect of oxygen supply and temperature at the root on the physiology of kiwifruit vines. *New Phytologist*, 113(4), 431–437. https://doi.org/10.1111/j.1469-8137.1989.tb00354.x.

Sorrenti, G., Toselli, M., Reggidori, G., & Spinelli, F. (2016). Implicazioni della gestione idrica nella “moria del kiwi” del veronese. *Rivista di Frutticoltura e di Ortofloricoltura*, *78*(3), 45-51.

Spadaro, D., Galliano, A., Pellegrino, C., Gilardi, G., Garibaldi, A., & Gullino, M. L. (2010). Dry matter and mineral composition, together with commercial storage practices, influence the development of skin pitting caused by Cadophora luteo-olivacea on kiwifruit ‘Hayward’. *Journal of Plant Pathology*. http://www.jstor.org/stable/41998808.

Spadaro, D., Pellegrino, C., Garibaldi, A., & Gullino, M. L. (2011). Development of SCAR primers for the detection of Cadophora luteo-olivacea on kiwifruit and pome fruit and of Cadophora malorum on pome fruit. *Phytopathologia Mediterranea*, 50(3).

Sparks, M. E., Bansal, R., Benoit, J. B., Blackburn, M. B., Chao, H., Chen, M., Cheng, S., Childers, C., Dinh, H., Doddapaneni, H. V., Dugan, S., Elpidina, E. N., Farrow, D. W., Friedrich, M., Gibbs, R. A., Hall, B., Han, Y., Hardy, R. W., Holmes, C. J., Hughes, D. S. T., Ioannidis, P., Cheatle Jarvela, A.M., Johnston, J. S., Jones, J. W., & Gundersen-Rindal, D. E. (2020). Brown marmorated stink bug, Halyomorpha halys (Stål), genome: Putative underpinnings of polyphagy, insecticide resistance potential and biology of a top worldwide pest. *BMC Genomics*, 21(1), 227. https://doi.org/10.1186/s12864-020-6510-7.

Spies, C. F. J., Mazzola, M., & McLeod, A. (2011). Characterisation and detection of Pythium and Phytophthora species associated with grapevines in South Africa. *European journal of plant pathology*, *131*, 103-119. doi: 10.1007/s10658-011-9791-5.

Spigaglia, P., Barbanti, F., Marocchi, F., Mastroleo, M., Baretta, M., Ferrante, P., Caboni, E., Lucioli, S., & Scortichini, M. (2020). Clostridium bifermentans and C. subterminale are associated with kiwifruit vine decline, known as moria , in Italy. *Plant Pathology*, 69(4), 765–774. https://doi.org/10.1111/ppa.13161.

Sturrock, R. N., Frankel, S. J., Brown, A. V., Hennon, P. E., Kliejunas, J. T., Lewis, K. J., Worrall, J. J., & Woods, A. J. (2011). Climate change and forest diseases. *Plant pathology*, 60(1), 133-149. doi: 10.1111/j.1365-3059.2010.02406.x.

Tacconi, G., Paltrinieri, S., Mejia, J. F., Fuentealba, S. P., Bertaccini, A., Tosi, L., Giacopini, A., Mazzucchi, U., Favaron, F., Sella, L., & Bertaiola, F. (2015). Vine decline in kiwifruit:

climate change and effect on waterlogging and Phytophthora in North Italy. *Acta Horticulturae*, 1096, 93–97. https://doi.org/10.17660/ActaHortic.2015.1096.7.

Tacconi, G., Giacopini, A., Vittone, G., Nari, L., Spadaro, D., Savian, F., Ermacora, P., Saro, S., Morone, C., Bardi, L., & Tosi, L., (2019). "Moria del kiwi": situazione disastrosa al nord, preoccupante nel resto d'Italia. Kiwi Informa Aprile/Giugno:32-37.

Tosi, L., Tacconi, G., & Giacopini, A. (2015) La moria del kiwi, situazione e prospettive. L'Informatore Agrario 44:67–70.

Wang, T., Ji, H., Yu, Y., Wang, X., Cheng, Y., Li, Z., Chen, J., Guo, L., Xu, J., & Gao, C. (2021). Development of a loop-mediated isothermal amplification method for the rapid detection of phytopythium vexans. *Frontiers in Microbiology*, *12*, 720485. https://doi.org/10.3389/fmicb.2021.720485.

Williamson, B., Tudzynski, B., Tudzynski, P., & Van Kan, J. A. L. (2007). Botrytis cinerea: The cause of grey mould disease. *Molecular Plant Pathology*, 8(5), 561–580. https://doi.org/10.1111/j.1364-3703.2007.00417.x.

Wurms, K. V., Long, P. G., Sharrock, K. R., & Greenwood, D. R. (1999). The potential for resistance to Botrytis cinerea by kiwifruit. *Crop Protection*, 18(7), 427–435. https://doi.org/10.1016/S0261-2194(99)00047-2.

Xiloyannis, C., & Montanaro, G. (2004). Irrigazione e concimazione dell'Actinidia.

Yang, J. I., Ruegger, P. M., McKenry, M. V., Becker, J. O., & Borneman, J. (2012). Correlations between root-associated microorganisms and peach replant disease symptoms in a California soil. *PloS one* 7(10):e46420. https://doi.org/10.1371/journal.pone.0046420.

Yano, T., Shimizu, S., Miyoshi, T., Miyata, N., Immon, K., Shinozaki, T., Sawada, H., & Kageyama, K. (2010). Tolerant Actinidia species to Pythium helicoides and P. vexans causing root rot. In VII International Symposium on Kiwifruit 913:517-523.

Zandalinas, S. I., Peláez-Vico, M. Á., Sinha, R., Pascual, L. S., & Mittler, R. (2024). The impact of multifactorial stress combination on plants, crops, and ecosystems: how should we prepare for what comes next?. *The Plant Journal*, 117(6), 1800-1814. https://doi.org/10.1111/tpj.16557.

Chapter 2 - Soil, rhizosphere, and root microbiome in kiwifruit vine decline, an emerging multifactorial disease

Soil, rhizosphere, and root microbiome in kiwifruit vine decline, emerging multifactorial disease

Micol Guaschino[1,2], Marco Garello[1,2], Luca Nari[3], Yeka V. Zhimo[4], Samir Droby[4], Davide Spadaro[1,2*]

[1] Department of Agricultural, Forestry and Food Sciences (DiSAFA), University of Torino, via Paolo Braccini 2, 10095, Grugliasco, TO, Italy

[2] Interdepartmental Centre of Competence for the Innovation in the Agro-environmental Sector - AGROINNOVA, University of Turin, via Paolo Braccini 2, 10095, Grugliasco, TO, Italy

[3] Fondazione Agrion - Via Falicetto, 24, 12030, Manta, CN, Italy

[4] Department Postharvest Science, ARO, The Volcani Center, P.O. Box 15159, Rishon Lezion 7505101, Israel

*** Correspondence:**

Davide Spadaro

davide.spadaro@unito.it

Keywords: multifactorial disease; kiwifruit vine decline syndrome; microbiome; dysbiosis; *Phytopythium*; Next Generation Sequencing; metabarcoding

Bibliographic reference: *Guaschino, M., Garello, M., Nari, L., Zhimo, Y. V., Droby, S., & Spadaro, D. (2024). Soil, rhizosphere, and root microbiome in kiwifruit vine decline, an emerging multifactorial disease. Frontiers in Microbiology, 15, 1330865. https://doi.org/10.3389/fmicb.2024.1330865.*

Abstract

Kiwifruit vine decline syndrome (KVDS) is characterized by severe root system impairment which leads to irreversible wilting of the canopy. Plants usually collapse rapidly from the appearance of the first above ground symptoms, without recovery even in the following seasons. The syndrome has been negatively impacting kiwifruit yield in different areas of Italy, the main producing European country, since its first outbreak in 2012. To date, a unique, common causal factor is yet to be found and the syndrome is referred to as multifactorial. In this paper, we investigated the whole biotic community (fungi, bacteria, and oomycetes) associated with the development of KVDS in three different belowground matrices/compartments (soil, rhizosphere, and root). Sampling was performed in both healthy and affected sites located in the main kiwifruit producing area of Northwestern Italy. To address the multifactorial nature of the syndrome and to investigate potential roles of abiotic factors in shaping these communities, physicochemical analysis of soils was also performed. This study investigates the associations among taxonomic groups composing the microbiome and also between biotic and abiotic factors. Dysbiosis was considered as a driving event shaping KVDS microbial communities. The results obtained from this study highlight the role of the oomycete genus *Phytopythium,* which resulted predominant in the oomycete community composition of diseased matrices, though it was also present in healthy ones. Both bacterial and fungal communities resulted in a high richness of genera, and majorly correlated to sampling site and matrix, underlining the importance of multiple location sampling both geographically and spatially. Rhizosphere community associated to KVDS resulted as driven by a dysbiotic process. In addition, analysis of association network in diseased rhizosphere, revealed the presence of potential cross- kingdom competition for plant-derived carbon between saprobes, oomycetes and bacteria.

1. Introduction

In the framework of changing climate where average temperatures are rising and both frequency and intensity of extreme weather events are expected to increase, co-occurring stress factors are becoming the main drivers of severe decline in plant growth and survival (Zandalinas et al., 2021a). Woody plant declines are characterized by a degeneration of plant tissues brought on by multifactorial stress, which is defined as the combination of biotic, climate-driven, and/or soil-associated stress factors simultaneously impacting plant health, with a decrease of the overall productivity (Bettenfeld et al., 2020; Zandalinas et al., 2021b). In the last decade, several perennials including different woody plant species have been increasingly affected by decline. Affected agroecosystems include vineyards (Fontaine et al., 2016; Gramaje et al., 2018; Merot et al., 2023), olive groves (Luvisi et al., 2017), peach (Yang et al., 2012), apple (Mazzola and Manici, 2012; Nicola et al., 2018), citrus (Ezrari et al., 2021) and kiwifruit orchards (Savian et al., 2020). Global kiwifruit production totals approximately 3.5 million tons, with Italy ranking as the world's third-largest producer, following China and New Zealand (FAOSTAT). In 2022, Italy produced 523,120 tons of kiwifruit, of which 250,000 tons were exported (Balestra and Costa, 2020). Since 2012, a condition known as kiwifruit vine decline syndrome (KVDS) has affected over 10% (almost 2,900 hectares) of Italian kiwifruit orchards, spanning regions in the north (Veneto, Piedmont, Friuli Venezia Giulia), central (Lazio, Emilia Romagna) and southern Italy (Calabria) (Sorrenti et al., 2019). However, it is estimated that over 25% of Italian kiwifruit orchards are affected (Savian et al., 2020). KVDS symptoms lead to severe root decay and irreversible wilting and plants usually die within a few weeks from the appearance of the first symptoms in the canopy. Aboveground symptoms include leaf curl, necrosis, and twig wilting, which appear long after impairment of the root system. Roots are characterized by central stele break off, cortex detachment, rotting areas and disappearance of finer feeding roots (Donati et al., 2020). The main pathogens associated with disease development, based on isolation techniques, are mainly soilborne oomycetes belonging to the genera *Phytopythium* and *Phytophthora*, although, they cannot be considered as the exclusive causal factors (Tacconi et al., 2015; Bardi et al., 2020). Both oomycete genera are characterized by a lifestyle that requires water for zoospore spread and show an optimal growth at high temperature (Brasier et al., 2022; Prencipe et al., 2023), therefore waterlogging and climate change are considered as co-factors for KVDS development. Kiwifruit

has been reported to be sensitive to both root anoxia caused by flooding events and high transpiration demand together with high soil temperatures (Save and Serrano, 1986; Smith et al., 1989). In 2020, Donati et al. isolated bacterial, fungal and oomycete communities from roots with different KVDS incidence located in Northeastern Italy, followed by inoculation of fungal and oomycete isolates on potted kiwi vines. In the same paper the inoculation of *Phytopythium* spp., *Phytophthora* spp., *Desarmillaria tabescens* and oomycete reference strains was performed together with waterlogging of pots. The results showed the reproduction of symptoms by all the isolates, regardless the irrigation strategy, suggesting a crucial role of multiple oomycete genera in the disease. In another recent study by Savian et al. (2020), the relationship between waterlogging, soil-borne pathogens and KVDS was investigated. In this study, historical rainfall data of two locations in Northeastern Italy was analyzed and greenhouse trials designed to evaluate the contribution of waterlogging to KVDS onset were conducted. Inoculation of kiwi plantlets with naturally infected in combination with waterlogging permitted symptom reproduction. Pathogen isolation revealed a high occurrence of the species: *Phytopythium vexans*, *Phytopythium chamaehyphon* and *Fusarium solani* (Savian et al., 2020). *P. vexans* was also previously described as being pathogenic towards kiwifruit roots in Turkey (Polat et al. 2017). In Italy, inoculation of *P. vexans* isolates combined with waterlogging was performed in greenhouse trials by Prencipe et al. (2020) to confirm pathogenicity. Similarly, *P. chamaehyphon* pathogenicity was confirmed by Savian et al. (2021) on kiwifruit. In addition, oomycetes were isolated from KVDS symptomatic plants in the northwestern area of Italy in 2016, 2017 and 2019 (Prencipe et al. 2023). Oomycetes belonging to the species *P. vexans*, *P. chamaehyphon*, *Phytopythium helicoides* and *Phytopythium litorale* were recovered at the highest rates. In the same study, their pathogenicity in kiwifruit was verified (and Koch postulates satisfied), by symptom reproduction with waterlogging treatment.

Phytopythium spp. have also been reported more broadly as root rot causal agents on kiwifruit in different countries, like China (Wang et al., 2015), Turkey (Türkkan et al., 2022) and Japan (Shimizu et al., 2005). *Phytophthora* has also been isolated and identified as a kiwi root rot pathogen with symptoms similar to KVDS in France (Baudry et al., 1991) and Turkey (Akilli et al., 2011; Kurbetli and Ozan, 2013).

In recent years, more in-depth studies using Next Generation Sequencing (NGS) techniques have been performed with the objective of defining the whole biotic community associated with the syndrome. In Central Italy biotic components of KVDS were characterized by Manici et al. (2022)

combining isolation techniques for fungal endophytes with qPCR quantification (of fungal and bacterial DNA) and NGS techniques for soil bacterial composition analysis. The study evidenced a reduction of bacterial communities in diseased samples as contributing to reduced plant growth. In Northeastern Italy, Savian et al. (2022) used a metabarcoding approach to describe oomycete and fungal communities in root endosphere and rhizosphere of healthy vs. diseased samples, evidencing the role of *Phytophthora sojae* and *Phytopythium* spp. in KVDS.

Microbial populations (namely fungi, bacteria, oomycetes, protists, archaea, and viruses) are deeply influenced by geographic location, by environmental properties (e.g., soil composition, plant host species/ genotypes) and agronomic practices (Fitzpatrick et al., 2020). Moreover, woody plants and their associated microbiota, are particularly susceptible to global change factors (Bettenfeld et al., 2020). Climate change can impact soil properties and generate environmental fluctuation which can affect the bulk soil microbiome, the main source/pool of potential plant colonizing microorganisms. Microorganisms in turn, can exert different responses to adverse conditions depending on lifestyle, infection strategy and sensitivity to abiotic factors (Zandalinas et al., 2021a). In comparison to bulk soil, the rhizosphere (the first plant-influenced habitat) is actively shaped by plant factors including root morphology, immune response, physiological changes (e.g. adaptation responses to climate change) and root exudate production (Trivedi et al., 2022). In the root endosphere, the enrichment of microbial groups is influenced by all these factors and by the filtration effect from the plant immune system (Singh et al., 2020).

As previously mentioned, microbial populations are subjected to change, especially in conditions of long-term abiotic stress imposed by climate change. In particular, the expansion of niches for novel pathogens is favored by rising temperatures (Bebber et al., 2013; Cavicchioli et al., 2019). In this framework, plants exert less control over the associated microbiome, increasing the possibility for dysbiosis, leading to higher disease susceptibility of the plant and the inability to balance host associated microbiome composition when external stressors are present. At the same time in the interaction between the plant and its microbiome, community assembly and interactions may vary, determining stress resilience and resistance (Trivedi et al., 2022). The Anna Karenina Principe (AKP) proposes that the microbiome associated with dysbiotic communities is subjected to an increase in stochastic assembly processes leading to more variability compared to healthy ones (Arnault et al., 2023).

The objective of the present work was to characterize the entire community associated to KVDS, considering bacteria, fungi and oomycetes. The biotic component was characterized in three different belowground compartments (soil, rhizosphere and roots) of kiwifruit orchards located in Northwest Italy. Besides characterizing the communities, secondary aims were to determine the associations between taxa and to evaluate the possible involvement of a dysbiosis process in community assembly. To address the contribution of the abiotic component in the syndrome, association networks between physicochemical characteristics of soils and rhizosphere taxa were assessed.

2. Materials and methods

2.1 Orchard location, sampling, and DNA extraction

Eight sites in four separate locations of Cuneo province, north-west Italy, were selected to sample three different matrices (soil, rhizosphere, and root) both in diseased and healthy orchards (**Figure 1; Supplementary Table 1**). From each sampling site, random plants were selected, and soil was collected at a depth of 30 cm after removing the topsoil. At the same time, roots and the attached soil were collected from different parts of the radical apparatus. Collected roots were symptomatic but without excessive necrosis. Each sample of soil, rhizosphere and root was collected in five biological replicates and treated independently. Roots were further processed in the laboratory to detach the soil attached to the root surface, following a previously reported protocol (Simmons et al., 2018) with minor modifications.

Prior to DNA extraction, washed roots were crushed using mortar and pestle with liquid nitrogen. Further breakage of the roots was achieved with metal beads and TissueLyser II (Qiagen, Hilden, Germany). Total DNA extraction from all the belowground matrices was performed with the DNeasy Powersoil kit (Qiagen, Hilden, Germany) following the manufacturer instructions. The extracted DNA was quantified, and quality checked with the Nanodrop 2000 spectrophotometer (ThermoFisher, Waltham, USA) and stored at -20°C.

2.2 Metabarcoding sequencing

Metabarcoding sequencing was performed by IGATech (Udine, Italy) with different primer sets for fungi, bacteria, and oomycetes. For bacteria, primers 341f (Klindworth et al., 2013) and 806r (Apprill et al., 2015) were selected. For both fungi and oomycetes, the reverse primer ITS4ngs

(Tedersoo et al., 2014) was used, while the selected forward primers were fITS7 (Ihrmark et al., 2012) and ITS3oo (Riit et al., 2016, 2018), respectively. Libraries were prepared by following the Illumina 16S Metagenomic Sequencing Library Preparation protocol (Illumina, 2013) in two amplification steps: 1) an initial PCR amplification using locus-specific PCR primers and 2) a subsequent amplification that integrates relevant flow-cell binding domains and unique indices (NexteraXT Index Kit, FC-131-1001/FC-131-1002). Peptide nucleic acid (PNA) clamping was applied during the first amplification step to block amplification of host chloroplast and mitochondrial 16S sequences following the manufacturer's protocol (PNA Bio Inc, Newbury Park, CA). For the locus specific amplification of 16S and ITS libraries 35 and 29 cycles were applied in the first PCR reaction, respectively. Libraries were sequenced on NovaSeq6000 instruments (Illumina, San Diego, CA) using 250-bp paired-end mode. During the analysis, 15 samples associated with oomycetes did not result in a viable sequencing library and thus had to be dropped. Therefore, the total number of samples was 120 for fungi and bacteria and 105 for oomycetes.

2.3 Bioinformatics for taxonomic assignment and alpha and beta-diversity

Sequence analysis for oomycetes, fungi and bacteria was performed separately using the QIIME2 suite (Bolyen et al., 2019), version 2021.2. Primer contamination removal was carried out using Cutadapt (Martin 2011; via q2-cutadapt), while read merging, ASV calling, and chimera removal were done using DADA2 (Callahan et al., 2016; via q2-dada2) with default settings. In this step, based on base quality values distribution, no 5’ trimming was performed for either forward or reverse reads. Taxonomic assignment of ASVs was achieved using the q2-feature-classifier (Bokulich et al., 2018) with a naive Bayes predictor. For fungi and oomycetes, the predictor was trained on the UNITE database, version 8.3-eukaryotes-global (Abarenkov et al., 2021), which was integrated with ITS sequences taken from the National Center for Biotechnology Information nucleotide database (NCBI; Available from: https://www.ncbi.nlm.nih.gov/nucleotide/). For bacteria, the predictor was trained on the SILVA database, version 138 (Glöckner et al., 2017), elaborated with the RESCRIPt plugin (Bokulich et al., 2023), after sequences were trimmed down to the V3V4 regions (via q2-features-classifier). In all three analyses, a ASV filtering step was performed: first matrix contaminations were removed (via q2-taxa), then ASVs with a frequency less than 0.0001 % of total ASVs were removed, as well as ASVs which appeared in less than 5 biological replications (for fungi and bacteria) or 3 biological replications (for oomycetes) (via q2-

feature-table). Normalization for alpha and beta diversity was carried out with SRS (Heidrich et al., 2021) (via q2- srs), with a depth of 81,336 (fungi), 35,900 (bacteria) and 600 (oomycetes) ASVs. Shannon Index (Shannon and Weaver, 1949), number of observed features (DeSantis et al., 2006) and Pielou evenness (Pielou, 1966) were chosen as alpha diversity metrics and calculated with the default q2-diversity plugin, while Robust Aitchison distance was selected as beta diversity metric and calculated with DEICODE (Martino et al., 2019; via q2-deicode).

Statistical analyses of alpha diversity results were performed using the stats package R implementation of the non-parametric Kruskal-Wallis test (Kruskal and Wallis, 2012). Post-hoc analysis for statistically significant results was carried out with the Dunn post-hoc test as implemented in the FSA R package (Ogle et al., 2023), with Benjamini-Hochberg false discovery rate (FDR) correction (Benjamini and Hochberg, 1995). Beta diversity results were used to carry out a Principal Coordinates Analysis (PCoA) with DEICODE (with auto-rpca method) and a Permutational Analysis of Variance (PERMANOVA) test using the Adonis plugin (Anderson, 2001) with 999 permutations. Differences in variance were assessed with the permadisp/betadisp test (Anderson, 2006), also with 999 permutations. Results of the PCoA were used to generate 2D plots by using packages ggplot2 (Wickham, 2016), ggpubr (Kassambara, 2023), rcompanion (Mangiafico, 2023) and dplyr (Wickham et al., 2023).

2.4 Microbial community composition, association networks and evaluation of ecological processes

Visualization of microbial community composition in the matrices was done by collapsing ASVs absolute frequencies at the genus level and by converting them to relative frequencies. Differential abundance of taxa between different health statuses for each matrix was measured with ALDEx2 (Fernandes et al., 2013; Fernandes et al., 2014; Gloor et al., 2016), via the q2-aldex2 plugin. For visualization, statistically significant comparisons were selected where relative abundance was at least 1% in either thesis or change was at least two-fold.

Association networks were calculated using the CoNet plugin (Faust and Raes, 2016) in combination with Cytoscape version 3.9.1 (Shannon et al., 2003) and visualized with Gephi (Bastian et al., 2009). A correlation cutoff of +/- 0.60 was selected to filter collinear variables.

The impact of stochastic and deterministic processes on microbiota composition was investigated by calculating the βNTI (beta Nearest Taxon Index) and the modified Raup-Crick metric based on

Bray-Curtis dissimilarity, as described in a previous study (Stegen et al., 2013). For the Raup-Crick metric, an optimized script was employed (Richter-Heitmann et al., 2020). To calculate these metrics, representative sequences from each taxon were aligned with MAFFT (Katoh and Standley, 2013) and a phylogenetic tree was calculated with FastTree (Price et al., 2010). These results were plotted with packages ggplot2 and ggpubr.

2.5 Physicochemical analysis of soils

Soil samples for physicochemical analysis were collected from the same sites used for metabarcoding analysis. This was done by collecting 0.5 kg of soil from between 20 and 40 cm deep. For each site, three diagonal sampling points were pooled and sent to Laboratorio Agrochimico Regionale (LAR; https://servizi.regione.piemonte.it/catalogo/analisi-dei-terreni-altre-analisi-chimiche-agrichim) of Piedmont Region (Torino, Italy) for analysis. The considered parameters were percentages of clay, loam, limestone, soil organic substance and sand for soil composition. Soil water pH, organic carbon, total nitrogen content in soil were measured. Mineral exchanges and assimilations (ppm) were also calculated. For explorative visualization of the physicochemical data with dimensionality reduction, a non-metric multidimensional scaling (NMDS) was performed with the metaMDS function of the vegan package (Oksanen et al., 2020), with bray-curtis as metric.

Physicochemical variables of considered soils were included as meta variables for interactions between biotic and abiotic factors in the association networks, previously described.

2.6 qPCR quantification of *P. vexans* and oomycete isolation

Quantification of the target species *P. vexans* to confirm sequencing results was performed in three biological replicates for each sample considered. The quantification was performed by using *P. vexans* phylotype-specific primers and a qPCR protocol from Bent et al. (2009). Standard deviation for the sample quantification was calculated based on the three technical qPCR replicates. Culture-based isolation of oomycetes from roots of diseased orchards was performed by using a semiselective substrate. Macro and micromorphological analyses were performed on the isolates. In addition, molecular identification was performed, as described by Prencipe et al. (2023).

3. Results

3.1 Metabarcoding sequencing

Overall, sequencing of 120 samples for fungi and bacteria and 105 samples for oomycetes resulted in 58,603,041(fungi), 41,229,343 (bacteria) and 5,205,191 (oomycetes) sequences associated with 20,306, 150,349 and 3,414 features, respectively. Subsequent filtering of contaminants and very low abundance ASVs resulted in 50,916,370 (fungi), 20,992,728 (bacteria) and 2,223,433 (oomycetes) sequences associated with 893, 1,711 and 190 features, respectively. On average, each sample represented 424,303, 174,939 and 21,175 sequences, respectively. Sequences were deposited in the European Nucleotide Archive (ENA; https://www.ebi.ac.uk/ena/browser/) database under project accession PRJEB70619.

3.2 Alpha and beta diversity

Alpha (**Supplementary Table 2**) and beta diversity indexes were calculated for each matrix for bacteria, fungi, and oomycetes.

For bacterial communities, differences in overall diversity between diseased and healthy matrices, based on the Shannon Index, were statistically significant for rhizosphere and soil samples, whereas no significant differences were found in roots (**Figure 2a**). In both cases, healthy samples presented lower diversity compared to diseased samples. In addition, both rhizosphere and soil samples, regardless of health status, presented higher diversity values compared to their root equivalents (**Figure 2a**). Differences in the number of observed features were significant only between healthy and diseased rhizosphere samples, but not in soil and root samples (**Figure 2b**). Samples associated with healthy plants did not show statistically significant differences between matrices. However, rhizosphere samples associated with diseased plants contained a significantly higher number of observed features compared to both root and soil samples (**Figure 2b**). Finally, evenness of bacterial ASV (**Figure 2c**) was tested with the Pielou index, which returned no significant difference between health status for roots, soil, and rhizosphere, although statistically significant differences were identified between root samples and non-root samples.

Unlike bacterial communities, the Shannon Index for fungal communities was not significantly different between health status for all considered matrices. However similar to bacteria, both rhizosphere and soil samples had a higher diversity of fungi compared to root samples, regardless

of health status (**Figure 3a**). The number of observed features (**Figure 3b**) in the fungal community of healthy plants was significantly lower than that of diseased plants in rhizosphere and soil but not in root samples. The number of observed features (**Figure 3b**) in the fungal communities of healthy plants was significantly lower than that of diseased plants in rhizosphere and soil but not in root samples. A significant reduction in the number of observed features was observed in healthy root tissue relative to healthy soil, but not rhizosphere. The number of observed features was also significantly lower in diseased root relative to both diseased soil and rhizosphere samples. For Pielou evenness (**Figure 3c**), the only statistically significant difference was found between healthy and diseased root samples, with the former having higher values compared to the latter (q value= 0.002).

For oomycetes, no statistically significant differences were identified for either the Shannon Index or the Pielou Evenness (**Figure 4a, c**) between matrices and health status. However, like bacteria and fungi, the oomycete communities of diseased soil and rhizosphere were found to contain significantly more observed features than healthy rhizosphere (**Figure 4b**). In addition, diseased root communities were not significantly different, in terms of observed features, compared to rhizosphere and soil regardless of health status (**Figure 4b**).

The effect of sampling site on microbial community composition along with disease status, matrix, and the interaction between these factors, was measured by means of a permutational analysis of variance (PERMANOVA) on Robust Aitchison distances (**Table 1**).

Obtained values of R^2 indicated that the major effect on bacterial community composition was exerted by matrix, which accounted for 87% of the variance (Pr=0.001; **Table 1**). Pairwise comparisons with permanova and permdisp between matrices (**Table 2**) identified significant differences in bacterial community composition between all matrix combinations; significant differences in dispersion were also identified. The effect of matrix on bacterial community composition was mirrored in the PCoA plot (**Figure 5a**), in which roots formed a distinct cluster from soil and rhizosphere.

By comparison, the effect of site explained the largest amount of variance in fungal community composition 68% (Pr=0.001). Therefore, relative to bacterial communities, fungal communities were highly location specific with matrix having less of an effect (9%; Pr=0.001). Pairwise comparisons between matrices identified statistically significant differences between root samples and rhizosphere/soil samples, with no statistically significant difference in dispersion. On the other

hand, pairwise comparisons between sites identified statistically significant differences in fungal community composition between all sites (Fossano, Manta, Scarnafigi, Verzuolo), except for Manta vs. Scarnafigi. In addition, permdisp identified statistically significant differences in dispersion between sites. Fungal communities associated with Manta had comparable dispersion with those of Fossano and Scarnafigi (**Table 2**). This location effect on fungi was mirrored in the PCoA plot (**Figure 5b**), in which points associated with Verzuolo and Fossano formed distinct clusters, while points associated with Manta and Scarnafigi did not form distinct clusters.

Significant dissimilarities in oomycete communities were largely related to the matrix (24%; Pr=0.001), site (13%; Pr=0.001) and disease status (9%; Pr=0.001). The statistical significance of the effect of disease status on oomycetes community structure was confirmed by pairwise comparison, although a dispersion effect could not be ruled out. Additionally, pairwise comparisons indicated statistically significant differences in oomycete community composition between all matrices, with no significant differences in dispersion. Regarding site, pairwise permanova indicated a statistically significant differences in oomycete community composition between Verzuolo and all other locations, although a statistically significant difference in dispersion was found between Scarnafigi and all other geographical locations. The presence of multiple factors with relatively low effect size was mirrored by the PCoA plot (**Figure 5c**), in which no clear clustering patterns were identified.

3.3 Bacterial community composition

Bacterial communities across the three matrices – soil, rhizosphere, and root (**Figure 6a, 6b, 6c**) – did not show any dominant genera but contained a diversity of taxa, even when grouped by geographic location.

In terms of relative abundance (**Figure 6a**), *Bacillus* was the most abundant genus in both healthy (6.85 %) and diseased (4.08%) orchard soil. In both healthy and diseased soil, all bacterial genera were similar in composition and abundance, and included *Methyloligellaceae* (2-3%), *Gaiella* (~2%), *Streptomyces* (~1%) and *Acidibacter* (~1%).

As in soil, in the rhizosphere (**Figure 6b**), *Bacillus* was the most abundant bacterial genera. However, its relative abundance was roughly double in healthy plants (10.00 %) relative to diseased plants (5.32%). No other significant differences in bacterial relative abundance were identified between healthy and diseased plants. Bacterial genera identified also included

Xanthobacteriaceae (~3%), *Vicinamibacteriales* (~2%), *Vicinamibacteraceae* (~1-2%), *Micrococcaceae* (~1-2%), *Gemmata* (~1-2%), *Streptomyces* (~1-2*%), Gemmatimonadaceae* (~1-2%), *Pirellulaceae* (~1%) and *Methyloligellaceae* (~1-2%). In healthy root tissues (**Figure 6c**) the most abundant genus was *Acidovorax* (2.87%) followed by *Bacillus* (2.25%), *Allorhizobium* (1.91%), *Acidibacter* (1.74%), *Dongia* (1.43%). Other genera including *Niastella*, *Ohtaekwangia*, *Verrucomicrobium*, *Neorhizobium* and SH-PL14 represented approximately 2% of the root community composition. In KVDS-affected roots (**Figure 6c**) the most abundant genera were *Niastella* (5.36%) and *Allorhizobium* (5.19%), followed by *Verrucomicrobium* (3.38%), *Ohtaekwangia* (2.12%), *Neorhizobium* (1.70%), SH-PL14 (1.22%) while the remaining 2.29% of the root bacterial community was made up by *Acidibacter*, *Acidovorax*, *Bacillus* and *Dongia*.

3.4 Fungal community composition

Like bacteria, fungal communities also contained a wide diversity of genera in the three matrices (**Figure 6a, 6b, 6c**).

The most abundant fungal genera in soil (**Figure 6a**) were *Gibelluliopsis* in both healthy (5.19%) and diseased orchards (3.05%), followed by *Mortierella* spp. both in healthy (2.81%) and diseased (2.17%) orchards. Other major genera composing the fungal community in diseased soil were: *Dactylonectria* (1.55%), *Astrosphaeriella* (1.54%), *Pleosporales* (1.02%) followed by the less abundant *Preussia* (0.88%), *Plectosphaerellaceae* (0.82%), *Talaromyces* (0.75%) and *Cordomyces* (0.58%). The fungal community composition was similar in healthy soils, with minor differences in relative abundance: *Plectosphaerellaceae* (2.80%), *Talaromyces* (1.69%), *Preussia* (1.66%), *Pleosporales* (1.37%), *Chordomyces* (1.10%), *Dactylonectria* (0.40%) and *Astrosphaeriella* (0.32%).

In rhizosphere (**Figure 6b**) the predominant genus was *Fusarium* (9.31%) in diseased sites followed by *Linnemania* (3.85%), *Dactylonectria* (3.02%), *Gibellulopsis* (2.31%), *Tetracladium* (1.34%), *Podila* (1.14%), *Brunneochlamydosporium* (1.13%), *Trichoderma* (1.04%), *Exophiala* (0.85%) and *Talaromyces* (0.57%). As in soil, differences between fungal genera in healthy vs. diseased rhizosphere were small (**Figure 6b**).

In roots however (**Figure 6c**), *Dactylonectria* was highly present in KVDS affected tissues (16.89%), followed by unknown Branch06 (2.70%), *Sordariomycetes* (2.62%), *Sebacinales* (1.97%), *Oculimacula* (1.94%), *Veronaea* (1.68%), *Brunneochlamydosporium* (1.65%), *Oliveonia*

(1.61%) and *Tetracladium* (1.52%). In healthy tissues *Dactylonectria* was less predominant (6.31%) while *Tetracladium* (7.96%) was the most abundant fungal genera followed by unknown Branch06 (6.86%). Less abundant genera included *Sordariomycetes* (1.05%) and *Oliveonia* (0.58%) while *Sebacinales*, *Oculimacula*, *Veronaea* and *Brunneochlamydosporium* accounted for less than 1%.

3.5 Oomycete community composition

Among oomycetes detected in soil, a significant difference in the relative abundance of *Phytopythium* spp. was observed between healthy and diseased sites. In samples collected from diseased orchards, the abundance of *Phytopythium* was as high as 30.94%. In healthy soil, relative abundance was 3.09% (**Figure 7**).

The same trend was observed in the rhizosphere where *Phytopythium* relative abundance was 56.97% and 14.27% of the total oomycete community at diseased sites and in healthy sites, respectively (**Figure 7**).

In comparison, *Phytopythium* relative abundance reached 70.92% in diseased roots and 15.90% in healthy roots (**Figure 7**). *Pythium* spp., another KVDS-associated genus. was also detected in the roots of healthy (1.57%) and affected (16.10%) plants (**Figure 6c**). In soil (**Figure 6a**) and rhizosphere (**Figure 6b**) *Pythium* spp. did not reach a frequency above 1% and were therefore not listed in **Figure 6**.

3.6 Association networks among microbial taxa

Cross-kingdom co-occurrence networks based on relative abundance profiles among fungi, bacteria and oomycetes were investigated with CoNet (**Supplementary Figure 1**). In all networks, bacteria represented the most abundant kingdom, followed by fungi (**Table 3**). Other taxa were far less abundant, with oomycetes having a relatively higher presence in the rhizosphere compared to root and soil. Comparison between healthy and diseased plants (**Table 3**) indicated a reduction of co-presence connections (indicating positive associations among taxa) and an increase in co-exclusion connections (indicating negative associations among taxa) in diseased rhizosphere and soil, while the opposite was true for root samples. It is also notable that in diseased (relative to healthy) root tissue, there was an increase in the relative abundance of oomycete nodes, average number of neighbors, network heterogeneity, network centralization and the number of connected

components. Taken together, these results suggest that the microbial endophytic network becomes increasingly more unequal due to the disease condition (**Table 3**). In soil, the decrease of connected components was associated with a reduction in both the number of nodes and edges, while in the rhizosphere this was associated with an increase in both metrics. Average number of neighbors was higher for healthy samples compared to diseased samples in root and soil and slightly lower in rhizosphere, while network radius was higher for healthy samples in soil, lower in rhizosphere and did not change in roots.

For *Phytopythium*, statistically significant association were identified in soil and rhizosphere, but not in root (**Figure 8**). In the rhizosphere (**Figure 8a**), *P. vexans* ASV1 was found to be negatively correlated with ASVs belonging to *Pochonia chlamydosporia* and an unknown *Glomeromycota*; *P. vexans* ASV2 was also negatively correlated with ASVs belonging to the genera *Minimelanolocus* and *Cyphellophora*, as well as unknown organisms in the *Chaetothyriales* order and Oomycota class, but also with the genus *Minimelanolocus*. Finally, *P. vexans* ASV3 was negatively correlated with an ASV of species *Kernia columnaris*, ASVs belonging to the genera *Minimelanolocus* and *Cyphellophora*, as well as unknown organisms in the *Didymellaceae* family and TM7a phylum, and with the genus *Minimelanolocus*. In addition, both species of *P. vexans*, as well as an additional ASV belonging to the genus *Phytopythium* were negatively correlated with an ASV associated with unknown *Didymellaceae*. In soil (**Figure 8b**), *Phytopythium* (as genus, as the species *P. vexans* and as *P. vexans* ASV3) was negatively correlated with the healthy status.

3.7 Evaluation of rhizosphere ecological processes

The impact of stochastic and deterministic processes on microbial composition was extrapolated via comparative analysis of beta Nearest Taxon Index (bNTI) values across different samples. In particular, bNTI values higher than 2 or lower than -2 can be considered the result of prevailing deterministic processes (i.e. selection), while values between -2 and 2 are associated with a predominance of stochastic processes (Stegen et al., 2013). Fungal communities had a lower average percentage of turnover explained by selection (1.84%) than bacteria (12.63%) and oomycetes (29.47%). When the health status of these communities was considered, differences emerged between taxa. For fungal and oomycetes communities, selection had a greater impact in the turnover of diseased communities (2.62% and 43.16%, respectively) than on healthy communities (1.05% and 17.54%, respectively). In contrast, for bacterial communities, there was

a higher impact of selection on the turnover of healthy communities (16.31%) than diseased communities (8.94%). Despite these differences among taxa, stochastic processes represented the main driver of community turnover for all taxa, with an impact of 98.16%, 87.37% and 70.53% for fungal, bacterial and oomycete communities, respectively. Stochastic processes can be additionally classified according to Bray-Curtis derived Raup-Crick (RCbray) values. RCbray < -0.95 is considered the result of homogenizing dispersal (a combination of drift and high dispersal), RCbray > 0.95 is considered the result of dispersal limitation (a combination of drift and low dispersal) and -0.95 < RCbray < 0.95 is considered the result of ecological drift (drift acting alone; Stegen et al., 2013). For fungi and bacteria (**Supplementary Figures 2 and 3**) dispersal limitation was the main stochastic process both in healthy communities (80.00% and 78.61%, respectively) and diseased communities (80.92% and 76.10%, respectively). For healthy fungal communities, ecological drift was higher (12.23%) than homogenizing dispersal (7.44%), while in diseased communities the opposite (8.10% versus 11.89%, respectively) was predicted. For bacterial communities, homogenizing dispersal was similarly high in healthy communities (16.76%) and diseased communities (16.89%), while ecological drift was marginal for both kinds of communities (2.31% and 6.92%, respectively). For oomycetes (**Supplementary Figure 4**), no dispersal limitation was observed, and homogenizing dispersal was measured only in diseased communities (6.48%). In contrast to both fungi and bacteria, oomycetes communities were predicted to have high values of ecological drift in both diseased communities (93.52%) and healthy communities (100.00%).

3.8 Physicochemical characteristics of soils and correlation with biotic components

Chemical-physical analysis of the sampled soils considered different variables as soil composition in terms of physical properties and presence/exchange of chemical elements (**Supplementary Table 3**). NMDS analysis of this data indicated that healthy and diseased soils did not cluster separately (**Supplementary Figure 5**). This result suggests an absence of chemical/physical factors strictly associated with disease status and/or microbiome assembly. Soil physicochemical properties have been reported as important drivers of soil microbial communities which represent the main reservoir for the rhizosphere microbiome (Plassart et al., 2019). Therefore, this data was integrated with the rhizosphere network (**Figure 9**).

Associations with microbial taxa were considered for assimilated copper (ppm), assimilated manganese (ppm), assimilated phosphorous (ppm), total sand (%), total limestone (%), C/N ratio, exchanged magnesium (ppm), exchanged potassium (ppm) and water pH. Although these parameters did not show any direct interaction with the main oomycete *Phytopythium* spp., third (or higher) degree associations with the genera interacting with *Phytopythium* were identified in the rhizosphere (**Figure 9**). Health status was also included as a parameter and resulted in third degree associations with exchanged potassium and assimilated manganese. Assimilated manganese showed a positive association with *Ramicandelaber longisporus* which was also negatively associated with the healthy status of the plant that is, in turn, negatively linked to *P. vexans* (ASV1). Exchanged potassium was negatively associated with the genus *Fusidium* and *Fusidium* (ASV1), which were negatively correlated with the healthy status of the plant. At higher degree of association, compared to *Phytopythium* or the healthy status, exchanged potassium is positively correlated with assimilated phosphorus while assimilated manganese is negatively associated with total limestone. Exchanged magnesium was positively associated with an unknown *Pirellula* ASV1 which was negatively associated with *P. vexans* ASV3. The C/N ratio was negatively correlated with an unknown *Minimelanolocus* ASV1 which was negatively correlated with *P. vexans* ASV3. Other parameters including assimilated copper and total sand were associated (at higher degrees) of neighborhood with both the healthy status of the plant and *P. vexans* ASVs, making their effects difficult to predict.

3.9 Quantification of *P. vexans* across matrices via qPCR and isolation from plant roots

Relative quantification of the oomycete *P. vexans* in soil, rhizosphere and roots was obtained by generating a standard curve (R^2=0.994, E=95%) from seven ten-fold dilutions (ranging from 20 fg to 20 ng) of *P. vexans* genomic DNA (strain CBS 119.80). The quantification of the target was calculated using linear regression with the equation associated with the curve y=-3.4578x + 20.465, the results are listed in **Supplementary Table 4**. Isolates of *P. vexans* were constantly reisolated from diseased plant roots (sampled from diseased orchards) and identified by using macro and micromorphological analysis and sequencing, as described in Prencipe et al. (2023). Five representative isolates were deposited in the Turin University Culture Collection (TUCC; **Supplementary Table 5**).

4. Discussion

So far, most of the research on KVDS has been focused on defining the causal agents of the disease using traditional and omic-based techniques. This body of research has revealed the involvement of multiple species of oomycetes belonging to the genera *Phytopythium* and *Phytophthora* in the onset of the syndrome in different producing areas of Italy. In this study, we not only characterized the bacterial, fungal and oomycete communities present in eight different orchard locations in Cuneo province (four healthy and four affected sites), but we also explored microbial community dynamics across three different belowground compartments. In addition, cross-kingdom microbial networks were constructed to explore potential interactions between taxa and address the possibility of dysbiosis. Potential associations between microbial taxa and soil associated abiotic factors were also explored. The finding that *Phytopythium* spp. were present both in healthy and diseased orchards suggests that the onset of KVDS is likely related to a shift in the larger microbial community rather than being solely due to these oomycetes. In this study, *Phytophthora* spp. were not identified as being abundant in any sample type (< 1% relative abundance). When all locations were considered, oomycetes were strongly correlated with disease status compared to fungi and bacteria. More specifically, relative abundances of *Phytopythium* spp. were significantly higher in all diseased matrices compared to healthy ones. However, no significant differences in oomycetes alpha diversity metrics were identified between matrices, except that healthy rhizosphere had a reduced number of observed features relative to diseased rhizosphere. This trend was also observed for fungal and bacterial communities and may suggest a dramatic shift in the way microbial communities interact with each other and with the host (Somera and Mazzola, 2022).

Previous studies conducted in Northeast Italy by Savian et al. (2022) characterized KVDS associated communities of kiwi root endosphere and rhizosphere using a metabarcoding approach. Compared to our study, this analysis only considered one healthy site and three sampling points from a single diseased orchard. Savian et al. (2022) identified *P. vexans* in both diseased and healthy root endosphere and rhizosphere. In addition, *Ph. sojae* was related to KVDS onset, though its pathogenicity on *Actinidia deliciosa* has not yet been verified, by reproduction of KVDS symptoms after inoculation. The involvement of *Phytopythium* genus in KVDS was also reported in a previous work by Savian et al. (2020) in which isolation from roots was performed, resulting in a high occurrence of Pythiaceae. Most notably, *P. chamaehyphon* and *P. vexans* were reported

to be associated with the syndrome. In another study performed on root tissues of kiwi vines sampled in northern Italy, the oomycete genera *Phytophthora* and *Phytopythium* were isolated both from both health statuses, with a higher percentage in diseased plants (Donati et al., 2020). The presence of the same oomycete genera (*Phytophthora* spp., *Phytopythium* spp. and *Pythium* spp.) was also observed in both diseased and healthy soybean rhizospheres (Noel et al., 2020). This finding suggests that a quantitative imbalance of species may contribute to symptoms development rather than simply the presence or absence of highly pathogenic species.

Phytopythium spp. pathogenicity on kiwifruit and the ability to reproduce symptoms in controlled conditions has been verified by different authors. Prencipe et al. (2020) tested the pathogenicity of *P. vexans* on kiwifruit plantlets and reproduced KVDS symptoms fulfilling Koch postulates. Savian et al. (2021) verified the pathogenicity of another species, *P. chamaehyphon*, on *Actinidia deliciosa* cv. Hayward and observed the typical wilting symptoms with disease progression similar to field conditions. A previous study in Northwestern Italy, which included the orchards considered in this work, revealed a high occurrence of *Phytopythium* spp. isolated from root tissues of kiwi plants showing clear symptoms of KVDS (Prencipe et al., 2023). These findings complement the metabarcoding results of this study.

Analyses of fungal communities associated with KVDS, in healthy and diseased samples was also explored. Fungal alpha diversity did not show any statistically significant difference in Shannon Index comparing healthy and diseased matrices. However, root tissue diversity (in terms of observed features) was lower than that of soil and rhizosphere. This observed reduction is expected due to the numerous factors differentiating root communities from the surrounding compartments (Bulgarelli et al., 2013). This finding was observed also in previous studies conducted in forest ecosystems (Frey et al., 2021). In addition, fungal evenness was significantly lower only in diseased roots, as a combination of the presence of a prevalent pathogenic taxon and the effect of continuous cropping as previously observed in *Panax notoginseng* gardens (Tan et al., 2017).

In this study, *Fusarium* was the main fungal genus in the rhizosphere, regardless of disease status, whereas *Linnemania* and *Dactylonectria* characterized diseased samples. Although *Dactylonectria* was the main genus in affected roots, it was also present in healthy roots in lower abundance. These findings are consistent with Savian et al. (2022), who found a high abundance of Nectriaceae in both root tissue and rhizosphere regardless KVDS. Our findings on fungal community composition in kiwifruit orchard soils is consistent with previous works. *Dactylonectria* (or *Cylindrocarpon*-

like species) was isolated from kiwifruit orchard soils and already associated with kiwifruit cultivation (Tacconi et al., 2015; Manici et al., 2022). *Cylindrocarpon* spp. pathogenicity on kiwifruit was verified in a previous work, where symptoms of root rot were reproduced 60 days after inoculation (Erper et al., 2013). Savian et al. (2020) isolated Hypocreaceae, Ceratobasidiaceae and Nectriaceae from KVDS affected roots, with a high occurrence of *F. solani*. *Fusarium* spp. were recently reported as root rot agents on kiwifruit cultivated in poor drained soils in China (Song et al., 2023), but the ability to reproduce KVDS symptoms was not directly verified. In previous studies conducted on apple replant disease (ARD), which affects apple trees worldwide, both Nectriaceae and *Fusarium* spp. were reported as fungal components of the biotic complex associated to the disease (Franke-Whittle et al., 2015). *Fusarium* spp. were frequently isolated from apple orchards but resulted as non-pathogenic or weakly virulent when inoculated on plantlets, depending on the species (Tewoldemedhin et al., 2011a). Pathogenicity of *Cylindrocarpon* spp. on apple was tested in a previous work and virulence resulted strain dependent (Tewoldemedhin et al., 2010). Recent studies conducted on secondary metabolites produced by *Fusarium* spp. and Nectriaceae (*Cylindrocarpon*-like) showed the ability of these filamentous fungi, frequently isolated from multifactorial pathosystems, to significantly impact fruit tree growth by releasing phytotoxic compounds in soil (Manici et al., 2017; 2021). Based on these findings, the roles of *Fusarium* spp. and *Cylindrocarpon* spp. in KVDS need further investigation.

In regard to bacterial abundance, a wide variety of genera were identified but were not correlated with the health status of the orchard, instead they were matrix specific. Significant differences in bacterial community composition were identified in rhizosphere and soil between healthy and diseased orchards. In both soil and rhizosphere matrices, *Bacillus* was the most prevalent genera, but we were not able to identify species-level differences characterizing KVDS affected orchards. Bacterial alpha diversity metrics, in particular Shannon Index and number of observed features, were higher in diseased samples of soil and rhizosphere (but not root) compared to healthy ones. Previous results highlighted the presence of higher bacterial diversity in samples associated with different microhabitats of diseased plants (Hossain et al., 2021; Obieze et al., 2023). In addition, root samples had a lower richness (in terms of observed features) compared to both rhizosphere and soil, which also aligned with previous observations of bacterial populations in plants (Bulgarelli et al., 2012; Lundberg et al., 2012; Mukhtar et al., 2021; Yuan et al., 2022). Only a few

studies on the biotic factors involved in KVDS onset have considered bacterial microbiota. For example, Donati et al. (2020) characterized the bacterial communities in root samples from three kiwifruit orchards with different KVDS severity. In contrast to our findings, the bacterial communities of healthy roots were characterized by higher biodiversity than KVDS affected roots. In another study, soil bacterial composition of different kiwifruit orchards was characterized using NGS techniques (Manici et al., 2022). A shift toward nitrifying bacterial genera in soil samples from old orchards, showing typical decline symptoms, together with a strong reduction of the overall bacterial community was observed.

The results of beta diversity analyses from this study confirm the large impact of the belowground compartment in defining the composition of bacterial communities, while geographical location had by far the highest impact on fungal community composition. The impact of the microhabitat on bacterial communities was previously investigated and was shown to be the main parameter behind beta-diversity variation (Bulgarelli et al., 2015; Jin et al., 2017; Yuan et al., 2018). On the other hand, soil physico-chemistry and site-specific soil properties, rather than host effects, are reported to strongly drive fungal assemblages (Adamo et al., 2021).

For oomycetes, statistically significant differences in observed features between healthy and diseased sites were observed, except for root tissue, with a greater number of ASVs associated with diseased conditions. However, neither matrix nor sampling location explained a significant part of composition variance in the oomycete beta diversity. A study conducted in soybean rhizosphere, showed a similar increase in richness associated with the diseased condition and a statistically significant effect of the sampling site in community composition (Noel et al., 2020).

In ARD, no single biological organism was identified as a causal agent, leading to ambiguity in defining the determining factors. In the ARD pathosystem, species belonging to the genera *Rhizoctonia*, *Phytophthora*, *Cylindrocarpon*, *Pythium* and *Phytopythium* have been identified as causal agents (Tewoldemedhin et al., 2011b; Mazzola and Manici, 2012; Tilston et al., 2018), presenting many resemblances with KVDS. Another woody plant decline system that presents similarities with KVDS is peach replant disease, in which *P. vexans* dominates the diseased community (Yang et al., 2012). This oomycete species was frequently identified both by culture dependent and independent methods, correlating with disease development but also varied in abundance, which was attributed to interactions with abiotic factors. In addition, *F. solani* was also associated with the community of peach replant disease, similarly to our findings in kiwifruit.

Co-exclusion/co-occurrence networks can help to provide a better picture of the structure of microbial communities. In general, no difference was found in the taxon composition of nodes across different microhabitats and health statuses of orchards in this study. Bacteria were the most represented kingdom, followed by fungi. In diseased soil, the reduction of both the number of edges and nodes, together with a reduction in the number of connected components and average number of neighbors, suggests a decrease in interaction within the microbial network. In contrast, in the diseased rhizosphere an increase in edge and node number was observed, with a slight increase in average number of neighbors. This, combined with a decrease in connected components, may indicate a reduction in associations between pre-existing components and the appearance of new associations in diseased plants. Finally, in the network associated with diseased roots, an increase in the number of nodes and a decrease in the number of edges were observed relative to healthy roots. This was also associated with a decrease in the average number of neighbors and an increase in connected components. As in the rhizosphere, these data suggest a decrease in connections inside connected components, with the formation/appearance of new ones. A particular focus was given to associations between *Phytopythium* and other taxa, both in soil and rhizosphere. In the root network analysis, however, *Phytopythium* was not significantly correlated with other taxa. Among detected *Phytopythium* ASVs, *P. vexans* ASV3 was the only taxon with a direct negative correlation with healthy soil, suggesting a predominant role of *P. vexans* in KVDS. In the diseased rhizosphere, this ASV was negatively correlated with multiple ASVs of Chaetothyriales (black yeasts), which includes the families Herpotrichiellaceae and Cyphellophoraceae (Teixeira et al., 2017). The family Cyphellophoraceae includes both *Cyphellophora* and *Phialophora* genera. *Cyphellophora* is a fungal genus with several plant associated species and characterized by tolerance to high temperatures (Feng et al., 2014). The family Herpotrichiellaceae, is largely composed of saprobic species, and includes *Minimelanolocus,* a freshwater lignicolous fungal genus associated with decaying submerged wood debris (Shearer et al., 2007; Wang et al., 2019). The genus *Minimelanolocus* and *Minimelanolocus* ASV1 were both predicted to be co-exclusive with *P. vexans* ASV2 and ASV3. Similarly to the oomycetes associated with KVDS (Prencipe et al., 2023), this group of fungi is characterized by an optimal growth at high temperatures (Hyde et al., 2016). In addition, *Cyphellophora* ASV1 and *Chaetothyriales* ASV1 were co-exclusive with *P. vexans* ASV2. *P. vexans* ASV3 was also co-exclusive with the fungus *Kernia columnaris* ASV1 (homotypic

synonym: *Cephalotrichum columnare*), a soil saprobe with a worldwide distribution (Sandoval-Denis et al., 2016). *P. vexans* ASV2 was also negatively correlated with the ubiquitous bacterial phylum *Candidatus saccharibacteria* ASV1 (formerly Candidate Division TM7), which has been to be commonly found in soils, sediments, and wastewater (Ferrari et al., 2014). The observed co-exclusive associations of saprobes and saccharibacteria with *P. vexans* ASVs in the rhizosphere, may imply a cross-kingdom competition for plant derived carbon. Saccharibacteria can digest the plant cellular wall and ferment soil necromass and root exudates (Starr et al., 2018) therefore competing for nutrients. Negative correlations were also found between *P. vexans* ASV1 and beneficial organisms like Unknown *Glomeromycota* ASV1 and *Pochonia chlamydosporia* ASV1. *Glomeromycota* spp. are obligate biotrophs which have been reported to form arbuscular mycorrhizas (AMs) with kiwifruit 'Hayward' (Zhang et al., 2017). The nematophagous endophyte *Pochonia chlamydosporia* has been shown to promote root growth tomato and banana (Zavala-Gonzalez et al., 2015; Mingot-Ureta et al., 2020). Finally, *P. vexans,* was predicted to be co-exclusive with Didymellaceae ASV1. Didymellaceae is a fungal family rich in species inhabiting different ecosystems and has been reported to associate with a broad range of plant hosts including *Actinidia* spp.. Most species of Didymellaceae are plant pathogens causing leaf and stem lesions (Chen et al., 2017): *Phoma* and *Didymella* are reported as pathogenic on kiwifruit (Kwon et al., 2016; Zou et al., 2020).

To explore the role of dysbiosis in KVDS affected orchards, bNTI values were calculated. The results showed that fungal community assembly processes were mainly stochastic in nature for both healthy and diseased orchards. For abundant fungal taxa, defined as greater than or equal to 1% relative abundance, Jiao and Lu (2020) found stochastic assembly to be dominant in agricultural fields (maize and rice). Similarly, Xiong et al. (2021) observed a large effect of stochastic processes, matrix, and crop in shaping crop fungal communities of maize, wheat, and barley. These results show a common dynamic of fungal assemblies in agricultural soils.

By comparison, bacterial community assembly was largely driven by stochastic processes in diseased orchards relative to healthy ones. According to Arnault et al. (2023) this finding is consistent with an expected increase in stochastic processes in disease associated microbiota, leading to higher variability of communities under stress conditions.

For oomycetes however, deterministic processes had 2.5 times higher impact in diseased communities compared to healthy ones. At the same time, closer inspection of bNTI values (100%

bNTI < -2) associated with these processes indicated the presence of the Anti Anna Karenina Principle (Anti-AKP), in which dysbiosis is regulated mainly by deterministic processes due to modification of the host biology permitting the onset of a novel and potentially pathogenic community (Arnault et al., 2023). Taken together, these findings suggest that different components of the rhizosphere microbiome associated with KVDS undergo an evolution compatible with dysbiotic processes.

Physicochemical properties of soils were integrated in the network analysis to assess their role in changing the plant's ability to withstand abiotic stress while influencing the plant associated microbiome (Giovannetti et al., 2023). Similar to grapevine decline, where physicochemical parameters of soils alone could not explain the presence of decline in affected vineyards compared to asymptomatic ones (Darriaut et al., 2021), KVDS affected and healthy orchards did not cluster differently based on soil physicochemical properties measured in this study. In vineyards, further investigation revealed a dysbiosis phenomenon in microbial communities and dysregulation of ecosystem processes linking soil status to vine fitness (Darriaut et al., 2021).

However, different soil parameters, including assimilated and exchanged minerals showed indirect (third or higher degree) associations with genera interacting with *Phytopythium* in the rhizosphere. It is also worth noting that health status had a third-degree association with exchanged potassium and assimilated manganese, which are key elements for healthy kiwifruit that influence both fruit set and size (Clark and Smith, 1988) as well as root growth (Buwalda and Hutton, 1988).

5. Conclusions

KVDS is a multifactorial syndrome in which multiple biotic components and abiotic stress brought about by climate change act synergically. Bacteria, fungi, and oomycetes were considered together in three different matrices, representing a spatial gradient of the belowground system, sampled in the main production area of Northwestern Italy. Together, with the microbial populations associated with the syndrome, physicochemical parameters of soils were also investigated revealing their roles in shaping fungal communities. Further analysis of the association networks between soil physiochemical characteristics and rhizosphere communities revealed indirect associations with *Phytopythium* spp. or with the plant health status. These abiotic factors play a role in reshaping the plant microbiota and may promote dysbiosis, especially when the plant is

already weakened. The oomycete genera *Phytopythium* previously reported in several studies as associated with the syndrome (Prencipe et al., 2020; Savian et al., 2021) was present in healthy and diseased fields, albeit in different relative abundances. Association networks of co-occurrence and co-exclusion between taxa were investigated for the first time in this pathosystem, unveiling the correlation of *Phytopythium* spp. with the diseased status of orchards in soils. In the rhizosphere, the oomycete ASVs were negatively associated with saprobes and plant growth promoting fungal genera such as AM fungi. Network analyses of rhizosphere communities showed bacterial and fungal associations were established with different *P. vexans* ASVs, thus revealing strain specific characteristics which require further investigation. The dynamic emerging from our analysis of the ecological processes driving rhizosphere community assembly, highlights the possibility of a dysbiosis phenomenon, driven by Anti-AKP in oomycete communities. Unlike fungal communities and bacterial assemblies in diseased samples that were dominated by stochastic processes. This study highlights the importance of considering multifactorial stressors and their interaction in emerging pathosystems. Environmental variations like flooding and higher temperatures in soil are likely to favor genera whose lifestyle requires such conditions, and these factors should be included in future analysis. Therefore, a relevant consideration for future studies is the investigation of water management and moisture levels in the soil close to roots and the possible correlation with the oomycete community development and soil temperature in the field. Soil enzymatic activity and/or metagenomic studies should also be considered to further investigate the functional role of communities associated with symptomatic orchards.

Acknowledgments

This research was funded by Piedmont Region (Italy) with the project “KIRIS - Kiwifruit Vine Decline Syndrome: deepening the etiology and development of prevention and control tool”, by Italian Ministry of University and Research with the project “KVD-Biome - Unveiling the plant exposome to dissect a multifactorial disease: the kiwifruit vine decline”, by AGER – Foundations Network for Agrifood Research with the project “SOS-KIWI - From SOil to Soil: origin and remediation to KIWIfruit Vine Decline Syndrome”, and by the European Commission – NextGenerationEU, Project SUS-MIRRI.IT "Strengthening the MIRRI Italian Research Infrastructure for Sustainable Bioscience and Bioeconomy”, code n. IR0000005. The Authors

would like to express their gratitude to Dr. Tracey Somera for her accurate revision of the manuscript.

References

Abarenkov, K., Zirk, A., Piirmann, T., Pöhönen, R., Ivanov, F., Nilsson, R. H., and Kõljalg, U. (2021). UNITE QIIME release for eukaryotes 2. UNITE Community. doi: 10.15156/BIO/126486.

Adamo, I., Castaño, C., Bonet, J. A., Colinas, C., Martínez de Aragón, J., and Alday, J. G. (2021). Soil physico-chemical properties have a greater effect on soil fungi than host species in Mediterranean pure and mixed pine forests. Soil Biology and Biochemistry 160, 108320. doi: 10.1016/j.soilbio.2021.108320.

Akilli, S., Serçe, Çi. U., Zekaİ Katircioğlu, Y., Karakaya, A., and Maden, S. (2011). Involvement of Phytophthora citrophthora in Kiwifruit Decline in Turkey: Involvement of Phytophthora citrophthora on Kiwifruit. Journal of Phytopathology 159, 579–581. doi: 10.1111/j.1439-0434.2011.01798.x.

Anderson, M. J. (2001). A new method for non-parametric multivariate analysis of variance: Non-parametric MANOVA for ecology. Austral Ecology 26, 32–46. doi: 10.1111/j.1442-9993.2001.01070.pp.x.

Anderson, M. J. (2006). Distance-Based Tests for Homogeneity of Multivariate Dispersions. Biometrics 62, 245–253. doi: 10.1111/j.1541-0420.2005.00440.x.

Apprill, A., McNally, S., Parsons, R., and Weber, L. (2015). Minor revision to V4 region SSU rRNA 806R gene primer greatly increases detection of SAR11 bacterioplankton. Aquat. Microb. Ecol. 75, 129–137. doi: 10.3354/ame01753.

Arnault, G., Mony, C., and Vandenkoornhuyse, P. (2023). Plant microbiota dysbiosis and the Anna Karenina Principle. Trends in Plant Science 28, 18–30. doi: 10.1016/j.tplants.2022.08.012.

Balestra, G.M., and Costa, G. (2020). La situazione in Italia: Evoluzione varietale sì, ma con tante avversità. Rivista di Frutticoltura 82, 10–16.

Bardi, L. (2020). Early Kiwifruit Decline: A Soil-Borne Disease Syndrome or a Climate Change Effect on Plant–Soil Relations? Frontiers in Agronomy 2. Available at: https://www.frontiersin.org/articles/10.3389/fagro.2020.00003 [Accessed July 20, 2023].

Bastian, M., Heymann, S., and Jacomy, M. (2009). Gephi: An Open Source Software for Exploring and Manipulating Networks. Proceedings of the International AAAI Conference on Web and Social Media 3, 361–362. doi: 10.1609/icwsm.v3i1.13937.

Baudry, A., Morzieres, J. P., and Ellis, R. (1991). Effect of Phytophthora spp. on kiwifruit in France. New Zealand Journal of Crop and Horticultural Science 19, 395–398. doi: 10.1080/01140671.1991.10422883.

Bebber, D. P., Ramotowski, M. A. T., and Gurr, S. J. (2013). Crop pests and pathogens move polewards in a warming world. Nature Clim Change 3, 985–988. doi: 10.1038/nclimate1990.

Benjamini, Y., and Hochberg, Y. (1995). Controlling the False Discovery Rate: A Practical and Powerful Approach to Multiple Testing. Journal of the Royal Statistical Society: Series B (Methodological) 57, 289–300. doi: 10.1111/j.2517-6161.1995.tb02031.x.

Bent, E., Loffredo, A., Yang, J., McKenry, M. V., Becker, J. O., and Borneman, J. (2009). Investigations into peach seedling stunting caused by a replant soil: Peach seedling stunting caused by a replant soil. FEMS Microbiology Ecology 68, 192–200. doi: 10.1111/j.1574-6941.2009.00668.x.

Bettenfeld, P., Fontaine, F., Trouvelot, S., Fernandez, O., and Courty, P.-E. (2020). Woody Plant Declines. What's Wrong with the Microbiome? Trends in Plant Science 25, 381–394. doi: 10.1016/j.tplants.2019.12.024.

Bokulich, N. A., Kaehler, B. D., Rideout, J. R., Dillon, M., Bolyen, E., Knight, R., et al. (2018). Optimizing taxonomic classification of marker-gene amplicon sequences with QIIME 2's q2-feature-classifier plugin. Microbiome 6, 90. doi: 10.1186/s40168-018-0470-z.

Bokulich, N., Robeson, M., Dillon, M. R., Ziemski, M., Kaehler, B., mirand863, et al. (2023). bokulich-lab/RESCRIPt: 2023.5.0. doi: 10.5281/zenodo.8004808.

Bolyen, E., Rideout, J. R., Dillon, M. R., Bokulich, N. A., Abnet, C. C., Al-Ghalith, G. A., et al. (2019). Reproducible, interactive, scalable and extensible microbiome data science using QIIME 2. Nat Biotechnol 37, 852–857. doi: 10.1038/s41587-019-0209-9.

Brasier, C., Scanu, B., Cooke, D., and Jung, T. (2022). Phytophthora: an ancient, historic, biologically and structurally cohesive and evolutionarily successful generic concept in need of preservation. IMA Fungus 13, 12. doi: 10.1186/s43008-022-00097-z.

Bulgarelli, D., Rott, M., Schlaeppi, K., Ver Loren van Themaat, E., Ahmadinejad, N., Assenza, F., et al. (2012). Revealing structure and assembly cues for Arabidopsis root-inhabiting bacterial microbiota. Nature 488, 91–95. doi: 10.1038/nature11336.

Bulgarelli, D., Schlaeppi, K., Spaepen, S., van Themaat, E. V. L., and Schulze-Lefert, P. (2013). Structure and Functions of the Bacterial Microbiota of Plants. Annual Review of Plant Biology 64, 807–838. doi: 10.1146/annurev-arplant-050312-120106

Bulgarelli, D., Garrido-Oter, R., Münch, P. C., Weiman, A., Dröge, J., Pan, Y., et al. (2015). Structure and Function of the Bacterial Root Microbiota in Wild and Domesticated Barley. Cell Host & Microbe 17, 392–403. doi: 10.1016/j.chom.2015.01.011.

Buwalda, J. G., and Hutton, R. C. (1988). Seasonal changes in root growth of kiwifruit. Scientia Horticulturae 36, 251–260. doi: 10.1016/0304-4238(88)90059-3.

Callahan, B. J., McMurdie, P. J., Rosen, M. J., Han, A. W., Johnson, A. J. A., and Holmes, S. P. (2016). DADA2: High-resolution sample inference from Illumina amplicon data. Nat Methods 13, 581–583. doi: 10.1038/nmeth.3869.

Cavicchioli, R., Ripple, W. J., Timmis, K. N., Azam, F., Bakken, L. R., Baylis, M., et al. (2019). Scientists' warning to humanity: microorganisms and climate change. Nat Rev Microbiol 17, 569–586. doi: 10.1038/s41579-019-0222-5.

Chen, Q., Hou, L. W., Duan, W. J., Crous, P. W., and Cai, L. (2017). Didymellaceae revisited. Studies in Mycology 87, 105–159. doi: 10.1016/j.simyco.2017.06.002.

Clark, C. J., and Smith, G. S. (1988). Seasonal accumulation of mineral nutrients by kiwifruit 2. Fruit. New Phytologist 108, 399–409. doi: 10.1111/j.1469-8137.1988.tb04180.x.

Darriaut, R., Martins, G., Dewasme, C., Mary, S., Darrieutort, G., Ballestra, P., et al. (2021). Grapevine decline is associated with difference in soil microbial composition and activity. OENO One 55. doi: 10.20870/oeno-one.2021.55.3.4626.

DeSantis, T. Z., Hugenholtz, P., Larsen, N., Rojas, M., Brodie, E. L., Keller, K., et al. (2006). Greengenes, a Chimera-Checked 16S rRNA Gene Database and Workbench Compatible with ARB. Appl Environ Microbiol 72, 5069–5072. doi: 10.1128/AEM.03006-05.

Donati, I., Cellini, A., Sangiorgio, D., Caldera, E., Sorrenti, G., and Spinelli, F. (2020). Pathogens Associated to Kiwifruit Vine Decline in Italy. Agriculture 10, 119. doi: 10.3390/agriculture10040119.

Erper, I., Agustí-Brisach, C., Tunali, B., and Armengol, J. (2013). Characterization of root rot disease of kiwifruit in the Black Sea region of Turkey. Eur J Plant Pathol 136, 291–300. doi: 10.1007/s10658-012-0163-6

Ezrari, S., Mhidra, O., Radouane, N., Tahiri, A., Polizzi, G., Lazraq, A., et al. (2021). Potential Role of Rhizobacteria Isolated from Citrus Rhizosphere for Biological Control of Citrus Dry Root Rot. Plants 10, 872. doi: 10.3390/plants10050872.

FAOSTAT. License: CC BY-NC-SA 3.0 IGO. Extracted from: https://www.fao.org/faostat/en/. Data of Access: 21-01-2024

Faust, K., and Raes, J. (2016). CoNet app: inference of biological association networks using Cytoscape. F1000Res 5, 1519. doi: 10.12688/f1000research.9050.2.

Feng, P., Lu, Q., Najafzadeh, M. J., Gerrits van den Ende, A. H. G., Sun, J., Li, R., et al. (2014). Cyphellophora and its relatives in Phialophora: biodiversity and possible role in human infection. Fungal Diversity 65, 17–45. doi: 10.1007/s13225-012-0194-5.

Fernandes, A. D., Macklaim, J. M., Linn, T. G., Reid, G., and Gloor, G. B. (2013). ANOVA-Like Differential Expression (ALDEx) Analysis for Mixed Population RNA-Seq. PLOS ONE 8, e67019. doi: 10.1371/journal.pone.0067019.

Fernandes, A. D., Reid, J. N., Macklaim, J. M., McMurrough, T. A., Edgell, D. R., and Gloor, G. B. (2014). Unifying the analysis of high-throughput sequencing datasets: characterizing RNA-seq, 16S rRNA gene sequencing and selective growth experiments by compositional data analysis. Microbiome 2, 15. doi: 10.1186/2049-2618-2-15.

Ferrari, B., Winsley, T., Ji, M., and Neilan, B. (2014). Insights into the distribution and abundance of the ubiquitous Candidatus Saccharibacteria phylum following tag pyrosequencing. Sci Rep 4, 3957. doi: 10.1038/srep03957.

Fitzpatrick, C. R., Salas-González, I., Conway, J. M., Finkel, O. M., Gilbert, S., Russ, D., et al. (2020). The Plant Microbiome: From Ecology to Reductionism and Beyond. Annu. Rev. Microbiol. 74, 81–100. doi: 10.1146/annurev-micro-022620-014327.

Fontaine, F., Pinto, C., Vallet, J., Clément, C., Gomes, A. C., and Spagnolo, A. (2016). The effects of grapevine trunk diseases (GTDs) on vine physiology. Eur J Plant Pathol 144, 707–721. doi: 10.1007/s10658-015-0770-0.

Franke-Whittle, I. H., Manici, L. M., Insam, H., and Stres, B. (2015). Rhizosphere bacteria and fungi associated with plant growth in soils of three replanted apple orchards. Plant Soil 395, 317–333. doi: 10.1007/s11104-015-2562-x.

Frey, B., Walthert, L., Perez-Mon, C., Stierli, B., Köchli, R., Dharmarajah, A., et al. (2021). Deep Soil Layers of Drought-Exposed Forests Harbor Poorly Known Bacterial and Fungal Communities. Front. Microbiol. 12, 674160. doi: 10.3389/fmicb.2021.674160.

Giovannetti, M., Salvioli Di Fossalunga, A., Stringlis, I. A., Proietti, S., and Fiorilli, V. (2023). Unearthing soil-plant-microbiota crosstalk: Looking back to move forward. Front. Plant Sci. 13, 1082752. doi: 10.3389/fpls.2022.1082752.

Glöckner, F. O., Yilmaz, P., Quast, C., Gerken, J., Beccati, A., Ciuprina, A., et al. (2017). 25 years of serving the community with ribosomal RNA gene reference databases and tools. Journal of Biotechnology 261, 169–176. doi: 10.1016/j.jbiotec.2017.06.1198.

Gloor, G. B., Macklaim, J. M., and Fernandes, A. D. (2016). Displaying Variation in Large Datasets: Plotting a Visual Summary of Effect Sizes. Journal of Computational and Graphical Statistics 25, 971–979. doi: 10.1080/10618600.2015.1131161.

Gramaje, D., Úrbez-Torres, J. R., and Sosnowski, M. R. (2018). Managing Grapevine Trunk Diseases With Respect to Etiology and Epidemiology: Current Strategies and Future Prospects. Plant Disease 102, 12–39. doi: 10.1094/PDIS-04-17-0512-FE.

Heidrich, V., Karlovsky, P., and Beule, L. (2021). 'SRS' R Package and 'q2-srs' QIIME 2 Plugin: Normalization of Microbiome Data Using Scaling with Ranked Subsampling (SRS). Applied Sciences 11, 11473. doi: 10.3390/app112311473.

Hossain, Z., Hubbard, M., Gan, Y., and Bainard, L. D. (2021). Root rot alters the root-associated microbiome of field pea in commercial crop production systems. Plant Soil 460, 593–607. doi: 10.1007/s11104-020-04779-8.

Hyde, K. D., Fryar, S., Tian, Q., Bahkali, A. H., and Xu, J. (2016). Lignicolous freshwater fungi along a north–south latitudinal gradient in the Asian/Australian region; can we predict the impact of global warming on biodiversity and function? Fungal Ecology 19, 190–200. doi: 10.1016/j.funeco.2015.07.002.

Ihrmark, K., Bödeker, I. T. M., Cruz-Martinez, K., Friberg, H., Kubartova, A., Schenck, J., et al. (2012). New primers to amplify the fungal ITS2 region - evaluation by 454-sequencing of artificial and natural communities. FEMS Microbiol Ecol 82, 666–677. doi: 10.1111/j.1574-6941.2012.01437.x.

Illumina. (2013). 16S metagenomic sequencing library preparation. https://support.illumina.com/documents/documentation/chemistry_documentation/16s/16s-metagenomic-library-prep-guide-15044223-b.pdf.

Jiao, S., and Lu, Y. (2020). Abundant fungi adapt to broader environmental gradients than rare fungi in agricultural fields. Global Change Biology 26, 4506–4520. doi: 10.1111/gcb.15130.

Jin, T., Wang, Y., Huang, Y., Xu, J., Zhang, P., Wang, N., et al. (2017). Taxonomic structure and functional association of foxtail millet root microbiome. GigaScience 6, 1–12. doi: 10.1093/gigascience/gix089.

Kassambara, A. (2023). _ggpubr: 'ggplot2' Based Publication Ready Plots_. R package version 0.6.0,

https://CRAN.R-project.org/package=ggpubr.

Katoh, K., and Standley, D. M. (2013). MAFFT Multiple Sequence Alignment Software Version 7: Improvements in Performance and Usability. Molecular Biology and Evolution 30, 772–780. doi: 10.1093/molbev/mst010.

Klindworth, A., Pruesse, E., Schweer, T., Peplies, J., Quast, C., Horn, M., et al. (2013). Evaluation of general 16S ribosomal RNA gene PCR primers for classical and next-generation sequencing-based diversity studies. Nucleic Acids Research 41, e1–e1. doi: 10.1093/nar/gks808.

Kruskal, W. H., and Wallis, W. A. (2012). Use of Ranks in One-Criterion Variance Analysis. Journal of the American Statistical Association. Available at: https://www.tandfonline.com/doi/abs/10.1080/01621459.1952.10483441 [Accessed June 7, 2023].

Kurbetli, İ., and Ozan, S. (2013). Occurrence of Phytophthora Root and Stem Rot of Kiwifruit in Turkey. J Phytopathol 161, 887–889. doi: 10.1111/jph.12145.

Kwon, Y., Hong, S., Kwack, Y.-B., and Kwak, Y.-S. (2016). First report of leaf spot on kiwifruit caused by Phoma sp. in Korea. New Zealand Journal of Crop and Horticultural Science 44, 227–230. doi: 10.1080/01140671.2016.1164198.

Lundberg, D. S., Lebeis, S. L., Paredes, S. H., Yourstone, S., Gehring, J., Malfatti, S., et al. (2012). Defining the core Arabidopsis thaliana root microbiome. Nature 488, 86–90. doi: 10.1038/nature11237.

Luvisi, A., Nicolì, F., and Luigi De Bellis (2017). Sustainable Management of Plant Quarantine Pests: The Case of Olive Quick Decline Syndrome. Sustainability 9, 659. doi: 10.3390/su9040659.

Mangiafico, S. S. (2023). rcompanion: Functions to Support Extension Education Program Evaluation. Rutgers Cooperative Extension, New Brunswick, New Jersey. version 2.4.34, https://CRAN.R-project.org/package=rcompanion/.

Manici, L. M., Caputo, F., and Saccà, M. L. (2017). Secondary metabolites released into the rhizosphere by Fusarium oxysporum and Fusarium spp. as underestimated component of nonspecific replant disease. Plant Soil 415, 85–98. doi: 10.1007/s11104-016-3152-2.

Manici, L. M., Caboni, E., Caputo, F., Frattarelli, A., and Lucioli, S. (2021). Phytotoxins from Dactylonectria torresensis involved in replant disease of fruit trees. Rhizosphere 17, 100300. doi: 10.1016/j.rhisph.2020.100300.

Manici, L. M., Saccà, M. L., Scotti, C., and Caputo, F. (2022). Quantitative reduction of soil bacteria and qualitative microbial changes: biotic components associated to kiwifruit decline. Plant Soil 477, 613–628. doi: 10.1007/s11104-022-05470-w.

Martin, M. (2011). Cutadapt removes adapter sequences from high-throughput sequencing reads. EMBnet.journal 17, 10–12. doi: 10.14806/ej.17.1.200.

Martino, C., Morton, J. T., Marotz, C. A., Thompson, L. R., Tripathi, A., Knight, R., et al. (2019). A Novel Sparse Compositional Technique Reveals Microbial Perturbations. mSystems 4, e00016-19. doi: 10.1128/mSystems.00016-19.

Mazzola, M., and Manici, L. M. (2012). Apple Replant Disease: Role of Microbial Ecology in Cause and Control. Annu. Rev. Phytopathol. 50, 45–65. doi: 10.1146/annurev-phyto-081211-173005.

Merot, A., Coulouma, G., Smits, N., Robelot, E., Gary, C., Guerin-Dubrana, L., et al. (2023). A systemic approach to grapevine decline diagnosed using three key indicators: plant mortality, yield loss and vigour decrease. OENO One 57, 133–149. doi: 10.20870/oeno-one.2023.57.1.5575.

Mingot-Ureta, C., Lopez-Moya, F., and Lopez-Llorca, L. V. (2020). Isolates of the Nematophagous Fungus Pochonia chlamydosporia Are Endophytic in Banana Roots and Promote Plant Growth. Agronomy 10, 1299. doi: 10.3390/agronomy10091299.

Mukhtar, S., Mehnaz, S., and Malik, K. A. (2021). Comparative Study of the Rhizosphere and Root Endosphere Microbiomes of Cholistan Desert Plants. Front. Microbiol. 12, 618742. doi: 10.3389/fmicb.2021.618742.

Nicola, L., Insam, H., Pertot, I., and Stres, B. (2018). Reanalysis of microbiomes in soils affected by apple replant disease (ARD): Old foes and novel suspects lead to the proposal of extended model of disease development. Applied Soil Ecology 129, 24–33. doi: 10.1016/j.apsoil.2018.04.010.

Noel, Z. A., Chang, H.-X., and Chilvers, M. I. (2020). Variation in soybean rhizosphere oomycete communities from Michigan fields with contrasting disease pressures. Applied Soil Ecology 150, 103435. doi: 10.1016/j.apsoil.2019.103435.

Obieze, C. C., George, P. B. L., Boyle, B., and Khasa, D. P. (2023). Black pepper rhizomicrobiome: Spectrum of plant health indicators, critical environmental factors and

community compartmentation in Vietnam. Applied Soil Ecology 187, 104857. doi: 10.1016/j.apsoil.2023.104857.

Ogle, D. H., Doll, J. C., Wheeler, A.P., Dinno, A. (2023). FSA: Simple Fisheries Stock Assessment Methods. R package version 0.9.4. https://CRAN.R-project.org/package=FSA.

Oksanen, J., Blanchet, F. G., Friendly, M., Kindt, R., Legendre, P., McGlinn, D., Minchin, P. R., O'Hara, R. B., Simpson, G. L., Solymos, P., Stevens, M. H. H. , Szoecs, E., and Wagner, H. (2020). _vegan: Community Ecology Package_. R package version 2.5-7, <https://CRAN.R-project.org/package=vegan>.

Pielou, E. C. (1966). The measurement of diversity in different types of biological collections. Journal of Theoretical Biology. 13,131-144.

Plassart, P., Prévost-Bouré, N. C., Uroz, S., Dequiedt, S., Stone, D., Creamer, R., et al. (2019). Soil parameters, land use, and geographical distance drive soil bacterial communities along a European transect. Sci Rep 9, 605. doi: 10.1038/s41598-018-36867-2.

Polat, Z., Awan, Q. N., Hussain, M., and Akgül, D. S. (2017). First Report of Phytopythium vexans Causing Root and Collar Rot of Kiwifruit in Turkey. Plant Disease 101, 1058. doi: 10.1094/PDIS-11-16-1554-PDN.

Prencipe, S., Savian, F., Nari, L., Ermacora, P., Spadaro, D., and Martini, M. (2020). First Report of Phytopythium vexans Causing Decline Syndrome of Actinidia deliciosa ‘Hayward’ in Italy. Plant Disease 104, 2032. doi: 10.1094/PDIS-10-19-2101-PDN.

Prencipe, S., Schiavon, G., Rosati, M., Nari, L., Schena, L., and Spadaro, D. (2023). Characterization of Phytopythium Species Involved in the Establishment and Development of Kiwifruit Vine Decline Syndrome. Microorganisms 11, 216. doi: 10.3390/microorganisms11010216.

Price, M. N., Dehal, P. S., and Arkin, A. P. (2010). FastTree 2 – Approximately Maximum-Likelihood Trees for Large Alignments. PLoS ONE 5, e9490. doi: 10.1371/journal.pone.0009490.

R Core Team. (2003). R: A Language and Environment for Statistical Computing. R Foundation for Statistical Computing. Vienna, Austria. https://www.R-project.org.

Richter-Heitmann, T., Hofner, B., Krah, F.-S., Sikorski, J., Wüst, P. K., Bunk, B., et al. (2020). Stochastic Dispersal Rather Than Deterministic Selection Explains the Spatio-Temporal Distribution of Soil Bacteria in a Temperate Grassland. Front. Microbiol. 11, 1391. doi: 10.3389/fmicb.2020.01391.

Riit, T., Tedersoo, L., Drenkhan, R., Runno-Paurson, E., Kokko, H., and Anslan, S. (2016). Oomycete-specific ITS primers for identification and metabarcoding. MC 14, 17–30. doi: 10.3897/mycokeys.14.9244.

Riit, T., Tedersoo, L., Drenkhan, R., Runno-Paurson, E., Kokko, H., and Anslan, S. (2018). Corrigendum for: “Oomycete-specific ITS primers for identification and metabarcoding” published in MycoKeys, doi: 10.3897/mycokeys.14.9244. MC 41, 119–120. doi: 10.3897/mycokeys.41.30558.

Sandoval-Denis, M., Guarro, J., Cano-Lira, J. F., Sutton, D. A., Wiederhold, N. P., de Hoog, G. S., et al. (2016). Phylogeny and taxonomic revision of Microascaceae with emphasis on synnematous fungi. Studies in Mycology 83, 193–233. doi: 10.1016/j.simyco.2016.07.002.

Save, R., and Serrano, L. (1986). Some physiological and growth responses of kiwifruit (Actinidia chinensis) to flooding. Physiol Plant 66, 75–78. doi: 10.1111/j.1399-3054.1986.tb01236.x.

Savian, F., Ginaldi, F., Musetti, R., Sandrin, N., Tarquini, G., Pagliari, L., et al. (2020). Studies on the aetiology of kiwifruit decline: interaction between soil-borne pathogens and waterlogging. Plant Soil 456, 113–128. doi: 10.1007/s11104-020-04671-5.

Savian, F., Prencipe, S., Filippini, N., Nari, L., Martini, M., Ermacora, P., et al. (2021). Pathogenicity of Phytopythium chamaehyphon : A New Player in Kiwifruit Vine Decline Syndrome of Actinidia chinensis var. deliciosa 'Hayward' in Italy. Plant Disease 105, 2781–2784. doi: 10.1094/PDIS-01-21-0143-SC.

Savian, F., Marroni, F., Ermacora, P., Firrao, G., and Martini, M. (2022). A Metabarcoding Approach to Investigate Fungal and Oomycete Communities Associated with Kiwifruit Vine Decline Syndrome in Italy. Phytobiomes Journal 6, 290–304. doi: 10.1094/PBIOMES-03-22-0019-R.

Shannon, C. E., and Weaver, W. (1949). The mathematical theory of communication. University of Illinois Press, Champaign, Illinois.

Shannon, P., Markiel, A., Ozier, O., Baliga, N. S., Wang, J. T., Ramage, D., et al. (2003). Cytoscape: A Software Environment for Integrated Models of Biomolecular Interaction Networks. Genome Res. 13, 2498–2504. doi: 10.1101/gr.1239303.

Shearer, C. A., Descals, E., Kohlmeyer, B., Kohlmeyer, J., Marvanová, L., Padgett, D., et al. (2007). Fungal biodiversity in aquatic habitats. Biodivers Conserv 16, 49–67. doi: 10.1007/s10531-006-9120-z.

Shimizu, S., Miyoshi, T., Yano, T., Tachibana, Y., 2005. First report of Kiwifruit root rot caused by Pythium spp. Japanese Journal of Phytopathology 71,210.

Simmons, T., Caddell, D. F., Deng, S., and Coleman-Derr, D. (2018). Exploring the Root Microbiome: Extracting Bacterial Community Data from the Soil, Rhizosphere, and Root Endosphere. JoVE (Journal of Visualized Experiments), e57561. doi: 10.3791/57561.

Singh, B. K., Trivedi, P., Egidi, E., Macdonald, C. A., and Delgado-Baquerizo, M. (2020). Crop microbiome and sustainable agriculture. Nat Rev Microbiol 18, 601–602. doi: 10.1038/s41579-020-00446-y.

Smith, G. S., Buwalda, J. G., Green, T. G. A., and Clark, C. J. (1989). Effect of oxygen supply and temperature at the root on the physiology of kiwifruit vines. New Phytol 113, 431–437. doi: 10.1111/j.1469-8137.1989.tb00354.x.

Somera, T. S., and Mazzola, M. (2022). Toward a holistic view of orchard ecosystem dynamics: A comprehensive review of the multiple factors governing development or suppression of apple replant disease. Frontiers in Microbiology 13 - 2022. doi: 10.3389/fmicb.2022.949404.

Song, W., Song, S., Lan, J., Zheng, D., Xu, X., Huang, L., et al. (2023). First Report of Root Rot Caused by Fusarium solani and F. breve on Kiwifruit in China. Plant Disease 107, 1635. doi: 10.1094/PDIS-09-22-2103-PDN.

Sorrenti, G., Tacconi, G., Tosi, L., Vittone, G., Nari, L., Savian, F., Saro, S., Ermacora, P., Graziani, S., and Toselli, M. (2019). Avanza la “moria del kiwi”: Evoluzione e primi riscontri della ricerca. Rivista di Frutticoltura 81 (2), 34–42.

Starr, E. P., Shi, S., Blazewicz, S. J., Probst, A. J., Herman, D. J., Firestone, M. K., et al. (2018). Stable isotope informed genome-resolved metagenomics reveals that Saccharibacteria utilize microbially-processed plant-derived carbon. Microbiome 6, 122. doi: 10.1186/s40168-018-0499-z

Stegen, J. C., Lin, X., Fredrickson, J. K., Chen, X., Kennedy, D. W., Murray, C. J., et al. (2013). Quantifying community assembly processes and identifying features that impose them. ISME J 7, 2069–2079. doi: 10.1038/ismej.2013.93.

Tacconi, G., Paltrinieri, S., Mejia, J. F., Fuentealba, S. P., Bertaccini, A., Tosi, L., et al. (2015). Vine decline in kiwifruit: climate change and effect on waterlogging and Phytophthora in North Italy. Acta Hortic., 93–97. doi: 10.17660/ActaHortic.2015.1096.7.

Tan, Y., Cui, Y., Li, H., Kuang, A., Li, X., Wei, Y., et al. (2017). Rhizospheric soil and root endogenous fungal diversity and composition in response to continuous Panax notoginseng cropping practices. Microbiological Research 194, 10–19. doi: 10.1016/j.micres.2016.09.009

Tedersoo, L., Bahram, M., Põlme, S., Kõljalg, U., Yorou, N. S., Wijesundera, R., et al. (2014). Global diversity and geography of soil fungi. Science 346, 1256688. doi: 10.1126/science.1256688.

Teixeira, M. M., Moreno, L. F., Stielow, B. J., Muszewska, A., Hainaut, M., Gonzaga, L., et al. (2017). Exploring the genomic diversity of black yeasts and relatives (Chaetothyriales , Ascomycota). Studies in Mycology 86, 1–28. doi: 10.1016/j.simyco.2017.01.001.

Tewoldemedhin, Y. T., Mazzola, M., Mostert, L., and McLeod, A. (2011). Cylindrocarpon species associated with apple tree roots in South Africa and their quantification using real-time PCR. Eur J Plant Pathol 129, 637–651. doi: 10.1007/s10658-010-9728-4

Tewoldemedhin, Y. T., Mazzola, M., Botha, W. J., Spies, C. F. J., and McLeod, A. (2011a). Characterization of fungi (Fusarium and Rhizoctonia) and oomycetes (Phytophthora and Pythium) associated with apple orchards in South Africa. Eur J Plant Pathol 130, 215–229. doi: 10.1007/s10658-011-9747-9.

Tewoldemedhin, Y. T., Mazzola, M., Labuschagne, I., and McLeod, A. (2011b). A multi-phasic approach reveals that apple replant disease is caused by multiple biological agents, with some agents acting synergistically. Soil Biology and Biochemistry 43, 1917–1927. doi: 10.1016/j.soilbio.2011.05.014

Trivedi, P., Batista, B. D., Bazany, K. E., and Singh, B. K. (2022). Plant–microbiome interactions under a changing world: responses, consequences and perspectives. New Phytologist 234, 1951–1959. doi: 10.1111/nph.18016.

Türkkan, M., Özer, G., Karaca, G., Erper, İ., and Derviş, S. (2022). Characterization and Pathogenicity of Pythium-Like Species Associated with Root and Collar Rot of Kiwifruit in Turkey. Plant Disease 106, 854–863. doi: 10.1094/PDIS-05-21-0961-RE.

Wang, K. X., Xie, Y. L., Yuan, G. Q., Li, Q. Q., and Lin, W. (2015). First Report of Root and Collar Rot Caused by Phytopythium helicoides on Kiwifruit (Actinidia chinensis). Plant Disease 99, 725. doi: 10.1094/PDIS-08-14-0817-PDN.

Wang, G.-N., Yu, X.-D., Dong, W., Bhat, D. J., Boonmee, S., Zhang, D., et al. (2019). Freshwater hyphomycetes in Eurotiomycetes: a new species of Minimelanolocus and a new collection of Thysanorea papuana (Herpotrichiellaceae). Mycol Progress 18, 511–522. doi: 10.1007/s11557-019-01473-7.

Wickham, H. (2016). ggplot2: Elegant Graphics for Data Analysis. Springer-Verlag New York. ISBN 978-3-319-24277-4. https://ggplot2.tidyverse.org.

Wickham H, François R, Henry L, Müller K, Vaughan D (2023). _dplyr: A Grammar of Data Manipulation_. R package version 1.1.2, https://CRAN.R-project.org/package=dplyr.

Xiong, C., He, J., Singh, B. K., Zhu, Y., Wang, J., Li, P., et al. (2021). Rare taxa maintain the stability of crop mycobiomes and ecosystem functions. Environmental Microbiology 23, 1907–1924. doi: 10.1111/1462-2920.15262.

Yang, J., Ruegger, P. M., McKenry, M. V., Becker, J. O., and Borneman, J. (2012). Correlations between root-associated microorganisms and peach replant disease symptoms in a California soil. PLoS One 7, e46420. doi: 10.1371/journal.pone.0046420

Yuan, J., Zhao, J., Wen, T., Zhao, M., Li, R., Goossens, P., et al. (2018). Root exudates drive the soil-borne legacy of aboveground pathogen infection. Microbiome 6, 156. doi: 10.1186/s40168-018-0537-x.

Yuan, Z., Liu, F., He, S., Zhou, L., and Pan, H. (2022). Community structure and diversity characteristics of rhizosphere and root endophytic bacterial community in different Acacia species. PLoS ONE 17, e0262909. doi: 10.1371/journal.pone.0262909.

Zandalinas, S. I., Fritschi, F. B., and Mittler, R. (2021a). Global Warming, Climate Change, and Environmental Pollution: Recipe for a Multifactorial Stress Combination Disaster. Trends in Plant Science 26, 588–599. doi: 10.1016/j.tplants.2021.02.011.

Zandalinas, S. I., Sengupta, S., Fritschi, F. B., Azad, R. K., Nechushtai, R., and Mittler, R. (2021b). The impact of multifactorial stress combination on plant growth and survival. New Phytol 230, 1034–1048. doi: 10.1111/nph.17232.

Zavala-Gonzalez, E. A., Escudero, N., Lopez-Moya, F., Aranda-Martinez, A., Exposito, A., Ricaño-Rodríguez, J., et al. (2015). Some isolates of the nematophagous fungus Pochonia chlamydosporia promote root growth and reduce flowering time of tomato. Ann Appl Biol 166, 472–483. doi: 10.1111/aab.12199.

Zhang, C., WeiJie, L., Li, W., Yao, H., Luo, C., Xu, H., and Shen, X. (2017). Correlation study on the diversity of the AM fungi and soil nutrients in the rhizosphere of different kiwifruit cultivars. Journal of Fruit Science 34, 344–353.

Zou, M. F., Wang, Y. X., Yan, M. F., Zhou, Y., Xiong, G. H., and Jiang, J. X. (2020). First Report of Leaf Spot on Kiwifruit Caused by Didymella bellidis in China. Plant Disease 104, 287. doi: 10.1094/PDIS-06-19-1257-PDN.

Tables

Table 1 - results of multivariate permutational analysis of variance (PERMANOVA) on Robust Aitchison distance matrix values for fungi, bacteria and oomycetes, performed with package *adonis*. Considered parameters include disease status, sampling matrix, sampling site and their intersections. F.model is the F statistic for the test, while R2 is the explained variance, expressed as percentage of total variance. Pr (>F) is the false discovery rate (FDR) adjusted p-value.

Community	**Effect**	**F.model**	**R2 (%)**	**Pr(>F)**
Fungi	Disease status	16.97	0.7	0.001
	Matrix	109.77	8.9	0.001
	Site	554.74	67.9	0.001
	Disease status and Matrix	9.55	0.8	0.001
	Disease status and Site	92.64	11.3	0.001
	Matrix and Site	14.42	3.5	0.001
	Disease status and Matrix and Site	11.87	2.9	0.001
	Residuals	NA	4	NA
Bacteria	Disease status	0.097	0	0.808
	Matrix	1837.34	86.9	0.001
	Site	96.19	7	0.001
	Disease status and Matrix	29.84	1.4	0.001
	Disease status and Site	4.46	0.3	0.001
	Matrix and Site	11.28	1.6	0.001
	Disease status and Matrix and Site	4.49	0.6	0.001
	Residuals	NA	2.2	NA
Oomycetes	Disease status	24.83	9	0.001
	Matrix	34.26	24	0.001
	Site	12.33	13	0.001
	Disease status and Matrix	1.03	0.6	0.386
	Disease status and Site	13.67	14.2	0.001
	Matrix and Site	3.82	8	0.001
	Disease status and Matrix and Site	1.98	2.7	0.06
	Residuals	NA	28.5	NA

Table 2 - Results of the Permutational multiple analysis of variance (PERMANOVA) and multivariate dispersion analysis (PERMDISP) for bacteria, fungi and oomycetes communities, with comparisons between matrices, sampling sites and disease status. Pseudo-F and F-value are the test metrics for PERMANOVA and PERMDISP, respectively. Q-value indicates the false discovery rate (FDR) adjusted p-value. Significance threshold for null hypothesis rejection was set at 0.05.

	PERMANOVA		**PERMDISP**	
Comparison	**Pseudo-F**	**q-value**	**F-value**	**q-value**
Bacteria - matrix				
Rhizosphere – Root	335.16	0.001	2.85	0.048
Rhizosphere - Soil	52.41	0.001	10.47	0.004
Root – Soil	886.47	0.001	2.56	0.004
Bacteria - site				
Fossano – Manta	1.14	0.300	0.14	0.739
Fossano – Scarnafigi	5.02	0.132	0.13	0.739
Fossano – Verzuolo	3.88	0.132	0.52	0.739
Manta – Scarnafigi	2.12	0.217	0.61	0.739
Manta – Verzuolo	3.09	0.132	0.09	0.739
Scarnafigi – Verzuolo	1.59	0.258	1.67	0.739
Bacteria – disease status				
Healthy – Diseased	< 0.01	0.990	1.40	0.237
Fungi - matrix				
Rhizosphere – Root	5.72	0.018	2.13	0.207
Rhizosphere - Soil	1.18	0.261	0.17	0.690
Root – Soil	9.86	0.003	4.23	0.123
Fungi - site				
Fossano – Manta	12.55	0.001	1.32	0.316
Fossano – Scarnafigi	25.53	0.001	5.86	0.034
Fossano – Verzuolo	314.69	0.001	4.47	0.016
Manta – Scarnafigi	0.99	0.344	0.23	0.657
Manta – Verzuolo	147.24	0.001	4.02	0.016
Scarnafigi – Verzuolo	192.12	0.001	13.30	0.006
Fungi – disease status				

Healthy – Diseased	0.82	0.385	1.29	0.261
Oomycetes - matrix				
Rhizosphere – Root	13.16	0.001	3.50	0.147
Rhizosphere - Soil	8.77	0.001	0.48	0.473
Root – Soil	31.00	0.001	1.43	0.319
Oomycetes - site				
Fossano – Manta	1.73	0.304	0.00	0.964
Fossano – Scarnafigi	0.50	0.620	8.88	0.009
Fossano – Verzuolo	14.36	0.003	1.57	0.205
Manta – Scarnafigi	0.64	0.570	14.45	0.006
Manta – Verzuolo	5.64	0.024	2.81	0.121
Scarnafigi – Verzuolo	14.48	0.003	8.97	0.012
Oomycetes – disease status				
Healthy – Diseased	9.68	0.001	6.68	0.011

Table 3 - Network metrics and parameters for root, rhizosphere, and soil microbiota. For each matrix and status, the relative abundance of nodes (for fungi, bacteria and oomycetes) in each network is reported. In addition, the relative abundance of co-presence/co-exclusion nodes is indicated.

Average number of neighbors: average number of nodes connected to each node; network diameter: value of the highest eccentricity of the graph; network radius: length of the lowest eccentricity of the graph; characteristic path length: average path length of the graph; clustering coefficient: average of the clustering coefficient of the graph nodes, defined as the ratio between the number of edges connecting the neighbor nodes and the maximum theoretical number of edges connecting the neighbor nodes; network density: ratio between the number of edges and the theoretical maximum number of edges in the graph; network heterogeneity: measure of the tendency of a graph to present hub nodes, which are nodes with high number of edges; network centralization: measure of the tendency of the graph to have a single hub node; number of connected components: indicates the number of so called “connected components”, which are subgraphs where each node has a pairwise connection to every other node.

	Root		**Rhizosphere**		**Soil**	
	Healthy	Diseased	Healthy	Diseased	Healthy	Diseased
Bacteria	69.47	69.17	62.11	64.25	62.35	63.58
Fungi	29.42	29.09	36.11	34.2	36.28	35.43
Oomycetes	0.07	0.37	1.11	0.6	0.12	0.2
Rhizaria	0.53	0.43	0.48	0.43	0.06	0.07
Archaea	0	0	0	0.33	0.37	0.2
Ichthyosporia	0	0	0.24	0	0.25	0
Unidentified	0.53	1.33	0.36	0.6	0.56	0.52
Copresence	54.21	59.19	54.39	51.6	53.04	48.59
Coexclusion	45.79	40.81	45.61	48.4	46.96	51.41
Number of nodes	1523	1612	1681	1845	1615	1524
Number of edges	8893	8030	9426	10992	8953	8165

Avg. number of neighbors	14.03	19.21	12.15	22.53	14.01	11.5
Network diameter	13	13	12	13	16	12
Network radius	7	7	7	7	8	6
Characteristic path length	8.49	10.53	10.21	8.24	9.13	16.13
Clustering coefficient	2.54	0.19	0.18	3.04	3.03	2.59
Network density	0.01	0.08	0.08	0.07	0.08	0.08
Network heterogeneity	1.28	7.03	4.34	2.57	5.54	7.33
Network centralization	1.07	1.26	1.43	0.59	1.18	2.41
Number of connected components	126	149	88	66	100	60

Figures

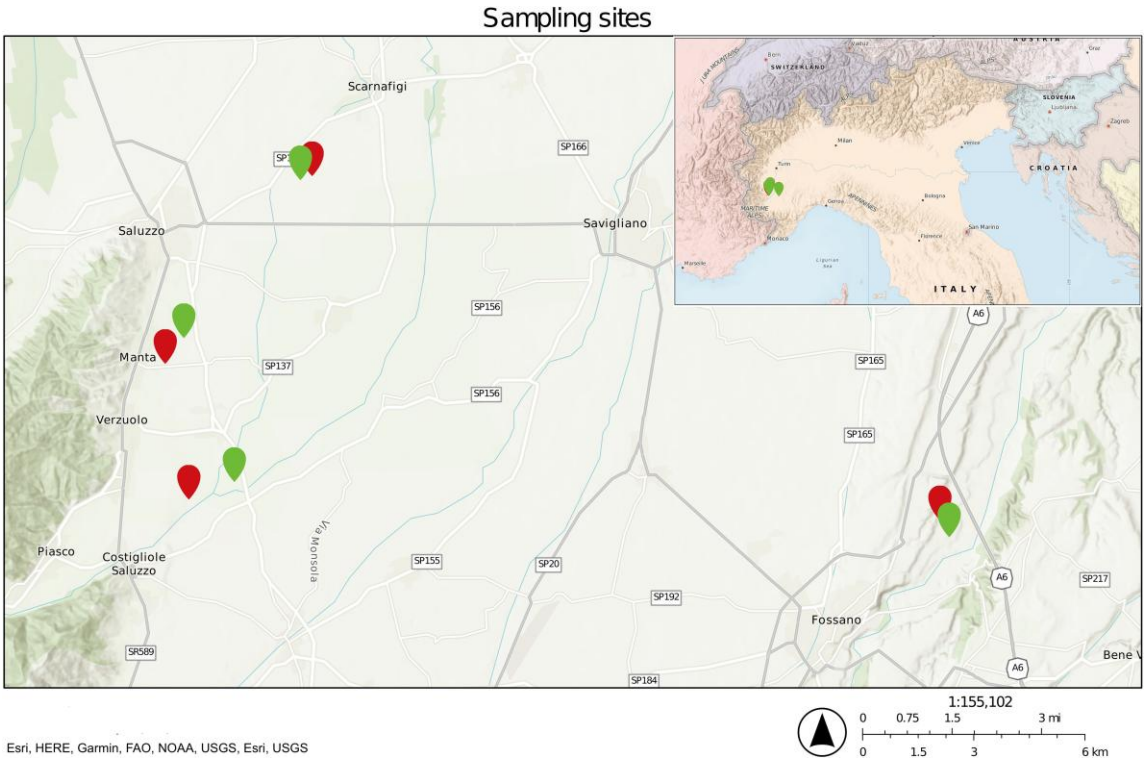


Figure 1 - Sampling site map, green pinpoints refer to healthy sites while red pinpoints to diseased ones.

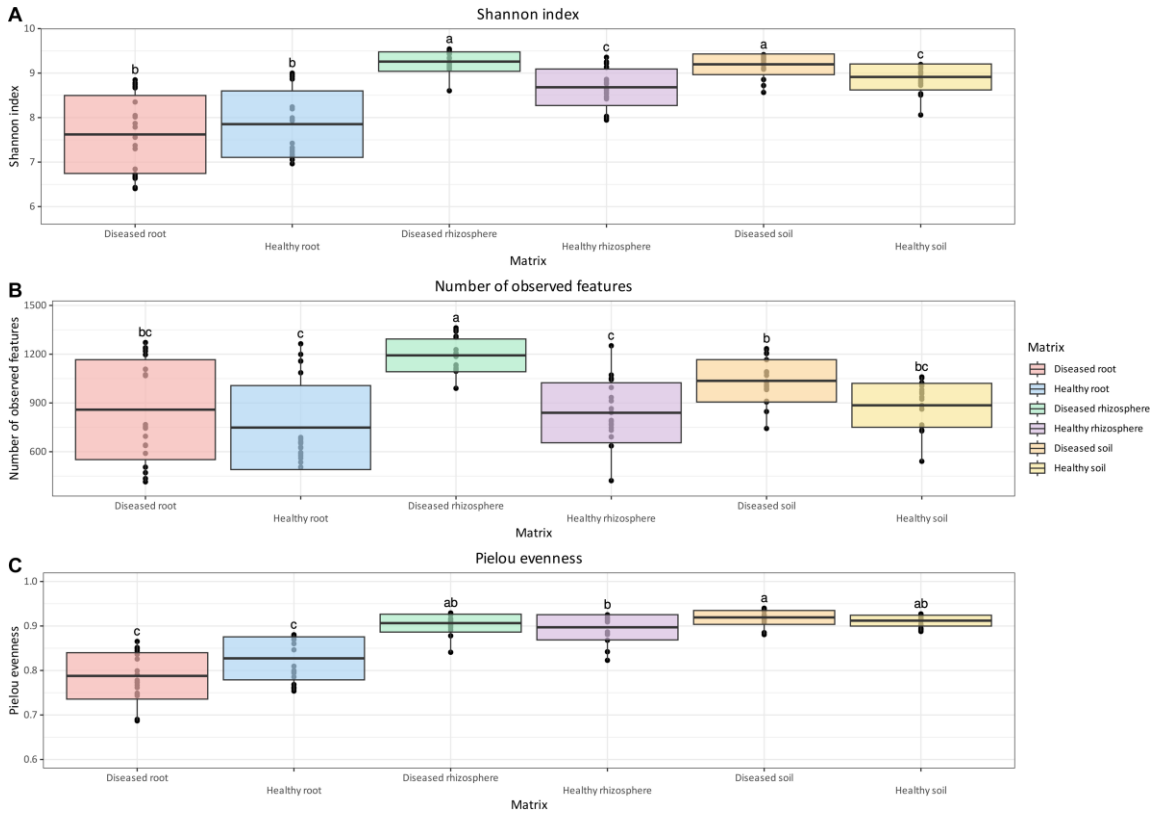


Figure 2 - Box and whisker plot of Shannon Index, number of observed features and Pielou evenness measured across matrix and health status for bacteria. Whiskers extend to ±1.5 interquartile range. Presence of statistically significant differences was assessed by means of a Kruskal-Wallis test, followed by a Dunn post-hoc test with Benjamini-Hochberg p-value correction. Value for H_0 rejection was set at 0.05.

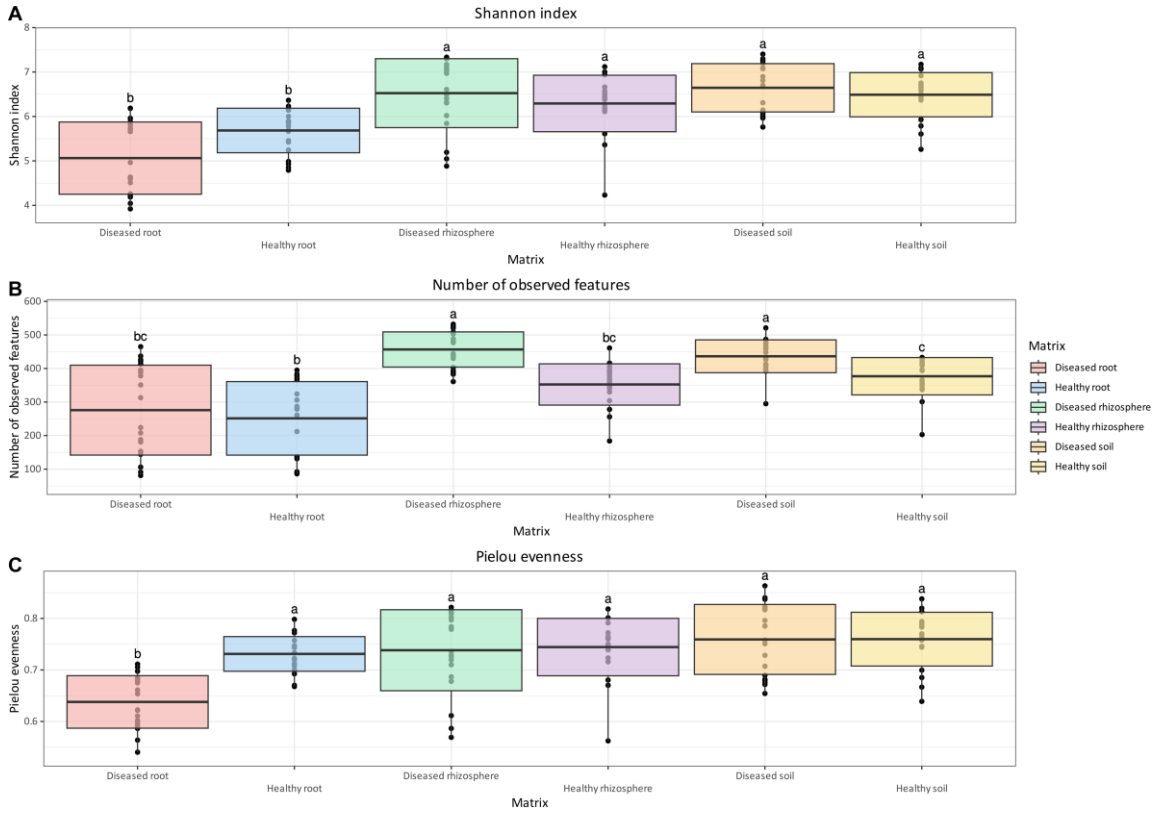


Figure 3 - Box and whisker plot of Shannon Index, number of observed features and Pielou evenness measured across matrix and health status for fungi. Whiskers extend to ±1.5 interquartile range. Presence of statistically significant differences was assessed by means of a Kruskal-Wallis test, followed by a Dunn post-hoc test with Benjamini-Hochberg p-value correction. Value for H_0 rejection was set at 0.05.

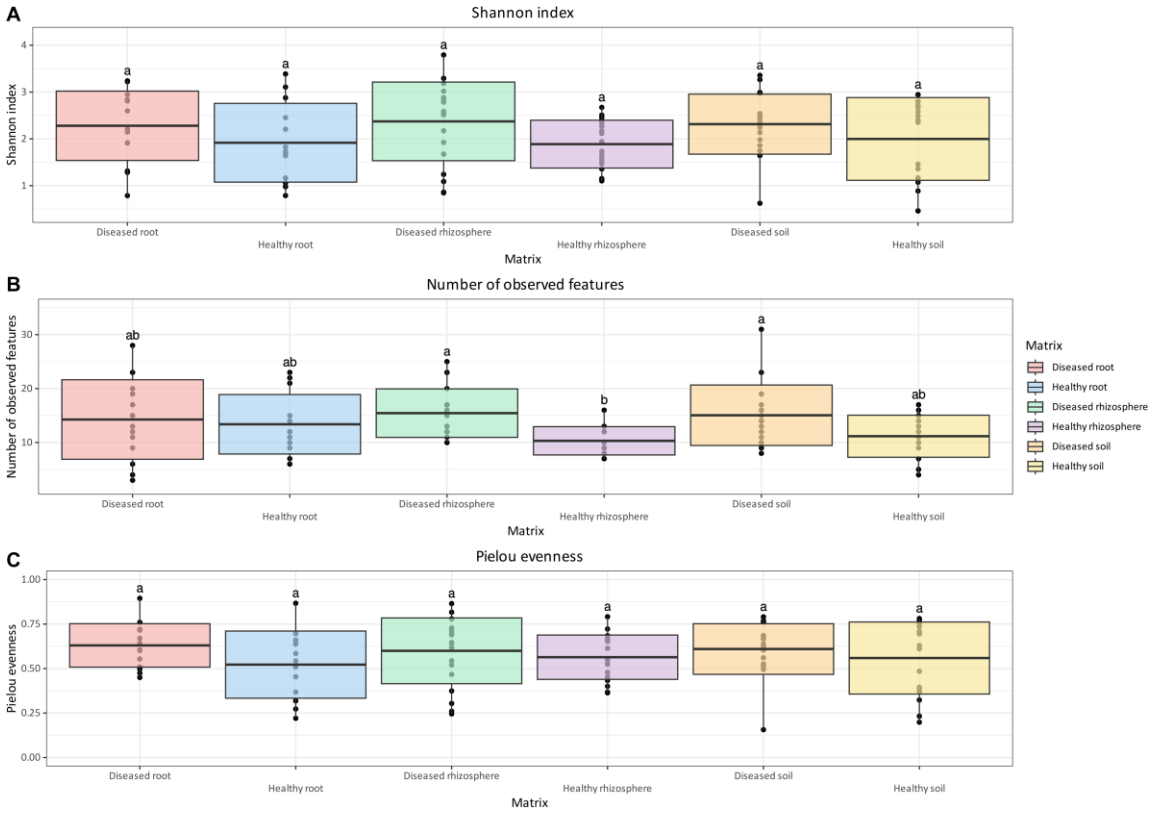


Figure 4 - Box and whisker plot of Shannon Index, number of observed features and Pielou evenness measured across matrix and health status for oomycetes. Whiskers extend to ±1.5 interquartile range. Presence of statistically significant differences was assessed by means of a Kruskal-Wallis test, followed by a Dunn post-hoc test with Benjamini-Hochberg p-value correction. Value for H_0 rejection was set at 0.05.

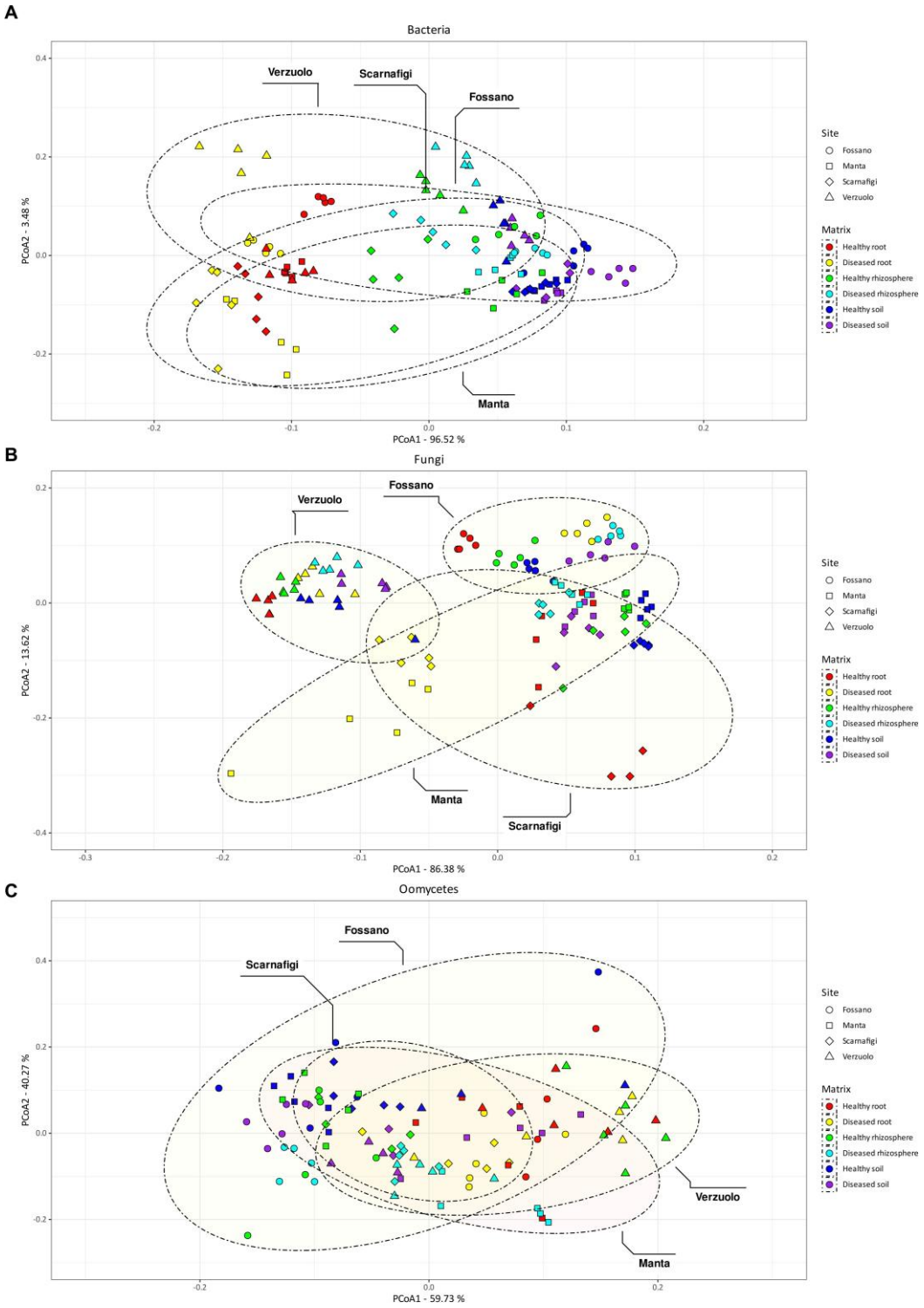


Figure 5 - Non-metric multidimensional scaling (NMDS) plot of Aitchison distances between bacterial samples (a), fungal samples (b) and oomycetes (c). Colors indicate different matrix/health status combination, while shape and ellipsoids are associated with sampling site.

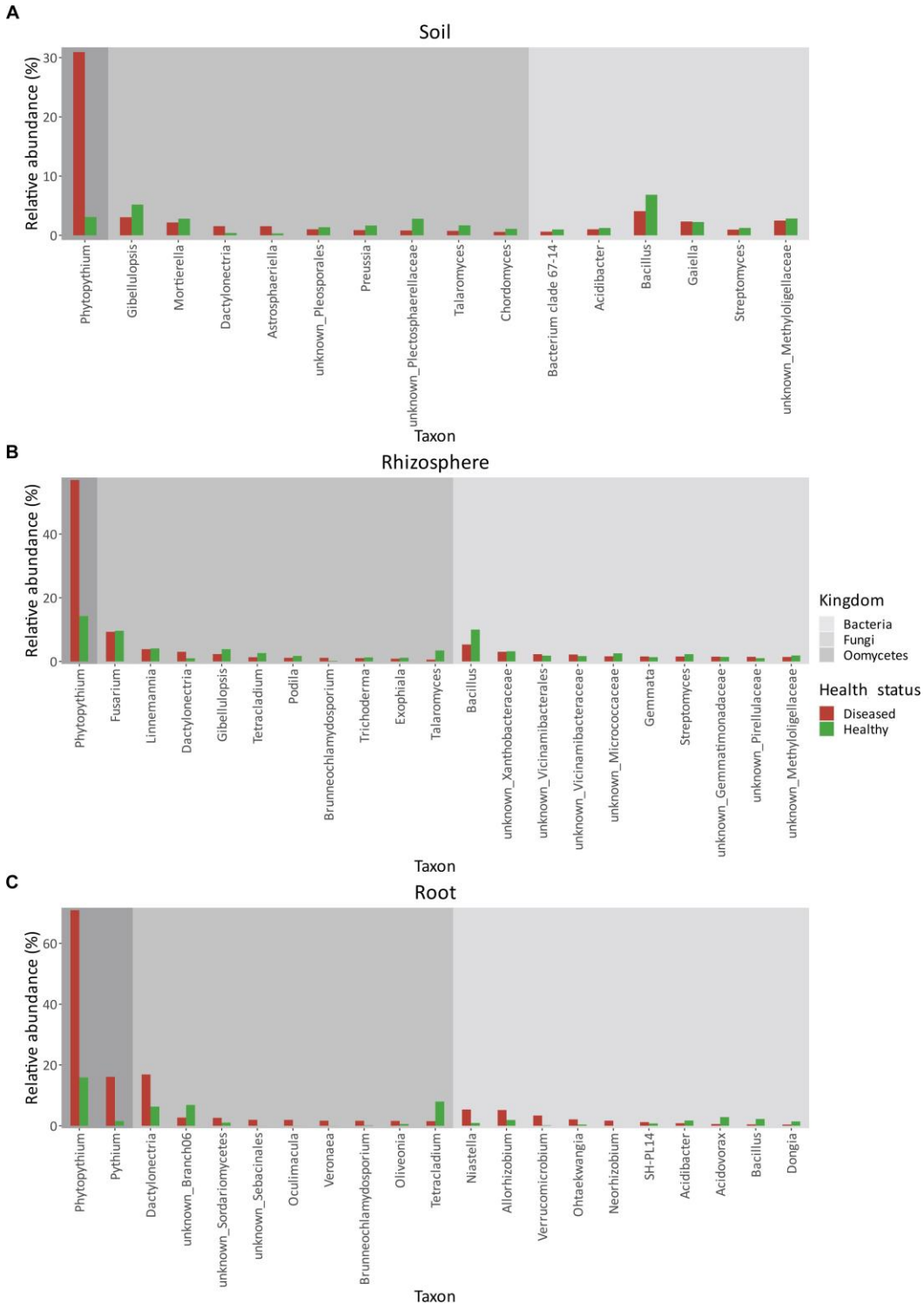


Figure 6 - Relative abundances (%) of bacteria, fungi and oomycetes in soil (a), rhizosphere (b) and root (c) between healthy and diseased orchards. Only taxa with a relative abundance higher than 1% in either condition were considered.

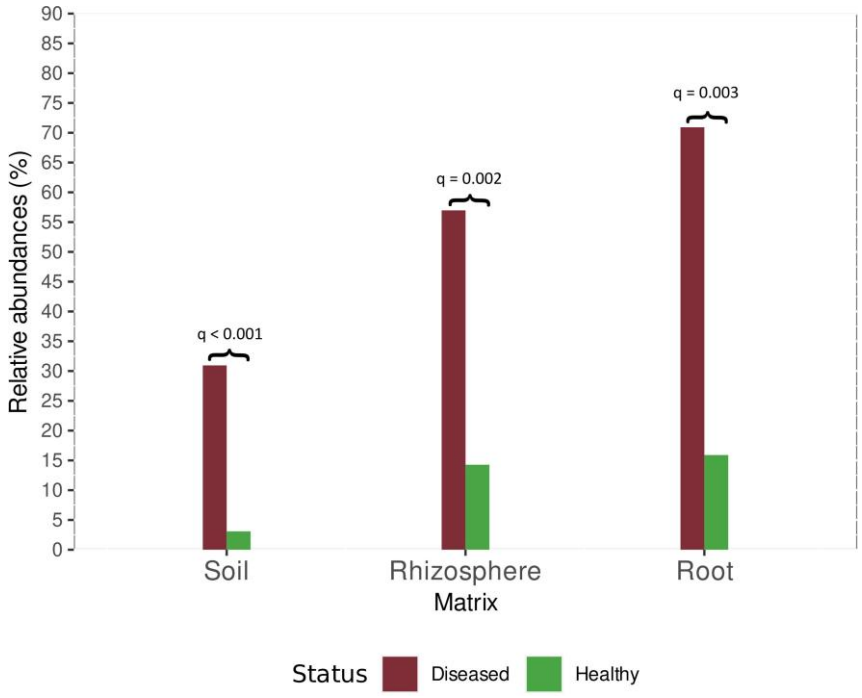


Figure 7 - Relative abundance of *Phytopythium* in healthy and diseased plants for root, rhizosphere, and soil samples. For each comparison the Bonferroni-adjusted p-value is provided, as returned by the Aldex2 analysis.

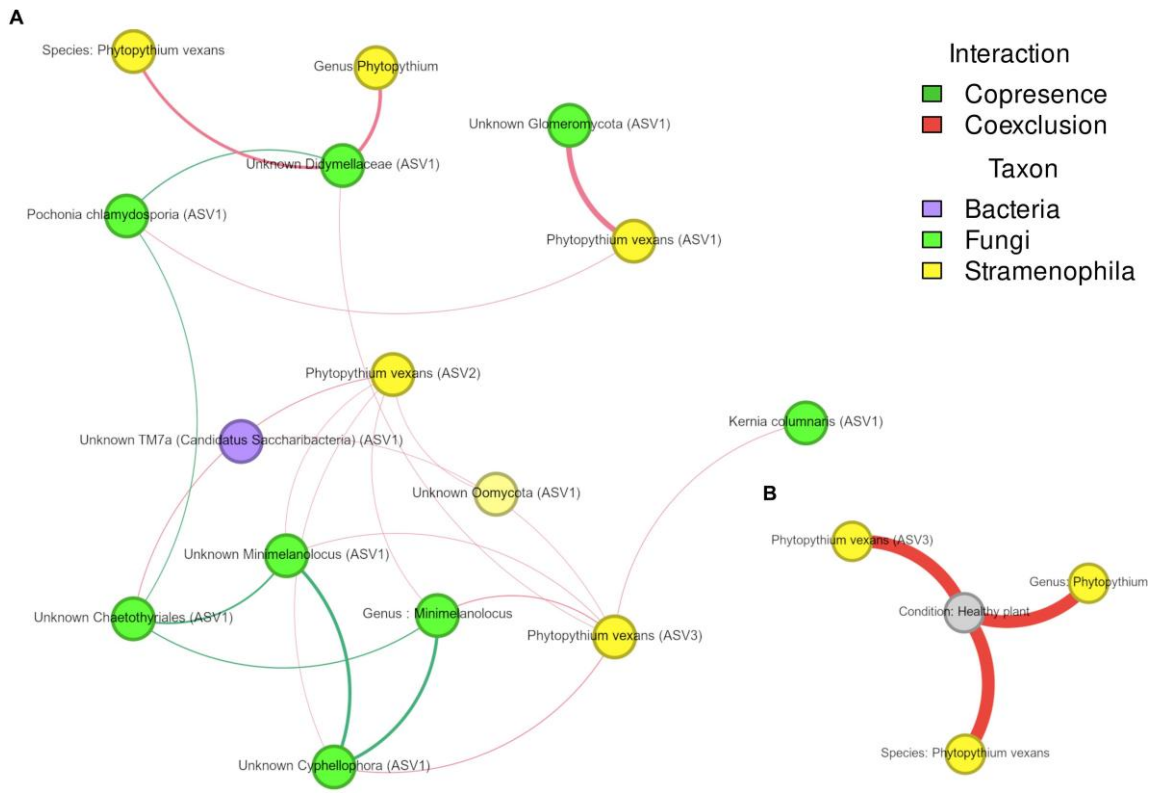


Figure 8 a, b - Association network of *Phytopythium* in microbial communities associated with kiwi plant rhizosphere (a) and soil (b). Edge colour represents association type (co-presence of co-exclusion), while node colour refers to their taxonomic kingdom. Node size is proportional to the number of connections (i.e. degree).

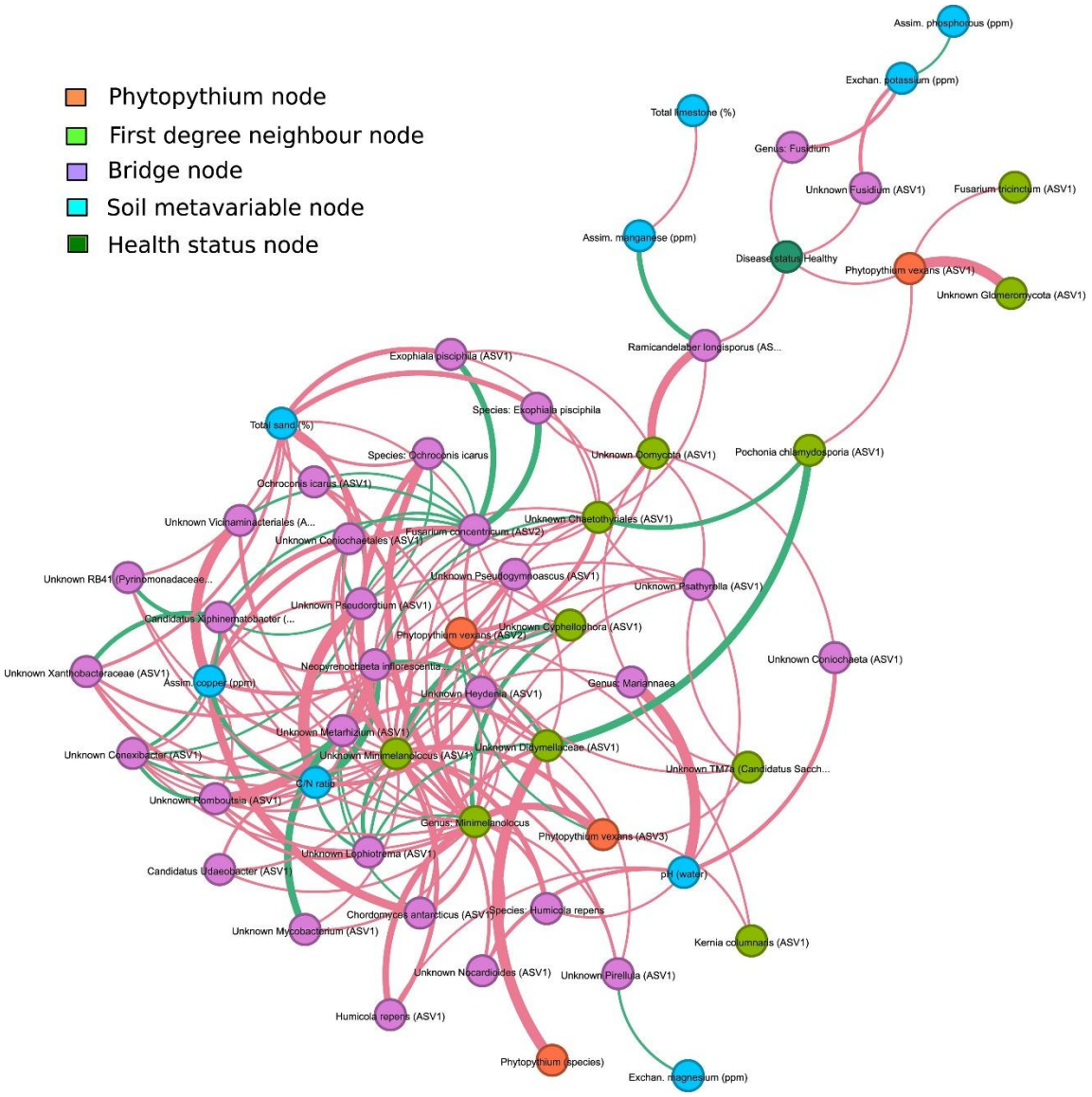


Figure 9 - Interaction network of the rhizosphere microbiome and soil metavariables, filtered to underline interactions between *Phytopythium*, interacting taxa and meta variables. Orange nodes are associated with *Phytopythium*; light green nodes are the first degree neighbour nodes of *Phytopythium*, i.e. have a direct interaction with *Phytopythium*; blue nodes are associated with soil meta variables; dark green nodes are associated with the health status of communities; finally, the purple nodes are bridge nodes, which are defined as nodes sitting on the shortest path between *Phytopythium* and soil metavariables. Edges are coloured based on interaction, which can be either copresence (green) and co exclusion (red). Edge thickness is directly proportional to the strength of interaction.

Supplementary material

Supplementary Table 1 – Sampling locations coordinates and disease incidence as percentage of affected plants.

Orchard code	Health status	City \ Location	North coordinates	East coordinates	Cultivar	Year of plantation	Total surface (ha)	Incidence of diseased plants (%)
S1-PIE01	Healthy	Manta (CN), Italy	N 44.620674	E 7.503988	HAYWARD	2017	1,65	0%
S1-PIE06	Healthy	Scarnafigi (CN), Italy	N 44.658897	E 7.543637	DORI'	2018	1,9	0%
S1-PIE07	Healthy	Fossano (CN), Italy	N 44.572412	E 7.764205	HAYWARD	2017	10,18	0%
S1-PIE09	Healthy	Verzuolo (CN), Italy	N 44.585809	E 7.521155	HAYWARD	1992	1,7	0%
S1-PIE013	Diseased	Manta (CN), Italy	N 44.614417	E 7.497665	HAYWARD	2017	0,73	20%
S1-PIE016	Diseased	Scarnafigi (CN), Italy	N 44.659875	E 7.547601	JINTAO	2016	NA	40%
S1-PIE017	Diseased	Fossano (CN), Italy	N 44.576531	E 7.761048	HAYWARD	2016	6,87	30%
S1-PIE020	Diseased	Verzuolo (CN), Italy	N 44.581535	E 7.505679	HAYWARD	1985	0,8	20%

Supplementary Table 2 – Alpha diversity values

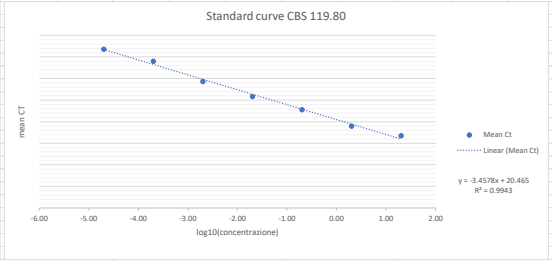
			Shannon			Pielou			Observed features		
Community	Group 1	Group 2	Value 1	Value 2	q value	Value 1	Value 2	q value	Value 1	Value 2	q value
Bacteria	Diseased_rhizosphere (n=20)	Diseased_root (n=20)	9.26±0.22	7.62±0.88	7.880E-10	0.91±0.02	0.79±0.05	5.300E-07	1192.85±100.64	858.80±307.39	1.30E-04
	Diseased_rhizosphere (n=20)	Diseased_soil (n=20)	9.26±0.22	9.20±0.23	7.229E-01	0.91±0.02	0.92±0.02	1.274E-01	1192.85±100.64	1036.20±130.32	4.568E-02
	Diseased_root (n=20)	Diseased_soil (n=20)	7.62±0.88	9.20±0.23	4.000E-09	0.79±0.05	0.92±0.02	4.230E-11	858.80±307.39	1036.20±130.32	1.099E-01
	Diseased_rhizosphere (n=20)	Healthy_rhizosphere (n=20)	9.26±0.22	8.68±0.41	4.187E-04	0.91±0.02	0.90±0.03	5.576E-01	1192.85±100.64	839.60±184.56	1.850E-05
	Diseased_root (n=20)	Healthy_rhizosphere (n=20)	7.62±0.88	8.68±0.41	8.517E-03	0.79±0.05	0.90±0.03	7.270E-06	858.80±307.39	839.60±184.56	6.558E-01
	Diseased_soil (n=20)	Healthy_rhizosphere (n=20)	9.20±0.23	8.68±0.41	1.397E-03	0.92±0.02	0.90±0.03	3.490E-02	1036.20±130.32	839.60±184.56	3.998E-02
	Diseased_rhizosphere (n=20)	Healthy_root (n=20)	9.26±0.22	7.85±0.75	8.110E-09	0.91±0.02	0.83±0.05	3.240E-05	1192.85±100.64	748.65±258.35	1.090E-07
	Diseased_root (n=20)	Healthy_root (n=20)	7.62±0.88	7.85±0.75	6.373E-01	0.79±0.05	0.83±0.05	4.028E-01	858.80±307.39	748.65±258.35	1.505E-01
	Diseased_soil (n=20)	Healthy_root (n=20)	9.20±0.23	7.85±0.75	5.130E-08	0.92±0.02	0.83±0.05	1.090E-08	1036.20±130.32	748.65±258.35	1.494E-03
	Healthy_rhizosphere (n=20)	Healthy_root (n=20)	8.68±0.41	7.85±0.75	2.915E-02	0.90±0.03	0.83±0.05	3.438E-04	839.60±184.56	748.65±258.35	3.542E-01
	Diseased_rhizosphere (n=20)	Healthy_soil (n=20)	9.26±0.22	8.91±0.29	1.026E-02	0.91±0.02	0.91±0.01	5.124E-01	1192.85±100.64	885.55±135.16	5.700E-05
	Diseased_root (n=20)	Healthy_soil (n=20)	7.62±0.88	8.91±0.29	3.414E-04	0.79±0.05	0.91±0.01	1.170E-08	858.80±307.39	885.55±135.16	8.043E-01
	Diseased_soil (n=20)	Healthy_soil (n=20)	9.20±0.23	8.91±0.29	2.560E-02	0.92±0.02	0.91±0.01	3.884E-01	1036.20±130.32	885.55±135.16	6.927E-02
	Healthy_rhizosphere (n=20)	Healthy_soil (n=20)	8.68±0.41	8.91±0.29	3.341E-01	0.90±0.03	0.91±0.01	2.661E-01	839.60±184.56	885.55±135.16	8.002E-01
	Healthy_root (n=20)	Healthy_soil (n=20)	7.85±0.75	8.91±0.29	1.644E-03	0.83±0.05	0.91±0.01	1.420E-06	748.65±258.35	885.55±135.16	2.221E-01
Fungi	Diseased_rhizosphere (n=20)	Diseased_root (n=20)	6.52±0.78	5.06±0.81	2.000E-06	0.74±0.08	0.64±0.05	3.890E-05	456.70±52.42	275.85±134.01	3.00E-06
	Diseased_rhizosphere (n=20)	Diseased_soil (n=20)	6.52±0.78	6.65±0.54	7.929E-01	0.74±0.08	0.76±0.07	6.71E-01	456.70±52.42	436.40±48.98	5.470E-01
	Diseased_root (n=20)	Diseased_soil (n=20)	5.06±0.81	6.65±0.54	6.480E-07	0.64±0.05	0.76±0.07	3.73E-06	275.85±134.01	436.40±48.98	4.270E-05
	Diseased_rhizosphere (n=20)	Healthy_rhizosphere (n=20)	6.52±0.78	6.29±0.64	4.267E-01	0.74±0.08	0.74±0.06	9.24E-01	456.70±52.42	352.35±61.52	6.470E-05
	Diseased_root (n=20)	Healthy_rhizosphere (n=20)	5.06±0.81	6.29±0.64	1.059E-04	0.64±0.05	0.74±0.06	3.33E-05	275.85±134.01	352.35±61.52	4.900E-01
	Diseased_soil (n=20)	Healthy_rhizosphere (n=20)	6.65±0.54	6.29±0.64	2.999E-01	0.76±0.07	0.74±0.06	6.94E-01	436.40±48.98	352.35±61.52	6.669E-04
	Diseased_rhizosphere (n=20)	Healthy_root (n=20)	6.52±0.78	5.68±0.50	2.845E-04	0.74±0.08	0.73±0.03	5.25E-01	456.70±52.42	251.35±109.64	6.240E-09
	Diseased_root (n=20)	Healthy_root (n=20)	5.06±0.81	5.68±0.50	2.975E-01	0.64±0.05	0.73±0.03	1.99E-03	275.85±134.01	251.35±109.64	2.610E-01
	Diseased_soil (n=20)	Healthy_root (n=20)	6.65±0.54	5.68±0.50	1.042E-04	0.76±0.07	0.73±0.03	2.24E-01	436.40±48.98	251.35±109.64	1.230E-07
	Healthy_rhizosphere (n=20)	Healthy_root (n=20)	6.29±0.64	5.68±0.50	8.197E-03	0.74±0.06	0.73±0.03	5.09E-01	352.35±61.52	251.35±109.64	6.824E-02
	Diseased_rhizosphere (n=20)	Healthy_soil (n=20)	6.52±0.78	6.49±0.50	8.486E-01	0.74±0.08	0.76±0.05	6.84E-01	456.70±52.42	376.95±55.69	3.655E-03
	Diseased_root (n=20)	Healthy_soil (n=20)	5.06±0.81	6.49±0.50	3.620E-06	0.64±0.05	0.76±0.05	3.81E-06	275.85±134.01	376.95±55.69	7.953E-02
	Diseased_soil (n=20)	Healthy_soil (n=20)	6.65±0.54	6.49±0.50	6.937E-01	0.76±0.07	0.76±0.05	9.63E-01	436.40±48.98	376.95±55.69	2.096E-02
	Healthy_rhizosphere (n=20)	Healthy_soil (n=20)	6.29±0.64	6.49±0.50	5.166E-01	0.74±0.06	0.76±0.05	7.032E-01	352.35±61.52	376.95±55.69	2.886E-01
	Healthy_root (n=20)	Healthy_soil (n=20)	5.68±0.50	6.49±0.50	5.235E-04	0.73±0.03	0.76±0.05	2.003E-01	251.35±109.64	376.95±55.69	3.497E-03
Oomycetes	Diseased_rhizosphere (n=20)	Diseased_Root (n=15)	2.37±0.84	2.28±0.74	7.484E-01	0.60±0.18	0.63±0.12	9.661E-01	15.45±4.50	14.27±7.37	4.896E-01
	Diseased_rhizosphere (n=20)	Diseased_Soil (n=18)	2.37±0.84	2.31±0.64	7.879E-01	0.60±0.18	0.61±0.14	9.641E-01	15.45±4.50	15.06±5.61	6.760E-01
	Diseased_Root (n=15)	Diseased_Soil (n=18)	2.28±0.74	2.31±0.64	9.983E-01	0.63±0.12	0.61±0.14	1.000E+00	14.27±7.37	15.06±5.61	6.489E-01
	Diseased_rhizosphere (n=20)	Healthy_rhizosphere (n=19)	2.37±0.84	1.89±0.51	2.531E-01	0.60±0.18	0.56±0.12	9.401E-01	15.45±4.50	10.32±2.63	7.871E-03
	Diseased_Root (n=15)	Healthy_rhizosphere (n=19)	2.28±0.74	1.89±0.51	2.904E-01	0.63±0.12	0.56±0.12	8.043E-01	14.27±7.37	10.32±2.63	1.102E-01
	Diseased_Soil (n=18)	Healthy_rhizosphere (n=19)	2.31±0.64	1.89±0.51	4.803E-01	0.61±0.14	0.56±0.12	6.697E-01	15.06±5.61	10.32±2.63	2.772E-02
	Diseased_rhizosphere (n=20)	Healthy_Root (n=13)	2.37±0.84	1.92±0.84	3.383E-01	0.60±0.18	0.52±0.19	1.000E+00	15.45±4.50	13.38±5.52	2.884E-01
	Diseased_Root (n=15)	Healthy_Root (n=13)	2.28±0.74	1.92±0.84	4.096E-01	0.63±0.12	0.52±0.19	1.000E+00	14.27±7.37	13.38±5.52	6.452E-01
	Diseased_Soil (n=18)	Healthy_Root (n=13)	2.31±0.64	1.92±0.84	5.225E-01	0.61±0.14	0.52±0.19	7.979E-01	15.06±5.61	13.38±5.52	4.505E-01
	Healthy_rhizosphere (n=19)	Healthy_Root (n=13)	1.89±0.51	1.92±0.84	8.040E-01	0.56±0.12	0.52±0.19	8.451E-01	10.32±2.63	13.38±5.52	2.709E-01
	Diseased_rhizosphere (n=20)	Healthy_Soil (n=18)	2.37±0.84	2.00±0.88	4.461E-01	0.60±0.18	0.56±0.20	9.010E-01	15.45±4.50	11.17±3.90	6.825E-02
	Diseased_Root (n=15)	Healthy_Soil (n=18)	2.28±0.74	2.00±0.88	6.310E-01	0.63±0.12	0.56±0.20	9.954E-01	14.27±7.37	11.17±3.90	3.851E-01
	Diseased_Soil (n=18)	Healthy_Soil (n=18)	2.31±0.64	2.00±0.88	6.660E-01	0.61±0.14	0.56±0.20	8.648E-01	15.06±5.61	11.17±3.90	1.587E-01
	Healthy_rhizosphere (n=19)	Healthy_Soil (n=18)	1.89±0.51	2.00±0.88	5.966E-01	0.56±0.12	0.56±0.20	1.000E+00	10.32±2.63	11.17±3.90	4.725E-01
	Healthy_Root (n=13)	Healthy_Soil (n=18)	1.92±0.84	2.00±0.88	7.594E-01	0.52±0.19	0.56±0.20	7.754E-01	13.38±5.52	11.17±3.90	5.764E-01

Supplementary Table 3 – Chemico-physical analysis of soils

	Healthy orchards				Diseased orchards			
Orchard code	S1-PIE01	S1-PIE06	S1-PIE07	S1-PIE09	S1-PIE013	S1-PIE016	S1-PIE017	S1-PIE020
Clay (%)	8.18	9.65	7.28	5.13	10.78	8.95	8.77	6.97
Silt (%)	48.10	43.40	33.08	25.55	49.02	45.15	31.95	36.88
Sand (%)	43.72	46.95	59.65	69.33	40.20	45.90	59.27	56.15
pH (water)	6.24	7.41	6.80	7.45	6.71	7.23	6.98	7.36
Total limestone (%)	0.39	0.59	0.78	0.78	0.39	0.39	0.59	0.39
Organic matter (%)	2,047	2,358	3,803	2,514	1,389	1,841	4,170	2,496
Organic carbon (%)	1,190	1,371	2,211	1,462	0.807	1,070	2,424	1,451
Total nitrogen (%)	0.1551	0.1740	0.2430	0.1556	0.1008	0.1483	0.2789	0.1575
C/N ratio	7.7	7.9	9.1	9.4	8.0	7.2	8.7	9.2
CSC (meq/100g)	15.1	11.3	14.0	10.2	11.8	11.9	14.6	12.2
Exchanged calcium (ppm)	1709	1649	1701	1651	1496	1570	1909	1904
Exchanged calcium (meq/100g)	8.53	8.23	8.49	8.24	7.46	7.83	9.53	9.50
Exchanged calcium on CSC (%)	56.6	72.8	60.4	81.0	63.5	65.6	65.4	78.1
Exchanged magnesium (ppm)	157	163	144	101	159	174	192	118
Exchanged magneisum (meq/100g)	1.29	1.34	1.19	0.83	1.31	1.43	1.58	0.97
Exchanged magnesium on CSC (%)	8.6	11.9	8.5	8.2	11.1	12.0	10.8	8.0
Exchanged potassium (ppm)	76	474	437	89	99	71	482	61
Exchanged potassium (meq/100g)	0.195	1,212	1,117	0.227	0.254	0.181	1,232	0.157
Exchanged potassium on CSC (%)	0.013	0.107	0.080	0.022	0.022	0.015	0.085	0.013
Ca/Mg ratio	6.6	6.1	7.1	9.9	5.7	5.5	6.0	9.8
Ca/K ratio	43.7	6.8	7.6	36.3	29.4	43.4	7.7	60.7
Mg/K ratio	6.6	1.1	1.1	3.7	5.1	7.9	1.3	6.2
Basic saturation	66.4	95.4	76.8	91.5	76.7	79.0	84.7	87.3
Phosphorous assim. (ppm)	17.2	95.6	179.4	52.8	43.7	21.2	186.4	41.5
Phosphorous pentoxide assim. (ppm)	39.3	218.9	410.9	120.9	100.0	48.6	426.8	95.1
Iron assim. (ppm)	150	75	132	45	86	51	147	56
Manganese assim. (ppm)	12.8	7.9	5.7	4.4	15.2	13.0	9.3	13.9
Zinc assim. (ppm)	2.6	2.3	14.5	6.5	3.6	1.8	18.2	6.5
Copper assim. (ppm)	4.7	2.2	13.5	13.5	5.7	4.9	11.7	25.3
B solubile (ppm)	0.2340	0.3380	0.4710	0.2530	0.3210	0.2460	0.4720	0.2060

Supplementary Table 4 - qPCR quantification of *Ph ytopythium vexans* in samples

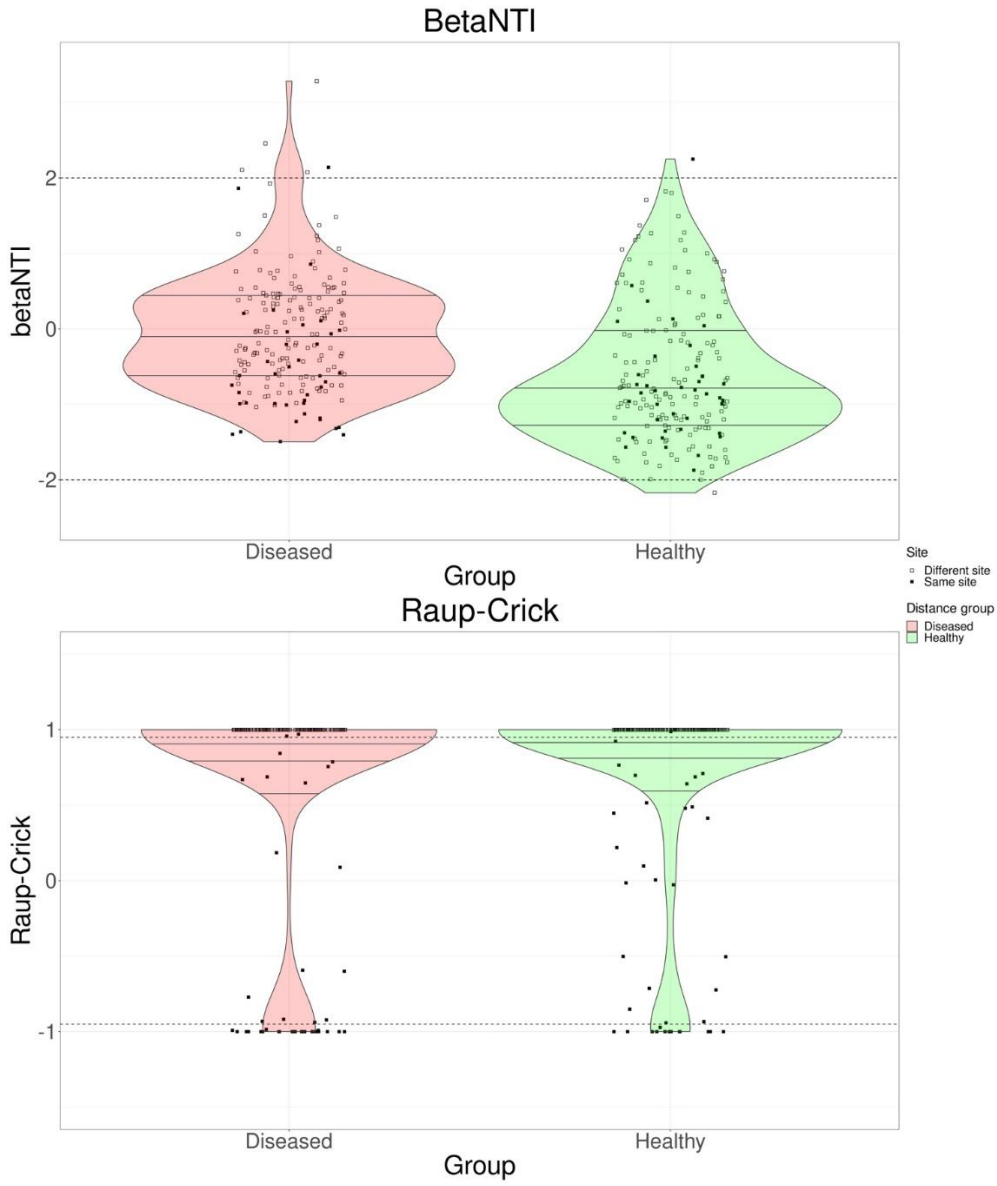
Sample	[ng/uL]	Dilution factor	Ct	Ct Mean	Dev. St	X log	Mean Ct
A rep1	20.00	1.00E+00	16.6732635	16.73	0.07	1.30	16.73
A rep2	20.00	1.00E+00	16.6345139			0.30	18.94
A rep3	20.00	1.00E+00	16.8157005			-0.70	22.79
B rep1	20.00	1.00E+00	16.8048744			-1.70	25.80
B rep2	20.00	1.00E+00	16.7276955			-2.699	29.32
B rep3	20.00	1.00E+00	16.743351			-3.6990	34.01
A rep1	2.00	1.00E-01	18.5842304	18.9433673	0.4677695	-4.69897	36.79
A rep2	2.00	1.00E-01	18.8185005				
A rep3	2.00	1.00E-01	18.2549362				
B rep1	2.00	1.00E-01	19.383955				
B rep2	2.00	1.00E-01	19.3917999				
B rep3	2.00	1.00E-01	19.2267818				
A rep1	0.20	1.00E-02	23.0799847	22.7877763	0.27793844		
A rep2	0.20	1.00E-02	22.986536				
A rep3	0.20	1.00E-02	22.6634769				
B rep1	0.20	1.00E-02	22.3780575				
B rep2	0.20	1.00E-02	23.0056572				
B rep3	0.20	1.00E-02	22.6129456				
A rep1	0.02	1.00E-03	26.6639919	25.8031286	0.87960207		
A rep2	0.02	1.00E-03	26.8112221				
A rep3	0.02	1.00E-03	26.2960453				
B rep1	0.02	1.00E-03	25.079916				
B rep2	0.02	1.00E-03	25.0195217				
B rep3	0.02	1.00E-03	24.9480743				
A rep1	0.002	1.00E-04	30.8242931	29.3150228	0.91921875		
A rep2	0.002	1.00E-04	29.4278316				
A rep3	0.002	1.00E-04	29.8747387				
B rep1	0.002	1.00E-04	28.7035866				
B rep2	0.002	1.00E-04	28.6136379				
B rep3	0.002	1.00E-04	28.4460487				
A rep1	0.0002	1.00E-05	37.0895424	34.0102135	2.005745		
A rep2	0.0002	1.00E-05	34.1145401				
A rep3	0.0002	1.00E-05	35.5915833				
B rep1	0.0002	1.00E-05	31.963213				
B rep2	0.0002	1.00E-05	32.9955444				
B rep3	0.0002	1.00E-05	32.3068581				
A rep1	0.00002	1.00E-06	38.1553688	36.7861195	19.0369774		
A rep2	0.00002	1.00E-06	38.1555862				
A rep3	0.00002	1.00E-06	35.7635536				
B rep1	0.00002	1.00E-06	Undetermine				
B rep2	0.00002	1.00E-06	Undetermine				
B rep3	0.00002	1.00E-06	35.0699692				



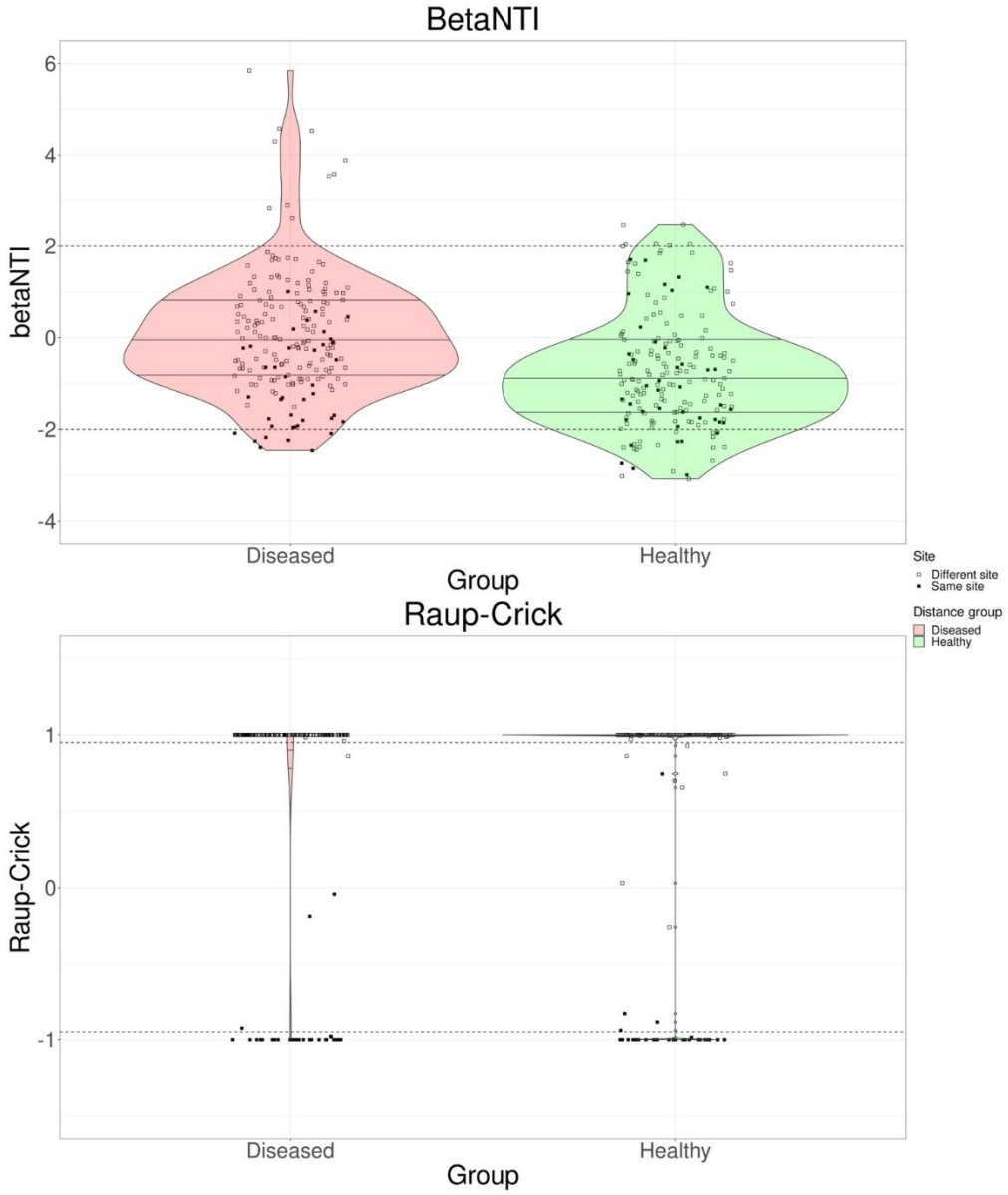
Slope	-3.4578428
Y-intercept	20.465
Efficiency (%	95%
R^2	0.994
amplific. Eff	1.94624562

Quantification of samples

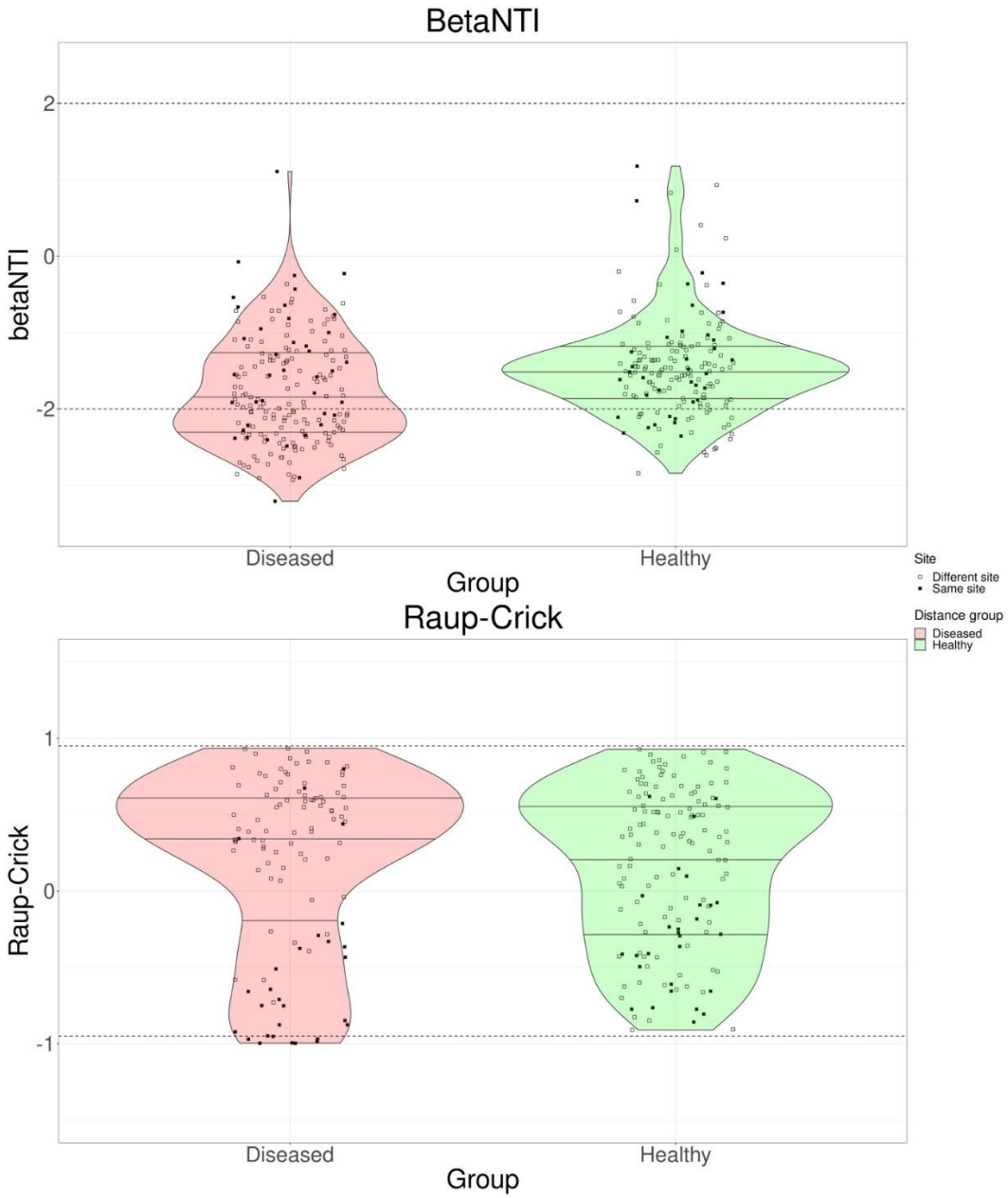
sample ID		Ct samples			mean Ct (Y)	X (expressed as log)	Target quantity	Standard Deviation				
SOIL	7	34.930397	34.8259392	33.8186531	34.52499644	-4.0660988	8.59E-05	0.61393692				
	7	34.2942123	34.8527718	34.7581978	34.63506063	-4.0979291	7.98E-05	0.29894686				
	7	34.7000771	34.6364861	34.9335632	34.75670878	-4.1331094	7.36022E-05	0.15642595				
	17	33.4827309	33.9374466	33.9190559	33.77974447	-3.8505737	0.000141067	0.25738563				
	17	34.1619263	33.6009598	34.4167175	34.05986786	-3.9315847	0.000117062	0.41734532			ng/uL target	status
	17	33.7270164	34.9504204	33.4896164	34.05568441	-3.9303748	0.000117388	0.78390308		S7	7.98E-03	healthy
	9	35.2378578	34.1233444	37.0473595	35.46952057	-4.3392529	4.57875E-05	1.47570889		S17	0.01251725	diseased
	9	30.7824421	31.3992081	31.4613037	31.21431796	-3.1086583	0.000778649	0.37530193		S9	0.04847188	healthy
	9	31.4932842	31.7664566	31.339592	31.53311094	-3.2008525	0.00062972	0.21620124		S20	0.01307076	diseased
	20	34.3526192	34.0279045	33.7165565	34.03236008	-3.9236295	0.000119226	0.31805472		S1	0.01111712	healthy
	20	33.9360657	33.3867302	33.7497444	33.69084676	-3.8248647	0.00014967	0.27936368		S13	0.00706071	diseased
	20	34.0787964	33.9579544	33.9116287	33.98279317	-3.9092949	0.000123227	0.08630747		S6	0.0088356	healthy
	1	34.4050713	34.2703285	33.7514229	34.14227422	-3.9554164	0.000110811	0.34512676		S16	0.00901601	diseased
	1	33.4050636	34.3427467	33.8660088	33.87127304	-3.8770435	0.000132726	0.46886372				
	1	34.7770348	34.655735	33.9324036	34.45505778	-4.0458727	8.99761E-05	0.45667711				
	13	34.5057373	33.8982277	34.6007156	34.33489354	-4.0111215	9.74717E-05	0.38113386				
	13	34.8268013	34.72929	34.6507263	34.73560588	-4.1270065	7.46438E-05	0.08820724				
	13	35.3936577	35.7301216	35.9268379	35.68353907	-4.4011466	3.97058E-05	0.26962519				
	6	34.3611298	33.5576591	33.6877518	33.86884689	-3.8763419	0.000132941	0.43126307				
	6	34.9390717	34.4335976	34.6087723	34.6604805	-4.1052804	7.84729E-05	0.25667357				
	6	35.3504829	34.9372711	35.406517	35.2314237	-4.2703959	5.36542E-05	0.25627965				
	16	33.967392	34.0086975	33.6918793	33.88932292	-3.8822635	0.00013114	0.17223394				
	16	35.7651787	35.9509506	36.6722031	36.12944412	-4.5301013	2.95052E-05	0.47913282				
	16	34.0984459	33.9439201	34.4243279	34.15556463	-3.95926	0.000109835	0.24524438				
ROOT	7	35.8526955	35.1574326	34.2259712	35.07869975	-4.2262285	5.9398E-05	0.8162151				
	7	34.8937721	37.007328	35.5737381	35.82494609	-4.4420412	3.61376E-05	1.07893871				
	7	35.3769379	34.4161949	34.7841034	34.85907873	-4.1627146	6.8752E-05	0.48473986				
	17	36.8907089	34.7762756	34.8222809	35.49642181	-4.3470327	4.49746E-05	1.20770714				
	17	34.9579277	36.5552444	35.0105247	35.50789897	-4.3503519	4.46322E-05	0.90740896			ng/uL target	status
	17	35.9609528	36.0754051	35.9694901	36.00194931	-4.4932301	3.21196E-05	0.06375765		R7	5.48E-03	healthy
	9	35.4862595	35.9001312	35.068222	35.48487091	-4.3436922	4.53219E-05	0.41595633		R17	4.06E-03	diseased
	9	35.5149078	35.2312622	35.963974	35.57004801	-4.3683252	4.28228E-05	0.36945497		R9	4.44E-03	healthy
	9	35.0816383	35.4482155	35.9491386	35.49299749	-4.3460424	4.50773E-05	0.4354805		R20	6.30E-03	diseased
	20	34.6927643	35.0832977	34.8254318	34.86716461	-4.165053	6.83828E-05	0.19858326		R1	7.55E-03	healthy
	20	34.650013	33.998333	34.5472527	34.39853287	-4.0295258	9.34274E-05	0.35037107		R13	1.41E-03	diseased
	20	37.0111313	35.7504997	36.0045547	36.25539525	-4.566526	2.71315E-05	0.66669986		R6	3.11E-03	healthy
	1	36.668335	37.0426407	39.5983009	37.76975886	-5.0044764	9.89746E-06	1.59458483		R16	3.17E-03	diseased
	1	33.5532265	33.1509972	34.5178413	33.74068832	-3.8392787	0.000144784	0.70244018				
	1	33.7324524	33.9319992	36.7083359	34.79092916	-4.1430059	7.19439E-05	1.6635177				
	13	Undetermine	Undetermine	37.2405777	37.2405777	-4.8514385	1.40787E-05	#DIV/0!				
	13	Undetermine	Undetermine	Undetermine	#DIV/0!	#DIV/0!	#DIV/0!	#DIV/0!				
	13	Undetermine	Undetermine	Undetermine	#DIV/0!	#DIV/0!	#DIV/0!	#DIV/0!				
	6	37.2102852	33.5955505	35.4770813	35.42763901	-4.3271409	4.70825E-05	1.80787446				
	6	37.2889786	36.7859955	37.2965164	37.12383016	-4.8176754	1.52168E-05	0.29259769				
	6	Undetermine	Undetermine	Undetermine	#DIV/0!	#DIV/0!	#DIV/0!	#DIV/0!				
	16	36.9658775	35.9762306	36.8309708	36.59102631	-4.6635898	2.16975E-05	0.53668451				
	16	36.1062241	36.2993813	35.1242332	35.84327952	-4.4473431	3.56991E-05	0.63015719				
	16	36.5949974	35.4494095	35.2254143	35.75660706	-4.4222777	3.78201E-05	0.73465451				
RHIZOSPHERE	7	34.2326508	33.7108078	33.800499	33.91465251	-3.8895887	0.000128947	0.27902203				
	7	33.8931389	34.4019737	34.5132256	34.26944606	-3.9921942	0.000101814	0.33060483				
	7	33.932682	33.5866966	33.1667557	33.56204478	-3.7876154	0.000163074	0.3835578				
	17	33.5802422	33.6588173	33.9726868	33.7372487	-3.838284	0.000145116	0.20764588				
	17	33.6068459	33.4105072	33.887146	33.63483302	-3.8086656	0.000155358	0.23954873			ng/uL target	status
	17	33.5789375	34.3794937	33.9363861	33.96493912	-3.9041315	0.000124701	0.40104115		RS7	0.00013128	healthy
	9	33.7332191	33.8828697	33.9244041	33.846831	-3.8699749	0.000134904	0.10055853		RS17	0.00014173	diseased
	9	33.7106972	33.7388916	33.9765053	33.80869802	-3.858947	0.000138374	0.1460075		RS9	0.00011872	healthy
	9	34.6388016	34.6888733	34.4074249	34.5783666	-4.0815333	8.28832E-05	0.15014188		RS20	0.00014901	diseased
	20	33.9349251	33.9467468	33.5165901	33.79942067	-3.856264	0.000139231	0.24500976		RS1	0.00013731	healthy
	20	33.6148376	33.4222946	33.7162971	33.58447647	-3.7941026	0.000160656	0.14933427		RS13	7.368E-05	diseased
	20	33.7036858	33.7748566	33.6706848	33.71640905	-3.8322572	0.000147144	0.05323861		R6	0.00018202	healthy
	1	34.3727379	33.6283951	33.8527908	33.95130793	-3.9001894	0.000125838	0.38182557		R16	0.00013201	diseased
	1	33.7800064	33.8124542	33.6281319	33.7401975	-3.8391368	0.000144832	0.0983984				
	1	33.9326706	33.5988274	33.8019409	33.77781296	-3.8500151	0.000141249	0.16822439				
	13	34.4333954	34.2700577	33.9467392	34.21673075	-3.9769491	0.000105451	0.24767192				
	13	Undetermine	Undetermine	Undetermine	#DIV/0!	#DIV/0!	0	#DIV/0!				
	13	34.180954	33.9286995	34.1269493	34.07886759	-3.9370794	0.00011559	0.13282308				
	6	33.9740448	33.5805321	33.4927673	33.68244807	-3.8224358	0.00015051	0.25631456				
	6	32.4789085	33.4625816	32.9638519	32.96844737	-3.6159484	0.000242132	0.49185265				
	6	33.9353294	33.6806297	33.3451805	33.65371323	-3.8141257	0.000153417	0.29599377				
	16	34.9358788	33.7565918	34.6105766	34.43434906	-4.0398838	9.12255E-05	0.60907434				
	16	33.9057198	33.6317978	33.8802986	33.80593872	-3.858149	0.000138628	0.15134516				
	16	33.3027039	33.4459801	33.8522301	33.533638	-3.7794002	0.000166188	0.28505736				



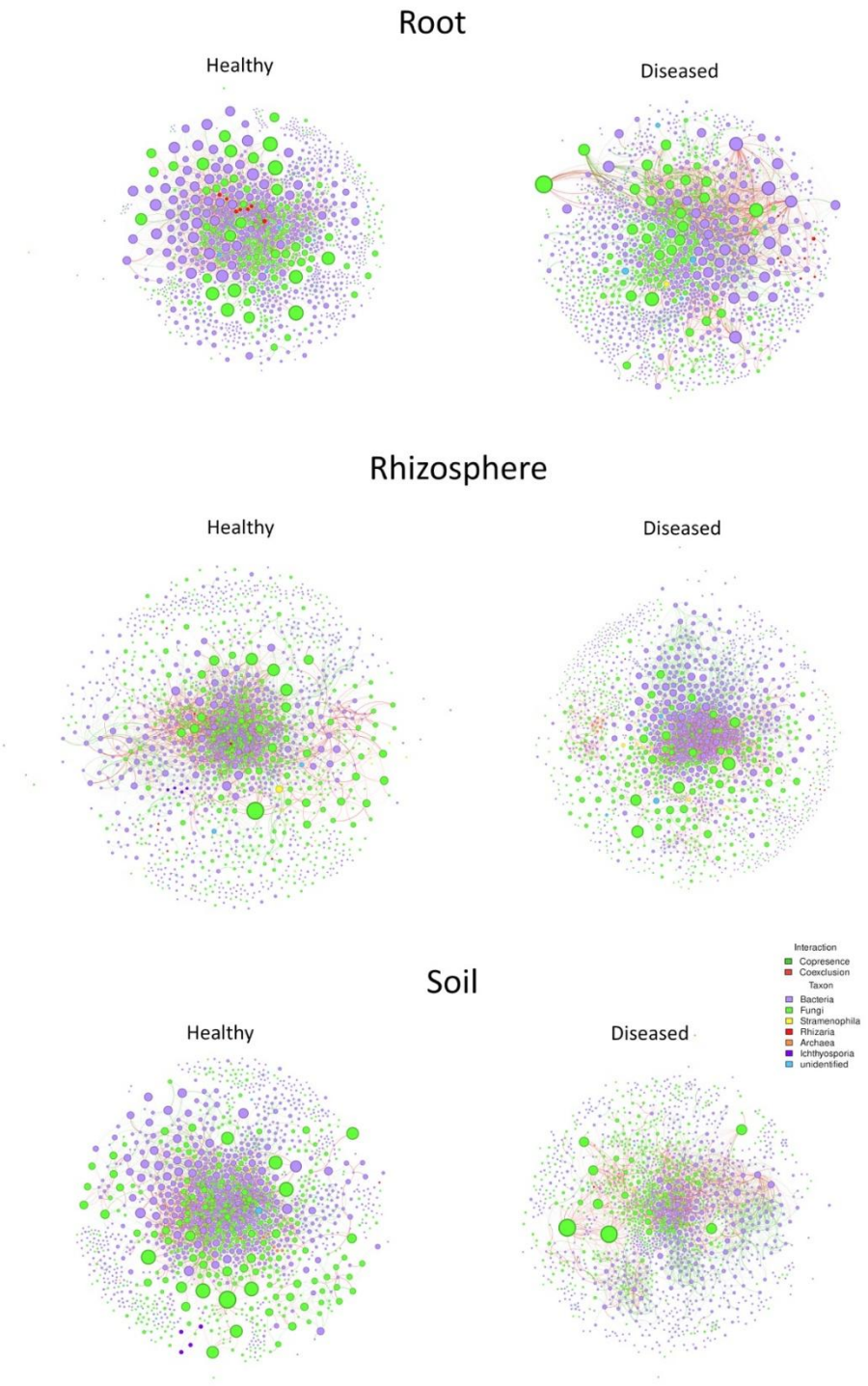
Supplementary Figure 1 - Violin plot for bNTI values (above) and Bray-Curtis derived Raup-Crick values (below) calculated on rhizosphere fungal communities. Values were calculated separately for diseased (left) and healthy (right) communities. Different point shape indicates whether the value refers to comparison conducted between communities in the same orchard (full square) or different orchards (empty square). In each plot the three continuous lines are associated with the first, second and third quartile of the point distribution. Dotted lines in both plots indicate significant threshold for the respective metric (2 and -2 for bNTI, -0.95 and 0.95 for Raup-Crick$_{Bray}$).



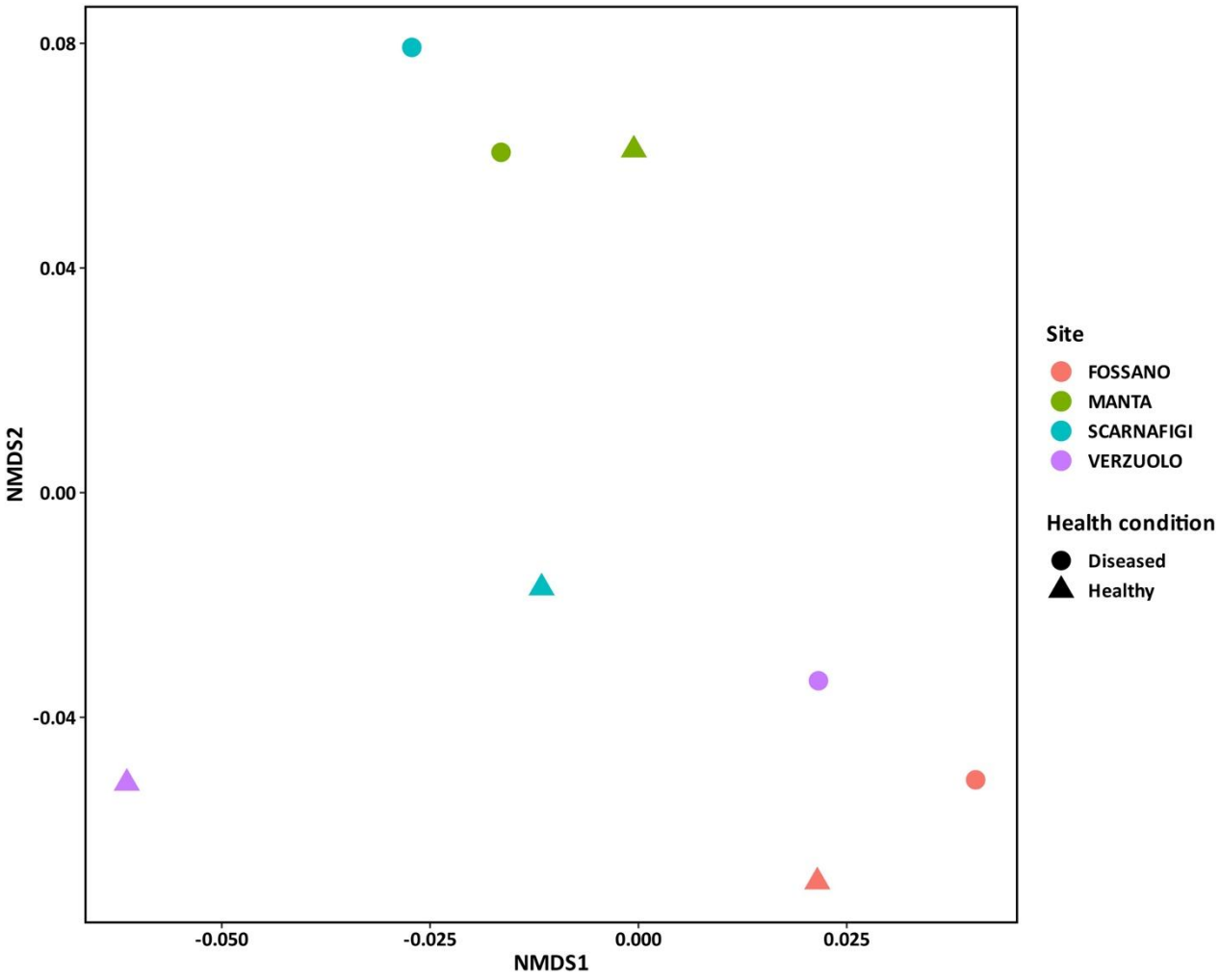
Supplementary Figure 2 - Violin plot for bNTI values (above) and Bray-Curtis derived Raup-Crick values (below) calculated on rhizosphere bacterial communities. Values were calculated separately for diseased (left) and healthy (right) communities. Different point shape indicates whether the value refers to comparison conducted between communities in the same orchard (full square) or different orchards (empty square). In each plot the three continuous lines are associated with the first, second and third quartile of the point distribution. Dotted lines in both plots indicate significant threshold for the respective metric (2 and -2 for bNTI, -0.95 and 0.95 for Raup-Crick$_{Bray}$).



Supplementary Figure 3 - Violin plot for bNTI values (above) and Bray-Curtis derived Raup-Crick values (below) calculated on rhizosphere oomycete communities. Values were calculated separately for diseased (left) and healthy (right) communities. Different point shape indicates whether the value refers to comparison conducted between communities in the same orchard (full square) or different orchards (empty square). In each plot the three continuous lines are associated with the first, second and third quartile of the point distribution. Dotted lines in both plots indicate significant threshold for the respective metric (2 and -2 for bNTI, -0.95 and 0.95 for Raup-Crick$_{Bray}$).



Supplementary Figure 4 - Association network of microbial communities associated with kiwi plant rhizosphere, root and soil. Edge colour is associated to interaction type (co-presence of co-exclusion), while node colour to their taxonomic kingdom. Node size is proportional to the number of connections (i.e. degree).



Supplementary Figure 5 - Non-metric multidimensional scaling (NMDS) plot of Bray-Curtis distances between soil samples. Colors indicate different sampling sites, while shapes are associated with health status

Chapter 3 - Development of a qPCR assay for early detection and quantification of *Phytopythium vexans* in kiwifruit plant and soil affected by Vine Decline Syndrome

Development of a qPCR assay for early detection and quantification of *Phytopythium vexans* in kiwifruit plant and soil affected by Vine Decline Syndrome

Guaschino, Micol[1,2]; Prencipe, Simona[1]; Somera, Tracey[3]; Tabone, Giulia[1]; Spadaro, Davide[1,2,*]

[1] Department of Agricultural, Forest and Food Sciences (DISAFA), University of Torino, Largo Paolo Braccini 2, 10095 Grugliasco (TO), Italy.

[2] AGROINNOVA, Interdepartmental Centre, University of Torino, Largo Paolo Braccini 2, 10095 Grugliasco (TO), Italy.

[3] USDA, Agricultural Research Service, Wenatchee, WA, United States.

* Corresponding author: D. Spadaro; davide.spadaro@unito.it

Bibliographic reference: *Guaschino, M., Prencipe, S., Somera, T., Tabone, G., & Spadaro, D. (2025). Development of a qPCR assay for early detection and quantification of* Phytopythium vexans *in kiwifruit plant and soil affected by Vine Decline Syndrome. Plant Disease, (in press). https://doi.org/10.1094/PDIS-09-24-2044-RE.*

Abstract

Kiwifruit Vine Decline Syndrome (KVDS) is a soilborne disease affecting *Actinidia* fruit trees in perennial cropping systems. Since its emergence in 2012, studies have increasingly identified the oomycete *Phytopythium vexans* as a major causative agent of the disease. *Phytopythium vexans* is also implicated in complex soilborne disease systems of woody perennial crops, including replant disease in apple and pear. To date, most molecular assays for the detection of *P. vexans* target the nuclear ribosomal internal transcribed spacer, a region which is ill-suited for distinguishing between closely related oomycete species. The cytochrome oxidase subunit I mitochondrial gene was targeted for the design of new primers because it was previously identified as a better marker for differentiating oomycete species. The FOR2/REV4RCA primer pair gave the best results regarding PCR specificity and was selected for use in a SYBR Green-based qPCR assay. The specificity of the qPCR assay was evaluated using 29 P. vexans strains (including different phylogenetic groups) as well as a wide variety of closely related off-target species associated with pathogenic soil communities of fruit trees. *Phytopythium vexans* strains were successfully quantified down to 20 fg in water and in DNA extracted from kiwifruit roots. *Phytopythium vexans* was also detected in artificially inoculated *Actinidia* plant roots as well as in a variety of naturally infected field samples of both kiwi and apple trees. These results suggest that the qPCR assay developed in this study is highly sensitive and specific to target pathogen, regardless of sample matrix.

Keywords: Woody plants; Fruit trees; Soil health; Kiwifruit Vine Decline Syndrome; Apple replant disease

1. Introduction

Kiwifruit Vine Decline Syndrome (KVDS; moria in Italian) is a soil-borne disease that has severely impacted *Actinidia* fruit trees in perennial cropping systems, particularly threatening kiwifruit production in Italy, but has also been reported in Turkey, Japan, and China (Shimizu et al. 2005, Wang et al. 2015, Türkkan et al. 2022). Since the emergence of KVDS in 2012, evidence has increasingly pointed to the oomycete *Phytopythium vexans* as a key biotic factor contributing to the disease (Donati et al. 2020; Prencipe et al. 2020; Savian et al. 2021, 2022; Prencipe et al. 2023). The species has been reported as pathogenic on many different economically relevant crops and it is characterized by a wide geographical distribution, as reported in the diagnostic guide by Ghimire and Baysal-Gurel (2023). In addition to causing root rot, it has also been implicated in more complex soilborne disease systems, particularly in woody perennial crops such as kiwifruit, pear, apple and grapevine, across the globe (Spies et al. 2011; Jabiri et al. 2021; Savian et al. 2022). Symptoms associated with infection by *P. vexans* include root necrotic lesions, root discoloration and rotting, leading to canopy wilting and plant decline. Interestingly, *P. vexans* has also been linked to Apple Replant Disease (ARD), playing a role in the decline of young apple trees in replant orchards (Tewoldemedhin et al. 2011).

Phytopythium vexans is characterized by a high level of genetic variation (Spies et al. 2011) and its trophic lifestyle tends to be necrotrophic (Adhikari et al. 2013; Broders et al. 2024). As a necrotroph, *P. vexans* targets roots that have already been compromised by abiotic stress factors (e.g., drought or flooding) or previous infections from other pathogens. Oomycetes, in general, are known to have a diverse lifestyle able to adapt to different conditions. Their ability to release zoospores in moisture (de Cock et al. 2015) and tolerate a wide range of temperatures (Prencipe et al. 2023), makes them particularly resilient across different ecosystems and climates.

Sequence-based analyses, especially those based on nuclear DNA, have been widely applied for identifying oomycetes and differentiating species. Initially, *Phytopythium* was classified within the Pythium genus, as clades were defined based on the nuclear ribosomal internal transcribed spacer (ITS) and large subunit rRNA (LSU) sequence analysis by Levesque and Cock (2004). However, subsequent studies revealed that the mitochondrial cytochrome oxidase

I (COI) region is a more reliable marker for species- level discrimination, complementing the data from the nuclear ITS region (Robideau et al. 2011). Building on these findings, de Cock et al. (2015) conducted a multi-locus analysis of nuclear and mitochondrial genes, which confirmed that Pythium species in clade "K" represented a distinct monophyletic genus, ultimately leading to the renaming of this group as Phytopythium.

Despite advances in molecular identification, managing diseases caused by plant pathogenic oomycetes, such as Phytopythium, remains a significant challenge. In European countries, traditional soil chemical fumigation is not an option due to the withdrawal of synthetic soil fumigants from EU market (Regulation (EC) No 1107/2009). Alternative strategies, like the potential use of organic amendments or biofumigation with brassica plant residues to control KVDS, have not yet been exploited and no effective biological control agents have been identified. Development of KVDS-resistant rootstocks is ongoing with promising results from grafting A. deliciosa or A. chinensis cultivars onto A. macrosperma genotypes, which has been shown to reduce symptoms and influence the oomycete community structure in the plant rhizo- and endosphere (Mian et al. 2023). However, successful use of resistant rootstocks as a management solution will require further evaluation of graft compatibility together with effects on yield and fruit quality.

Oomycete pathogens, including those involved in KVDS, primarily originate in soil, but nursery material and irrigation water can also contribute to the spread of inoculum (Moein et al. 2019a). A survey conducted on woody ornamental plants by Puertolas et al. (2021) traced the presence of oomycete inoculum (considering three genera: *Phytopythium*, *Pythium* and *Phytophthora*), both with traditional and molecular techniques. Notably, molecular assays confirmed the presence of oomycetes in all tested plants, across both compost and plant material, underscoring a critical issue for international nursery trades in Europe, where phytosanitary regulations are less restrictive compared to other countries like Australia, New Zealand, and the USA. Among these genera, *Phytopythium* stands out as a significant concern due to its role in diseases of perennial fruit trees.

In this framework, effective disease management and inoculum reduction requires monitoring of putative infection sources with efficient pathogen quantification techniques (Moein et al. 2019b). A variety of DNA-based assays for the detection of *P. vexans* have been developed. Most assays target ITS nuclear region via different techniques: quantitative PCR (qPCR; Yang et al. 2012), TaqMan probes (Spies et al. 2011; Yano et al. 2011) and Loop-Mediated

Isothermal Amplification (LAMP; Wang et al. 2021). Other previously developed qPCR assays for the detection of P. vexans targeted the small subunit rRNA gene in peach seedlings (Bent et al. 2009) and a putative inositol polyphosphate 5- phosphatase region in apple roots (Moein et al. 2019b). The aim of the research was to develop a diagnostic tool, based on the COI mitochondrial gene region, for early detection of *P. vexans* in soils and plant roots. Primers were designed by considering the different phylogenetic groups belonging to the species and the optimal couple validated following the European and Mediterranean Plant Protection Organization (EPPO) standard PM 7/98 (5) (EPPO 2021). Fungal and oomycete species reported as involved in the KVDS pathosystem were considered as off-targets for specificity evaluation, together with species commonly found in agricultural soil communities. Assay validation was carried out using *Actinidia deliciosa* cv. Hayward as host, which is a variety susceptible to oomycetes, but still the main cultivar in Italian orchards. To explore the potential for applying this molecular assay to other woody perennial plants with similar disease systems, the assay was also used to screen soils sampled from ARD-affected orchards. The diagnostic tool could be employed in nurseries to test infected plants and in orchards to monitor both infected soils and plants, thereby avoiding the spread of diseases caused by P. vexans and mitigate further damage to the roots of perennial crops.

2.Materials and methods

2.1 Oomycete and fungal strains

Strains of *P. vexans* isolated from root tissue of *Actinidia deliciosa* cv. Hayward cultivated in North-West Italy (Piedmont) from 2016-2021 were considered in this study (Table 1). These isolates were previously characterized by molecular phylogeny and belong to different phylogenetic groups (Prencipe et al. 2023). Furthermore, mono-hyphal cultures were obtained from newly isolated strains, molecularly characterized following the methods described in Prencipe et al. (2023) and kept at 18°C in soil extract for long-term storage. The reference strain of the target organism (*P. vexans* CBS 119.80), closely related and off- target species were provided by the Westerdijk Institute (*A. tabescens* CBS 137.32, *Ph. cryptogea* CBS 141726, *Ph. megasperma* CBS 118733, *Ph. infestans* CBS 147289, *P. chamaehyphon* CBS 259.30, *P. citrinum* CBS 119171, *P. helicoides* CBS 286.31, *P. litorale* CBS 118360, *Ph. mirpurense* CBS 124523). Additionally, 17 strains were provided by the University of Torino collection, including species commonly found in agricultural soils, associated with KVDS

and/or reported as pathogenic towards kiwifruit in the literature (Table 2). While *P. chamaehyphon* strain PChUd was provided by the University of Udine. All fungal and oomycete strains used in this study were mono-hyphal cultures. Representative strains isolated from kiwifruit (*Actinidia deliciosa*) cv. Hayward were deposited in Turin University Culture Collection (TUCC, University of Turin). All strains of P. vexans isolated from *A. deliciosa* roots during 2021 were grown on pimaricin-ampicillin- rifampicin-pentachloronitrobenzene – corn meal agar (PARP-CMA, Prencipe et al. 2023) at 25±1 °C for 5 days, and mono-hyphal cultures were obtained. Fungal species were grown on malt extract agar (MEA, 15 g/L agar, 30 g/L alt extract, 5 g/L mycological peptone) for 10 days. Oomycete and fungal genomic DNA was extracted with Omega EZNA Fungal DNA Mini Kit (Omega Bio-Tek, Darmstadt, Germany) following the manufacturer instructions. The quantity and quality of the DNA was verified using a Nanodrop 2000 Spectrophotometer (Thermo Fischer Scientific, Waltham, MA, USA) and diluted to a concentration of 20 ng/µL.

2.2 Sequence analysis and primer design

Sequences of the COI mitochondrial gene belonging to *P. vexans* strains and to off-target species were retrieved from the National Centre of Biotechnology Information website (NCBI; https://www.ncbi.nlm.nih.gov/). These sequences were aligned with MAFFT software (Katoh and Standley, 2013) for a total of 300 sequences belonging to 25 different species (*P. vexans, P. helicoides, P. litorale, P.chamaehyphon, P. delawarense, P. mirpurense, P. boreale, P. carbonicum, P. citrinum, P. kandeliae, P. montanum, P. oedochilum, P. ostracodes, P. sindhum, P. mercuriale, Calycofera operculata, Globisporangium sylvaticum, Pythium ultimum, Py. intermedium, Pseudomonas syringae pv. actinidiae, Phytophthora cinnamomi, Ph. citrophthora, Ph. drechsleri, Ph. lateralis, Ph. palmivora*). The identifiers of sequences considered in the alignment are listed in Supplementary Table 1. The aligned sequences were then used as input for DECIPHER v2.0 (Wright, 2016) to identify regions which were different between *P. vexans* and the off-target species. After identification of the best regions, primer sets given as output by DECIPHER v2.0 were revised manually to design the final primer sets, which are listed in Table 3. For in-silico validation of the primer sets, both Primer Blast (https://www.ncbi.nlm.nih.gov/tools/primer-blast/) and OligoCalc (http://biotools.nubic.northwestern.edu/OligoCalc.html) were used to identify possible off-target amplification, potential self-annealing sites and hairpin formation.

2.3 Amplification with end-point PCR and qPCR

As stated above, different primer pairs were designed on the COI mitochondrial gene of *P. vexans* (Table 3). Conventional end-point PCR was used as a preliminarily check for best performing primer pairs using genomic DNA from *P. vexans* strains and off-target species (Tables 1 and 2). End-point PCR reactions were performed using the Taq DNA polymerase kit (Qiagen, Hilden, Germany) in a total volume of 25 µL. Each reaction contained 17.45 µL of molecular grade water, 2.5 µL Buffer 10x, 0.8 µL of MgCl2 (25 mM), 1 µL of dNTPs (10 mM), 1 µL of each primer (5 µM), 0.25 µL of Taq DNA polymerase (5 units / µL) and 20 ng of genomic DNA. Thermal cycling was performed as follows: 5 minutes at 95 °C followed by 34 cycles of 95 °C for 30 seconds, 62 °C for 30 seconds, 72 °C for 1 minute with a final TM extension of 5 minutes using a T100 Thermal Cycler (Bio-Rad, Hercules, CA, USA). In order to check primer specificity, PCR products were run on 1.5 % agarose gel in 1x Tris- Borate-EDTA buffer (TBE) and visualized using the Quantity One software (Bio-Rad). The primer pairs with specific amplification for *P. vexans* were further evaluated for specificity in qPCR reactions, using different primer concentrations in the working solution ranging from 2.5 µM to 10 µM. SYBR Green qPCR reactions were carried out using 7.5 µL SsoAdvanced Universal SYBR Green Supermix 2x (Bio-Rad) in a final volume of 15 µL with 1 µL of DNA (~20 ng) and 1.2 µL of each primer (5 µM). Assays were carried out using a CFX96 Real- Time PCR Detection System (Bio-Rad) with 96 well-plates (Bio-Rad) sealed with optical adhesive film (Bio-Rad). Thermal conditions were 95 °C for 10 min, followed by 40 cycles of the annealing temperature for 1 min and 95 °C for 15 s. After each run, the melting curve step was performed by ramping the temperature from 60 °C to 90 °C. In each run, a negative control (biological grade water) and a positive control (*P. vexans* CBS 119.80 genomic DNA) were always included in triplicate. Data from qPCR reactions used to quantify the amount of *P. vexans* target DNA in a particular sample were collected and Cq (quantification cycle) values were interpolated into a standard curve generated with serial dilutions of the target DNA (*P. vexans* CBS 119.80 genomic DNA).

2.4 Specificity, sensitivity, selectivity, repeatability, and reproducibility of the qPCR assay

Validation of the qPCR assay was carried out by following the EPPO standard PM 7/98 (5) (EPPO 2021) guidelines. For evaluating the specificity of the assay, 29 *P. vexans* strains (4 strains isolated in 2021 from root tissue, 24 provided by the University of Torino, the reference *P. vexans* strain CBS 119.80 and 27 isolates belonging to 18 non-target species (Tables 1 and 2) were used. Off-target species included closely related ones, other species reported as pathogenic to kiwifruit, species commonly found in agricultural soil communities, and fungal

species associated with pathogenic soil communities involved in multifactorial diseases of fruit trees where *P. vexans* is also present. To confirm the specific amplification of the target organism through qPCR, the amplicons of three samples with positive results were sequenced in both directions by BMR Genomics (Padova, Italy) using the same primer set used for the assay. The resulting consensus sequences were compared using BLASTN (http://blast.ncbi.nlm.nih.gov/Blast.cgi) with those deposited in the GenBank (http://www.ncbi.nlm.nih.gov/genbank/) repository. For assay sensitivity and limit of detection (LOD) determination, a standard calibration curve was obtained by performing serial dilutions ranging from 20 ng to 2 fg of CBS 119.80 and PP3 strains in sterile biological-grade water. These strains belong to two different phylogenetic clusters of *P. vexans* (Prencipe et al. 2023). Dilutions were performed twice (using biological duplicates) and run in triplicate (technical replicates). The standard curve based on the PP3 strain was used as an internal control for quantification of target DNA concentration (Figure 1). Selectivity was tested by diluting the target DNA into *A. deliciosa* cv. Hayward root DNA at a concentration of 10 ng/µL, to determine the influence of the host on target detection (Figure 2). The repeatability was checked by performing two different assays by the same operator, whereas the reproducibility of the assay was tested by two different operators in two different laboratories on different days. The qPCR assay was further validated using DNA extracted from symptomatic and asymptomatic matrices sampled in the field (Figure 3) and on artificially inoculated samples as described below.

2.5 Testing of qPCR in naturally and artificially inoculated tissues

The assay was tested on three artificially inoculated *A. deliciosa* cv. Hayward plants, infected with 47 g of *P. vexans* strain T4B as described in Prencipe et al. (2020) and three control plants. Roots were sampled 48 h after inoculation, freeze-dried and processed with mortar and pestle. Both untreated (control) and inoculated plants were sampled at the same time point to compare pathogen quantity. DNA was then extracted with the Qiagen DNeasy Plant Mini Kit (Qiagen) from both inoculated and control plants. Naturally infected matrices of kiwifruit roots, rhizosphere and bulk soil were also used to test the qPCR assay. Field samples were collected during summer 2021 in both symptomatic and asymptomatic commercial orchards located in Piedmont, Cuneo province, Italy to test for the presence of *P. vexans*. Sampling sites and methods are described in Guaschino et al. (2024). Four bulk soil samples, four rhizosphere soil samples and three root samples for each condition (symptomatic and asymptomatic) were collected and analyzed in technical triplicate. DNA from the different matrices was extracted

with the Qiagen Power Soil kit (Qiagen). Different matrices were considered to test for inhibitory effects of plant and soil extracts on the specificity and sensitivity of the assay. The qPCR assay was also used to screen ARD-affected orchard soil samples collected throughout the apple production region of central Washington state (USA) in 11 different orchard locations (Supplementary Table 2). Soil samples were collected from the tree root zone (15–60 cm from trunk) in summer of 2021 and 2022 using a 2.5 cm soil core to a depth of 20 cm. For each sample, microbial DNA was extracted from 5 g of soil using the Qiagen Power Soil kit (Qiagen). DNA samples were screened for the presence of *P. vexans* by performing the qPCR assay as described in Section 2.3.

2.6 Data analysis

Baseline range and Cq values were generated using CFX Maestro software (Bio-Rad). The Wilcoxon-Mann-Whitney test was performed in RStudio (Posit team, 2024) with R v. 4.3.3 (R Core Team, 2024) to analyze both repeatability and reproducibility of the assay with $p<0.05$.

3. Results

3.1 Optimization of SYBR Green qPCR assay

The mitochondrial marker COI was selected because of its ability to distinguish closely related oomycete species. Nine primer sets were designed for the detection of *P. vexans* (Table 3). The FOR2/REV4RCA primer pair gave the best result in terms of specificity in end-point PCR and was therefore optimized for the SYBR Green qPCR assay. Various primer concentrations and annealing temperatures were tested, with the optimal conditions determined to be 0.4 µM for primer concentration and 62°C for annealing temperature.

3.2 Specificity, sensitivity, selectivity, repeatability, and reproducibility of the assay

Amplification of the target 193 bp fragment was evaluated using 29 strains of *P. vexans* belonging to different phylogenetic groups (Table 1). Specificity of the assay was verified by considering 27 isolates belonging to 18 different off-target species (Table 2). Of these, isolates were either phylogenetically close to *P. vexans* or previously reported as pathogenic to *Actinidia* plants, and/or species commonly occurring in agricultural soils.

To establish the limit of detection (LOD) of the target organism, *P. vexans* DNA from two different strains (CBS 119.80 and PP3) was serially diluted from 20 ng to 2 fg. For both strains, the target DNA was detectable from 20 ng down to 20 fg with an average LOD Cq of 33.37 ±

0.74. For off-target species, no amplification was detected before the established LOD Cq threshold. Standard curve equations for CBS 119.80 and PP3 strains were y = -3.47 x + 36.35 (R2=0.99) and y = -3.62 x + 37.24 (R2=0.99), respectively. The reaction efficiency for CBS 119.80 was 94% while for PP3 it was 96%. In terms of selectivity, no statistically significant differences were found between target DNA dilutions performed in water and DNA extracted from kiwi roots (Figure 2). In comparison of the standard curves obtained with the two different strains, the only statistically significant difference was found at 0.0002 ng (p-value = 0.03571) (Figure 1).

3.3 Detection of P. vexans in artificially inoculated *Actinidia* roots

For the detection of *P. vexans* in artificially inoculated tissue, 18 samples were considered. Samples were a biological triplicate, each run as a technical triplicate. The qPCR assay detected the pathogen in both uninoculated (control) and inoculated root tissue after 48 h; average Cq values were 31.22 (corresponding to 5.11 x 101 ng in average) and 21.57 (corresponding to 2.33 x 104 ng in average), respectively (Supplementary Table 3).

3.4 Detection of *P. vexans* in naturally infected soil, rhizosphere and roots of symptomatic and asymptomatic kiwifruit and apple orchards

Twenty-two kiwifruit samples were analyzed (half symptomatic and half asymptomatic). The target DNA in soil samples was amplified with a Cq ranging from 29.45 to 38.88, detecting up to 9.21 x 101 *P. vexans* ng in asymptomatic ones (Figure 3). No target DNA was detected in symptomatic soil samples. In symptomatic rhizosphere soil the lowest (earliest) Cq value recorded was 28.02, while for symptomatic root tissue the value was 31.09. Symptomatic rhizosphere showed the highest value of *P. vexans* ng (3.17 x 102), while the highest quantity in root tissue was detected in asymptomatic samples (7.09 x 101 ng). Samples were considered negative when the signal exceeded the Cq corresponding to the assay LOD. When all samples were considered, *P. vexans* was detected in a greater percentage of rhizosphere (62%) and root (50%) samples than soil samples (12.5%). In addition, a total of 24 soil samples collected from 11 different ARD-affected orchard locations in Washington State were screened for the presence of P. vexans using the qPCR assay. *Phytopythium vexans* was identified in 2/11 of these locations (5/24 samples).

4. Discussion

In this study, we developed a molecular diagnostic tool for early detection of the plant pathogenic oomycete *P. vexans* which was validated on *Actinidia*, where the pathogen is involved in causing vine decline syndrome. The relevance of *P. vexans* as a root pathogen in different crops across the globe has risen in the last decade (Türkkan et al. 2022, Ghimire and Baysal-Gurel, 2023).

To our knowledge, this assay represents the first species-specific qPCR assay based on the COI mitochondrial gene region tested on both kiwi vine decline syndrome samples and apple replant disease (including soil, rhizospheric soil and roots).

The first species-specific primers for the detection of different phylogenetic groups of *P. vexans* were developed to quantify the inoculum associated with grapevine decline in South Africa (Spies et al. 2011). In this study, Spies and colleagues performed the validation in grapevine roots and primer specificity was checked using a panel of *Pythium* and *Phytophthora* species. However, unlike our study, other off-target organisms normally present in agricultural samples were not included. The sensitivity reported in Spies et al. (2011) reached 6.9 fg/µL (27.2 fg / reaction) in one *P. vexans* phylogenetic group, whereas our assay was able to equally quantify 20 fg for both phylogenetic groups considered. In this study, standard curves obtained with *P. vexans* strains CBS 119.80 and PP3 showed a significant statistical difference at a single point of the curve. This variability in standard curve construction was likely due to different qPCR efficiencies between phylogenetic groups.

For better comparison, we performed an alignment of COI sequences and generated a new tree (data not shown) comparing the strains included in Spies et al. (2011) and the *P. vexans* strains isolated from kiwifruit and previously characterized by Prencipe et al. (2021), which confirmed the same phylogenetic grouping of kiwifruit isolates, as previously observed in grapevine.

In another paper by Moein et al. (2019b), which aimed to improve the Spies et al. (2011) assay, a novel Taqman-based qPCR assay targeting *P. vexans* was designed for the quantification of oomycetes species involved in Apple Replant Disease (ARD). With the development of the Taqman assay, which targeted a single copy gene (polyphosphate 5- phosphatase gene), sensitivity decreased to 2,000 fg/reaction for all the phylogenetic groups belonging to the target species. The Taqman probe from Moein et al. (2019b) was evaluated in KVDS naturally infected soil, rhizosphere and roots of both symptomatic and asymptomatic trees, but no

amplification was observed using this technique, except for the positive control. To compare sensitivity, a standard curve with the TaqMan assay was performed using a *P. vexans* strain isolated from KVDS affected roots, obtaining different Cq from what reported in the paper underestimating the pathogen quantity (Moein et al. 2019b).

Compared to our study, the assays used in Spies et al. (2011) and Moein et al. (2019b) were less sensitive, but most importantly they were not validated on off-target species characteristic of orchard soils, which makes the quantification of *P. vexans* in naturally infected samples vulnerable to false positives. The assay of Moein, developed for quantification of *P. vexans* in ARD pathosystems, was also tested on irrigation water and nursery trees. Quantification of the target oomycete with the TaqMan probe failed in nursery trees (Moein et al. 2019a), while in this study pathogen quantification in artificially inoculated and naturally infected roots was successful with the developed assay. *Phytopythium vexans* was detected in both symptomatic and asymptomatic samples, which is consistent with the KVDS model proposed in another study (Guaschino et al. 2024). However, it should be noted that quantification of *P. vexans* in environmental samples resulted in fewer positives, probably due to the presence of reaction inhibitors especially in soil as observed by Schrader et al. (2012). While in the quantification performed in artificially inoculated roots, results indicate that the presence of the pathogen was greater in inoculated vs. uninoculated root tissue.

In conclusion, we developed a qPCR assay for the quantification of *P. vexans* based on the amplification of the COI mitochondrial gene. The assay resulted to be specific, selective and sensitive for the detection of the target oomycete, being able to equally quantify strains belonging to different phylogenetical groups. The development of a qPCR assay targeting a concerning pathogen of perennial crops is a useful tool for monitoring the inoculum spread, pathogen load and to ensure the health of propagation materials. Being able to monitor pathogen quantities across various environmental matrices could support the development or optimization of agricultural management strategies in fruit tree orchards, particularly in countries where fungicide use is strictly regulated. Real time qPCR allows for faster and more accurate implementation of control measures or eradication procedures compared to traditional methods of pathogen isolation (Schaad and Frederick, 2010). Lastly, it is worth mentioning that there is evidence suggesting that *Phytopythium* spp. could be favored as average soil temperatures increase (Prencipe et al. 2023). Therefore, this approach to disease management is of relevance considering climate change projections, which may alter the global distribution of many plant pathogens including *P. vexans*.

Acknowledgements

This research was funded by Piedmont Region (Italy) with the project “KIRIS - Kiwifruit Vine Decline Syndrome: deepening the etiology and development of prevention and control tool” and “KIPOTRA – Kiwifruit Vine Decline Syndrome – Evaluation of the use of rootstocks as an agronomic tool to prevent symptom development”, by Italian Ministry of University and Research with the project “KVD-Biome - Unveiling the plant exposome to dissect a multifactorial disease: the kiwifruit vine decline”, by AGER – Foundations Network for Agrifood Research with the project “SOS-KIWI - From SOil to Soil: origin and remediation to KIWIfruit Vine Decline Syndrome”, and by the European Commission – NextGenerationEU, Project SUS-MIRRI.IT "Strengthening the MIRRI Italian Research Infrastructure for Sustainable Bioscience and Bioeconomy”, code n. IR0000005. The authors would like to acknowledge Marta Martini and Paolo Ermacora for Phytopythium chamaehyphon strain PChUd.

References

Bent, E., Loffredo, A., Yang, J. I., McKenry, M. V., Becker, J. O., and Borneman, J. 2009. Investigations into peach seedling stunting caused by are plant soil. FEMS Microbiology Ecology 68(2):192-200.

Broders, K., Capador-Barreto, H., Iriarte, G., Wright, J., Baur, M., Espinosa-Ortega, H., and Spear, E. 2024. Oomycete communities in lowland tropical forest soils vary in abundance and are composed of saprophytes and pathogens of seeds and seedlings of multiple plant species. bioRxiv 2024-02.

De Cock, A. W. A. M., Lodhi, A. M., Rintoul, T. L., Bala, K., Robideau, G. P., Abad, Z. G., Coffey, M. D., Shahzad, S., and Lévesque, C. A. 2015. Phytopythium: molecular phylogeny and systematics. Persoonia-Molecular phylogeny and evolution of fungi 34(1):25-39.

Donati, I., Cellini, A., Sangiorgio, D., Caldera, E., Sorrenti, G., and Spinelli, F. 2020. Pathogens associated to kiwifruit vine decline in Italy. Agriculture 10(4):119.

EPPO. 2021. PM 7/98 (5). Specific requirements for laboratories preparing accreditation for a plant pest diagnostic activity. EPPO Bulletin 51: 468-498.

Ghimire, B., and Baysal-Gurel, F. 2023. A diagnostic guide to Phytopythium helicoides and Phytopythium vexans causing root and crown rot diseases. Plant Health Progress 24(4):527-538.

Guaschino, M., Garello, M., Nari, L., Zhimo, Y. V., Droby, S., and Spadaro, D. 2024. Soil, rhizosphere, and root microbiome in kiwifruit vine decline, an emerging multifactorial disease. Frontiers in Microbiology15:1330865.

Jabiri, S., Bahra, C., MacLean, D., Radouane, N., Barka, E. A., Bendriss Amraoui, M., and Lahlali, R. (2021). Phytopythium vexans associated with apple and pear decline in the Saïss plain of Morocco. Microorganisms 9(9), 1916.

Katoh, K., and Standley, D. M. 2013. MAFFT Multiple Sequence Alignment Software Version 7: Improvements in Performance and Usability. Molecular Biology and Evolution 30:772.

Levesque, C. A., and De Cock, A. W. 2004. Molecular phylogeny and taxonomy of the genus Pythium. Mycological research 108(12):1363-1383.

Mian, G., Cipriani, G., Firrao, G., Martini, M., and Ermacora, P. 2023. Genetic diversity of Actinidia spp. shapes the oomycete pattern associated with Kiwifruit Vine Decline Syndrome (KVDS). Scientific Reports 13(1):16449.

Moein, S., Mazzola, M., Ntushelo, N. S., and McLeod, A. 2019a. Apple nursery trees and irrigation water as potential external inoculum sources of apple replant disease in South Africa. European Journal of Plant Pathology 153:1131-1147.

Moein, S., Mazzola, M., Spies, C. F. J., and McLeod, A. 2019b. Evaluating different approaches for the quantification of oomycete apple replant pathogens, and their relationship with seedling growth reductions. European Journal of Plant Pathology 154:243-257.

Posit team. 2024. RStudio: Integrated Development Environment for R. Posit Software, PBC, Boston, MA. URL http://www.posit.co/.

Prencipe, S., Savian, F., Nari, L., Ermacora, P., Spadaro, D., and Martini, M. 2020. First report of Phytopythium vexans causing decline syndrome of Actinidia deliciosa ‘Hayward’ in Italy. Plant Disease 104(7):2032-2032.

Prencipe, S., Schiavon, G., Rosati, M., Nari, L., Schena, L., and Spadaro, D. 2023. Characterization of Phytopythium species involved in the establishment and development of kiwifruit vine decline syndrome. Microorganisms 11(1):216.

Puertolas, A., Bonants, P. J., Boa, E., and Woodward, S. 2021. Application of real-time PCR for the detection and quantification of oomycetes in ornamental nursery stock. Journal of Fungi 7(2):87.

R Core Team. 2024. R: A Language and Environment for Statistical Computing. R Foundation for Statistical Computing, Vienna, Austria. <https://www.R-project.org/>.

Regulation (EC) No 1107/2009 of the European Parliament and of the Council of 21 October 2009 concerning the placing of plant protection products on the market and repealing Council Directives 79/117/EEC and 91/414/EEC. Official Journal of the European Union OJ L309 24.11.2009:1-50.

Robideau, G. P., De Cock, A. W., Coffey, M. D., Voglmayr, H., Brouwer, H., Bala, K., Chitty, D. W., Désaulniers, N., Eggertson, Q. A., Gachon, C. M. M., Hu, C. H., Kupper, F. C., Rintoul, T. L., Sarhan, E., Verstappen, E. C. P., Zhang, Y., Bonants, P. J. M., Ristaino, J., and André Lévesque, C. 2011. DNA barcoding of oomycetes with cytochrome c oxidase subunit I and internal transcribed spacer. Molecular ecology resources 11(6):1002-1011.

Savian, F., Prencipe, S., Filippini, N., Nari, L., Martini, M., Ermacora, P., and Spadaro, D. 2021. Pathogenicity of Phytopythium chamaehyphon: A new player in kiwifruit vine decline syndrome of Actinidia chinensis var. deliciosa 'Hayward' in Italy. Plant Disease 105(10):2781-2784.

Savian, F., Marroni, F., Ermacora, P., Firrao, G., and Martini, M. 2022. A metabarcoding approach to investigate fungal and oomycete communities associated with kiwifruit vine decline syndrome in Italy. Phytobiomes Journal 6(4):290-304.

Schaad, N. W., and Frederick, R. D. 2002. Real-time PCR and its application for rapid plant disease diagnostics. Canadian journal of plant pathology 24(3):250-258.

Schrader, C., Schielke, A., Ellerbroek, L., and Johne, R. 2012. PCR inhibitors–occurrence, properties and removal. Journal of applied microbiology 113(5):1014-1026.

Shimizu, S., Miyoshi, T., Yano, T., and Tachibana, Y. 2005. First report of kiwifruit root rot caused by Phytium spp. In papers presented at the 2005 annual meeting in Shizuoka). Annals of the Phytopathological Society of Japan 71:210.

Spies, C. F. J., Mazzola, M., and McLeod, A. 2011. Characterisation and detection of Pythium and Phytophthora species associated with grapevines in South Africa. European journal of plant pathology 131:103-119.

Tewoldemedhin, Y. T., Mazzola, M., Botha, W. J., Spies, C. F., and McLeod, A. 2011. Characterization of fungi (Fusarium and Rhizoctonia) and oomycetes (Phytophthora and Pythium) associated with apple orchards in South Africa. European Journal of Plant Pathology 130:215-229.

Türkkan, M., Özer, G., Karaca, G., Erper, İ., and Derviş, S. 2022. Characterization and Pathogenicity of Pythium-Like Species Associated with Root and Collar Rot of Kiwifruit in Turkey. Plant Disease 106:854–863.

Wang, K. X., Xie, Y. L., Yuan, G. Q., Li, Q. Q., and Lin, W. 2015. First Report of Root and Collar Rot Caused by Phytopythium helicoides on Kiwifruit (Actinidia chinensis). Plant Disease 99:725.

Wang, T., Ji, H., Yu, Y., Wang, X., Cheng, Y., Li, Z., Chen, J., Guo, L., Xu, J., and Gao, C. 2021. Development of a loop-mediated isothermal amplification method for the rapid detection of Phytopythium vexans. Frontiers in Microbiology 12:720485.

Wright E., S. 2016. Using DECIPHER v2.0 to Analyze Big Biological Sequence Data in R. The R Journal 8(1):352-359.

Yang, J. I., Ruegger, P. M., McKenry, M. V., Becker, J. O., and Borneman, J. 2012. Correlations between root-associated microorganisms and peach replant disease symptoms in a California soil. PloS one 7(10):e46420.

Yano, T., Shimizu, S., Miyoshi, T., Miyata, N., Immon, K., Shinozaki, T., Sawada, H., and Kageyama, K. 2010. Tolerant Actinidia species to Pythium helicoides and P. vexans causing root rot. In VII International Symposium on Kiwifruit 913:517-523.

Tables

Table 1 – Isolates of target species, representing different phylogenetic groups of *Phytopythium vexans*, and different years of isolation.

Strain ID	Host	Source	Origin	Year of isolation
13/16DR3	*Actinidia deliciosa* cv. Hayward	Roots	Italy	2016
13/16DR2	*Actinidia deliciosa* cv. Hayward	Roots	Italy	2016
TUCC00000470 (PPF)	*Actinidia deliciosa* cv. Hayward	Roots	Italy	2018
R1F	*Actinidia deliciosa* cv. Hayward	Roots	Italy	2019
TUCC00000474 (2V013N2)	*Actinidia deliciosa* cv. Hayward	Roots	Italy	2021
PP6	*Actinidia deliciosa* cv. Hayward	Roots	Italy	2018
TUCC00000469 (PPA)	*Actinidia deliciosa* cv. Hayward	Roots	Italy	2018
P8E	*Actinidia deliciosa* cv. Soreli	Roots	Italy	2019
12/16DR2	*Actinidia deliciosa* cv. Hayward	Roots	Italy	2016
PH1	*Actinidia deliciosa* cv. Hayward	Roots	Italy	2016
P8A	*Actinidia deliciosa* cv. Soreli	Roots	Italy	2019
R1C	*Actinidia deliciosa* cv. Hayward	Roots	Italy	2019
1M016Y2	*Actinidia deliciosa* cv. Hayward	Roots	Italy	2021
PP2	*Actinidia deliciosa* cv. Hayward	Roots	Italy	2018
PPC	*Actinidia deliciosa* cv. Hayward	Roots	Italy	2018
12/16CR1	*Actinidia deliciosa* cv. Hayward	Roots	Italy	2016
PH3	*Actinidia deliciosa* cv. Hayward	Roots	Italy	2016
TUCC00000472 (R1A)	*Actinidia deliciosa* cv. Hayward	Roots	Italy	2019
RE3	*Actinidia deliciosa* cv. Hayward	Roots	Italy	2019
2V013C1	*Actinidia deliciosa* cv. Hayward	Roots	Italy	2021
PP4	*Actinidia deliciosa* cv. Hayward	Roots	Italy	2018

P8F	*Actinidia deliciosa* cv. Soreli	Roots	Italy	2019
12/16AB1	*Actinidia deliciosa* cv. Hayward	Roots	Italy	2016
PP1	*Actinidia deliciosa* cv. Hayward	Roots	Italy	2018
R1D	*Actinidia deliciosa* cv. Hayward	Roots	Italy	2019
TUCC00000473 (2V013F1)	*Actinidia deliciosa cv. Hayward*	Roots	Italy	2021
PP8	*Actinidia deliciosa cv. Hayward*	Roots	Italy	2018
PP3	*Actinidia deliciosa cv. Hayward*	Roots	Italy	2018
P8D	*Actinidia deliciosa cv. Soreli*	Roots	Italy	2019

Table 2 – Strains belonging to off-target species considered for the validation of the specificity of the assay

Species	Strain ID	Host	Source	Origin
Armillaria tabescens	CBS 137.32	*Malus sylvestris*	Root, Seedling	United States of America
Dactylonectria pauciseptata	CVG 669	*Rubus idaeus* cv. Diamond Jubilee	Roots	Italy
Dactylonectria torrensis	CVG 670	*Rubus idaeus* cv. Diamond Jubilee	Roots	Italy
Dactylonectria hispanica	CVG 1011	*Rubus idaeus* cv. Grandeur	Roots	Italy
Fusarium commune	DB07	*Zea mays*	Roots	Italy
Fusarium oxysporum	203-4	*Allium cepa*	Roots	Italy
Fusarium oxysporum	MONC77	*Allium cepa*	Seed	Italy
Fusarium proliferatum	C136	*Allium cepa*	Roots	Italy
Fusarium verticilloides	5621	*Zea mays*	Crown	Italy
Globisporangium intermedium	13G1	*Actinidia deliciosa*	Roots	Italy
Globisporangium intermedium	PC3B	*Actinidia deliciosa*	Roots	Italy
Phytophthora cryptogea	CBS 141726	*Musa acuminata* 'Dwarf Cavendish'	Roots	Italy
Phytophthora megasperma	CBS 118733	*Prunus avium*	-	Italy
Phytophthora infestans	CBS 147289	*Solanum tuberosum*	-	Netherlands
Phytopythium chamaehyphon	TUCC00000481 (CA5)	*Actinidia deliciosa*	Roots	Italy
Phytopythium chamaehyphon	CBS 259.30	*Carica papaia*	-	Unknown
Phytopythium chamaehyphon	PChUd	*Actinidia deliciosa*	Roots	Italy
Phytopythium citrinum	CBS 119171	*Vitis vinifera*	Vineyard soil	France
Phytopythium helicoides	CBS 286.31	*Phaseolus vulgaris*	-	United States of America
Phytopythium helicoides	TUCC00000477 (3EB)	*Actinidia deliciosa*	Roots	Italy
Phytopythium litorale	TUCC00000475 (14A)	*Actinidia deliciosa*	Roots	Italy
Phytopythium litorale	CBS 118360	*Phragmites australis*	Reed rhizosphere soil	Germany

Phytopythium litorale	TUCC00000479 (P8H)	*Actinidia deliciosa*	Roots	Italy
Phytopythium litorale	TUCC00000478 (P8I)	*Actinidia deliciosa*	Roots	Italy
Phytopythium mirpurense	CBS 124523	-	Stagnant water	Pakistan
Trichoderma sp.	D6B1	*Zea mays*	Seed	Italy
Trichoderma sp.	SCP1	*Zea mays*	Seed	Italy

Table 3 – Primer pairs designed on the COI gene for the detection of P. vexans with SYBR Green qPCR assay

Primer name	Primer sequence (5'->3')	Tm	Amplicon size
FW1D	CAATAGTTGCAAC(A/T)GTAATGTCTGTA	61.7	123
REV2RC	TCATTAATAAACCATGTGCTGTAATCATA	62.1	
FW1D	CAATAGTTGCAAC(A/T)GTAATGTCTGTA	61.7	113
REV1RC	ACCATGTGCTGTAATCATAACATT	58.3	
FW1D	CAATAGTTGCAAC(A/T)GTAATGTCTGTA	61.7	115
REV3RC	AAACCATGTGCTGTAATCATAACATT	60.1	
FOR2	TATGATTACAGCACATGGTTTATTAATGA	62.1	193
REV4RC	CTATTAGTATC(A/T)TCTGCTTTAGTTGAATCA	63.9	
FOR4	AATGTTATGATTACAGCACATGGT	58.3	198
REV4RC	CTATTAGTATC(A/T)TCTGCTTTAGTTGAATCA	63.9	
FOR3	AATGTTATGATTACAGCACATGGTTT	60.1	198
REV4RC	CTATTAGTATC(A/T)TCTGCTTTAGTTGAATCA	63.9	
FOR2	TATGATTACAGCACATGGTTTATTAATGA	62.1	193
REV4RCA	TGATTCAACTAAAGCAGATGATACTAATAG	63.9	
FOR3	AATGTTATGATTACAGCACATGGTTT	60.1	198
REV4RCA	TGATTCAACTAAAGCAGATGATACTAATAG	63.9	
FOR4	AATGTTATGATTACAGCACATGGT	58.3	198
REV4RCA	TGATTCAACTAAAGCAGATGATACTAATAG	63.9	

Figures

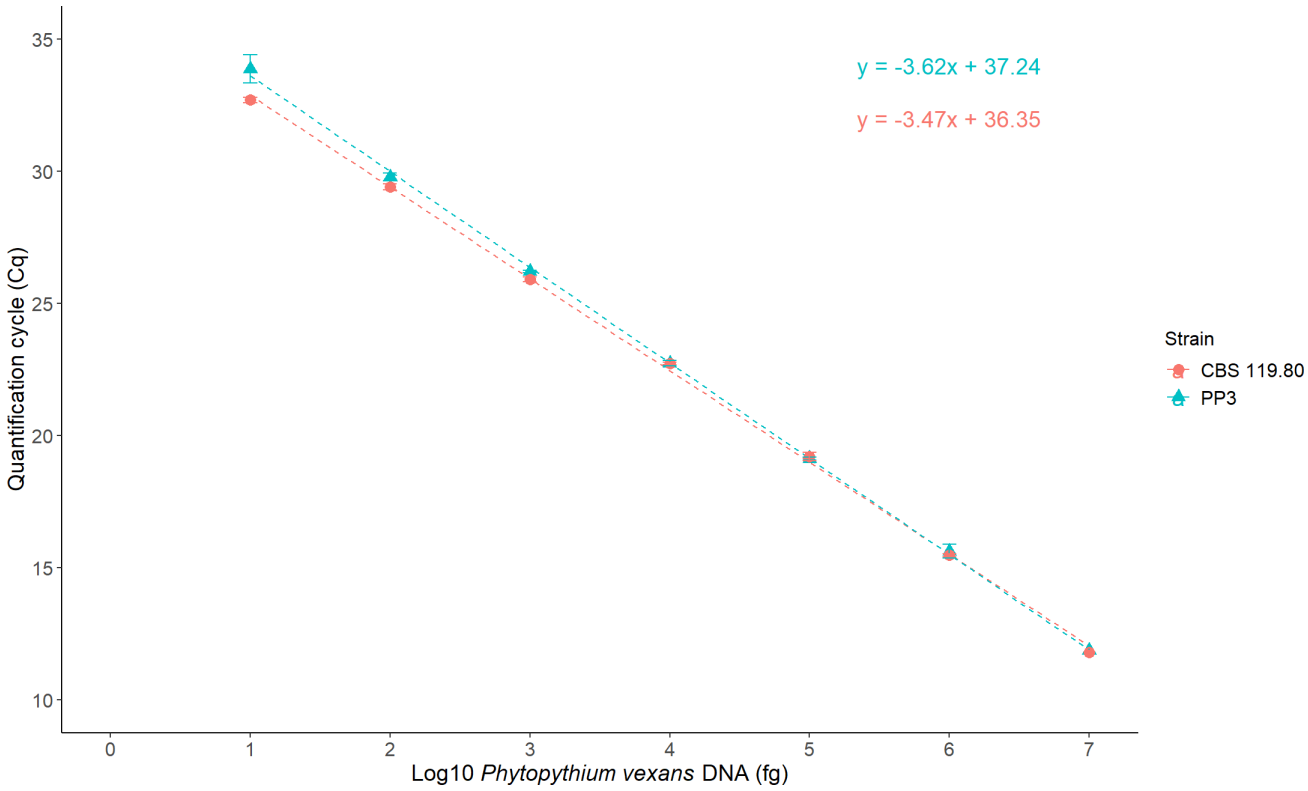


Figure 1 – Standard curves obtained with genomic DNA of two *Phytopythium vexans* strains CBS 11980 (red) and PP3 (blue) showing correlation with the amount of target DNA and the quantification cycle (Cq). Error bars represent the Cq standard deviation between runs.

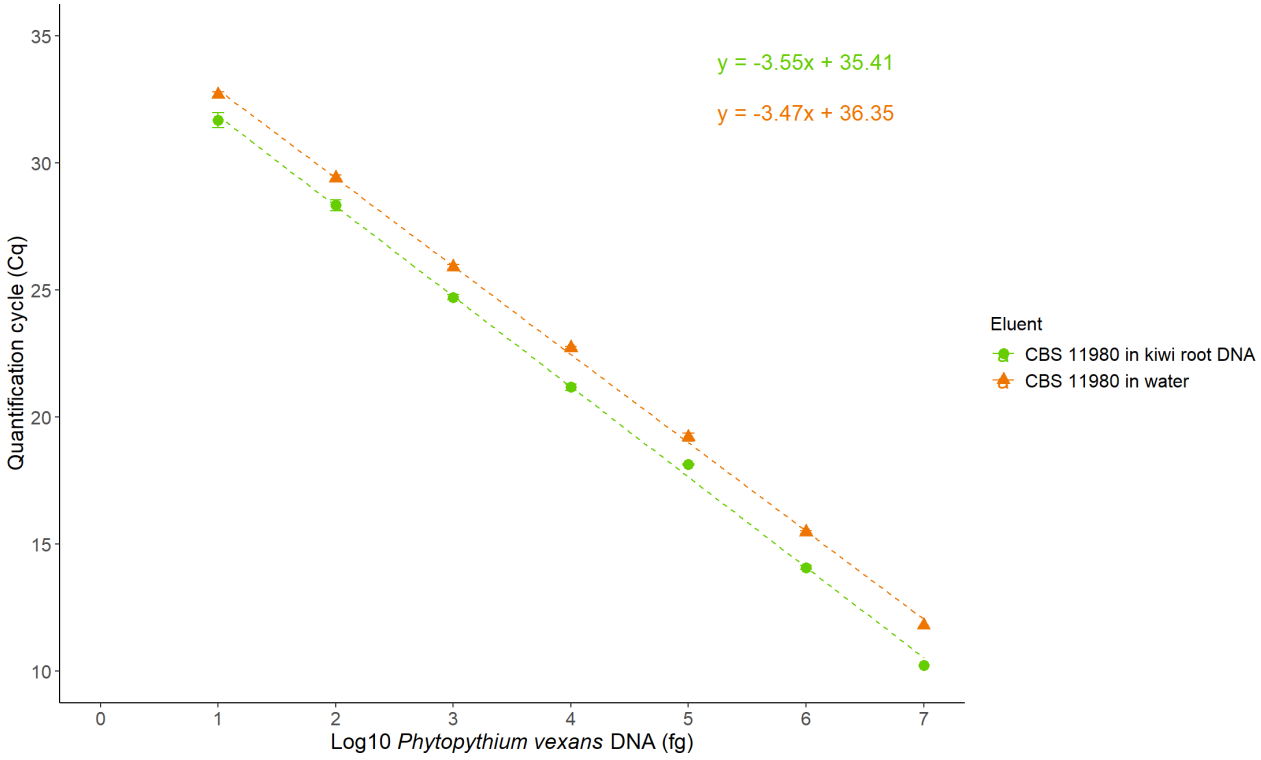


Figure 2 – Standard curves obtained with dilutions of the *Phytopythium vexans* strain CBS 119.80 in water (orange) and kiwifruit root DNA concentrated at 10 ng (green). Error bars represent the Cq standard deviation between runs.

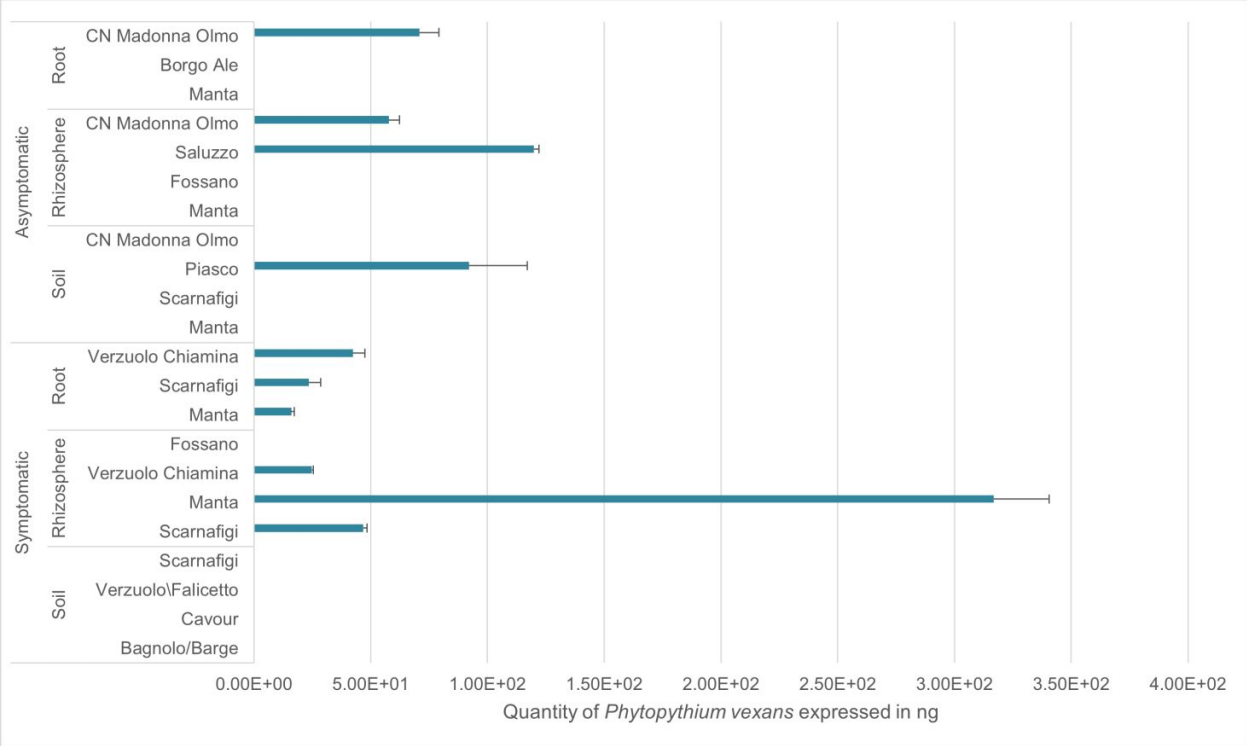


Figure 3 – Barplot representing the quantification of *Phytopythium vexans* expressed in ng, in naturally infected samples (root, soil and rhizosphere). Error bars represent the Cq standard error between runs.

Supplementary material

Supplementary Table 1 – List of COI sequences used to perform the alignment used as input for DECIPHER v2.0

Species	Strain	Gene	Accession number
Phytopythium helicoides	CA1	cytochrome oxidase subunit 1 (COI) partial cds	ON228523
Phytopythium helicoides	CA2	cytochrome oxidase subunit 1 (COI) partial cds	ON228524
Phytopythium helicoides	H5	cytochrome oxidase subunit 1 (COI) partial cds	AB690633.1
Phytopythium helicoides	CBS286.31	cytochrome oxidase subunit 1 (COI) partial cds	AB690645.1
Phytopythium helicoides	Chen 248	cytochrome oxidase subunit 1 (COI) partial cds	MF984145.1
Phytopythium helicoides	Chen 249	cytochrome oxidase subunit 1 (COI) partial cds	MF984146.1
Phytopythium helicoides	Chen 250	cytochrome oxidase subunit 1 (COI) partial cds	MF984147.1
Phytopythium helicoides	GB42A	cytochrome oxidase subunit 1 (COI) partial cds	MK879707.1
Phytopythium helicoides	GB450C	cytochrome oxidase subunit 1 (COI) partial cds	MK879708.1
Phytopythium helicoides	GB5796A	cytochrome oxidase subunit 1 (COI) partial cds	MK879709.1
Phytopythium helicoides	GB6038A	cytochrome oxidase subunit 1 (COI) partial cds	MK879710.1
Phytopythium helicoides	NA	cytochrome oxidase subunit 1 (COI) partial cds	MT188654.1
Phytopythium helicoides	NA	cytochrome oxidase subunit 1 (COI) partial cds	MT834959.1
Phytopythium helicoides	RMSD1	cytochrome oxidase subunit 1 (COI) partial cds	MW450815.1
Phytopythium chamaehyphon	CA3	cytochrome oxidase subunit 1 (COI) partial cds	ON228525
Phytopythium chamaehyphon	CA4	cytochrome oxidase subunit 1 (COI) partial cds	ON228526
Phytopythium chamaehyphon	CA5	cytochrome oxidase subunit 1 (COI) partial cds	ON228527
Phytopythium chamaehyphon	PH6	cytochrome oxidase subunit 1 (COI) partial cds	ON228528
Phytopythium chamaehyphon	4/16_DRE	cytochrome oxidase subunit 1 (COI) partial cds	ON228529
Phytopythium chamaehyphon	10/16_BR	cytochrome oxidase subunit 1 (COI) partial cds	ON228530
Phytopythium chamaehyphon	11/16_AB1	cytochrome oxidase subunit 1 (COI) partial cds	ON228531
Phytopythium chamaehyphon	62PPch	cytochrome oxidase subunit 1 (COI) partial cds	MT780641.1

Phytopythium chamaehyphon	CBS 259.30	cytochrome oxidase subunit 1 (COI) partial cds	AB690644.1
Phytopythium chamaehyphon	22PPch	cytochrome oxidase subunit 1 (COI) partial cds	MT780601.1
Phytopythium chamaehyphon	56PPch	cytochrome oxidase subunit 1 (COI) partial cds	MT780635.1
Phytopythium chamaehyphon	GUCC7026	cytochrome oxidase subunit 1 (COI) partial cds	AB690631.1
Phytopythium chamaehyphon	61PPch	cytochrome oxidase subunit 1 (COI) partial cds	MT780640.1
Phytopythium chamaehyphon	86PPch	cytochrome oxidase subunit 1 (COI) partial cds	MT780665.1
Phytopythium chamaehyphon	105PPch	cytochrome oxidase subunit 1 (COI) partial cds	MT780683.1
Phytopythium chamaehyphon	106PPch	cytochrome oxidase subunit 1 (COI) partial cds	MT780684.1
Phytopythium chamaehyphon	108PPch	cytochrome oxidase subunit 1 (COI) partial cds	MT780686.1
Phytopythium litorale	R3A	cytochrome oxidase subunit 1 (COI) partial cds	ON228532
Phytopythium litorale	4SBE_C2D	cytochrome oxidase subunit 1 (COI) partial cds	ON228533
Phytopythium litorale	4SBE_C2A	cytochrome oxidase subunit 1 (COI) partial cds	ON228534
Phytopythium litorale	4SBE_C2C	cytochrome oxidase subunit 1 (COI) partial cds	ON228535
Phytopythium litorale	4SBE_C2B	cytochrome oxidase subunit 1 (COI) partial cds	ON228536
Phytopythium litorale	P8G	cytochrome oxidase subunit 1 (COI) partial cds	ON228537
Phytopythium litorale	P8H	cytochrome oxidase subunit 1 (COI) partial cds	ON228538
Phytopythium litorale	P8I	cytochrome oxidase subunit 1 (COI) partial cds	ON228539
Phytopythium litorale	R10A	cytochrome oxidase subunit 1 (COI) partial cds	ON228540
Phytopythium litorale	R10B	cytochrome oxidase subunit 1 (COI) partial cds	ON228541
Phytopythium litorale	GUCC7167	cytochrome oxidase subunit 1 (COI) partial cds	AB690634.1
Phytopythium litorale	GUCC1072	cytochrome oxidase subunit 1 (COI) partial cds	AB920495.1
Phytopythium litorale	GUCC1132	cytochrome oxidase subunit 1 (COI) partial cds	AB920496.1
Phytopythium litorale	PPRI8629	cytochrome oxidase subunit 1 (COI) partial cds	GU133465.1
Phytopythium litorale	CBS122662	cytochrome oxidase subunit 1 (COI) partial cds	HQ708432.1
Phytopythium litorale	CBS118360	cytochrome oxidase subunit 1 (COI) partial cds	HQ708433.1
Phytopythium litorale	BR896	cytochrome oxidase subunit 1 (COI) partial cds	HQ708434.1
Phytopythium litorale	Lev3013	cytochrome oxidase subunit 1 (COI) partial cds	HQ708717.1
Phytopythium litorale	Lev3012	cytochrome oxidase subunit 1 (COI) partial cds	HQ708718.1

Phytopythium litorale	Lev3011	cytochrome oxidase subunit 1 (COI) partial cds	HQ708719.1
Phytopythium litorale	Lev3006	cytochrome oxidase subunit 1 (COI) partial cds	HQ708720.1
Phytopythium litorale	Lev3002	cytochrome oxidase subunit 1 (COI) partial cds	HQ708721.1
Phytopythium litorale	NA	cytochrome oxidase subunit 1 (COI) partial cds	KT247404.1
Phytopythium litorale	C12-19	cytochrome oxidase subunit 1 (COI) partial cds	KT692919.1
Phytopythium litorale	NNIBRFG9359	cytochrome oxidase subunit 1 (COI) partial cds	MK802185.1
Phytopythium litorale	W630	cytochrome oxidase subunit 1 (COI) partial cds	MK802186.1
Phytopythium litorale	NA	cytochrome oxidase subunit 1 (COI) partial cds	MT648515.1
Phytopythium litorale	PH-C	cytochrome oxidase subunit 1 (COI) partial cds	MT863263.1
Phytopythium vexans	RE3	cytochrome oxidase subunit 1 (COI) partial cds	ON228542
Phytopythium vexans	R1A	cytochrome oxidase subunit 1 (COI) partial cds	ON228543
Phytopythium vexans	R1B	cytochrome oxidase subunit 1 (COI) partial cds	ON228544
Phytopythium vexans	R1C	cytochrome oxidase subunit 1 (COI) partial cds	ON228545
Phytopythium vexans	R1D	cytochrome oxidase subunit 1 (COI) partial cds	ON228546
Phytopythium vexans	R1E	cytochrome oxidase subunit 1 (COI) partial cds	ON228547
Phytopythium vexans	R1F	cytochrome oxidase subunit 1 (COI) partial cds	ON228548
Phytopythium vexans	R1G	cytochrome oxidase subunit 1 (COI) partial cds	ON228549
Phytopythium vexans	R1H	cytochrome oxidase subunit 1 (COI) partial cds	ON228550
Phytopythium vexans	R7A	cytochrome oxidase subunit 1 (COI) partial cds	ON228551
Phytopythium vexans	R7B	cytochrome oxidase subunit 1 (COI) partial cds	ON228552
Phytopythium vexans	R7C	cytochrome oxidase subunit 1 (COI) partial cds	ON228553
Phytopythium vexans	R7D	cytochrome oxidase subunit 1 (COI) partial cds	ON228554
Phytopythium vexans	R7E	cytochrome oxidase subunit 1 (COI) partial cds	ON228555
Phytopythium vexans	R7F	cytochrome oxidase subunit 1 (COI) partial cds	ON228556
Phytopythium vexans	P8A	cytochrome oxidase subunit 1 (COI) partial cds	ON228557

Phytopythium vexans	P8B	cytochrome oxidase subunit 1 (COI) partial cds	ON228558
Phytopythium vexans	P8D	cytochrome oxidase subunit 1 (COI) partial cds	ON228559
Phytopythium vexans	P8E	cytochrome oxidase subunit 1 (COI) partial cds	ON228560
Phytopythium vexans	P8F	cytochrome oxidase subunit 1 (COI) partial cds	ON228561
Phytopythium vexans	T4A	cytochrome oxidase subunit 1 (COI) partial cds	ON228562
Phytopythium vexans	T4B	cytochrome oxidase subunit 1 (COI) partial cds	ON228563
Phytopythium vexans	13/16_DR2	cytochrome oxidase subunit 1 (COI) partial cds	ON228564
Phytopythium vexans	13/16_DR3	cytochrome oxidase subunit 1 (COI) partial cds	ON228565
Phytopythium vexans	PPA	cytochrome oxidase subunit 1 (COI) partial cds	ON228566
Phytopythium vexans	PPC	cytochrome oxidase subunit 1 (COI) partial cds	ON228567
Phytopythium vexans	PPD	cytochrome oxidase subunit 1 (COI) partial cds	ON228568
Phytopythium vexans	PPE	cytochrome oxidase subunit 1 (COI) partial cds	ON228569
Phytopythium vexans	PPF	cytochrome oxidase subunit 1 (COI) partial cds	ON228570
Phytopythium vexans	PP1	cytochrome oxidase subunit 1 (COI) partial cds	ON228571
Phytopythium vexans	PP2	cytochrome oxidase subunit 1 (COI) partial cds	ON228572
Phytopythium vexans	PP3	cytochrome oxidase subunit 1 (COI) partial cds	ON228573
Phytopythium vexans	PP4	cytochrome oxidase subunit 1 (COI) partial cds	ON228574
Phytopythium vexans	PP5	cytochrome oxidase subunit 1 (COI) partial cds	ON228575
Phytopythium vexans	PP6	cytochrome oxidase subunit 1 (COI) partial cds	ON228576
Phytopythium vexans	PP8	cytochrome oxidase subunit 1 (COI) partial cds	ON228577
Phytopythium vexans	GBI	cytochrome oxidase subunit 1 (COI) partial cds	ON228578
Phytopythium vexans	4SRE1	cytochrome oxidase subunit 1 (COI) partial cds	ON228579
Phytopythium vexans	4SRE2	cytochrome oxidase subunit 1 (COI) partial cds	ON228580
Phytopythium vexans	4SBE_2C1	cytochrome oxidase subunit 1 (COI) partial cds	ON228581
Phytopythium vexans	5/16_CBE	cytochrome oxidase subunit 1 (COI) partial cds	ON228582
Phytopythium vexans	6/16_BRE	cytochrome oxidase subunit 1 (COI) partial cds	ON228583

Phytopythium vexans	12/16_CR1	cytochrome oxidase subunit 1 (COI) partial cds	ON228584
Phytopythium vexans	12/16_AB1	cytochrome oxidase subunit 1 (COI) partial cds	ON228585
Phytopythium vexans	4SBE_C1A	cytochrome oxidase subunit 1 (COI) partial cds	ON228586

Globisporangium sylvaticum	C12-82	cytochrome oxidase subunit 1 (COI) partial cds	KT692839.1
Globisporangium sylvaticum	C12-85	cytochrome oxidase subunit 1 (COI) partial cds	KT692841.1
Globisporangium sylvaticum	C12-186	cytochrome oxidase subunit 1 (COI) partial cds	KT692843.1
Globisporangium sylvaticum	C12-92	cytochrome oxidase subunit 1 (COI) partial cds	KT692845.1
Globisporangium sylvaticum	C12-192	cytochrome oxidase subunit 1 (COI) partial cds	KT692847.1
Globisporangium sylvaticum	N17-112	cytochrome oxidase subunit 1 (COI) partial cds	MT222607.1
Globisporangium sylvaticum	N17-181	cytochrome oxidase subunit 1 (COI) partial cds	MT222676.1
Globisporangium sylvaticum	N17-185	cytochrome oxidase subunit 1 (COI) partial cds	MT222680.1
Globisporangium sylvaticum	N18-83	cytochrome oxidase subunit 1 (COI) partial cds	MT222839.1
Globisporangium sylvaticum	LPPY17	cytochrome oxidase subunit 1 (COI) partial cds	MT536761.1
Globisporangium sylvaticum	Iso9	cytochrome oxidase subunit 1 (COI) partial cds	MZ152005.1
Globisporangium sylvaticum	Iso82	cytochrome oxidase subunit 1 (COI) partial cds	MZ152021.1
Globisporangium sylvaticum	SAP18	cytochrome oxidase subunit 1 (COI) partial cds	OK020192.1
Globisporangium sylvaticum	SAP21_34	cytochrome oxidase subunit 1 (COI) partial cds	OK020193.1
Pythium ultimum	CBS 39851	cytochrome oxidase subunit 1 (COI) partial cds	HQ708906.1
Phytopythium delawarense	CBS 123040	cytochrome oxidase subunit 1 (COI) partial cds	KF853240.1
Phytopythium mirpurense	NA	cytochrome oxidase subunit 1 (COI) partial cds	KJ831612.1
Pythium aff. intermedium	C12-184	cytochrome oxidase subunit 1 (COI) partial cds	KT692881.1
Pseudomonas syringae pv. Actinidiae	ICMP 9617 C01_100	whole genome shotgun sequence	AOKP01000100.1:13928-14941
Pseudomonas syringae pv. Actinidiae	ICMP 9617 C01_185	whole genome shotgun sequence	AOKP01000185.1:5085-6527
Pseudomonas syringae pv. Actinidiae	ICMP 9617 C01_221	whole genome shotgun sequence	AOKP01000221.1:81364-83376

Pseudomonas syringae pv. Actinidiae	ICMP 9617 C01_232	whole genome shotgun sequence	AOKP01000232.1:131456-132895
Pseudomonas syringae pv. Actinidiae	str. NCPPB 3739 contig727	whole genome shotgun sequence	NZ_AFTH01000709.1
Pseudomonas syringae pv. Actinidiae	ICMP 9617 chromosome	whole genome shotgun sequence	NZ_CM002753.1:5468678-5470117

Pseudomonas syringae pv. Actinidiae	ICMP 9617 chromosome	whole genome shotgun sequence	NZ_CM002753.1:4980916-4982928
Pseudomonas syringae pv. Actinidiae	ICMP 9617 chromosome	whole genome shotgun sequence	NZ_CM002753.1:4133679-4135121
Phytopythium boreale	CBS 551.88	cytochrome oxidase subunit 1 (COI) partial cds	AB690647.1
Phytopythium boreale	P28	cytochrome oxidase subunit 1 (COI) partial cds	MT720660.1
Phytopythium boreale	P41	cytochrome oxidase subunit 1 (COI) partial cds	MT720661.1
Phytopythium boreale	P57	cytochrome oxidase subunit 1 (COI) partial cds	MT720662.1
Phytopythium carbonicum	CBS 112544	cytochrome oxidase subunit 1 (COI) partial cds	AB690648.1
Phytopythium carbonicum	CBS 112545	cytochrome oxidase subunit 1 (COI) partial cds	HQ708420.1
Phytopythium carbonicum	P24	cytochrome oxidase subunit 1 (COI) partial cds	MT720663.1
Phytopythium carbonicum	P25	cytochrome oxidase subunit 1 (COI) partial cds	MT720664.1
Phytophthora cinnamomi	P1	cytochrome oxidase subunit 1 (COI) partial cds	MN566591.1
Phytophthora cinnamomi	P8	cytochrome oxidase subunit 1 (COI) partial cds	MN566598.1
Phytophthora cinnamomi	P9	cytochrome oxidase subunit 1 (COI) partial cds	MN566599.1
Phytophthora cinnamomi	P10	cytochrome oxidase subunit 1 (COI) partial cds	MN566600.1
Phytophthora cinnamomi	P11	cytochrome oxidase subunit 1 (COI) partial cds	MN566601.1
Phytophthora cinnamomi	VN007	cytochrome oxidase subunit 1 (COI) partial cds	MN866061.1
Phytophthora cinnamomi	VN017	cytochrome oxidase subunit 1 (COI) partial cds	MN866062.1
Phytophthora cinnamomi	VN058	cytochrome oxidase subunit 1 (COI) partial cds	MN866066.1
Phytophthora cinnamomi	VN070	cytochrome oxidase subunit 1 (COI) partial cds	MN866069.1
Phytophthora cinnamomi	VN231	cytochrome oxidase subunit 1 (COI) partial cds	MN866082.1
Phytophthora cinnamomi	VN450	cytochrome oxidase subunit 1 (COI) partial cds	MN866086.1
Phytophthora cinnamomi	VN533	cytochrome oxidase subunit 1 (COI) partial cds	MN866089.1
Phytophthora cinnamomi	VN555	cytochrome oxidase subunit 1 (COI) partial cds	MN866093.1
Phytophthora cinnamomi	TXQ01	cytochrome oxidase subunit 1 (COI) partial cds	MT021460.1
Phytophthora cinnamomi	LEV6688	cytochrome oxidase subunit 1 (COI) partial cds	MT832898.1
Phytophthora cinnamomi	LEV6711	cytochrome oxidase subunit 1 (COI) partial cds	MT832899.1

Phytophthora cinnamomi	LEV6712	cytochrome oxidase subunit 1 (COI) partial cds	MT832900.1
Phytophthora cinnamomi	LEV6718	cytochrome oxidase subunit 1 (COI) partial cds	MT832901.1
Phytophthora cinnamomi	LEV6720	cytochrome oxidase subunit 1 (COI) partial cds	MT832902.1
Phytophthora cinnamomi	LEV6719	cytochrome oxidase subunit 1 (COI) partial cds	MT832903.1
Phytophthora cinnamomi	LEV6702	cytochrome oxidase subunit 1 (COI) partial cds	MT832904.1
Phytophthora cinnamomi	LEV6725	cytochrome oxidase subunit 1 (COI) partial cds	MT832905.1
Phytophthora cinnamomi	LEV6722	cytochrome oxidase subunit 1 (COI) partial cds	MT832906.1
Phytophthora cinnamomi	GB.647.z1	cytochrome oxidase subunit 1 (COI) partial cds	MT996347.1
Phytophthora cinnamomi	GB.5972.pear.a	cytochrome oxidase subunit 1 (COI) partial cds	MT996348.1
Phytophthora cinnamomi	GB.5973.ble.rt	cytochrome oxidase subunit 1 (COI) partial cds	MT996349.1
Phytophthora cinnamomi	GB.6378.soil	cytochrome oxidase subunit 1 (COI) partial cds	MT996350.1
Phytophthora cinnamomi	PDA1546	cytochrome oxidase subunit 1 (COI) partial cds	MW927569.1
Phytophthora citrophthora	CH88IC1	cytochrome oxidase subunit 1 (COI) partial cds	AB688195.1
Phytophthora citrophthora	STE-U6751	cytochrome oxidase subunit 1 (COI) partial cds	GU133458.1
Phytophthora citrophthora	M189	cytochrome oxidase subunit 1 (COI) partial cds	GU945471.1
Phytophthora citrophthora	P10341	cytochrome oxidase subunit 1 (COI) partial cds	HQ261283.1
Phytophthora citrophthora	CBS 111726	cytochrome oxidase subunit 1 (COI) partial cds	HQ708273.1
Phytophthora citrophthora	NJB2013-HR-27	cytochrome oxidase subunit 1 (COI) partial cds	KJ631594.2
Phytophthora citrophthora	NJB2013-MF-34	cytochrome oxidase subunit 1 (COI) partial cds	KJ631595.2
Phytophthora citrophthora	41-1-1	cytochrome oxidase subunit 1 (COI) partial cds	KU942419.1
Phytophthora citrophthora	WPC P3693	cytochrome oxidase subunit 1 (COI) partial cds	LC595908.1
Phytophthora citrophthora	GB.18-1244	cytochrome oxidase subunit 1 (COI) partial cds	MN513257.1
Phytophthora citrophthora	CBS 950.87	cytochrome oxidase subunit 1 (COI) partial cds	MT583654.1
Phytophthora citrophthora	PAB17.152A	cytochrome oxidase subunit 1 (COI) partial cds	MT583655.1
Phytophthora citrophthora	VHS33174	cytochrome oxidase subunit 1 (COI) partial cds	MT583656.1
Phytophthora citrophthora	P1159	cytochrome oxidase subunit 1 (COI) partial cds	MW597356.1
Phytophthora citrophthora	PDA1843	cytochrome oxidase subunit 1 (COI) partial cds	MW927570.1

Phytopythium citrinum	CBS119171	cytochrome oxidase subunit 1 (COI) partial cds	AB690649.1
Phytopythium citrinum	ADC9519	cytochrome oxidase subunit 1 (COI) partial cds	HQ708423.1
Phytopythium citrinum	ADC9515	cytochrome oxidase subunit 1 (COI) partial cds	HQ708424.1
Phytopythium citrinum	ADC9513	cytochrome oxidase subunit 1 (COI) partial cds	HQ708425.1
Phytopythium citrinum	ADC9512	cytochrome oxidase subunit 1 (COI) partial cds	HQ708426.1
Phytopythium citrinum	ADC9442	cytochrome oxidase subunit 1 (COI) partial cds	HQ708427.1
Phytopythium citrinum	C12-6	cytochrome oxidase subunit 1 (COI) partial cds	KT692918.1
Phytopythium delawarense	382B	cytochrome oxidase subunit 1 (COI) partial cds	AB690642.2
Phytopythium delawarense	CBS 123040	cytochrome oxidase subunit 1 (COI) partial cds	KF853240.1
Phytophthora drechsleri	C18	cytochrome oxidase subunit 1 (COI) partial cds	AY659597.1
Phytophthora drechsleri	Sa2	cytochrome oxidase subunit 1 (COI) partial cds	AY659602.1
Phytophthora drechsleri	LEV 6731	cytochrome oxidase subunit 1 (COI) partial cds	MH013472.1
Phytophthora drechsleri	CPHST BL 140	cytochrome oxidase subunit 1 (COI) partial cds	MH136880.1
Phytophthora drechsleri	23J5	cytochrome oxidase subunit 1 (COI) partial cds	MH620076.1
Phytophthora drechsleri	VN520	cytochrome oxidase subunit 1 (COI) partial cds	MN866087.1
Phytophthora drechsleri	LEV6696	cytochrome oxidase subunit 1 (COI) partial cds	MT832907.1
Phytophthora drechsleri	LEV6705	cytochrome oxidase subunit 1 (COI) partial cds	MT832909.1
Phytophthora drechsleri	LEV6730	cytochrome oxidase subunit 1 (COI) partial cds	MT832910.1
Phytophthora drechsleri	LEV6697	cytochrome oxidase subunit 1 (COI) partial cds	MT832911.1
Phytophthora drechsleri	LEV6698	cytochrome oxidase subunit 1 (COI) partial cds	MT832912.1
Phytophthora drechsleri	LEV6736	cytochrome oxidase subunit 1 (COI) partial cds	MT832913.1
Phytophthora drechsleri	LEV6710	cytochrome oxidase subunit 1 (COI) partial cds	MT832914.1
Phytophthora drechsleri	20-043	cytochrome oxidase subunit 1 (COI) partial cds	MW480541.1
Phytopythium kandeliae	P11614	cytochrome oxidase subunit 1 (COI) partial cds	HQ171169.1
Phytopythium kandeliae	P15209	cytochrome oxidase subunit 1 (COI) partial cds	HQ171176.1
Phytopythium kandeliae	CBS11391	cytochrome oxidase subunit 1 (COI) partial cds	HQ708206.1
Phytopythium kandeliae	CBS11191	cytochrome oxidase subunit 1 (COI) partial cds	HQ708207.1

Phytopythium kandeliae	AJM 26	cytochrome oxidase subunit 1 (COI) partial cds	KJ690246.1
Phytopythium kandeliae	AJM 85	cytochrome oxidase subunit 1 (COI) partial cds	KJ690247.1
Phytopythium kandeliae	AJM 95	cytochrome oxidase subunit 1 (COI) partial cds	KJ690248.1
Phytopythium kandeliae	NBRC 32620	cytochrome oxidase subunit 1 (COI) partial cds	MF397922.1
Phytophthora lateralis	CBS 168.42	cytochrome oxidase subunit 1 (COI) partial cds	AY564191.1
Phytophthora lateralis	SCRP390	cytochrome oxidase subunit 1 (COI) partial cds	AY659607.1
Phytophthora lateralis	isolate 368	cytochrome oxidase subunit 1 (COI) partial cds	EU124922.1
Phytophthora lateralis	isolate p51	cytochrome oxidase subunit 1 (COI) partial cds	GU945487.1
Phytophthora lateralis	Lev1213	cytochrome oxidase subunit 1 (COI) partial cds	HQ708320.1
Phytophthora lateralis	P2388	cytochrome oxidase subunit 1 (COI) partial cds	JX121322.1
Phytophthora lateralis	P2275	cytochrome oxidase subunit 1 (COI) partial cds	KP987113.1
Phytophthora lateralis	P2276	cytochrome oxidase subunit 1 (COI) partial cds	KP987115.1
Phytophthora lateralis	NA	cytochrome oxidase subunit 1 (COI) partial cds	KU532174.1
Phytophthora lateralis	NA	cytochrome oxidase subunit 1 (COI) partial cds	KU532175.1
Phytophthora lateralis	ex-type CPHST BL 42	cytochrome oxidase subunit 1 (COI) partial cds	MH136917.1
Phytophthora lateralis	isolate 22H9	cytochrome oxidase subunit 1 (COI) partial cds	MH620089.1
Phytophthora lateralis	OSU JP-15-23	cytochrome oxidase subunit 1 (COI) partial cds	MK792735.1
Phytophthora lateralis	OSU JP-15-25	cytochrome oxidase subunit 1 (COI) partial cds	MK792737.1
Phytophthora lateralis	OSU JP-15-27	cytochrome oxidase subunit 1 (COI) partial cds	MK792739.1
Phytophthora lateralis	OSU JP-14-2	cytochrome oxidase subunit 1 (COI) partial cds	MK792741.1
Phytophthora lateralis	OSU JP-14-5	cytochrome oxidase subunit 1 (COI) partial cds	MK792744.1
Phytophthora lateralis	OSU JP-14-6	cytochrome oxidase subunit 1 (COI) partial cds	MK792745.1
Phytophthora lateralis	P2451	cytochrome oxidase subunit 1 (COI) partial cds	MW323672.1
Phytopythium montanum	CBS111349	cytochrome oxidase subunit 1 (COI) partial cds	AB690637.1
Phytopythium montanum	ADC9766	cytochrome oxidase subunit 1 (COI) partial cds	HQ708437.1
Phytopythium montanum	ADC9762	cytochrome oxidase subunit 1 (COI) partial cds	HQ708438.1
Phytopythium oedochilum	CBS252.70	cytochrome oxidase subunit 1 (COI) partial cds	AB690643.1

Phytopythium oedochilum	CBS292.37	cytochrome oxidase subunit 1 (COI) partial cds	AB690646.1
Phytopythium oedochilum	GUCC5091	cytochrome oxidase subunit 1 (COI) partial cds	AB920493.1
Phytopythium oedochilum	GUCC5078	cytochrome oxidase subunit 1 (COI) partial cds	AB920494.1
Phytopythium oedochilum	CBS 292.37	cytochrome oxidase subunit 1 (COI) partial cds	EF408873.1
Phytopythium oedochilum	STE-U6748	cytochrome oxidase subunit 1 (COI) partial cds	GU133468.1
Phytopythium oedochilum	CBS29237	cytochrome oxidase subunit 1 (COI) partial cds	HQ708439.1
Phytopythium oedochilum	CBS73994	cytochrome oxidase subunit 1 (COI) partial cds	HQ708440.1
Phytopythium oedochilum	DAOM229148	cytochrome oxidase subunit 1 (COI) partial cds	HQ708756.1
Phytopythium ostracodes	CBS768.73	cytochrome oxidase subunit 1 (COI) partial cds	AB690638.1
Phytopythium ostracodes	P45	cytochrome oxidase subunit 1 (COI) partial cds	MT720666.1
Phytopythium ostracodes	P64	cytochrome oxidase subunit 1 (COI) partial cds	MT720667.1
Phytopythium ostracodes	P121	cytochrome oxidase subunit 1 (COI) partial cds	MT720668.1
Phytophthora palmivora	93Ppal	cytochrome oxidase subunit 1 (COI) partial cds	MT780672.1
Phytophthora palmivora	115Ppal	cytochrome oxidase subunit 1 (COI) partial cds	MT780691.1
Phytophthora palmivora	201Ppal	cytochrome oxidase subunit 1 (COI) partial cds	MT780698.1
Phytophthora palmivora	203Ppal	cytochrome oxidase subunit 1 (COI) partial cds	MT780700.1
Phytophthora palmivora	207Ppal	cytochrome oxidase subunit 1 (COI) partial cds	MT780704.1
Phytophthora palmivora	211Ppal	cytochrome oxidase subunit 1 (COI) partial cds	MT780706.1
Phytophthora palmivora	NA	cytochrome oxidase subunit 1 (COI) partial cds	MT780708.1
Phytophthora palmivora	213Ppal	cytochrome oxidase subunit 1 (COI) partial cds	MT780710.1
Phytophthora palmivora	215Ppal	cytochrome oxidase subunit 1 (COI) partial cds	MT780712.1
Phytophthora palmivora	217Ppal	cytochrome oxidase subunit 1 (COI) partial cds	MT780714.1
Phytophthora palmivora	227Ppal	cytochrome oxidase subunit 1 (COI) partial cds	MT780724.1
Phytophthora palmivora	229Ppal	cytochrome oxidase subunit 1 (COI) partial cds	MT780726.1
Phytophthora palmivora	CBS 179.26	cytochrome oxidase subunit 1 (COI) partial cds	MZ782838.1
Phytophthora palmivora	Phoenix4	cytochrome oxidase subunit 1 (COI) partial cds	MZ782840.1
Phytophthora palmivora	GRE1	cytochrome oxidase subunit 1 (COI) partial cds	MZ782841.1

Phytophthora palmivora	MD5	cytochrome oxidase subunit 1 (COI) partial cds	MZ782842.1
Phytophthora palmivora	MD6	cytochrome oxidase subunit 1 (COI) partial cds	MZ782843.1
Phytopythium sindhum	CBS:124520	cytochrome oxidase subunit 1 (COI) partial cds	HM244821.1
Phytopythium sindhum	CBS:124518	cytochrome oxidase subunit 1 (COI) partial cds	HM244822.1
Phytopythium sindhum	Chen 265	cytochrome oxidase subunit 1 (COI) partial cds	MF984149.1
Phytopythium mercuriale	CBS122443	cytochrome oxidase subunit 1 (COI) partial cds	AB690636.1
Phytopythium mercuriale	GUCC1132	cytochrome oxidase subunit 1 (COI) partial cds	AB920497.1
Phytopythium mercuriale	suto5ssT3	cytochrome oxidase subunit 1 (COI) partial cds	AB920498.1
Phytopythium mercuriale	STE-U6127	cytochrome oxidase subunit 1 (COI) partial cds	GU133464.1
Phytopythium mercuriale	Chen 314	cytochrome oxidase subunit 1 (COI) partial cds	MN271343.1
Phytopythium mercuriale	P50	cytochrome oxidase subunit 1 (COI) partial cds	MT720665.1

Supplementary Table 2 - Orchard locations in central Washington state where soil samples were collected and screened for the presence of *Phytpopythium vexans*

Sample Name	Year sampled	County in WA State	Longitude	Latitude	*Phytopythium vexans* detected
GF118	2021	Okanogan	-119.8545755	48.08615251	
GF119	2021	Okanogan	-119.8554016	48.0867832	
CK 120	2021	Douglas	-119.5030809	48.07118808	
CK 121	2021	Douglas	-119.507587	48.07120242	
COL 114	2021	Chelan	-120.0137771	47.86464248	
COL 115	2021	Chelan	-120.0134338	47.86462809	
LOS116	2021	Okanogan	-119.6013894	48.89383011	
LOS117	2021	Okanogan	-119.6029344	48.89367493	
MF110	2021	Yakima	-120.1864915	46.38586389	X
MF111	2021	Yakima	-120.1955395	46.42884028	X
MF112	2021	Yakima	-120.2746969	46.42505395	
MF113	2021	Yakima	-120.1822429	46.39243041	X
OTT109	2021	Okanogan	-119.4147811	48.78616521	
OTT108	2021	Okanogan	-119.4148884	48.7866459	
TA104	2021	Okanogan	-119.4005654	48.94962791	
TA105	2021	Okanogan	-119.4390604	48.94404792	
W106	2021	Okanogan	-119.4586978	48.78193546	
W107	2021	Okanogan	-119.4574532	48.78185769	
ALD 132	2022	Grant	-119.5781538	46.941106	X
ALD 133	2022	Grant	-119.5781538	46.941106	X
FH136	2022	Grant	-119.3782089	46.9353431	
FH 137	2022	Grant	-119.42751	46.9634	
HB134	2022	Okanogan	-119.7279022	48.2598876	
HB135	2022	Okanogan	-119.72554	48.25901	

Supplementary Table 3 – Results of the quantification of *Phytopythium vexans* in artificially inoculated kiwifruit roots

Condition	Sample ID	Ct	*Phytopythium vexans* quantity (ng)	Mean of *Phytopythium vexans* quantity (ng)	DS	Technical replicate aggregate (ng)
Control	NS 48 1	31.992	2.82×10^{1}	5.11×10^{1}	2.41×10^{1}	5.61×10^{1}
Control	NS 48 1	30.536	7.11×10^{1}			
Control	NS 48 1	30.584	6.90×10^{1}			
Control	NS 48 2	31.418	4.06×10^{1}			3.09×10^{1}
Control	NS 48 2	32.105	2.62×10^{1}			
Control	NS 48 2	32.131	2.58×10^{1}			
Control	NS 48 3	30.156	9.06×10^{1}			6.63×10^{1}
Control	NS 48 3	31.483	3.89×10^{1}			
Control	NS 48 3	30.572	6.95×10^{1}			
Inoculated	I 48 1	22.449	1.22×10^{4}	2.33×10^{4}	9.69×10^{3}	1.24×10^{4}
Inoculated	I 48 1	22.478	1.20×10^{4}			
Inoculated	I 48 1	22.339	1.31×10^{4}			
Inoculated	I 48 2	21.486	2.25×10^{4}			2.28×10^{4}
Inoculated	I 48 2	21.375	2.41×10^{4}			
Inoculated	I 48 2	21.535	2.18×10^{4}			
Inoculated	I 48 3	20.911	3.24×10^{4}			3.46×10^{4}
Inoculated	I 48 3	20.707	3.69×10^{4}			
Inoculated	I 48 3	20.82	3.44×10^{4}			

Chapter 4 - Transcriptional dynamics of kiwifruit roots under combined biotic and abiotic stressors: insights into multifactorial stress responses

Transcriptional dynamics of kiwifruit roots under combined biotic and abiotic stressors: insights into multifactorial stress responses

Micol Guaschino[1,2,*], Heidi Hargarten[3] Chris Cook[4], Huiting Zhang[5], Loren Honaas[3], Tracey Somera[3], and Davide Spadaro[1,2]

1 Department of Agricultural, Forest and Food Sciences (DISAFA), University of Torino, Largo Paolo Braccini 2, 10095 Grugliasco (TO), Italy.

2 AGROINNOVA, Interdepartmental Centre, University of Torino, Largo Paolo Braccini 2, 10095 Grugliasco (TO), Italy.

3 United States Department of Agriculture, Agricultural Research Service, Tree Fruit Research Laboratory, 1104 N. Western Ave, Wenatchee, WA 98801, USA

4 Tree Fruit Research and Extension Center, Washington State University, 1100 N Western Ave., Wenatchee, WA 98801, USA

5 Department of Horticulture, Washington State University, Pullman, Washington, USA

** Corresponding author: M. Guaschino; micol.guaschino@unito.it*

In preparation

Abstract

First reported in Italy in 2012, Kiwifruit Vine Decline Syndrome (KVDS) has emerged as a major threat to *Actinidia deliciosa* vines in the Mediterranean region, significantly impacting kiwifruit production. Although infection with biotic agents alone (e.g., *Phytopythium vexans*) has proven insufficient to reproduce KVDS symptoms, multiple studies have suggested that root flooding plays a key role in KVDS development. To date, research has provided insights into the response of *A. deliciosa* to individual stress factors (including flooding); however, little is known about how these plants cope with stress combinations. To study the impact of a multifactorial stress combination on kiwi plants, we characterized the transcriptomic response of *Actinidia deliciosa* cv. Hayward over time under biotic stress (inoculation with *P. vexans*), abiotic stress (root flooding), and their combination, mimicking KVDS symptoms under controlled conditions. The study revealed that while typical responses to flooding (e.g. anaerobic metabolism shift, ethylene signaling cascade) were also observed in combined stress treatments, the transcriptomic profile of the multifactorial condition was distinct and could not be predicted from individual-stress responses. Notably, in presence of flooding key biotic defense mechanisms were suppressed, including phenylpropanoid biosynthesis and auxin signaling, despite their upregulation during infection alone. These results support the hypothesis that KVDS arises from a synergistic interaction between biotic and abiotic stressors, where the plant's stress adaptation mechanisms come at the cost of its defense capabilities. To our knowledge, this is the first investigation of biotic-abiotic interactions in *Actinidia*, providing novel insights into the adaptive strategies of kiwi plants under multifactorial/combined stress conditions.

1.Introduction

Plants constantly encounter a wide range of environmental challenges, including biotic and abiotic stresses, which can significantly impact their growth, development, and productivity. Understanding plant stress responses is crucial for improving agricultural resilience, especially in the context of climate change, where fluctuating environmental conditions and emerging pathogens threaten global food security (Zandalinas et al., 2023). *Actinidia deliciosa* (kiwifruit) is an economically important crop valued for its nutritional and commercial significance (Satpal et al., 2021); however, it is highly susceptible to various stressors, including soilborne pathogens and environmental factors. Kiwifruit Vine Decline Syndrome (KVDS) was first reported in Italy in 2012 (Tacconi et al., 2015). Since then, KVDS has emerged as a major threat to *A. deliciosa* vines throughout the Mediterranean region (Polat et al., 2017; Prencipe et al., 2020). The syndrome causes severe root damage, leading to rapid and irreversible canopy wilting, significantly impacting kiwifruit production (Guaschino et al., 2024).

Several studies, using both traditional and novel approaches, have attempted to uncover the causes of KVDS by integrating biotic and abiotic stress factors (Donati et al., 2020; Prencipe et al., 2023; Savian et al., 2021, 2022; Guaschino et al., 2024). Soilborne oomycetes belonging to *Phytopythium* and *Phytophthora* genera have been frequently isolated and identified in metabarcoding studies as being related to the development of the disease in different areas. The genus *Phytopythium* has been recently divided from the *Pythium* genus (Levesque and de Cock 2004). Additionally, multiple studies have suggested that root flooding—linked to extreme weather events driven by climate change—plays a key role in the syndrome development (Tacconi et al., 2015; Savian et al., 2020). Although research has shown that the development of KVDS may be related to the action of many soilborne organisms, *Phytopythium vexans* has been identified as one of the main causal agents of the disease (Prencipe et al., 2020; 2023). Although pathogenesis of *P. vexans* in woody plants has been widely reported (Ghimire and Baysal-Gurel; 2023), the molecular mechanisms underlying the infection process are only partially understood, with recent studies highlighting the involvement of transmembrane transport, sugar-binding activities, and peptidase domains in the secretome of *P. vexans* (Adhikari et al., 2013).

Flooding itself, on the other hand, is a well-known abiotic stress factor impacting plants, and its effects have been extensively studied not only in model plants but also in *Actinidia* spp. (Reid et al., 1991; 1992; Beppu et al., 2022). Molecular mechanisms underlying root flooding responses

in *Actinidia* spp. have been investigated through transcriptomic and RNA-seq approaches (Gao et al., 2022; Xing et al., 2023; Baldi et al., 2024). In response to waterlogging stress, kiwifruit roots exhibited a greater number of down-regulated than up-regulated genes, highlighting the fact that induction of the stress response requires the coordinated suppression of a large number of genes involved in growth-related processes including metabolism, enzyme activity, and cell membrane integrity (Gao et al., 2022). At the same time, key metabolic pathways such as the MAPK signaling pathway and glycolysis/gluconeogenesis are upregulated, alongside the activation of transcription factors like MYB, AP2-EREBP, and WRKY. Waterlogging has also been shown to induce significant upregulation of *Ad*ADH1 and *Ad*ADH2, enzymes central to ethanolic fermentation and correlated with increased acetaldehyde and ethanol production (Xing et al., 2023).

Plants respond differently to different abiotic and biotic stressors, with pests and pathogens often thriving under extreme conditions, increasing disease risk. While extensive research has provided insights into plant responses to individual stress factors, much less is known about how plants cope with stress combinations (Zandalinas et al., 2022). While *Actinidia* response to waterlogging has been documented, its reactions to biotic (soilborne oomycetes) and combined stressors remain poorly understood. Despite the importance of combined stress interactions, research on *Actinidia* physiological, morphological, and molecular responses under such conditions is limited, unlike studies in model crops (Dixit et al., 2023). In general, however, many unanswered questions remain regarding the connections between metabolic pathways, gene regulatory networks, and hormones that govern plant stress responses, as well as how these pathways are regulated under multiple, simultaneous stress conditions. The interplay of multiple stressors triggers various response mechanisms, networks, and pathways that regulate key hormones influencing plant adaptation to stress including ethylene, abscisic acid, jasmonic acid, and salicylic acid (Nawaz et al., 2023).

This study aims to characterize differentially expressed genes (DEGs) in *Actinidia deliciosa* cv. Hayward, the most widely cultivated kiwifruit cultivar, under biotic stress (pathogen inoculation), abiotic stress (root flooding), and their combination, mimicking KVDS symptoms under controlled conditions. By analyzing transcriptomic responses in root tissue over time, we seek to identify key molecular pathways involved in stress tolerance or susceptibility and explore potential crosstalk mechanisms between biotic and abiotic stress responses. Additionally, qPCR gene expression analysis was conducted on select genes to validate transcriptomic findings and assess correlations

with RNA-seq data. To our knowledge, this is the first transcriptomic investigation of *Actinidia* under combined abiotic and biotic stressors. We aim to provide novel insights into the adaptive strategies of kiwifruit plants under multifactorial stress combinations as well as how the multi-stress combination alters the plant-pathogen interaction.

2. Materials and Methods

2.1 Plant material and treatments

One year old, non-grafted, *Actinidia deliciosa* cv. Hayward plants were grown in 7 L pots with peat and soil 1:1 (v/v) and kept in the glasshouse during May-August 2023. An equal number of 12 plants was used for each of the following four treatment groups: 1) Inoculated with *Phytopythium vexans* (I), 2) Flooded for 48 h (F), 3) Combined (both inoculated and flooded; IF), and 4) Control without stress application (NS). The experiment followed a randomized block design, with 4 biological replicates per treatment. Each biological replicate was collected by pooling root tissue from 3 different individuals. Considered time points were: 0, 48, 72, 144 hours and 14 days (hereby referred to as T0, T48, T72, T144 and T14d respectively). The full experimental design and sampling scheme is presented in Figure 1. Roots were harvested for all the treatments, at each time point, to impose the same stress level from root detachment throughout the experiment. However, only treatments NS and I at T0 and T48 were sequenced. Isolate *P. vexans* T4B, from the University of Torino collection (Prencipe et al., 2023) was used to inoculate kiwifruit plants in soil surrounding the roots. To perform inoculation, 6.7 g/L of *P. vexans* mycelium—harvested from PARP-CMA plates after 5 days of incubation at 25 °C—was thoroughly mixed into the soil. Flooding occurred 48 h after inoculation in the combined treatment. Both combined and flooded plants were submerged for 48 h by placing potted plants in bigger containers which were then filled up to the crown level with tap water.

2.2 Pathogen load quantification with qPCR

The presence of *P. vexans* in sampled *A. deliciosa* roots was successfully quantified using a species-specific qPCR assay, with DNA extraction, standard curve generation, and quantification procedures according to Guaschino *et al.* (2025). The samples were extracted by pooling biological samples and by performing 4 technical replicates for each treatment at each time point.

2.3 RNA isolation and sequencing

Root samples were collected, rinsed with water, flash dried in liquid nitrogen and kept at -80 °C until total RNA extraction with the Spectrum Plant Total RNA Kit (Merck KGaA, Darmstadt, Germany) could be performed following the manufacturer's instructions. RNA extraction yield and purity was checked with a Nanodrop 2000 spectrophotometer (Thermo Fisher Scientific, Waltam, USA) and samples were shipped to Novogene (Cambridge, UK) for quality control of the RNA samples, mRNA capture, RNA-seq library preparation, and sequencing. Libraries were then pooled and sequenced with Illumina technology on a NovaSeq X Plus (150 PE) (Novogene, Cambridge, UK). Read data are publicly available at the Sequencing Read Archive (SRA) under the BioProject code PRJNA1259424. A total of 3,470,814,234 raw reads were generated from sequencing 48 root samples.

2.4 Processing of RNA-seq data for analysis

RNA-seq data was processed on Washington State University high performance computer cluster, Kamiak. GEMmaker nextflow workflow (Hadish et al., 2022) was used to automatically execute the following bioinformatics processes: quality assessment using FastQC and multiQC, adaptor and quality trimming with Trimmomatics, read mapping with STAR, and transcript quantification using Stringtie.

2.5 Reference genome selection

To select the best kiwifruit genome for read mapping, a BUSCO (Manni et al., 2021) analysis was performed on the annotated peptides from three selected genomes – *A. chinensis* Red5 Pilkington 2018, *Actinidia chinensis* hy Wu 2019, and *A. deliciosa* Xia 2023 (Pilkington et al., 2018; Wu et al., 2019; Xia et al., 2023). The putative peptide sequences were either downloaded or extracted from the genome assembly. First, gffutils was used to extract putative coding sequences with the genome assembly and GFF file as input. The extracted coding sequences were then translated into peptide using Geneious v9.0.5 (https://www.geneious.com). The eudicotodb_10 was selected as the database to search against, and all other parameters were set to default for the BUSCO analysis. The *A. deliciosa* Xia et al. (2023) genome was selected as reference because it is the same species used in this study, and it has a high BUSCO complete score. All the information about the

considered genomes and the BUSCO completeness assessment results can be found in **Supplementary Table 1**.

2.6 Differential gene expression and functional enrichment analyses

To perform differential expression (DE) analysis, the R package 'DESeq2' v.1.40.2 (Love et al., 2014) was used. The threshold for significance was set to alpha 0.05 using a Benjamini-Hochberg correction. Pairwise contrasts for DE identification between treatments are reported in **Supplementary Table 2**. Before proceeding with the enrichment analysis, subsetting of the up and down regulated genes was performed based on significance and Log Fold Change (LFC) > 0 to have enough statistical power. Next, a functional enrichment analysis was performed on this subset of DE genes. The putative peptide sequences extracted from the *A. deliciosa* Xia 2023 genome were functionally annotated with interproscan (version 5.59.91) by searching against all its databases, including GO terms. Functional enrichment analysis was performed using the R package 'topGo' v 2.58.0 (Alexa et al., 2024). To identify enriched GO terms among the genes of interest, we utilized the topGOdata object builder function, providing it with the list of gene names and their associated GO terms, obtained from interproscan, through the annFUN.gene2GO function. The topGOdata object was then used to assess GO enrichment significance via the getSigGroups function, employing the "weight01Count" enrichment method and the "weight01Count" algorithm (which accounts for the GO hierarchy) to perform Fisher's Exact tests for significance, with an alpha threshold of 0.05. Furthermore, topGO was also used to identify underrepresented terms. In addition, KO terms were obtained by using KEGG Mapper, while pathway enrichment was carried out with FUNC-E (https://github.com/SystemsGenetics/FUNC-E), where DEGs from comparisons of interests were used as the foreground and all the annotated genes from *A. deliciosa* (Xia et al., 2023) genome as background. To get a broader functional framework of DEGs, FUNC-e was also used to identify enriched IPR terms.

2.7 Hierarchical clustering and heatmap analysis of differentially expressed genes

2.7.1 Data processing and selection of differentially expressed genes

Gene expression data were obtained from the GEMmaker pipeline in the form of fragments per kilobase of transcript per million mapped reads (FPKM) table with averaged values. The table was imported into R, and differentially expressed (DE) genes were identified for each contrast of

interest. The DE gene list for each contrast of interest was extracted and merged with the corresponding FPKM values from the GEMmaker output. The merged dataset was saved for further analysis.

2.7.2 Data preparation for heatmap generation

The dataset was preprocessed by setting gene identifiers as row names and extracting only expression values for hierarchical clustering. To ensure proper clustering, treatments and time points were reordered based on predefined criteria. Columns were arranged first by treatment and then by time to maintain consistency in visualization. To handle missing data, zeros were converted to NA values, and genes with expression data missing for all but one condition were removed. The remaining missing values were replaced with zeros before clustering.

2.7.3 Hierarchical clustering and heatmap construction

A Euclidean distance matrix was computed for hierarchical clustering using the "average" linkage method. For heatmap visualization, the heat.clust function from the massageR package v 0.5 (https://gitlab.com/stanstrup_R_packages/massageR.git) was used to perform Z-score normalization across rows, scaling expression values between -2 and 2. The resulting transformed dataset was used to generate a heatmap using the heatmap.2 function from the gplots package. Row dendrograms were included to visualize hierarchical clustering, while column dendrograms were omitted to preserve the predefined treatment-time order.

2.8 qPCR validation of RNA-Seq

2.8.1 Candidate gene selection and primer design for quantitative Real Time-PCR

Candidate genes (CG) for qPCR validation of RNA-Seq data were selected using previously published selection criteria (Honaas et al., 2021; Waite et al., 2023; Hadish et al., 2024) applied to experiment-specific expression data. Briefly, 30 CGs were selected for primer design after genes from the GEM were filtered based on expression value (sum >5,000 counts across all treatments), standard deviation (SD 50-300), and pattern (linear, positive or negative). A BLAST database of *A. deliciosa* CDS sequences (see section 2.5) was created in Geneious v.9.1.8. Multiple primer pairs (n = 10) were developed and evaluated for each CG as described in Hargarten et al (2018). 15 CGs were ultimately selected for qPCR (**Supplementary Table 3**). Primers were synthesized

and handled as in Hargarten et al (2018). qPCR reference genes were selected *ab initio*, as opposed to the use of previously published reference genes, because the stability of reference genes can be species, tissue, and condition specific (Radonić et al., 2004) and would require validation in our experiment prior to use (Bustin et al., 2013). Using the same filtering criteria described above, three reference genes were ultimately selected (**Supplementary Table 3**).

cDNA was synthesized using the iScript™ gDNA Clear cDNASynthesis Kit (Bio-Rad, Hercules, CA) with a total RNA input of 1 ug per sample. A subset of 18 cDNA samples were used for qPCR validation of RNA-Seq results (**Supplementary Table 4**). For each CG, qPCR was carried out on all samples in technical triplicate, following the "sample maximization" scheme described by Hellemans et al. (2007). Each qPCR reaction was prepared by an epMotion® P5073 (Eppendorf, Hamburg, Germany). The reaction assay, machinery, and plastics were used according to Hargarten et al. (2018), with the following modifications to accommodate the epMotion® P5073 pipetting capabilities: 7.5 uL SsoAdvanced Universal SYBR® Green Supermix (Bio-Rad, Hercules, CA) and 2.5 uL nuclease free water to create a 15 uL reaction.

2.8.2 qPCR post-processing for normalized expression.

Postprocessing of qPCR for normalized expression was carried out as in Waite et al. (2023). Briefly, amplification and melt curves were manually inspected and filtered variance and anomalies. Reaction efficiency was calculated in R v4.4.1 (R Core Team, 2024) based on raw amplification data using the package 'qpcR' v1.4-1 (Ritz & Spiess 2008). Computed reaction efficiencies were in BioRad's CFX Maestro 1.0 software (4.0.2325.0418) and used to calculate relative normalized expression using the Pfaffl method (Pfaffle 2001). The built-in stability analysis in the CFX Maestro Software (geNorm; Vandesomple et al., 2002) was used to evaluate reference genes. Correlations between RNA-Seq (TPMs) and qPCR (normalized expression) were performed in R using pearson's correlation (cor(method='pearson')), and visualized with 'ggplot2' (Wickham 2016).

3. Results

3.1 Differential gene expression in *A. deliciosa* roots across treatments and time points

3.1.1 Differential gene expression within each treatment, across time

A time-course analysis was performed to evaluate transcriptional changes in kiwifruit roots under inoculation, flooding, and combined (multifactorial) stress. Differentially expressed genes (DEGs) were identified by comparing stress treatment conditions with the control condition (without stress application) for each time point. DEGs were categorized as either up- or downregulated (relative to no stress controls) at five distinct time points: T0, T48, T96, T144 and T14d (**Figure 1**). Based on the number of DEGs identified, the bulk of transcriptional reprogramming occurred at the 96 hr time point (T96), regardless of stress treatment (**Table 1**). It should be noted that T96 represents 96 h after inoculation with *P.vexans*, but only 48 h after flooding stress (**Figure 1**). It is also interesting to note that, across all treatments and timepoints, there were more stress-induced decreases than increases in DEG expression. Notably, the magnitude of transcriptomic changes over time was smaller in *P. vexans*-inoculated plants compared to those exposed to flooding or combined stresses. At all post-stress time points (T96, T144, and T14d), the total number of affected genes was greatest under combined stress, suggesting a cumulative effect of combined biotic and abiotic stressors on the transcriptional activity of kiwifruit roots. Additionally, the flooding- and inoculation-only treatments (but not the combined stress treatment) showed similar temporal DEG patterns: after a sharp decline at T144, the number of DEGs increased again by T14d. This pattern suggests that the combined stress condition may have impaired the plant's capacity to recover or re-establish a baseline transcriptional state following acute flooding stress, as indicated by the sustained low number of DEGs at T144 and the lack of rebound at T14d compared to the other stress treatments (flooding- and inoculation-only).

Treatment-specific subsets of DEGs (Inoculation, Flooding and Combined treatments at T96 vs. no stress control at T96) were also identified and used to generate hierarchical clustering heatmaps for visualizing FPKM RNA-Seq expression patterns (**Supplementary Figures 1**, **2** and **3**, respectively). These figures not only show that flooded-only and combined stress conditions greatly altered the transcriptome at T96, but also reveal a high degree of similarity in terms of the specific gene responses (**Supplementary Figures 2** and **3**). After two-weeks (T14d), however,

more similar gene expression profiles were observed across all stress treatments, which remained distinguishable from the no stress control.

3.1.2 Comparison of DEGs among treatments at the 96 hour timepoint

To better understand the potential overlaps and differences in gene expression patterns between treatments at T96—the peak transcriptional response time point—Venn diagrams were generated. The Venn diagram shown in **Figure 2** illustrates the distribution of both unique and shared *upregulated* genes across the different stress treatments. Only 9 genes were shared across all three treatments, possibly indicative of a core set (or network) of general stress responsive genes. This aligns with findings that plant stress responses combine shared and stressor-specific components (De Nadal et al., 2011; Kreps et al., 2022) with stimulus specific responses becoming more prominent over time. Along these same lines, 35 genes were identified as being *downregulated*, regardless of stress treatment (**Figure 3**). These results are in agreement with previous studies suggesting that plant stress responses are likely to be rather specific, depending on the stressor (Hahn et al., 2013), reflecting the need for tailored and efficient physiological and molecular adjustments to distinct biotic or abiotic challenges. Climate change is expected to exacerbate this complexity by altering pathogen prevalence and virulence. Plants must efficiently navigate the crosstalk between biotic and abiotic stress signaling pathways, transcription factors regulate these responses and play a key role in mediating both biotic and abiotic stress signaling (Singh et al., 2002; Leisner et al., 2022).

In contrast, the number of up- and downregulated genes shared between the flooded-only and combined treatment was markedly higher (5,724 and 8,990 genes, respectively) than those shared between the inoculation-only and combined (3 and 11 genes, respectively) or inoculation-only and flooded-only treatments (2 and 13 genes, respectively). These results indicate that, overall, the transcriptomic responses of *A. deliciosa* cv. Hayward in response to flooding vs. flooding + exposure to *P. vexans* are highly similar. However, the combined stress condition resulted in a larger number of unique up- and downregulated genes (2,225 and 1,777 genes, respectively) than flooding (1,109 and 1,359 genes, respectively) or inoculation alone (29 and 402 genes, respectively). This result likely reflects the combined impact of abiotic and biotic stress factors under these conditions.

3.2 Functional enrichment analysis of Biological Processes and KEGG pathways in kiwifruit roots exposed to *P. vexans* 96 hours post-inoculation

3.2.1 GO enrichment analysis of up- and down regulated genes

A functional enrichment analysis of the 504 DEGs upregulated (43) downregulated (461) in response to biotic stress (relative to the no stress control) at T96 was conducted (**Figure 4**). Due to the low number of upregulated genes at this treatment x time point, statistical analysis of overrepresented GO terms was not possible. At this time point, only three upregulated genes had an Log2 Fold Change (FLC) > 2, with the highest being *Acde02g00614.1* (LFC = 17.62) and *Acde03g00407.1* (LFC = 17.26), indicating that although most upregulated DEGs exhibited modest changes, a few showed strong transcriptional upregulation to *P. vexans* infection (confirmed via qRT-PCR; **Supplementary Table 5**). At this time, downregulated DEGs were associated with GO terms related to protein production/turnover (GO:0006355, GO:0006457, GO:0006418, GO:0016567), energy production via oxidative phosphorylation (GO:0042773), and cell growth (GO:0008283) as further described below.

3.2.2 In-depth analysis of the top 10 up- and down regulated genes in response to biotic stress

Analysis of the top 10 DEG upregulated in response to biotic stress, based on p-values, revealed significant induction (**Figure 4**, **Table 2**). While these genes were significantly upregulated, we were unable to perform GO enrichment analysis due to annotation limitations, and thus, they do not have associated GO terms. In contrast, expression analysis of the top 10 downregulated genes revealed several genes that were significantly repressed across multiple biological processes (**Figure 4**, **Table 2**). Among these, the most downregulated gene was *Acde29g00858.1* associated with GO:0006355, the regulation of DNA-templated transcription. Five additional genes in the 'top 10 downregulated genes' were associated with the same GO term: *Acde19g01072.1, Acde13g01591.1, Acde09g00889.1, Acde12g01064.1,* and *Acde25g00613.1* (**Table 2**). It is also interesting to note that GO:00016567 (protein ubiquitination) was downregulated during this time, suggesting a reduction in protein turnover. Other top 10 downregulated genes included annotations with ATP synthesis coupled electron transport (*Acde001100s00016.1*), protein folding (*Acde15g00062.1*) cell proliferation (*Acde06g01046.1*), and response to auxin stimulus (*Acde23g00039.1*). Taken together, these results suggest the top 10 most downregulated genes

following exposure to *P. vexans* are associated with shutting down processes related to plant cell growth and energy production. The patterns of expression of these selected genes through time are visible in **Figure 5**.

3.2.3 KEGG enrichment analysis of up- and downregulated genes in response to biotic stress

Several DEGs identified as significantly up- or downregulated in response to root infection by *P. vexans* were enriched in KEGG terms. Selected KEGG terms, highlighting key metabolic and regulatory pathway components of the response to biotic stress, are further discussed and listed in Table 3. Notably, multiple elements associated with specific phytohormone signaling pathways were significantly enriched among upregulated DEGs. These include ABA-responsive element binding factor (K14432) and EREBP-like factor (K09286) (p = 0.024 and 0.016, respectively) and suggest the involvement of the hormones abscisic acid (ABA) and ethylene, respectively. The enrichment of Indole-3-pyruvate monooxygenase (K11816) (p = 0.022), a key enzyme in auxin/indole-3-acetic acid biosynthesis, further highlights the role of auxin signaling in regulating growth and defense in response to infection by *P. vexans*. Also enriched was the enzyme protein phosphatase 2C (K14497) (p = 0.022), suggesting enhanced regulation of signal transduction pathways via dephosphorylation by phosphatases.

The upregulation of chalcone synthase (K00660) (p = 0.021), an enzyme required for initiating flavonoid biosynthesis, indicates regulation of phenolic and or secondary metabolite content of root and/or root exudates 96h post-inoculation. Flavonoid biosynthesis pathways were also recently implicated in resistance to infection by *Pseudomonas syringae* in kiwifruit leaves (Ma et al., 2025). Along these same lines, primary-amine oxidase (K00276) (p = 0.022), an enzyme that converts primary monoamines to into aldehydes, ammonia or hydrogen peroxide, points to the production of reactive oxygen species as part of the root response to biotic stress. In addition, the upregulation of aquaporin PIP (K09872) (p = 0.022) suggests an increase in cell membrane permeability for water, although PIP-type aquaporins may also function in the transport of H_2O_2 across the plasma membrane to counteract pathogen invasion (Li et al., 2020). Finally, significant enrichment of NPF2 transporters (K26552) may also be related to the need for specialized transport of metabolites across cell membranes.

Similar to the GO term analysis, KEGG terms enriched in downregulated genes suggest suppression of essential cellular and metabolic processes under pathogen attack. Notably, glutathione S-transferase (K00799), with a highly significant p-value of 0.0004 suggests a reduced

ability to protect cells from oxidative stress, possibly rendering the plant more sensitive to stress. Downregulation of ndhH, NAD(P)H-quinone oxidoreductase subunit H (K05579), a protein that functions as part of the NADH-quinone oxidoreductase complex (NDH-1), suggests reduced energy production via oxidative phosphorylation. Aminocyclopropane carboxylate oxidase (K05933), a key enzyme in ethylene biosynthesis, was also downregulated ($p = 0.043$), suggesting reduced levels of ethylene under biotic stress. Ethylene biosynthesis has long been associated with the expression of a variety of plant defense-related genes (Ecker and Davis, 1987). In some studies, however, ethylene production has been shown to promote and/or be associated with disease development (Lund et al., 1998). Downregulation of multiple E3 ubiquitin-protein ligases such as RNF14 (K11971), CBLL1 (K15685), and AIP2 (K16274) (all with *p*-values of 0.047; **Table 3**) involved in protein ubiquitination, points to reduced proteolytic activity during this time. Moreover, HSP20 family protein (K13993), involved in endoplasmic reticulum-associated protein degradation, was also highly enriched among downregulated genes (p = 1.4e-27). Finally, the enzymes 15-cis-phytoene desaturase (K02293) (involved in carotenoid biosynthesis) and threonine synthase (K01733) (essential for synthesis of the amino acid threonine) were also overrepresented among downregulated genes (p = 0.047). Together, these findings reveal a complex regulatory landscape in which hormonal signals (ABA, IAA and reduced levels of ethylene) mediate the plant response to *P. vexans*. This may include increased production/transport of flavonoid-based metabolites and H_2O_2. At the same time, suppression of key cellular and metabolic processes required for plant cell growth (inc. oxidative phosphorylation and protein synthesis/turnover) also appear to be important for helping plants adapt to biotic stress.

3.3 Functional enrichment analysis of Biological Processes and KEGG pathways in kiwifruit roots exposed to root flooding 48 hours after treatment

3.3.1 GO enrichment analysis of up- and downregulated genes 48 hours post-flooding (T96)

In response to abiotic stress induced by root flooding, a relatively large number of upregulated genes (53 in total) were associated with the broad GO term biosynthetic process (GO:0009058**,** p = 0.00078) (**Figure 6**), suggesting an overall enhancement of biosynthetic activity in response to flooding stress. The most significantly enriched upregulated biological process was GO:0016567 (protein ubiquitination, p = 0.00036). This signifies a need for protein degradation or turnover and

could point to an accumulation of misfolded proteins in response to waterlogging stress. In contrast, in response to inoculation, the same GO term (GO:0016567) was enriched in *down*regulated DEG (as described in section 3.2.1). In addition to protein ubiquitination, other terms associated with the processing/modification of existing mRNA transcripts included: GO:0006396 (RNA processing, p = 0.001), GO:0006388 (tRNA splicing, p = 0.00159), and GO:0008033 (tRNA processing, p = 0.00866). Among GO terms enriched in *down*regulated DEGs in response to flooding stress, GO:0006412 (translation) represented one of the most downregulated (average LFC =5; **Figure 6**). This is a broad GO term in which positive vs. negative regulation of protein synthesis is not specified. However, a number of key processes required for new protein synthesis and proper protein function including: GO:0006414 (translational elongation), GO:0006457 (protein folding) and GO:0006486 (protein glycosylation) were significantly enriched with downregulated DEGs. Limiting new protein synthesis and promoting the degradation of misfolded proteins may help maintain protein homeostasis under stressful conditions. These results may also point towards rapid synthesis and breakdown of proteins, crucial processes for allowing cells to adjust protein levels in order to adapt to various stressors.

Waterlogging is often associated with a decrease in soil redox potential which can lead to increased solubility/mobility (and potentially toxic concentrations) of certain metal ions (esp. manganese and iron) (Shabala et al., 2014). Thus, the ability to maintain ion homeostasis is also a key component of waterlogging tolerance in plants. Consequently, GO:0030001 (metal ion transport, p = 0.00441), GO:0030026 (intracellular manganese ion homeostasis), GO:0006820 (monoatomic anion transport), GO:0006817 (phosphate ion transport), GO:0071805 (potassium ion transmembrane transport) and GO:0015706 (nitrate transmembrane transport) were all enriched in downregulated DEGs. This indicates that the membrane transport activity of many nutrients essential for plant growth was reduced. On the other hand, these changes may contribute to osmotic/cytosolic homeostasis under anoxic conditions. It is worth noting that in addition to GO:0015706 (nitrate transmembrane transport), GO:0010167 (response to nitrate) was also enriched in downregulated DEG. As soil redox potential decreases, nitrate availability is also likely to decrease. This is because denitrification is more likely to occur as waterlogged soil becomes more reduced. Not only is nitrate the most common readily available nitrogen source used by plants, but it also serves as an environmental signal for effecting changes in plant growth and physiology (including stimulating root growth and metabolism) (Redinbaugh and Campbell,

1991). Likewise, a variety of cell growth-related processes were enriched in downregulated DEGs in response flooding, particularly those related to the production/assembly of plant cells. For example, L-arabinose is a constituent of hemicellulose, a major component of plant cell walls. The enrichment of downregulated DEGs in the nested GO terms GO:0008299 (isoprenoid biosynthetic process), GO:0016126 (sterol biosynthetic process) and GO:0046373 (L-arabinose metabolic process) as well as GO:0016126 (cellulose biosynthetic process) suggests a reduction in the production of essential components of plant cell walls.

Under low oxygen conditions, cells increase their reliance on glycolysis (while limiting mitochondrial respiration) to maintain ATP production. GO:0006096 (glycolytic process, $p = 0.00242$) was significantly enriched in upregulated DEGs. At the same time, a number of GO terms enriched in downregulated DEG pointed to energy deprivation resulting from exposure to flooding stress including: GO: 0006099 (tricarboxylic acid cycle), GO:0015986 (proton motive force-driven ATP synthesis), glucose metabolic process (GO:0006006), and fatty acid biosynthetic process (GO:0006633). Lastly, the upregulation of GO:0005985 (sucrose metabolic process, $p = 0.00328$) and GO:0005992 (trehalose biosynthetic process, $p = 0.00537$) is also notable. In kiwi and in other plants, the accumulation of soluble sugars (esp. sucrose and trehalose) in roots has been identified as an important aspect of the adaptive response to waterlogging and hypoxia, which may facilitate osmotic adjustment and/or adventitious root formation (Li et al., 2020; Ji and Hyun, 2023).

3.3.2 In depth analysis of the top 10 up- and downregulated genes in response to abiotic stress

In response to root flooding, the top 10 upregulated genes were selected for a more in-depth exploration of key biological processes associated with stress adaptation (**Table 2**; **Figure 6**). Among the genes associated with GO:0009058 (biosynthetic process), *Acde24g00960.1* showed strong upregulation with a LFC of 18.37 ($p = 0.00078$). Other genes belonging to the same GO term, such as *Acde24g00926.1*, *Acde19g00475.1*, *Acde07g00013.1*, *Acde18g00476.1*, *Acde21g00949.1* and *Acde15g01156.1*, further emphasize the activation of pathways related to biosynthetic activities. One gene (*Acde10g01179.1*; LFC of 4.16) was significantly enriched in both GO:0006096 (glycolytic process) ($p = 0.00242$) and GO:0019752 (carboxylic acid metabolic process) ($p = 0.04093$). Along these same lines, genes belonging to GO:0015031 (protein transport) ($p = 0.0381$) were also upregulated, (e.g., *Acde02g00864.1*, LFCFC = 5.52;

Acde28g00379.1, LFC = 5.48) highlighting the need for enhanced transport of proteins into, out of and/or within cells in response to flooding stress (possibly stress-related proteins). Among the top 10 genes downregulated in response to root flooding, *Acde000000s00035.1* was the most extreme, with a LFC of -23.49. This gene was associated with multiple processes including: GO:0006412 (translation) (p = < 1e-30), GO:0006807 (nitrogen compound metabolic process) (p = 0.00239) and GO:0071704 (organic substance metabolic process) (p = 0.00434). Strong downregulation was also exhibited by *Acde28g00092.1* (LFC = -11.04) belonging to GO:0071704. It should be mentioned that, due to hierarchical relationships between GO terms (in which terms higher up in the hierarchy are more general than those further down), genes are often associated with multiple GO terms. Alternatively, genes associated with multiple GO terms may play multiple roles in the transcriptional response. Interestingly, the GO terms GO:0071704 (organic substance metabolic process) and GO:0006807 (nitrogen compound metabolic process) were consistently associated with several genes: *Acde12g00105.1*, *Acde09g00923.1*, *Acde18g00394.1*, *Acde03g01667.1*, *Acde08g00322.1*, *Acde22g00339.1* and *Acde10g01004.1*). The LFC values for these genes were similar (**Table 2**), demonstrating uniformity in the degree of downregulation. These results may point to a coordinated transcriptional response. Notably, *Acde26g00444.1* was associated with GO:0006633 (fatty acid biosynthetic process) (p = 0.01637) and with GO:0071704 (organic substance metabolic process) (**Table 2**). Along with the upregulation of glycolytic processes, reduced levels of fatty acid biosynthesis point to energy deprivation resulting from exposure to flooding stress. Changes in expression through time are evidenced in **Figure 7**.

3.3.3 KEGG enrichment analysis of up- and downregulated genes 48 hours post-flooding (T96)

Several DEGs identified as significantly up- or downregulated in response to flooding were enriched in KEGG terms (**Table 3**), highlighting critical roles in transcriptional regulation, protein metabolism, and ethylene signaling pathways. Similar to GO term analysis, exploration of enriched KEGG terms indicated an increase in ubiquitin-mediated protein degradation (e.g. K11855 - ubiquitin carboxyl-terminal hydrolase 36/42; $p = 0.033$). Along these same lines, upregulation of peptide chain release factor subunit 1 (K03265) ($p = 0.033$), which is a component of mRNA surveillance pathways, suggests the involvement of mechanisms for detection/degradation of abnormal mRNA (including prematurely terminated mRNA). Finally, the suppression of the enzyme peptidyl-prolyl isomerase (K01802) ($p = 0.046$), which catalyzes a rate-limiting step in

the folding of proteins, provides additional evidence for downregulation of protein folding resulting from flooding stress. As previously mentioned, these effects are likely related to the need for cells to rapidly adjust protein levels in response to waterlogging stress.

Consistent with previous reports on flooding responses in soybean and rice, we observed significant upregulation of ADH1, alcohol dehydrogenase class-P (K18857), in the flooding treatment. ADH is a key enzyme involved in anaerobic respiration and plays a central role in allowing plants to cope with hypoxic conditions by facilitating energy production through fermentation pathways. In terms of stress sensing/signaling, the transcription factors WRKY33 (K13424) and WRKY22 (K13425) (p = 0.033 and 0.036, respectively) were upregulated. These transcription factors are involved in MAPK signaling pathways, which are known to be activated in response to a wide variety of environmental stresses (de Nadal et al., 2011). WRKY33 and WRKY22 are components of signaling pathways sensing pathogen infection/attack; however, recent studies have also suggested that members of this gene family participate in hypoxia stress response in a variety of plants (Tang et al., 2020). In addition, upregulation of EIN3-binding F-box protein (K14515) and ethylene-insensitive protein 3 (K14514) (p = 0.033 and 0.037, respectively) indicate elevated levels of ethylene, as both are components of a MAPK signaling pathway which is activated by ethylene. Ethylene gas typically tends to accumulate in the tissues of flooded plants (Voesenek et al., 2006) and has been previously implicated in regulating the kiwifruit response to waterlogging/hypoxia (Li et al., 2020).

Downregulation of specific KEGG terms reflected suppression of key cellular processes required for plant growth. For example, tubulin beta (K07375), a protein required for the formation and function of microtubules (major components of the cytoskeleton), was downregulated (p = 0.046). This would limit plant cell growth and/or intracellular transport in response to flooding stress. Results also showed that RAC1 (K04392), a Ras-related GTPase protein, was downregulated (p = 0.046). This protein acts as a downstream effector in MAPK signaling pathways helping to regulate cell growth, differentiation, and cytoskeletal reorganization/cell cycle progression. Also notable was the downregulation of acid phosphatase type 7 (K22390). Phosphatases are key enzymes involved in phosphate utilization, which is essential for plant growth.

One of the most interesting findings from this analysis was the downregulation of phenylalanine ammonia-lyase (K10775) (p = 0.046). Phenylalanine ammonia-lyase (PAL) catalyzes the first step of the phenylpropanoid biosynthetic pathway, converting L-phenylalanine to trans-cinnamic acid.

This is a key precursor in the biosynthesis of a variety of secondary metabolites, including flavonoids. As previously mentioned in Section 3.2.3, chalcone synthase (crucial for flavonoid biosynthesis) appears to be upregulated in response to infection with *P. vexans*. Consequently, downregulation of PAL in response to flooding may weaken kiwi defense response against *P. vexans* infection. The downregulation of this enzyme was also previously observed in avocado in response to flooding (Reeksting et al., 2016). The fact that GO:0009094 (L-phenalaline biosynthetic process) was enriched in downregulated DEGs in this treatment provides support for this hypothesis. As mentioned above, L-phenylalanine plays a crucial role in plant defense by serving as a precursor for the phenylpropanoid pathway. Moreover, GO:0006952 (defense response) was enriched in downregulated DEGs in response to flooding. In a recent study, flooding was shown to deactivate wound-induced defense against herbivore attack in *Arabidopsis thaliana* (Lee et al., 2020). This "deactivation" was linked to ethylene signaling and the expression of ethylene-responsive genes which increased after short-term submergence. In the current study, suppression of ethylene biosynthesis/signaling appeared to be a factor in meditating the response to infection by *P. vexans*. Therefore, accumulation of ethylene gas in the root tissues of flooded kiwi plants may have a negative effect on defense against *P. vexans.* This may be one way that the combination of flooding + inoculation alters plant-pathogen interaction dynamics and promotes KVDS.

3.4 Functional enrichment analysis of Biological Processes and KEGG pathways in kiwifruit roots exposed to combined stress conditions: 48 hours post-flooding/96 hours post-inoculation

3.4.1 GO enrichment analysis of up- and downregulated genes in response to combined stress conditions (inoculation + flooding, T96)

Analysis of genes that were upregulated across significantly enriched biological processes revealed several GO terms with relatively high numbers of associated genes (**Table 2**; **Figure 8**). These included: GO:0009058 (biosynthetic process, 71 genes, $p = 0.00011$), GO:0006351 (regulation of transcription, 41 genes, $p = 0.00863$) and GO:0006508 (proteolysis, 74 genes, $p = 0.02$). As in the other two treatments, upregulated genes were enriched in the nested GO terms GO:0007165 (signal transduction) and GO:0000160 (phosphorelay signal transduction system).

In the combined stress treatment, a large number of enriched GO terms were dedicated to transcriptional regulation and the control of mRNA biogenesis including: GO:0006351 (DNA-templated transcription), GO:0006352 (DNA-templated transcription initiation), GO:0006338 (chromatin remodeling, p = 0.00901), and GO:00016570 (histone modification). The GO terms GO:0015031 (protein transport, p = 0.00352), GO:0006606 (protein import into the nucleus), and GO:0006913 (nucleocytoplasmic transport), may also be related to the regulation of transcription. Enriched GO terms which seemed to support RNA processing after transcription included: GO:0006413 (translational initiation), GO:0006396 (RNA processing, p = 0.00028), GO:0008033 (tRNA maturation), GO:0006388 (tRNA splicing), and GO:0000398 (mRNA splicing, via spliceosome). In terms of post-translational modifications regulating protein stability, a number of GO terms enriched in upregulated genes appeared to be at odds with each other. For example, GO:0016579 (protein de-ubiquitination) suggests a need to rescue proteins marked for degradation while GO:0006508 (proteolysis) and GO:0006511 (ubiquitin-dependent protein catabolic processes) imply increasing rates of protein degradation. Increased protein degradation and decreased protein folding were also processes associated with flooding alone. Taken together, these processes highlight the intricate balance between ubiquitination/deubiquitination in maintaining cellular homeostasis under combined stress conditions. These findings may also reflect the need to decrease production of growth-related proteins while increasing production of stress-related proteins. Finally, as in the flooding alone treatment, GO terms associated with the need to maintain osmotic homeostasis (GO:009415 - response to water, p = 0.00364; GO:0005992 - trehalose biosynthetic process; GO:0005985 - sucrose metabolic processes, p = 0.00714) and cellular energy production (GO:0019752 - carboxylic acid metabolic processes, 8 genes, p = 0.01493; GO:0006096 - glycolytic process, 3 genes, p = 0.00376) were significantly enriched in upregulated genes.

Among biological processes significantly enriched with *down*regulated DEGs in response to combined stress, GO:0006412 (translation) represented the most significantly enriched term (p < 1e-30) (**Figure 8**). As previously mentioned, positive vs. negative regulation of protein synthesis for this GO term is not specified. However, the finding that GO:0006413 (translational initiation) was enriched with *up*regulated DEGs supports an increase in translation under combined stress conditions. Nevertheless, key processes associated with protein functionality including GO:0006457 (protein folding), GO:0000413 (protein peptidyl-prolyl isomerization) and

GO:0006486 (protein glycosylation) were enriched with downregulated DEGs (decreased protein folding and glycosylation was also associated with flooding alone). In both flooding and combined stress conditions, control of gene expression via the modification of existing transcripts appears to be particularly valuable. Like flooding alone, a variety of cell growth and energy related processes were enriched in downregulated DEGs in response to combined stress including: GO:0006260 (DNA replication), GO:0006355 (regulation of DNA-templated transcription) and GO:0015986 (proton motive force-driven ATP synthesis). Also as in flooding alone, these processes specifically included those related to the production/assembly of plant cell membranes and walls. Enrichment of downregulated DEGs in the nested GO terms GO:0006629 (lipid metabolic processes), GO:0008299 (isoprenoid biosynthetic process), and GO:0016126 (sterol biosynthetic process) suggests a reduction in the production of essential components of plant cell membranes. Downregulated DEGs were also enriched in GO:0010215 (cellulose microfibril organization) and GO:0046373 (L-arabinose metabolic process).

Similar to flooding alone, GO enrichment analysis of the combined stress treatment provided clear evidence of a number of adaptive responses to waterlogging for maintaining osmotic and cellular homeostasis. For example, GO:0030001 (metal ion transport, $p = 0.00441$), GO:0006820 (monoatomic anion transport), GO:0006817 (phosphate ion transport) and GO:0071805 (potassium ion transmembrane transport) were significantly enriched in downregulated genes (all 4 of these GO terms were also enriched in flooding alone). Reduced oxygen availability in the soil resulting from flooding typically disrupts potassium ion (K+) transport in root cells. This disruption can lead to impaired K+ uptake and leakage from cells (Gill et al., 2018). In both flooding alone and combined treatments GO:0006820 (ammonium transmembrane transport) and GO:0006546 (glycine catabolic process) were enriched in downregulated genes. The significance of reduced ammonium transport and glycine breakdown and under waterlogging conditions is unclear. Also enriched in downregulated genes in both flooding and combined stress treatments was GO:0010274 (hydrotropism). This result suggests that waterlogging not only reduces the expression of genes involved in cell growth but also those affecting growth orientation (i.e. root growth towards water).

The ability to effectively manage reactive oxygen species where oxygen is limited is especially important. Surprisingly, analysis of GO Terms enriched in downregulated DEGs suggested a

reduced ability to attenuate oxidative stress (relative to non-stressed control plants) in both flooding and combined stress treatments. In both treatments, this was supported by GO:0006979 (response to oxidative stress), and GO:0006284 (base-excision repair, $p = 0.00912$). In a previous study, *A. deliciosa* (Hayward) was categorized as a relatively sensitive genotype in terms of its tolerance to waterlogging compared to *A. valvata* (KR5), a finding which was partly due to a greater increase in superoxide dismutases in KR5 roots (Li et al., 2020). That said, a reduced ability for reactive oxygen scavenging was something that was reflected in GO and/or KEGG term analysis regardless of treatment (biotic, abiotic or combined).

Finally, as in flooding alone (but not biotic stress) GO:0006952 (defense response) was enriched in downregulated DEGs. Also, GO:0009094 (L-phenylalanine biosynthetic process) was enriched in downregulated DEGs in both flooding and combined stress treatments. L-phenylalanine is an important precursor for the production of various compounds, including flavonoids, which appear to be important components of the plant response to infection by *P. vexans* (see section 3.2.3). Changes in gene expression patterns through time are shown in **Figure 7**.

3.4.2 In depth analysis of the top 10 up and down regulated genes in response to combined stress conditions (inoculation and flooding) 96 hours post treatment

Analysis of the top 10 *up*regulated genes in response to combined stress highlights the involvement of multiple GO terms, particularly those related to signal transduction, transcription, protein transport/regulation and the cellular response to water (**Table 2**). The LFC values shown in Table 2 range from 4-19 (16-15,4288 times the gene expression value of the non-treated control at T96), with the highest upregulation (LFC = 19) exhibited by *Acde24g00960.1* (associated with GO:0006351 - DNA-templated transcription) and GO:0009058 - biosynthetic process). Also associated with the same GO terms were *Acde24g00926.1* (LFC = 8.40) and *Acde19g00475.1* (LFC = 8). These results indicate that rates of RNA transcription were greatly elevated under combined stress. In contrast, during infection by *P. vexans,* rates of DNA-templated transcription were downregulated in *A. deliciosa* roots (Table 2, and also mentioned in section 3.2.2). These differences highlight the role of mRNA translation as an important regulatory mechanism/control point for gene expression in response to different stressors.

The top 10 genes *up*regulated in response to combined stress also included *Acde03g01777.1* (LFC = 6.8), associated with GO:0009058 (biosynthetic process) and GO:0006396 (RNA processing) as

well as *Acde10g01033.1* (LFC = 7.7) and *Acde13g00767.1* (LFC = 4.3), both of which were associated with GO:0006508 (proteolysis). In comparison, GO:00016567 (protein ubiquitination) was enriched in *down*regulated DEG during infection by *P. vexans*. Simultaneous up (or down) regulation of protein synthesis and degradation is most likely related to the need to regulate net accumulation of intracellular proteins under different stressors.

Several *up*regulated genes exhibited similar average LFC values (~4.0). These included *Acde25g00656.1*, associated with signal transduction (GO:0000160, GO:0007165) and *Acde28g00379.1*, associated with protein transport (GO:0015031) and the nested GO processes: nucleocytoplasmic transport (GO:0006913), and protein import into the nucleus (GO:0006606). Upregulation of *Acde10g01179.1* (LFC = 4.26) was important for maintaining ATP production under hypoxic conditions (GO:0006096, GO:0019752). *Acde10g01112.1* (LFC = 3.97) was also associated with adaptation to flooding (GO:0009415; response to water stimulus).

The top 10 genes *down*regulated under combined stress exhibited significant suppression with LFC values ranging from -22.9 to -9.0 (**Table 2**). The most downregulated gene, *Acde000000s00035.1* (LFC = -22.9), was linked to GO:0006412 (translation), GO:0006807 (obsolete nitrogen compound metabolic process), and GO:0071704 (obsolete organic substance metabolic process). This was surprising, considering that the most upregulated gene (*Acde24g00960.1*) was associated with DNA-templated transcription. This indicates that although the cell is producing more RNA transcripts from genes, those transcripts are not being efficiently converted into functional proteins. This may help plants root cells rapidly respond to multiple environmental changes associated with combined stress treatment (e.g. by upregulating the transcription of stress response genes but downregulating the translation of other genes). Along these same lines, *Acde09g00923.1* (LFC = -11.5), *Acde03g01708.1* (LFC = -10.5), *Acde14g00259.1* (LFC = -10.2), and *Acde08g00277.1* (L2FC = -9.1) while associated with GO:0071704 and GO:0006807, were also linked to GO:0006355 (*regulation* of DNA-templated transcription). Regulation of DNA-templated transcription could be positive or negative. Based on our survey of the top 10 upregulated genes, this most likely indicates diminished expression of genes involved in negative regulation.

It is also worth noting that *Acde01g00258.1*, associated with GO:0006979 (response to oxidative stress), was among the top 10 downregulated genes (LFC = -10). As previously mentioned in section 3.4.1, this finding suggests a reduction in the plant's ability to attenuate oxidative stress

and may play a key role in increasing plant susceptibility to individual (esp. flooding) and combined stressors. Lastly, *Acde03g01652.1* (LFC = -9.56) was associated with GO:0010215 (cellulose microfibril organization), again highlighting a reduction in the production of essential components of plant cell walls (as discussed in section 3.4.1). in response to the combined stress treatment.

3.4.3 KEGG enrichment analysis of up- and downregulated genes in response to combined stress conditions (inoculation and flooding) 96 hours post treatment

KEGG enrichment analysis of up regulated genes revealed that as with flooding alone, the combined stress treatment led to increased expression of WRKY transcription factor 33 (K13424) ($p = 0.045$) and EIN3; ethylene-insensitive protein 3 (K14514) (Table 3). As previously described in section 3.3.3, this is indicative of ethylene-mediated activation of MAPK signaling pathways of the hypoxic stress response. As in the flooding treatment, upregulation of ADH1; alcohol dehydrogenase (K18857) is indicative of adaptation to hypoxic conditions via energy production through fermentation/glycolysis.

The ubiquitin ligase, ARIH1; ariadne-1 (K11968) ($p = 0.045$) was also upregulated, again highlighting the role of ubiquitin-mediated protein degradation. Additionally, PPM1L, PP2CE (K17506), a protein phosphatase, and USP36_42 (K11855) ($p = 0.045$), a ubiquitin carboxyl-terminal hydrolase, point toward active protein regulation and turnover.

In comparison, pathways associated with metabolism, transport, and structural integrity were significantly downregulated. Laccase (K05909) ($p = 0.037$) was downregulated, indicating reduced lignin biosynthesis and oxidative processes. Additionally, the MATE family transporter (K03327) and ABCG2 (K05681) ($p = 0.041$) were suppressed, reflecting reduced activity of multidrug transporters and ABC transport proteins under stress. Downregulation of cellulose synthase (K10999) ($p = 0.046$) and tubulin beta (K07375) suggests impairment in cell wall biosynthesis and cytoskeletal organization, likely limiting structural maintenance under stress. Auxin transport processes were also suppressed, as evidenced by the downregulation of PIN (K13947) and AUX1/LAX (K13946) ($p = 0.046$), indicating disruption in auxin influx and efflux during stress. Additionally, (and also supported by GO term analysis) the downregulation of phenylalanine ammonia-lyase (PAL, K10775) ($p = 0.049$) implies reduced phenylpropanoid biosynthesis, potentially affecting plant defense and secondary metabolite production.

3.5 Effect of treatment on *P. vexans* root infection

Quantification of *P. vexans* DNA in root tissue revealed a substantial increase in pathogen load in inoculated (I and IF) relative to non-inoculated plants (NS and F) over time (T0-T14d), confirming root infection (**Supplementary Table 6**). In inoculated-only (I) plants, the highest quantities of pathogen DNA (2.95 x 10^4 ng) were detected 48 hours post-inoculation (T48); however, pathogen loads appeared to slowly decline over time (T96-T14d). In comparison, the application of flooding + inoculation resulted in pathogen loads which increased over time. As a result, by T14d, higher pathogens loads were detected in IF (1.33 x 10^4 ng) than in I (5.7 x 10^3 ng).

3.6 qPCR validation of RNA-Seq Data

Of the 15 candidate genes selected for qPCR, 11 were used for final correlation comparisons while four candidate genes were dropped due to evidence of non-specific *in vitro* primer binding, low or no fluorescence across a majority of the samples, and/or poor reaction performance (Supplemental Table). Two of the three reference genes passed the quality control and stability analysis and were used for expression normalization (*Acde08g00052.1* & *Acde17g00362.1* M=0.81). The third reference gene (*Acde03g01935.1*) was omitted due to poor performance across repeat qPCR runs. qPCR relative expression was correlated with RNA-Seq TPM normalized expression.

4. Discussion

In this study, by analyzing transcriptomic responses in kiwifruit root tissue over time, we identified key molecular pathways involved in the plant response to different stressors, applied individually and in combination. To our knowledge, this is the first transcriptomic investigation of *Actinidia* under abiotic and biotic stressors combined. The results of our study not only support well-documented mechanisms underlying plant adaptive responses to flooding and biotic stress, but also offer unexpected and novel insight into less understood aspects of these stress responses, including hormonal crosstalk. As previously mentioned, infection with *P. vexans* or flooding alone have proven insufficient to reproduce KVDS symptoms. The results from this study shed new light on specific hormonal crosstalk mechanisms involved in biotic vs. abiotic stress responses which are likely to oppose each other, altering the plant-pathogen interaction and reducing the plant's ability to mitigate biotic stress. The massive re-organization of the transcriptional program triggered by flooding stress response appears to "swamp" and suppress the biotic defense response.

This hypothesis is also supported by the amount of *P. vexans* detected in root tissue; by T14d, the level P. *vexans* root infection was higher in the combined stress treatment than with waterlogging or inoculation alone. These findings provide new evidence about how different stressors work together to influence KVDS disease development.

In terms of transcriptional reprogramming, downregulation was shown to be an integral part of the plant's adaptive response, regardless of stress treatment. Although several genes were significantly upregulated, there were more stress-induced decreases than increases in DEG expression, regardless of treatment or timepoint. At T96, these included multiple genes related to plant cell growth and energy production. The ability of cells to rapidly adjust rates of protein production/turnover appeared to be a critical aspect of both individual and combined stress responses. In addition, the combined stress condition resulted in a larger number of unique up- and downregulated genes than with flooding or inoculation alone, demonstrating the dramatic effect of combined stressors on the transcriptome.

4.1 Hormonal crosstalk, flavonoid biosynthesis and reduced proteolysis underscore the kiwi root transcriptome response to *P. vexans*.

As previously described in Section 3.2, a number of phytohormone signaling pathways appeared to be involved in mediating the plant response to *P. vexans* infection including the hormones abscisic acid (ABA), ethylene (ET) and indole acetic acid (IAA). In many studies, ABA has been shown to be a key player in modulating abiotic stress tolerance in plants; however, the role of ABA in plant disease resistance/susceptibility is less well-understood (Bharath et al., 2021; Mauch-Mani and Mauch, 2005).

In *Arabidopsis*, ABA has been shown to contribute to defense against necrotrophic oomycetes through at least two distinct mechanisms. One well-established pathway involves ABA-dependent priming of callose deposition, which strengthens the cell wall by forming β-1,3-glucan-rich papillae at infection sites, thereby providing a physical barrier against pathogen entry (Ton and Mauch-Mani, 2004). A second, less direct mechanism links ABA to the activation of jasmonic acid (JA) biosynthesis and downstream JA-dependent defense gene expression (Adie et al., 2007). Notably, in our kiwifruit–*Phytopythium* pathosystem, we observed an upregulation of ABA-related responses but no significant induction of JA-associated genes. This suggests that in this

host-pathogen interaction, ABA may primarily function through callose-associated physical defenses rather than via JA-mediated signaling.

There is also strong evidence that ABA interacts with ethylene (ET) and that high ABA concentrations typically inhibit ET production (LeNoble et al., 2004). In our study, downregulation of aminocyclopropane carboxylate oxidase (K05933) at T96 during infection with *P. vexans*, suggests that the rate of ethylene biosynthesis decreased during pathogen infection. On the other hand, K09286 (EREBP-like factor) was enriched with upregulated DEGs, suggestive of ethylene-mediated regulation of gene expression. As previously noted, ethylene biosynthesis has been associated with the expression of a variety of plant defense-related genes (Ecker and Davis, 1987; Broekaert et al., 2006). In some studies, however, ethylene production has been shown to promote and/or be associated with disease development (Lund et al., 1998). In this study, due to the above evidence, it is difficult to link ethylene production to the induction of defense response genes.

The upregulation of YUCCA (K11816), implies indole-3-acetic acid (IAA) may also be involved in mediating the plant response to infection. IAA is crucial in regulating plant responses to developmental and environmental cues, including pathogen attacks. In kiwifruit, IAA has been shown to induce resistance against the postharvest fungal pathogen *Botrytis cinerea* (Li et al., 2023). Defense responses against necrotrophic pathogens (including *Phytopythium*) are typically governed by complex signaling pathways involving connections between JA/ET-dependent signaling (Pandey, et al., 2016) and auxins (Truman et al., 2010; Hentrich et al., 2013); however, no clear JA-related transcriptional signature emerged in this study. The interplay between multiple phytohormones observed in this study, including ET, ABA, and IAA, is consistent with the current understanding of hormonal crosstalk and exemplifies the fine-tuned coordination required to mount plant defense responses (Verma et al., 2016).

In the Li et al. (2023) study mentioned above, IAA treatment was also linked to the activation of the phenylpropanoid pathway, including the production of flavonoids and phenols. The significant induction of chalcone synthase (K00660) at T96, underscores the importance of flavonoid biosynthesis in *A. deliciosa* defense and signaling. It is also interesting to note that chalcone synthase (CHS) upregulation was previously observed in response to inoculation with *P. ultimum* in apple (Zhu et al., 2019). Apple replant disease is similar to KVDS in many ways; in both pathosystems, *Phytopythium*/*Pythium* spp. are key causative agents while *Dactylonectria* and/or

Ilyonectria/Cylindrocarpon may also be involved. In the Zhu et al. study, CHS upregulation was detected in both susceptible and resistant genotypes, primarily at 72 hours post-inoculation.
In addition to flavonoid biosynthesis, the upregulation of specific transport proteins (e.g. aquaporin and NPF2 transporters) indicated that defenses related to the transport of specialized metabolites (including H_2O_2) were also induced. In comparison, a number of aspects related to growth and cellular maintenance were suppressed in the face of pathogen invasion, indicative of a defense/growth trade-off. Most noticeable was the suppression of multiple E3 ubiquitin-protein ligases and other genes associated with protein degradation. The accumulation of certain proteins may be particularly valuable for biotic stress responses; reduced proteolysis may reflect a stabilization of stress-related proteins during the plant-microbe interaction. Signs of reduced energy production via oxidative phosphorylation and production of reactive oxygen species (ROS) coupled with a reduced ability to attenuate ROS damage, highlight less beneficial aspects of the root response to biotic stress.

4.2 Kiwi root transcriptome response to flooding indicates a highly coordinated response in which adaptations to osmotic and hypoxic stress are prioritized over other processes.
Enrichment of multiple processes involved in transcriptional regulation suggests a massive reorganization in the transcriptional program in response to flooding (a finding which is also evident in Table 2). A large part of the kiwi root response to flooding stress appeared to be associated with the ability to efficiently control gene expression and maintain protein homeostasis. This was accomplished via several different strategies including: downregulation of new protein synthesis (translation) and folding activity in combination with processing/modification of existing mRNA transcripts, as well as increased ubiquitin-mediated protein degradation and mRNA surveillance activities. Protein transport was also upregulated, indicating enhanced transport of proteins into, out of and/or within cells in response to flooding stress. As mentioned previously, these processes are likely crucial for allowing cells to rapidly adjust protein levels in order to adapt to waterlogging.
Key adaptive mechanisms which can be predicted from the transcriptomic response to flooding also include alterations in gene expression related to maintaining ion and osmotic homeostasis across cell membranes. In addition to metal ions, the membrane transport activity of many nutrients essential for plant growth was reduced (including phosphate, nitrate and potassium

transport). Along these same lines, the upregulation of processes related to the accumulation of soluble sugars (esp. sucrose and trehalose) in roots was identified as an important aspect of the adaptive response to waterlogging in *A. deliciosa*. Together, these changes likely contribute to osmotic adjustment/cytosolic homeostasis.

In terms of environmental sensing/signaling, ethylene signaling in response to flooding has been shown to be central to hypoxia tolerance in many plants. As mentioned earlier, ethylene gas typically tends to accumulate in the tissues of flooded plants. Ethylene was previously implicated in regulating the response to waterlogging/hypoxia in kiwifruit (Li et al., 2020). In this study, two components of the ethylene signaling pathway, EIN3 (K14514) and EBF1/2 (K14515), were upregulated in the flooding alone treatment. Ethylene signaling begins with ethylene binding to a family of receptors and culminates in a transcriptional cascade involving EIN3/EIL and ERF transcription factors (Potuschak et al., 2003; Mao et al., 2006; Khan et al., 2020). The upregulation of EBF1/2, which encodes F-box proteins that physically interact with EIN3/EIL, further emphasizes the intricate regulation of ethylene-responsive genes during flooding stress.

GO and KEGG-based enrichment analyses also provided valuable insight into how gene expression is specifically modulated (following stress signaling activated by ethylene) in order to adapt to hypoxic conditions. As mentioned in Section 3.3.3, significant upregulation of stress-responsive WRKY transcription factors underscores the *Actinidia* response to hypoxia at the root level (Gao et al., 2022; Xing et al., 2023). WRKY transcription factors are considered to be general stress-regulatory machinery; a variety of different WRKY transcription factors mediate responses to both abiotic and biotic stressors and interconnect hormonal responses (Friedel et al., 2012). In this study, we observed the upregulation of WRKY22 and WRKY33 in *A. deliciosa* in response to flooding stress, aligning with findings in which WRKY transcription factors, including WRKY22, are rapidly induced under submergence in *Arabidopsis* (Hsu et al., 2013). The involvement of WRKY33 in oxidative stress responses and hormone signaling has been particularly well-documented (Tang et al., 2020; 2021). The activation of WRKY33 in *A. deliciosa* during flooding stress underscores its conserved role in hypoxia tolerance, as initially established in *Arabidopsis* (Tang et al., 2020). In *Arabidopsis*, WRKY33 positively regulates submergence responses by targeting genes through the "TC box" cis-element and is predominantly expressed in roots (Jiang and Deyholos, 2008; Zhang et al., 2021). It is also worth noting that concurrent activation of WRKY33 and WRKY22 has been observed in *A. valvata* in response to prolonged waterlogging

(Gao et al., 2022). The activation of these transcription factors in *A. deliciosa* root tissue in this study further highlights its importance in adapting to hypoxic conditions resulting from waterlogging across species.

As previously noted, the enzyme ADH play an essential role in ethanol fermentation and is also considered to be a major marker for hypoxia stress in plants (Pan et al., 2021) including kiwifruit (Zhang et al., 2015; Li et al., 2021; Xing et al., 2023). A proteomic study by Hashiguchi et al. (2009) showed that proteins related to glycolysis, including ADH, are highly affected by flooding in soybean, while Komatsu et al. (2010; 2009) demonstrated increased ADH levels and transcription under waterlogged conditions. Komatsu et al. (2011) further reported that ADH expression is more strongly induced by flooding in soybean than in rice, highlighting its importance in less flood-tolerant species (e.g. kiwifruit). In a previous study conducted by Zhang et al. (2015) on prolonged hypoxia stress in *A. deliciosa,* two *Ad*ADH genes were upregulated in response to 96 h of waterlogging. A more recent study by Xing et al. (2023) also confirmed the involvement of *Ad*ADH in wild *A. deliciosa*, which was highly expressed after 3 days of flooding. In another work by Li et al. (2021), *Ad*ADH was upregulated in two *Actinidia* rootstocks: *A. valvata* and *A. deliciosa*. The upregulation of ADH in our study reinforces the notion that kiwi roots respond to waterlogging by shifting towards anaerobic metabolism/glycolysis to maintain cellular energy homeostasis under oxygen-limited conditions. Following waterlogging, adaptations to osmotic and hypoxic stress are prioritized over cell growth and energy-related processes, via regulation of specific signaling pathways. However, flooding stress can also limit pathogen defenses in plants. For example, Mooney et al. (2024) demonstrated that flooding stress can interfere with PAMP-triggered immunity (PTI) by prioritizing hypoxia-related transcriptional responses over defense signaling. In their study, *Arabidopsis* plants exposed to the bacterial elicitor flg22 showed a blunted immune response when also subjected to hypoxia, likely due to resource limitations that led to suppression of developmental processes and defense pathways. This transcriptional reprogramming was mediated in part by hypoxia-associated ERF-VII transcription factors and accompanied by repression of key developmental transcription factor families. In the context of this study, downregulation of processes linked to secondary metabolite production (K10775, GO:0009094) and defense responses (GO:0006952), together with the upregulation of components of the ethylene signaling pathway EIN3 and EBF1/2, may not only weaken pathogen-specific defenses against *P. vexans*, (i.e. phenylpropanoid/flavonoid production), but may also play

a role in deactivating more general wound-induced defense responses (Lee et al., 2020). These findings support the idea that under combined stress, such as flooding and pathogen exposure, plants deprioritize biotic defense responses in favor of survival-related adjustments, thereby compromising their ability to resist infection. Additionally, flooding can create conditions that favor certain pathogens (especially oomycetes, which thrive in moist conditions), further increasing vulnerability. In the following section, we explore more specifically how flooding interacts with *P. vexans* inoculation to alter plant defense responses and disease outcomes.

4.3 Kiwi root transcriptome response to simultaneous biotic and abiotic stressors indicates a disruption of root immune responses and a trade-off favoring hypoxia survival.

GO and KEGG-based transcriptomic analyses of the response to flooding alone (F) and that of the combined stress conditions (IF) were very similar. In both cases, these analyses provided clear evidence of a host of adaptive responses to waterlogging related to the need to maintain osmotic and cellular homeostasis under hypoxic conditions. This included evidence for the role of ethylene-mediated activation of MAPK pathways/WRKY transcription factors in stress signaling, the central role of anaerobic fermentation pathways in maintaining ATP production, and downregulation of genes involved in the transport of metal ions and nutrients across cell membranes.

In particular, ADH induction/upregulation appears to be a common response to hypoxia across a variety of woody tree species including avocado and gray poplar (Reeksting et al., 2016; Kreuzwieser et al., 2009). In the Reeksting et al. study with avocado, no significant differences in ADH expression were reported between flooding alone and multifactorial treatments. In the current study, p-values for the ADH enzyme from KEGG enrichment analysis were highly similar between F and IF treatments. The consistent upregulation of ADH across these two stress scenarios in our study suggests that ADH activation is a conserved and robust mechanism in both single-stress and more complex, multifactorial waterlogging stress responses.

Also regarding signaling pathways, the activation of EIN3 (K14514) and WRKY33 (K13424) was consistent with the flooding alone treatment. That said, while we observed activation of EIN3 in multifactorial stress, this was the only component of the ethylene signaling pathway that was upregulated (i.e., EBF1/2 did not show a significant change in expression in this condition). In addition, we observed concurrent activation of WRKY33 and WRKY22 in *A. deliciosa* in response

to flooding stress (F); however, only one transcription factor (WRKY33) was upregulated in the multifactorial (IF) treatment. WRKY33 and WRKY22 are key positive regulators of plant responses to submergence, but are also components of signaling pathways sensing pathogen infection/attack. In *Arabidopsis*, hypoxia is known to induce the expression of disease resistance genes (Hsu et al., 2013), with WRKY33 extensively reported to positively regulate disease resistance mechanisms (in *Arabidopsis*) (Liu et al., 2017; Sham et al., 2017; Wang et al., 2018). This dual role in hypoxia tolerance and pathogen defense highlights the intricate interplay between stress response pathways. This is especially significant to understanding the development of KVDS, given that *A. deliciosa* is highly sensitive to flooding at the root level while oomycetes (including *P. vexans*) are generally favored by waterlogging conditions. However, as previously mentioned, in the context of this study system, waterlogging/hypoxia appeared to impair biotic defenses, while the plant focused energy on survival.

In keeping with this hypothesis, significant downregulation of the auxin transporters PIN (K13947) and AUX1 (K13946) was unique to the multifactorial stress condition. Auxin signaling and transport are critical for balancing growth and defense during stress conditions. These results suggest a disruption in polar auxin transport (PAT) and auxin homeostasis. The observed downregulation likely impacts both the polarity-dependent auxin transport and its systemic distribution via the phloem. Although the role of auxins in stress responses is multifaceted. Auxin accumulation has been shown to enhance susceptibility to necrotrophic pathogens while supporting resistance to biotrophic pathogens (Kazan et al., 2009). For example, in *Arabidopsis aux1* mutants, *Botrytis cinerea* infection leads to compromised ability of developing induced resistance against the same necrotrophic fungus (Korolev et al., 2007). Furthermore, the modulation of auxin signaling during pathogen attack has been widely reported. In kiwifruit, the auxin IAA has been shown to induce resistance against the postharvest fungal pathogen *B. cinerea* (Li et al., 2023). These observations suggest that the downregulation of multiple proteins which facilitate the movement of auxin may impair the plant's ability to respond to necrotrophic pathogens during multifactorial stress. Other investigations of *Arabidopsis* mutants with impaired auxin production or signaling revealed an increased vulnerability to infections caused by necrotrophic pathogens (Llorente et al., 2008; Tiryaki et al., 2002). That said, the downregulation of PIN and AUX1 in the IF treatment could represent a trade-off mechanism. Plants may suppress auxin transport to prioritize stress adaptation over growth, potentially altering susceptibility to

specific pathogens. It is also interesting to note that rates of DNA-templated transcription and translational initiation were elevated under combined (but not flooding alone) stress. In both treatments, however, translation and post-translational processes required for the generation of functional proteins were suppressed while proteolysis was upregulated. In contrast, key mechanisms for protein degradation appeared to be downregulated under biotic stress alone. Regardless of treatment, a large part of the kiwi root response to stress appears to be associated with the ability to maintain protein homeostasis (via several different processes which often appear to be opposing). Finally, as first discussed in Section 3.3.3, one of the most striking results was the downregulation of phenylalanine ammonia-lyase (PAL) in both F and IF treatments. This enzyme catalyzes the first step of the phenylpropanoid biosynthetic pathway, which, as revealed in this study, is likely to be a vital component of the chemical defense response to infection with *P. vexans*. As previously mentioned, PAL also plays a central role in the synthesis of lignin. Therefore, its reduced expression in the combined treatment (along with the downregulation of components required for the production/assembly of plant cell walls/membranes), may also weaken the plant's structural defenses under dual stress conditions.

5. Conclusion

This work provides new insight into the transcriptomic responses of *Actinidia deliciosa* roots to a multifactorial stress combination (infection with *Phytopythium vexans* inoculation + flooding stress) as well as to these stressors applied individually. It represents the first assessment of the impact of this multifactorial stress combination on kiwifruit. Although many “classical” aspects of the plant response to flooding were shared between F and IF treatments, the transcriptomic response to multifactorial stress was unique and could not be predicted from the response of roots to each of the different stressors. The most notable (and worrisome) finding from this study was the fact that the individual stressors (infection with *P. vexans* and flooding) appeared to have antagonistic effects on each other. The activation of multi-phytohormone signaling cascades and key enzymes (chalcone synthase) involved in phenylpropanoid biosynthesis appeared to play a major role in regulating root defense responses to *P. vexans* during infection. The effect of flooding was dominant to the effect of pathogen infection and the ability of *A. deliciosa* (Hayward) to mount an effective defense response (especially in terms of chemical defenses) was greatly reduced in

the presence of flooding. Consequently, even though the stressors applied individually to the plant have a negligible effect on plant growth/survival, the antagonistic effects between pathogen and flooding likely has a synergistic effect on the plant, leading to significant negative effects on plant growth and survival (i.e., the development of KVDS). Additionally, the pathogen infection transcriptome is likely to be altered in the presence of water. Analyzing the transcriptome of *P. vexans* while also characterizing other plant-microbiome interactions under infection alone and infection + flooding, may be one area for future research that could further enhance our understanding of KVDS development as well as the factors associated with resilience to (or mitigation of) this multifactorial stress combination.

Acknowledgements

This research was funded by Piedmont Region (Italy) with the project "KIRIS - Kiwifruit Vine Decline Syndrome: deepening the etiology and development of prevention and control tool" and "KIPOTRA – Kiwifruit Vine Decline Syndrome – Evaluation of the use of rootstocks as an agronomic tool to prevent symptom development", by Italian Ministry of University and Research with the project "KVD-Biome - Unveiling the plant exposome to dissect a multifactorial disease: the kiwifruit vine decline", by AGER – Foundations Network for Agrifood Research with the project "SOS-KIWI - From SOil to Soil: origin and remediation to KIWIfruit Vine Decline Syndrome", and by the European Commission – NextGenerationEU, Project SUS-MIRRI.IT "Strengthening the MIRRI Italian Research Infrastructure for Sustainable Bioscience and Bioeconomy", code n. IR0000005.

References

Adhikari, B.N., Hamilton, J.P., Zerillo, M.M., Tisserat, N., Lévesque, C.A. & Buell, C.R. (2013) Comparative Genomics Reveals Insight into Virulence Strategies of Plant Pathogenic Oomycetes. PLOS ONE, 8, e75072. https://doi.org/10.1371/journal.pone.0075072.

Adie, Bruce A.T., Pérez-Pérez, J., Pérez-Pérez, M.M., Godoy, M., Sánchez-Serrano, J.-J., Schmelz, E.A., et al. (2007) ABA Is an Essential Signal for Plant Resistance to Pathogens Affecting JA Biosynthesis and the Activation of Defenses in

Arabidopsis. The Plant Cell, 19, 1665–1681. https://doi.org/10.1105/tpc.106.048041.

Alexa A, Rahnenfuhrer J (2024). topGO: Enrichment Analysis for Gene Ontology. doi:10.18129/B9.bioc.topGO, R package version 2.59.0, https://bioconductor.org/packages/topGO.

Asselbergh, B., De Vleesschauwer, D. & Höfte, M. (2008) Global switches and fine-tuning-ABA modulates plant pathogen defense. Molecular plant-microbe interactions: MPMI, 21, 709–719. https://doi.org/10.1094/MPMI-21-6-0709.

Baldi, E., Pastore, C., Chiarelli, G., Quartieri, M., Spinelli, F. & Toselli, M. (2024) Molecular Responses to Drought and Waterlogging Stresses of Kiwifruit (Actinidia chinensis var. deliciosa) Potted Vines. *Horticulturae*, 10, 834. https://doi.org/10.3390/horticulturae10080834.

Beppu, K., Ogihara, Y., Ohtani, M. & Kataoka, I. (2022) Comparison of waterlogging tolerance between *Actinidia macrosperma* and *Actinidia deliciosa*. *Acta Horticulturae*, 219–226. https://doi.org/10.17660/ActaHortic.2022.1332.29.

Bharath, P., Gahir, S. & Raghavendra, A.S. (2021) Abscisic Acid-Induced Stomatal Closure: An Important Component of Plant Defense Against Abiotic and Biotic Stress. *Frontiers in Plant Science*, 12. https://doi.org/10.3389/fpls.2021.615114.

Broekaert, W.F., Delauré, S.L., Bolle, M.F.C.D. & Cammue, B.P.A. (2006) The Role of Ethylene in Host-Pathogen Interactions. Annual Review of Phytopathology, 44, 393–416. https://doi.org/10.1146/annurev.phyto.44.070505.143440.

Bürger, M. & Chory, J. (2019) Stressed Out About Hormones: How Plants Orchestrate Immunity. Cell Host & Microbe, 26, 163–172. https://doi.org/10.1016/j.chom.2019.07.006.

Bustin, S.A., Benes, V., Garson, J., Hellemans, J., Huggett, J., Kubista, M., et al. (2013) The need for transparency and good practices in the qPCR literature. *Nature Methods*, 10, 1063–1067. https://doi.org/10.1038/nmeth.2697.

Campos, M.L., Kang, J.-H. & Howe, G.A. (2014) Jasmonate-Triggered Plant Immunity. Journal of Chemical Ecology, 40, 657–675. https://doi.org/10.1007/s10886-014-0468-3.

Cao, F.Y., Yoshioka, K. & Desveaux, D. (2011) The roles of ABA in plant–pathogen interactions. Journal of Plant Research, 124, 489–499. https://doi.org/10.1007/s10265-011-0409-y.

Dao, T.T.H., Linthorst, H.J.M. & Verpoorte, R. (2011) Chalcone synthase and its functions in plant resistance. Phytochemistry Reviews, 10, 397–412. https://doi.org/10.1007/s11101-011-9211-7.

De Nadal, E. de, Ammerer, G. & Posas, F. (2011) Controlling gene expression in response to stress. *Nature Reviews Genetics*, 12, 833–845. https://doi.org/10.1038/nrg3055.

Dhawale, S., Souciet, G. & Kuhn, D.N. (1989) Increase of Chalcone Synthase mRNA in Pathogen-Inoculated Soybeans with Race-Specific Resistance Is Different in Leaves and Roots 1. Plant Physiology, 91, 911–916.

Dixit, S., Sivalingam, P.N., Baskaran, R.K.M., Senthil-Kumar, M. & Ghosh, P.K. (2024) Plant responses to concurrent abiotic and biotic stress: unravelling physiological and morphological mechanisms. Plant Physiology Reports, 29, 6–17. https://doi.org/10.1007/s40502-023-00766-0.

Donati, I., Cellini, A., Sangiorgio, D., Caldera, E., Sorrenti, G. & Spinelli, F. (2020) Pathogens Associated to Kiwifruit Vine Decline in Italy. Agriculture, 10, 119. https://doi.org/10.3390/agriculture10040119.

Ecker, J.R. & Davis, R.W. (1987) Plant defense genes are regulated by ethylene. *Proceedings of the National Academy of Sciences*, 84, 5202–5206. https://doi.org/10.1073/pnas.84.15.5202.

Friedel, S., Usadel, B., Von Wirén, N. & Sreenivasulu, N. (2012) Reverse Engineering: A Key Component of Systems Biology to Unravel Global Abiotic Stress Cross-Talk. Frontiers in Plant Science, 3. https://doi.org/10.3389/fpls.2012.00294.

Gao, Y., jiang, Z., Shi, M., Zhou, Y., Huo, L., Li, X., et al. (2022) Comparative transcriptome provides insight into responding mechanism of waterlogging stress in Actinidia valvata Dunn. Gene, 845, 146843. https://doi.org/10.1016/j.gene.2022.146843.

Ghimire, B. & Baysal-Gurel, F. (2023) A Diagnostic Guide to Phytopythium helicoides and Phytopythium vexans Causing Root and Crown Rot Diseases. Plant Health Progress, 24, 527–538. https://doi.org/10.1094/PHP-01-23-0003-DG.

Gietler, M., Fidler, J., Labudda, M. & Nykiel, M. (2020) Abscisic Acid—Enemy or Savior in the Response of Cereals to Abiotic and Biotic Stresses? International Journal of Molecular Sciences, 21, 4607. https://doi.org/10.3390/ijms21134607.

Gill, M.B., Zeng, F., Shabala, L., Böhm, J., Zhang, G., Zhou, M., et al. (2018) The ability to regulate voltage-gated K+-permeable channels in the mature root epidermis is

essential for waterlogging tolerance in barley. Journal of Experimental Botany, 69, 667–680. https://doi.org/10.1093/jxb/erx429.

Guaschino, M., Garello, M., Nari, L., Zhimo, Y.V., Droby, S. & Spadaro, D. (2024) Soil, rhizosphere, and root microbiome in kiwifruit vine decline, an emerging multifactorial disease. *Frontiers in Microbiology*, 15. https://doi.org/10.3389/fmicb.2024.1330865.

Hadish, J.A., Biggs, T.D., Shealy, B.T., Bender, M.R., McKnight, C.B., Wytko, C., et al. (2022) GEMmaker: process massive RNA-seq datasets on heterogeneous computational infrastructure. *BMC Bioinformatics*, 23, 156. https://doi.org/10.1186/s12859-022-04629-7.

Hadish, J.A., Hargarten, H.L., Zhang, H., Mattheis, J.P., Honaas, L.A. & Ficklin, S.P. (2024) Correction: Towards identification of postharvest fruit quality transcriptomic markers in Malus domestica. *PLOS ONE*, 19, e0306187. https://doi.org/10.1371/journal.pone.0306187.

Hahn, A., Kilian, J., Mohrholz, A., Ladwig, F., Peschke, F., Dautel, R., et al. (2013) Plant Core Environmental Stress Response Genes Are Systemically Coordinated during Abiotic Stresses. *International Journal of Molecular Sciences*, 14, 7617–7641. https://doi.org/10.3390/ijms14047617.

Hargarten, H., Waliullah, S., Kalcsits, L. & Honaas, L.A. (2018) Leveraging Transcriptome Data for Enhanced Gene Expression Analysis in Apple. https://doi.org/10.21273/JASHS04424-18.

Hashiguchi, A., Sakata, K. & Komatsu, S. (2009) Proteome analysis of early-stage soybean seedlings under flooding stress. *Journal of Proteome Research*, 8, 2058–2069. https://doi.org/10.1021/pr801051m.

Hellemans, J., Mortier, G., De Paepe, A., Speleman, F. & Vandesompele, J. (2007) qBase relative quantification framework and software for management and automated analysis of real-time quantitative PCR data. *Genome Biology*, 8, R19. https://doi.org/10.1186/gb-2007-8-2-r19.

Hentrich, M., Böttcher, C., Düchting, P., Cheng, Y., Zhao, Y., Berkowitz, O., et al. (2013) The jasmonic acid signaling pathway is linked to auxin homeostasis through the modulation of 8 and 9 gene expression. The Plant Journal, 74, 626–637. https://doi.org/10.1111/tpj.12152.

Honaas, L., Hargarten, H., Hadish, J., Ficklin, S.P., Serra, S., Musacchi, S., et al. (2021) Transcriptomics of Differential Ripening in 'd'Anjou' Pear (Pyrus communis L.). *Frontiers in Plant Science*, 12. https://doi.org/10.3389/fpls.2021.609684.

Hsu, F.-C., Chou, M.-Y., Chou, S.-J., Li, Y.-R., Peng, H.-P. & Shih, M.-C. (2013) Submergence Confers Immunity Mediated by the WRKY22 Transcription Factor in Arabidopsis. The Plant Cell, 25, 2699–2713. https://doi.org/10.1105/tpc.113.114447.

Ji, H.S. & Hyun, T.K. (2023) Physiological and sucrose metabolic responses to waterlogging stress in balloon flower (Platycodon grandiflorus (Jacq.) A. DC). *Physiology and Molecular Biology of Plants*, 29, 591–600. https://doi.org/10.1007/s12298-023-01310-y.

Jiang, Y. & Deyholos, M.K. (2008) Functional characterization of Arabidopsis NaCl-inducible WRKY25 and WRKY33 transcription factors in abiotic stresses. Plant Molecular Biology, 69, 91–105. https://doi.org/10.1007/s11103-008-9408-3.

Kazan, K. & Manners, J.M. (2009a) Linking development to defense: auxin in plant–pathogen interactions. Trends in Plant Science, 14, 373–382. https://doi.org/10.1016/j.tplants.2009.04.005.

Khan, M.I.R., Trivellini, A., Chhillar, H., Chopra, P., Ferrante, A., Khan, N.A., et al. (2020) The significance and functions of ethylene in flooding stress tolerance in plants. Environmental and Experimental Botany, 179, 104188. https://doi.org/10.1016/j.envexpbot.2020.104188.

Kohli, A., Sreenivasulu, N., Lakshmanan, P. & Kumar, P.P. (2013) The phytohormone crosstalk paradigm takes center stage in understanding how plants respond to abiotic stresses. Plant Cell Reports, 32, 945–957. https://doi.org/10.1007/s00299-013-1461-y.

Komatsu, S., Yamamoto, R., Nanjo, Y., Mikami, Y., Yunokawa, H. & Sakata, K. (2009) A Comprehensive Analysis of the Soybean Genes and Proteins Expressed under Flooding Stress using Transcriptome and Proteome Techniques. *Journal of Proteome Research*, 8, 4766–4778. https://doi.org/10.1021/pr900460x.

Komatsu, S., Sugimoto, T., Hoshino, T., Nanjo, Y. & Furukawa, K. (2010) Identification of flooding stress responsible cascades in root and hypocotyl of soybean using proteome analysis. *Amino Acids*, 38, 729–738. https://doi.org/10.1007/s00726-009-0277-0.

Komatsu, S., Thibaut, D., Hiraga, S., Kato, M., Chiba, M., Hashiguchi, A., et al. (2011) Characterization of a novel flooding stress-responsive alcohol dehydrogenase expressed in soybean roots. Plant Molecular Biology, 77, 309–322. https://doi.org/10.1007/s11103-011-9812-y.

Korolev, N., Rav David, D. & Elad, Y. (2008) The role of phytohormones in basal resistance and Trichoderma-induced systemic resistance to Botrytis cinerea in Arabidopsis thaliana. BioControl, 53, 667–683. https://doi.org/10.1007/s10526-007-9103-3.

Kreuzwieser, J., Hauberg, J., Howell, K.A., Carroll, A., Rennenberg, H., Millar, A.H., et al. (2009) Differential Response of Gray Poplar Leaves and Roots Underpins Stress Adaptation during Hypoxia. Plant Physiology, 149, 461–473. https://doi.org/10.1104/pp.108.125989.

Kreps, J.A., Wu, Y., Chang, H.-S., Zhu, T., Wang, X. & Harper, J.F. (2002) Transcriptome Changes for Arabidopsis in Response to Salt, Osmotic, and Cold Stress,. *Plant Physiology*, 130, 2129–2141. https://doi.org/10.1104/pp.008532.

Lee, H.-J., Park, J.-S., Shin, S.Y., Kim, S.-G., Lee, G., Kim, H.-S., et al. (2020) Submergence deactivates wound-induced plant defence against herbivores. *Communications Biology*, 3, 651. https://doi.org/10.1038/s42003-020-01376-4.

Leisner, C.P., Potnis, N. & Sanz-Saez, A. (2023b) Crosstalk and trade-offs: Plant responses to climate change-associated abiotic and biotic stresses. Plant, Cell & Environment, 46, 2946–2963. https://doi.org/10.1111/pce.14532.

LeNoble, M.E., Spollen, W.G. & Sharp, R.E. (2004) Maintenance of shoot growth by endogenous ABA: genetic assessment of the involvement of ethylene suppression. *Journal of Experimental Botany*, 55, 237–245. https://doi.org/10.1093/jxb/erh031.

Lévesque, A.C. & De Cock, A.W.A.M. (2004) Molecular phylogeny and taxonomy of the genus *Pythium*. *Mycological Research*, 108, 1363–1383. https://doi.org/10.1017/S0953756204001431.

Li, G., Chen, T., Zhang, Z., Li, B. & Tian, S. (2020) Roles of Aquaporins in Plant-Pathogen Interaction. *Plants*, 9, 1134. https://doi.org/10.3390/plants9091134.

Li, Z., Zhong, Y., Bai, D., Abid, M., Zhang, Y., Lin, M., et al. (2020) Comparative Transcriptome Analysis of Two Contrasting Kiwifruit (Actinidia) Genotypes under Waterlogging Stress. Preprints. https://doi.org/10.20944/preprints202007.0395.v1.

Li, Z., Bai, D., Zhong, Y., Abid, M., Qi, X., Hu, C., et al. (2021) Physiological Responses of Two Contrasting Kiwifruit (Actinidia spp.) Rootstocks against Waterlogging Stress. Plants, 10, 2586. https://doi.org/10.3390/plants10122586.

Li, Z., Yang, S., Wang, X., Liao, Q., Zhang, W., Liu, J.G., Liu, G., & Tang, J. (2023). Widely targeted metabolomics analysis reveals the effect of exogenous auxin on postharvest resistance to Botrytis cinerea in kiwifruit (Actinidia chinensis L.). *Postharvest Biology and Technology*.

Liu, S., Ziegler, J., Zeier, J., Birkenbihl, R.P. & Somssich, I.E. (2017) Botrytis cinerea B05.10 promotes disease development in Arabidopsis by suppressing WRKY33-mediated host immunity. *Plant, Cell & Environment*, 40, 2189–2206. https://doi.org/10.1111/pce.13022.

Llorente, F., Muskett, P., Sánchez-Vallet, A., López, G., Ramos, B., Sánchez-Rodríguez, C., et al. (2008) Repression of the Auxin Response Pathway Increases Arabidopsis Susceptibility to Necrotrophic Fungi. Molecular Plant, 1, 496–509. https://doi.org/10.1093/mp/ssn025.

Lorenzo, O., Piqueras, R., Sánchez-Serrano, J.J. & Solano, R. (2003) ETHYLENE RESPONSE FACTOR1 Integrates Signals from Ethylene and Jasmonate Pathways in Plant Defense[W]. The Plant Cell, 15, 165–178. https://doi.org/10.1105/tpc.007468.

Love, M.I., Huber, W. & Anders, S. (2014) Moderated estimation of fold change and dispersion for RNA-seq data with DESeq2. *Genome Biology*, 15, 550. https://doi.org/10.1186/s13059-014-0550-8.

Lund, S.T., Stall, R.E. & Klee, H.J. (1998) Ethylene Regulates the Susceptible Response to Pathogen Infection in Tomato. *The Plant Cell*, 10, 371–382. https://doi.org/10.1105/tpc.10.3.371.

Ma, C., Liu, W., Du, X., Zhao, C., Tian, R., Li, R., et al. (2025) The flavonoid metabolic pathway genes Ac4CL1, Ac4CL3 and AcHCT1 positively regulate the kiwifruit immune response to Pseudomonas syringae pv. actinidiae. *Plant Molecular Biology*, 115, 21. https://doi.org/10.1007/s11103-024-01546-6.

Maicas, S. & Mateo, J.J. (2020) Sustainability of Wine Production. Sustainability, 12, 559. https://doi.org/10.3390/su12020559.

Manni, M., Berkeley, M.R., Seppey, M., Simão, F.A. & Zdobnov, E.M. (2021) BUSCO Update: Novel and Streamlined Workflows along with Broader and Deeper Phylogenetic Coverage for Scoring of Eukaryotic, Prokaryotic, and Viral Genomes.

Molecular Biology and Evolution, 38, 4647–4654. https://doi.org/10.1093/molbev/msab199.

Mao, C., Wang, S., Jia, Q. & Wu, P. (2006a) OsEIL1, a Rice Homolog of the Arabidopsis EIN3 Regulates the Ethylene Response as a Positive Component. Plant Molecular Biology, 61, 141–152. https://doi.org/10.1007/s11103-005-6184-1.

Mauch-Mani, B. & Mauch, F. (2005) The role of abscisic acid in plant–pathogen interactions. *Current Opinion in Plant Biology*, 8, 409–414. https://doi.org/10.1016/j.pbi.2005.05.015.

Merlot, S., Gosti, F., Guerrier, D., Vavasseur, A. & Giraudat, J. (2001a) The ABI1 and ABI2 protein phosphatases 2C act in a negative feedback regulatory loop of the abscisic acid signalling pathway. The Plant Journal, 25, 295–303. https://doi.org/10.1046/j.1365-313x.2001.00965.x.

Merlot, S., Gosti, F., Guerrier, D., Vavasseur, A. & Giraudat, J. (2001b) The ABI1 and ABI2 protein phosphatases 2C act in a negative feedback regulatory loop of the abscisic acid signalling pathway. The Plant Journal, 25, 295–303. https://doi.org/10.1046/j.1365-313x.2001.00965.x.

Mooney, B.C., Doorly, C.M., Mantz, M., García, P., Huesgen, P.F. & Graciet, E. (2024) Hypoxia represses pattern-triggered immune responses in Arabidopsis. Plant Physiology, 196, 2064–2077. https://doi.org/10.1093/plphys/kiae432.

Nawaz, M., Sun, J., Shabbir, S., Khattak, W.A., Ren, G., Nie, X., et al. (2023) A review of plants strategies to resist biotic and abiotic environmental stressors. *Science of The Total Environment*, 900, 165832. https://doi.org/10.1016/j.scitotenv.2023.165832.

Negi, S., Sukumar, P., Liu, X., Cohen, J.D. & Muday, G.K. (2010) Genetic dissection of the role of ethylene in regulating auxin-dependent lateral and adventitious root formation in tomato. The Plant Journal, 61, 3–15. https://doi.org/10.1111/j.1365-313X.2009.04027.x.

Pan, J., Sharif, R., Xu, X. & Chen, X. (2021) Mechanisms of Waterlogging Tolerance in Plants: Research Progress and Prospects. *Frontiers in Plant Science*, 11. https://doi.org/10.3389/fpls.2020.627331.

Pandey, D., Rajendran, S.R.C.K., Gaur, M., Sajeesh, P.K. & Kumar, A. (2016) Plant Defense Signaling and Responses Against Necrotrophic Fungal Pathogens. *Journal of Plant Growth Regulation*, 35, 1159–1174. https://doi.org/10.1007/s00344-016-9600-7.

Pfaffl, M.W. (2001) A new mathematical model for relative quantification in real-time RT–PCR. *Nucleic Acids Research*, 29, e45. https://doi.org/10.1093/nar/29.9.e45.

Pilkington, S.M., Crowhurst, R., Hilario, E., Nardozza, S., Fraser, L., Peng, Y., et al. (2018) A manually annotated Actinidia chinensis var. chinensis (kiwifruit) genome highlights the challenges associated with draft genomes and gene prediction in plants. *BMC Genomics*, 19, 257. https://doi.org/10.1186/s12864-018-4656-3.

Polat, Z., Awan, Q. N., Hussain, M., & Akgül, D. S. (2017) First Report of Phytopythium vexans Causing Root and Collar Rot of Kiwifruit in Turkey. Plant Disease, 101:1058. https://doi.org/10.1094/PDIS-11-16-1554-PDN.

Prencipe, S., Savian, F., Nari, L., Ermacora, P., Spadaro, D., & Martini, M. (2020). First report of Phytopythium vexans causing decline syndrome of Actinidia deliciosa 'Hayward' in Italy. Plant Disease, 104:2032. https://doi.org/10.1094/PDIS-10-19-2101-PDN.

Prencipe, S., Schiavon, G., Rosati, M., Nari, L., Schena, L. & Spadaro, D. (2023) Characterization of Phytopythium Species Involved in the Establishment and Development of Kiwifruit Vine Decline Syndrome. *Microorganisms*, 11, 216. https://doi.org/10.3390/microorganisms11010216.

Potuschak, T., Lechner, E., Parmentier, Y., Yanagisawa, S., Grava, S., Koncz, C., et al. (2003) EIN3-Dependent Regulation of Plant Ethylene Hormone Signaling by Two Arabidopsis F Box Proteins. Cell, 115, 679–689. https://doi.org/10.1016/S0092-8674(03)00968-1.

R Core Team (2024). R: A language and environment for statistical computing. R Foundation for Statistical Computing, Vienna, Austria.

Radonić, A., Thulke, S., Mackay, I.M., Landt, O., Siegert, W. & Nitsche, A. (2004) Guideline to reference gene selection for quantitative real-time PCR. *Biochemical and Biophysical Research Communications*, 313, 856–862. https://doi.org/10.1016/j.bbrc.2003.11.177.

Rai, G.K., Khanday, D.M., Choudhary, S.M., Kumar, P., Kumari, S., Martínez-Andújar, C., et al. (2024) Unlocking nature's stress buster: Abscisic acid's crucial role in defending plants against abiotic stress. Plant Stress, 11, 100359. https://doi.org/10.1016/j.stress.2024.100359.

Redinbaugh, M.G. & Campbell, W.H. (1991) Higher plant responses to environmental nitrate. *Physiologia Plantarum*, 82, 640–650. https://doi.org/10.1111/j.1399-3054.1991.tb02958.x.

Reeksting, B.J., Olivier, N.A. & Berg, N. van den (2016) Transcriptome responses of an ungrafted Phytophthora root rot tolerant avocado (Persea americana) rootstock to flooding and Phytophthora cinnamomi. BMC Plant Biology, 16, 205. https://doi.org/10.1186/s12870-016-0893-2.

Reid, J. b., Tate ,K.G., Brown ,N.S. & Cheah, L. h. and (1991) Effects of flooding and alluvium deposition on kiwifruit (Actinidia deliciosa): 1. Early vine decline. *New Zealand Journal of Crop and Horticultural Science*, 19, 247–257. https://doi.org/10.1080/01140671.1991.10421808.

Reid, J.B., Tate ,K.G. & Brown, N.S. and (1992) Effects of flooding and alluvium deposition on kiwifruit (Actinidia deliciosa): 2. Vine performance the following season. *New Zealand Journal of Crop and Horticultural Science*, 20, 283–288. https://doi.org/10.1080/01140671.1992.10421769.

Ritz, C. & Spiess, A.-N. (2008) qpcR: an R package for sigmoidal model selection in quantitative real-time polymerase chain reaction analysis. *Bioinformatics*, 24, 1549–1551. https://doi.org/10.1093/bioinformatics/btn227.

Satpal, D., Kaur, J., Bhadariya, V. & Sharma, K. (2021) Actinidia deliciosa (Kiwi fruit): A comprehensive review on the nutritional composition, health benefits, traditional utilization, and commercialization. *Journal of Food Processing and Preservation*, 45, e15588. https://doi.org/10.1111/jfpp.15588.

Savian, F., Ginaldi, F., Musetti, R., Sandrin, N., Tarquini, G., Pagliari, L., et al. (2020) Studies on the aetiology of kiwifruit decline: interaction between soil-borne pathogens and waterlogging. *Plant and Soil*, 456, 113–128. https://doi.org/10.1007/s11104-020-04671-5.

Savian, F., Prencipe, S., Filippini, N., Nari, L., Martini, M., Ermacora, P., et al. (2021) Pathogenicity of Phytopythium chamaehyphon: A New Player in Kiwifruit Vine Decline Syndrome of Actinidia chinensis var. deliciosa 'Hayward' in Italy. *Plant Disease*, 105, 2781–2784. https://doi.org/10.1094/PDIS-01-21-0143-SC.

Savian, F., Marroni, F., Ermacora, P., Firrao, G. & Martini, M. (2022) A Metabarcoding Approach to Investigate Fungal and Oomycete Communities Associated with Kiwifruit Vine Decline Syndrome in Italy. Phytobiomes Journal, 6, 290–304. https://doi.org/10.1094/PBIOMES-03-22-0019-R.

Shabala, S., Shabala, L., Barcelo, J. & Poschenrieder, C. (2014) Membrane transporters mediating root signalling and adaptive responses to oxygen deprivation and soil

flooding. *Plant, Cell & Environment*, 37, 2216–2233. https://doi.org/10.1111/pce.12339.

Sham, A., Moustafa, K., Al-Shamisi, S., Alyan, S., Iratni, R. & AbuQamar, S. (2017) Microarray analysis of Arabidopsis WRKY33 mutants in response to the necrotrophic fungus Botrytis cinerea. *PLOS ONE*, 12, e0172343. https://doi.org/10.1371/journal.pone.0172343.

Shukla, V., Lombardi, L., Iacopino, S., Pencik, A., Novak, O., Perata, P., et al. (2019) Endogenous Hypoxia in Lateral Root Primordia Controls Root Architecture by Antagonizing Auxin Signaling in Arabidopsis. Molecular Plant, 12, 538–551. https://doi.org/10.1016/j.molp.2019.01.007.

Singh, K.B., Foley, R.C. & Oñate-Sánchez, L. (2002) Transcription factors in plant defense and stress responses. *Current Opinion in Plant Biology*, 5, 430–436. https://doi.org/10.1016/S1369-5266(02)00289-3.

Singh, A., Pandey, A., Srivastava, A.K., Tran, L.-S.P. & Pandey, G.K. (2016) Plant protein phosphatases 2C: from genomic diversity to functional multiplicity and importance in stress management. Critical Reviews in Biotechnology, 36, 1023–1035. https://doi.org/10.3109/07388551.2015.1083941.

Tacconi, G., Paltrinieri, S., Mejia, J.F., Fuentealba, S.P., Bertaccini, A., Tosi, L., et al. (2015) Vine decline in kiwifruit: climate change and effect on waterlogging and Phytophthora in North Italy. *Acta Horticulturae*, 93–97. https://doi.org/10.17660/ActaHortic.2015.1096.7.

Tang, H., Bi, H., Liu, B., Lou, S., Song, Y., Tong, S., et al. (2020) WRKY33 interacts with WRKY12 protein to up-regulate RAP2.2 during submergence induced hypoxia response in Arabidopsis thaliana. New Phytologist, 229, 106–125. https://doi.org/10.1111/nph.17020.

Tang, H. & Liu, H. (2021) Roles of single gene in plant hypoxia and pathogen responses. Plant Signaling & Behavior, 16, 1934295. https://doi.org/10.1080/15592324.2021.1934295.

Tiryaki, I. & Staswick, P.E. (2002) An Arabidopsis Mutant Defective in Jasmonate Response Is Allelic to the Auxin-Signaling Mutant axr1. Plant Physiology, 130, 887–894. https://doi.org/10.1104/pp.005272.

Ton, J., Flors, V. & Mauch-Mani, B. (2009) The multifaceted role of ABA in disease resistance. Trends in Plant Science, 14, 310–317. https://doi.org/10.1016/j.tplants.2009.03.006.

Ton, J. & Mauch-Mani, B. (2004) β-amino-butyric acid-induced resistance against necrotrophic pathogens is based on ABA-dependent priming for callose. The Plant Journal, 38, 119–130. https://doi.org/10.1111/j.1365-313X.2004.02028.x.

Truman, W.M., Bennett, M.H., Turnbull, C.G.N. & Grant, M.R. (2010) Arabidopsis Auxin Mutants Are Compromised in Systemic Acquired Resistance and Exhibit Aberrant Accumulation of Various Indolic Compounds. Plant Physiology, 152, 1562–1573. https://doi.org/10.1104/pp.109.152173.

Turner, J.G., Ellis, C. & Devoto, A. (2002) The Jasmonate Signal Pathway. The Plant Cell, 14, s153–s164. https://doi.org/10.1105/tpc.000679.

Vandesompele, J., De Preter, K., Pattyn, F., Poppe, B., Van Roy, N., De Paepe, A., et al. (2002) Accurate normalization of real-time quantitative RT-PCR data by geometric averaging of multiple internal control genes. Genome Biology, 3, research0034.1. https://doi.org/10.1186/gb-2002-3-7-research0034.

Verma, V., Ravindran, P. & Kumar, P.P. (2016) Plant hormone-mediated regulation of stress responses. BMC Plant Biology, 16, 86. https://doi.org/10.1186/s12870-016-0771-y.

Voesenek, L. a. C.J., Colmer, T.D., Pierik, R., Millenaar, F.F. & Peeters, A.J.M. (2006) How plants cope with complete submergence. *New Phytologist*, 170, 213–226. https://doi.org/10.1111/j.1469-8137.2006.01692.x.

Waite, J.M., Kelly, E.A., Zhang, H., Hargarten, H.L., Waliullah, S., Altman, N.S., et al. (2023) Transcriptomic approach to uncover dynamic events in the development of mid-season sunburn in apple fruit. *G3 Genes|Genomes|Genetics*, 13, jkad120. https://doi.org/10.1093/g3journal/jkad120.

Wang, D., Pajerowska-Mukhtar, K., Culler, A.H. & Dong, X. (2007) Salicylic Acid Inhibits Pathogen Growth in Plants through Repression of the Auxin Signaling Pathway. Current Biology, 17, 1784–1790. https://doi.org/10.1016/j.cub.2007.09.025.

Wang, Y., Schuck, S., Wu, J., Yang, P., Döring, A.-C., Zeier, J., et al. (2018) A MPK3/6-WRKY33-ALD1-Pipecolic Acid Regulatory Loop Contributes to Systemic Acquired Resistance. *The Plant Cell*, 30, 2480–2494. https://doi.org/10.1105/tpc.18.00547.

Wang, Y., Li, X., Fan, B., Zhu, C. & Chen, Z. (2021) Regulation and Function of Defense-Related Callose Deposition in Plants. *International Journal of Molecular Sciences*, 22, 2393. https://doi.org/10.3390/ijms22052393.

Wickham H (2016). ggplot2: Elegant Graphics for Data Analysis. Springer-Verlag New York. ISBN 978-3-319-24277-4, https://ggplot2.tidyverse.org.

Wu, H., Ma, T., Kang, M., Ai, F., Zhang, J., Dong, G., et al. (2019) A high-quality Actinidia chinensis (kiwifruit) genome. *Horticulture Research*, 6, 117. https://doi.org/10.1038/s41438-019-0202-y.

Xia, H., Deng, H., Li, M., Xie, Y., Lin, L., Zhang, H., et al. (2023) Chromosome-scale genome assembly of a natural diploid kiwifruit (Actinidia chinensis var. deliciosa). *Scientific Data*, 10, 92. https://doi.org/10.1038/s41597-023-02006-4.

Xing, M., Huang, K., Zhang, C., Xi, D., Luo, H., Pei, J., et al. (2023) Transcriptome Analysis Reveals the Molecular Mechanism and Responsive Genes of Waterlogging Stress in Actinidia deliciosa Planch Kiwifruit Plants. International Journal of Molecular Sciences, 24, 15887. https://doi.org/10.3390/ijms242115887.

Yang, L., Sun, Q., Geng, B., Shi, J., Zhu, H., Sun, Y., et al. (2023a) Jasmonate biosynthesis enzyme allene oxide cyclase 2 mediates cold tolerance and pathogen resistance. Plant Physiology, 193, 1621–1634. https://doi.org/10.1093/plphys/kiad362.

Yang, L., Sun, Q., Geng, B., Shi, J., Zhu, H., Sun, Y., et al. (2023b) Jasmonate biosynthesis enzyme allene oxide cyclase 2 mediates cold tolerance and pathogen resistance. Plant Physiology, 193, 1621–1634. https://doi.org/10.1093/plphys/kiad362.

Zandalinas, S.I. & Mittler, R. (2022) Plant responses to multifactorial stress combination. *New Phytologist*, 234, 1161–1167. https://doi.org/10.1111/nph.18087.

Zandalinas, S.I., Peláez-Vico, M.Á., Sinha, R., Pascual, L.S. & Mittler, R. (2023) The impact of multifactorial stress combination on plants, crops, and ecosystems: how should we prepare for what comes next? The Plant Journal, 117, 1800–1814. https://doi.org/10.1111/tpj.16557.

Zhang, J.-Y., Huang, S.-N., Mo, Z.-H., Xuan, J.-P., Jia, X.-D., Wang, G., et al. (2015) De novo transcriptome sequencing and comparative analysis of differentially expressed genes in kiwifruit under waterlogging stress. *Molecular Breeding*, 35, 208. https://doi.org/10.1007/s11032-015-0408-0.

Zhang, J.-Y., Huang, S.-N., Chen, Y.-H., Wang, G. & Guo, Z.-R. (2017) Identification and characterization of two waterlogging responsive alcohol dehydrogenase genes (AdADH1 and AdADH2) in Actinidia deliciosa. Molecular Breeding, 37, 52. https://doi.org/10.1007/s11032-017-0653-5.

Zhang, J., Liu, B., Song, Y., Chen, Y., Fu, J., Liu, J., et al. (2021) Genome-wide (ChIP-seq) identification of target genes regulated by WRKY33 during submergence stress in Arabidopsis. BMC Genomic Data, 22, 16. https://doi.org/10.1186/s12863-021-00972-5.

Zhu, Y., Shao, J., Zhou, Z. & Davis, R.E. (2019) Genotype-specific suppression of multiple defense pathways in apple root during infection by Pythium ultimum. Horticulture Research, 6, 10. https://doi.org/10.1038/s41438-018-0087-1.

Tables

Table 1. Number of significant DEGs ($p<0.05$) in kiwifruit roots under inoculation, flooding and combined (multifactorial) stress at each time point compared to the control "no stress" condition. Flooded and Multifactorial treatments were not sequenced at T 48.

Inoculated	48 h	96 h	144 h	14 d
UP	19	43	5	20
DOWN	15	461	13	46
Flooded	48 h	96 h	144 h	14 d
UP	-	6844	26	57
DOWN		10397	45	340
Multifactorial	48 h	96 h	144 h	14 d
UP	-	7961	253	167
DOWN		10813	532	285

Table 2. List of top 10 significantly up- or down- regulated genes identified under different stress conditions (biotic stress, abiotic stress, and multifactorial stress) after 96 hours (T96) with results of Gene Ontology (GO) and Kyoto Encyclopedia of Genes and Genomes (KEGG) pathway functional enrichment analysis. The table includes the gene ID, Log2 Fold-Change (Log2FC), and p-values for differential expression analysis (DE.pval). The associated GO terms and KEGG pathway annotations are also presented, along with their respective p-values. The GO terms describe biological processes linked to the genes, while the KEGG pathways provide additional insight into their functional roles.

	Gene.ID	Log2FC	DE.pval	GO.Term.ID	GO.Term.Description	GO.Term.enrichment.pval	KEGG.Term.ID	KEGG.Term.Description	KEGG.Term.enrichment.pval
	Biotic Stress, 96hrs								
Down Regulated Genes	Acde29g00858.1	-6.7	0.03	GO:0006355	regulation of transcription, DNA-templated	0.03	NA	NA	NA
	Acde001100s00016.1	-4.9	1.49E-05	GO:0042773	mitochondrial ATP synthesis	0.006	NA	NA	NA
	Acde25g00613.1	-4.4	0.004	GO:0006355	regulation of transcription, DNA-templated	0.03	NA	NA	NA
	Acde12g01064.1	-4.0	0.02	GO:0006355	regulation of transcription, DNA-templated	0.03	NA	NA	NA
	Acde15g00062.1	-4.0	0.002	GO:0006457	protein folding	0.05	K04079	HSP90A, htpG; molecular chaperone HtpG	0.02
	Acde09g00889.1	-3.5	0.05	GO:0006355	regulation of transcription, DNA-templated	0.03	NA	NA	NA
	Acde06g01046.1	-3.5	0.02	GO:0008283	cell proliferation	0.006	NA	NA	NA
	Acde23g00039.1	-3.4	0.001	GO:0009733	response to auxin stimulus	0.008	NA	NA	NA
	Acde13g01591.1	-3.0	0.05	GO:0006355	regulation of transcription, DNA-templated	0.03	NA	NA	NA
	Acde19g01072.1	-3.0	0.004	GO:0006355	regulation of transcription, DNA-templated	0.03	NA	NA	NA
	Abiotic Stress, 96hrs								
Up Regulated Genes	Acde24g00960.1	18.4	1.63E-05	GO:0009058	biosynthetic process	0.0008	NA	NA	NA
	Acde24g00926.1	8.5	0.008	GO:0009058	biosynthetic process	0.0008	NA	NA	NA
	Acde19g00475.1	8.0	0.0003	GO:0009058	biosynthetic process	0.0008	NA	NA	NA
	Acde02g00864.1	5.5	0.0006	GO:0015031	protein transport	0.04	NA	NA	NA
	Acde28g00379.1	5.5	1.89E-05	GO:0015031	protein transport	0.04	NA	NA	NA
	Acde07g00013.1	4.7	3.32E-05	GO:0009058	biosynthetic process	0.0008	NA	NA	NA
	Acde10g01179.1	4.2	1.13E-18	GO:0006096; GO:0019752	glycolytic process; carboxylic acid metabolic process	0.002; 0.04	NA	NA	NA

	Acde18g00476.1	3.9	5.95E-08	GO:0009058	biosynthetic process	0.0008	NA	NA	NA
	Acde21g00949.1	3.8	0.03	GO:0009058	biosynthetic process	0.0008	NA	NA	NA
	Acde15g01156.1	3.7	5.54E-10	GO:0009058	biosynthetic process	0.0008	NA	NA	NA
Down Regulated Genes	Acde000000s00035.1	-23.5	2.77E-13	GO:0006412; GO:0006807; GO:0071704	translation; obsolete nitrogen compound metabolic process; obsolete organic substance metabolic process	< 1e-30; 0.002; 0.004	NA	NA	NA
	Acde28g00092.1	-11	1.82E-10	GO:0071704	obsolete organic substance metabolic process	0.004	NA	NA	NA
	Acde12g00105.1	-10.3	1.32E-13	GO:0006807; GO:0071704	obsolete nitrogen compound metabolic process; obsolete organic substance metabolic process	0.002; 0.004	NA	NA	NA
	Acde09g00923.1	-8.9	2.50E-17	GO:0006807; GO:0071704	obsolete nitrogen compound metabolic process; obsolete organic substance metabolic process	0.002; 0.004	NA	NA	NA
	Acde18g00394.1	-8.9	3.52E-10	GO:0006807; GO:0071704	obsolete nitrogen compound metabolic process; obsolete organic substance metabolic process	0.002; 0.004	NA	NA	NA
	Acde03g01667.1	-8.7	4.30E-08	GO:0006807; GO:0071704	obsolete nitrogen compound metabolic process; obsolete organic substance metabolic process	0.002; 0.004	K16297	SCPL-II; serine carboxypeptidase-like clade II	0.05
	Acde08g00322.1	-8.7	1.40E-08	GO:0006807; GO:0071704	obsolete nitrogen compound metabolic process; obsolete organic substance metabolic process	0.002; 0.004	NA	NA	NA
	Acde22g00339.1	-8.7	7.75E-08	GO:0006807; GO:0071704	obsolete nitrogen compound metabolic process; obsolete organic substance metabolic process	0.002; 0.004	NA	NA	NA
	Acde26g00444.1	-8.7	1.66E-08	GO:0006633; GO:0071704	fatty acid biosynthetic process; obsolete organic substance metabolic process	0.02; 0.004	NA	NA	NA
	Acde10g01004.1	-8.7	5.64E-08	GO:0006807; GO:0071704	obsolete nitrogen compound metabolic process; obsolete organic substance metabolic process	0.002; 0.004	NA	NA	NA
	Multifactorial Stress, 96hrs								

Up Regulated Genes	Acde24g00960.1	19	6.53E-06	GO:0006351; GO:0009058	DNA-templated transcription; biosynthetic process	0.009; 0.0001	NA	NA	NA
	Acde24g00926.1	8.4	0.008	GO:0006351; GO:0009058	DNA-templated transcription; biosynthetic process	0.009; 0.0001	NA	NA	NA
	Acde19g00475.1	8	0.0003	GO:0006351; GO:0009058	DNA-templated transcription; biosynthetic process	0.009; 0.0001	NA	NA	NA
	Acde10g01033.1	7.7	4.26E-05	GO:0006508	proteolysis	0.02	NA	NA	NA
	Acde03g01777.1	6.8	0.001	GO:0006396; GO:0009058	RNA processing; biosynthetic process	0.0003; 0.0001	NA	NA	NA
	Acde28g00379.1	4.6	0.0003	GO:0006606; GO:0006913; GO:0015031	protein import into nucleus; nucleocytoplasmic transport; protein transport	0.02; 0.02; 0.003	NA	NA	NA
	Acde10g01179.1	4.3	1.52E-19	GO:0006096; GO:0019752	glycolytic process; carboxylic acid metabolic process	0.003; 0.01	NA	NA	NA
	Acde13g00767.1	4.3	0.02	GO:0006508	proteolysis	0.02	NA	NA	NA
	Acde25g00656.1	4.2	0.02	GO:0000160; GO:0007165	phosphorelay signal transduction system; signal transduction	0.05; 0.02	NA	NA	NA
	Acde10g01112.1	4	4.56E-37	GO:0009415	response to water	0.004	NA	NA	NA
Down Regulated Genes	Acde000000s00035.1	-22.9	1.08E-12	GO:0006412; GO:0006807; GO:0071704	translation; obsolete nitrogen compound metabolic process; obsolete organic substance metabolic process	< 1e-30; 0.002; 0.004	NA	NA	NA
	Acde09g00923.1	-11.5	1.97E-15	GO:0006355; GO:0006807; GO:0071704	regulation of DNA-templated transcription; obsolete nitrogen compound metabolic process; obsolete organic substance metabolic process	0.02; 0.002; 0.004	NA	NA	NA
	Acde28g00092.1	-10.7	5.76E-10	GO:0071704	obsolete organic substance metabolic process	0.004	NA	NA	NA
	Acde03g01708.1	-10.5	8.14E-12	GO:0006355; GO:0006807; GO:0071704	regulation of DNA-templated transcription; obsolete nitrogen compound metabolic process; obsolete organic substance metabolic process	0.02; 0.002; 0.004	NA	NA	NA

	Acde14g00259.1	-10.2	2.86E-10	GO:0006355; GO:0006807; GO:0071704	regulation of DNA-templated transcription; obsolete nitrogen compound metabolic process; obsolete organic substance metabolic process	0.02; 0.002; 0.004	NA	NA	NA
	Acde01g00258.1	-10	6.75E-13	GO:0006979	response to oxidative stress	0.03	NA	NA	NA
	Acde02g00270.1	-9.7	4.78E-10	GO:0006807; GO:0071704	obsolete nitrogen compound metabolic process; obsolete organic substance metabolic process	0.002; 0.004	K16297	SCPL-II; serine carboxypeptidase-like clade II	0.05
	Acde03g01652.1	-9.5	5.76E-09	GO:0010215	cellulose microfibril organization	0.04	NA	NA	NA
	Acde08g00277.1	-9.1	1.59E-08	GO:0006355; GO:0006807; GO:0071704	regulation of DNA-templated transcription; obsolete nitrogen compound metabolic process; obsolete organic substance metabolic process	0.02; 0.002; 0.004	NA	NA	NA
	Acde08g00551.1	-9	1.32E-09	GO:0006807; GO:0071704	obsolete nitrogen compound metabolic process; obsolete organic substance metabolic process	0.002; 0.004	K16297	SCPL-II; serine carboxypeptidase-like clade II	0.05

Table 3. Select KEGG terms and associated genes across treatments at T96: Inoculated with *Phytopythium vexans* (I), Flooded for 48 h (F), and Multifactorial (IF). The table includes: KEGG Term and Associated (overrepresented) DEGs, Regulation (up or down), a description of the KEGG term, and the p-value associated with each pathway (only those with $p<0.05$ are included).

Treatment	Kegg Term	Associated Genes	Regulation	Description	p_value
IF	K13424	*Acde02g00753.1,Acde03g00505.1,Acde13g00920.1,Acde15g00258.1,Acde23g01468.1,Acde28g00500.1*	up	WRKY33; WRKY transcription factor 33	0.0454
IF	K14514	*Acde13g01378.1,Acde13g01419.1,Acde13g01420.1,Acde23g00978.1,Acde23g00979.1,Acde23g01024.1,Acde28g01182.1*	up	EIN3; ethylene-insensitive protein 3	0.0454
IF	K18857	*Acde07g00384.1,Acde10g00781.1,Acde11g00699.1,Acde11g0070*	up	ADH1; alcohol dehydrogenase class-P [EC:1.1.1.1]	0.0454
IF	K11968	*Acde01g01121.1, Acde02g00504.1, Acde06g01193.1, Acde08g01009.1, Acde19g01401.1, Acde21g00280.1,*	up	ARIH1; ariadne-1 [EC:2.3.2.31]	0.0454
IF	K17506	*Acde02g01006.1, Acde03g00284.1, Acde04g00519.1, Acde04g00655.1, Acde13g01314.1, Acde14g00198.1, Acde15g00221.1, Acde17g00058.1, Acde20g00032.1,*	up	PPM1L, PP2CE; protein phosphatase 1L [EC:3.1.3.16]	0.0454
IF	K11855	*Acde04g00470.1, Acde10g00908.1, Acde12g00794.1, Acde13g00651.1, Acde16g00269.1, Acde20g00021.1,*	up	USP36_42; ubiquitin carboxyl-terminal hydrolase 36/42 [EC:3.4.19.12]	0.0454
IF	K10999	*Acde04g00604.1,Acde07g00339.1,Acde07g00731.1,Acde08g00525.1,Acde10g00811.1,Acde11g00436.1,Acde13g00670.1,Acde13g00754.1,Acde14g00108.1,Acde14g01026.1,Acde16g00248.1,Acde18g01131.1,Acde21g00642.1,Acde22g00296.1,Acde23g01626.1*	down	CESA; cellulose synthase A [EC:2.4.1.12]	0.0460
IF	K13947	*Acde04g00643.1,Acde05g00476.1,Acde12g00382.1,Acde16g00115.1,Acde18g00496.1,Acde21g00681.1,Acde25g00909.1,Acde26g0*	down	PIN; auxin efflux carrier family protein	0.0460
IF	K13946	*Acde02g00827.1,Acde02g00984.1,Acde03g00299.1,Acde03g00442.1,Acde06g01319.1,Acde08g01372.1,Acde10g00701.1,Acde15g0*	down	AUX1, LAX; auxin influx carrier (AUX1 LAX family)	0.0460
IF	K10775	*Acde03g01392.1,Acde08g01482.1,Acde18g01382.1,Acde18g01383.1,Acde18g01384.1,Acde24g00696.1,Acde26g00949.1,Acde28g0*	down	PAL; phenylalanine ammonia-lyase [EC:4.3.1.24]	0.0494
IF	K05909	*Acde02g00468.1, Acde02g00835.1, Acde02g01030.1, Acde03g00263.1, Acde03g00415.1, Acde03g00437.1, Acde03g01158.1, Acde04g00569.1, Acde08g01378.1, Acde08g01628.1, Acde09g00549.1, Acde10g00840.1, Acde13g00921.1, Acde13g00962.1, Acde15g00251.1, Acde21g00609.1, Acde22g00644.1, Acde22g00645.1, Acde22g00787.1, Acde23g01466.1, Acde24g00486.1, Acde28g00371.1, Acde29g00792.1*	down	E1.10.3.2; laccase [EC:1.10.3.2]	0.0375
IF	K03327	*Acde01g00560.1, Acde02g00727.1, Acde03g00153.1, Acde03g00535.1, Acde03g02002.1, Acde04g00839.1, Acde05g00286.1, Acde05g00901.1, Acde06g00165.1, Acde07g00167.1, Acde09g00394.1, Acde12g00132.1, Acde12g00422.1, Acde12g00423.1, Acde12g00934.1, Acde13g00294.1, Acde13g00295.1, Acde17g00304.1, Acde18g00242.1, Acde18g00965.1, Acde19g00562.1, Acde19g00960.1, Acde23g00359.1, Acde23g00716.1, Acde23g00951.1, Acde24g00231.1, Acde25g00395.1, Acde25g00867.1, Acde25g00868.1, Acde25g00869.1, Acde25g00870.1, Acde26g00469.1, Acde27g00412.1, Acde27g00415.1*	down	SLC47A, MATE, DTX; MATE family, multidrug and toxin extrusion protein	0.0417
IF	K05681	*Acde03g00874.1, Acde03g01466.1, Acde05g00252.1, Acde05g00808.1, Acde06g00975.1, Acde07g00411.1, Acde07g00474.1, Acde07g01046.1, Acde08g01447.1, Acde12g00483.1, Acde15g00669.1, Acde16g00040.1, Acde18g00645.1, Acde19g00678.1, Acde20g00287.1, Acde21g00802.1, Acde22g00263.1, Acde23g00593.1, Acde24g00623.1, Acde24g00624.1, Acde25g00584.1, Acde25g00753.1, Acde26g00263.1, Acde27g00307.1, Acde28g01133.1*	down	ABCG2, CD338; ATP-binding cassette, subfamily G (WHITE), member 2	0.0417
IF	K07375	*Acde000250s00003.1, Acde02g00393.1, Acde02g00860.1, Acde03g00420.1, Acde03g00928.1, Acde03g01507.1, Acde10g01142.1, Acde15g00149.1, Acde18g00314.1, Acde19g00577.1, Acde21g00135.1, Acde24g00191.1, Acde25g00439.1, Acde28g00408.1*	down	TUBB; tubulin beta	0.0460

I	K14432	*Acde04g00315.1*	up	ABF; ABA responsive element binding factor	0.0242
I	K09286	*Acde06g00011.1,Acde07g00013.1*	up	EREBP; EREBP-like factor	0.0167
I	K00660	*Acde22g00598.1*	up	CHS; chalcone synthase [EC:2.3.1.74]	0.0214
I	K00276	*Acde20g00476.1*	up	AOC3, AOC2, tynA; primary-amine oxidase	0.0224
I	K14497	*Acde02g00950.1*	up	PP2C; protein phosphatase 2C [EC:3.1.3.16]	0.0224
I	K11816	*Acde23g01606.1*	up	YUCCA; indole-3-pyruvate monooxygenase	0.0224
I	K09872	*Acde15g00699.1*	up	PIP; aquaporin PIP	0.0224
I	K26552	*Acde29g00584.1*	up	NPF2, GTR, NRT1; MFS transporter, POT/PTR family, nitrate/chloride/glucosinolate transporter	0.0214
I	K00799	*Acde05g01058.1,Acde17g00396.1,Acde17g00425.1,Acde17g00426.1,Acde17g00427.1,Acde29g00668.1*	down	GST, gst; glutathione S-transferase [EC:2.5.1.18]	0.0004
I	K11971	*Acde24g00075.1*	down	RNF14, ARA54; E3 ubiquitin-protein ligase RNF14	0.0468
I	K05579	*Acde000680s00018.1*	down	ndhH; NAD(P)H-quinone oxidoreductase subunit H	0.0468
I	K15685	*Acde02g00851.1*	down	CBLL1; E3 ubiquitin-protein ligase Hakai [EC:2.3.2.27]	0.0468
I	K16274	*Acde20g00356.1*	down	AIP2; E3 ubiquitin-protein ligase AIP2 [EC:2.3.2.27]	0.0468
I	K01733	*Acde16g01105.1*	down	thrC; threonine synthase [EC:4.2.3.1]	0.0468
I	K02293	*Acde06g01347.1*	down	PDS, crtP; 15-cis-phytoene desaturase [EC:1.3.5.5]	0.0468
I	K05933	*Acde10g00751.1,Acde17g00537.1*	down	E1.14.17.4; aminocyclopropanecarboxylate oxidase [EC:1.14.17.4]	0.0432
I	K13993	*Acde01g00120.1,Acde03g00775.1,Acde10g00573.1,Acde10g00574.1,Acde13g00331.1,Acde13g00973.1,Acde13g01015.1,Acde14g00540.1,Acde15g00377.1,Acde16g00928.1,Acde16g01147.1,Acde18g00194.1,Acde19g01025.1,Acde22g00872.1,Acde23g01373.1,Acde23g01418.1,Acde24g00500.1,Acde24g00501.1,Acde24g00502.1,Acde28g00181.1,Acde28g00399.1,Acde28g00401.1*	down	HSP20; HSP20 family protein	1.402E-27
F	K18857	*Acde07g00384.1,Acde10g00781.1,Acde11g00700.1,Acde11g0070*	up	ADH1; alcohol dehydrogenase class-P [EC:1.1.1.1]	0.0381
F	K13424	*Acde02g00753.1,Acde03g00505.1,Acde13g00920.1,Acde15g00258.1,Acde23g01468.1,Acde28g00500.1*	up	WRKY33; WRKY transcription factor 33	0.0335
F	K14515	*Acde01g00734.1,Acde09g01004.1,Acde13g00555.1,Acde14g00120.1,Acde20g00108.1,Acde29g01128.1*	up	EBF1_2; EIN3-binding F-box protein	0.0335
F	K14514	*Acde13g01419.1,Acde13g01420.1,Acde23g00978.1,Acde23g00979.1,Acde23g01024.1,Acde28g01182.1*	up	EIN3; ethylene-insensitive protein 3	0.0365
F	K13425	*Acde03g00878.1,Acde07g00927.1,Acde14g00798.1,Acde18g00127.1,Acde25g00463.1*	up	WRKY22; WRKY transcription factor 22	0.0365
F	K11855	*Acde04g00470.1,Acde10g00908.1,Acde11g00843.1,Acde12g00794.1,Acde13g00651.1,Acde16g00269.1,Acde20g00021.1,Acde23g00670.1,Acde25g00268.1*	up	USP36_42; ubiquitin carboxyl-terminal hydrolase 36/42 [EC:3.4.19.12]	0.0335
F	K03265	*Acde04g00556.1,Acde10g00851.1,Acde11g00786.1,Acde21g00595.1,Acde21g00596.1*	up	ETF1, ERF1; peptide chain release factor subunit 1	0.0335
F	K10775	*Acde03g01392.1,Acde08g01482.1,Acde18g01382.1,Acde18g01383.1,Acde18g01384.1,Acde24g00696.1,Acde26g00949.1,Acde28g00895.1*	down	PAL; phenylalanine ammonia-lyase [EC:4.3.1.24]	0.0464
F	K01802	*Acde06g01305.1,Acde07g01265.1,Acde09g00118.1,Acde14g00023.1,Acde15g00198.1,Acde18g01301.1,Acde19g01310.1,Acde22g00105.1,Acde24g00454.1,Acde24g00549.1,Acde25g00297.1,Acde28g00454.1*	down	E5.2.1.8; peptidylprolyl isomerase [EC:5.2.1.8]	0.0464
F	K07375	*Acde000250s00003.1,Acde02g00393.1,Acde02g00860.1,Acde03g00420.1,Acde03g00928.1,Acde03g01507.1,Acde10g01142.1,Acde15g00149.1,Acde18g00314.1,Acde19g00577.1,Acde21g00135.1,Acde24g00191.1,Acde25g00439.1,Acde28g00408.1*	down	TUBB; tubulin beta	0.0464
F	K04392	*Acde05g01144.1,Acde08g00283.1,Acde09g00086.1,Acde09g01061.1,Acde13g01325.1,Acde14g01104.1,Acde15g01040.1,Acde15g01160.1,Acde16g00625.1,Acde20g01067.1,Acde21g01147.1,Acde26g00582.1*	down	RAC1; Ras-related C3 botulinum toxin substrate 1	0.0464
F	K22390	*Acde04g00180.1,Acde06g01265.1,Acde07g00708.1,Acde08g01036.1,Acde08g01206.1,Acde10g00271.1,Acde10g00272.1,Acde13g00592.1,Acde13g00805.1,Acde15g00764.1,Acde19g00804.1,Acde21g00189.1,Acde23g00805.1,Acde27g00219.1,Acde27g00220.1,Acde27g00221.1*	down	ACP7; acid phosphatase type 7	0.0464

Figures

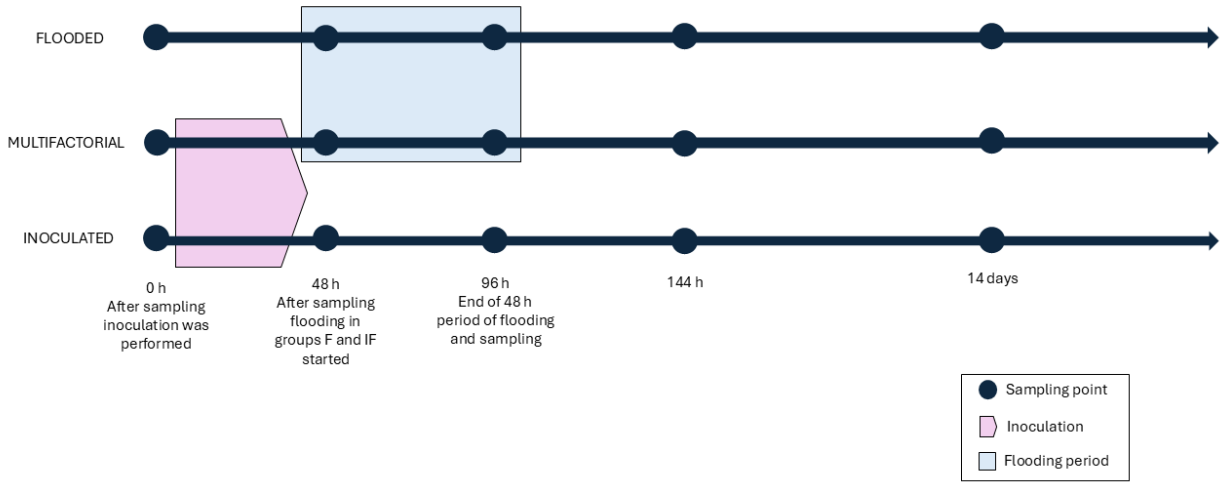


Figure 1. Diagram illustrating the experimental setup involving four treatment groups: Control (not shown), Inoculated, Multifactorial (inoculated and flooded), and Flooded. Sampling timepoints are represented by dark blue circles along the timeline, with key events annotated. The first sampling time point occurred at 0 h, immediately before inoculation (which is represented by the pink polygon). At 48 h, a second sampling was conducted just prior to flooding in the Flooded and Multifactorial groups. The flooding period is represented by a blue box. At 96 h, the flooding period ended, and another sampling was immediately performed. Additional sampling points were at 144 hours and 14 days.

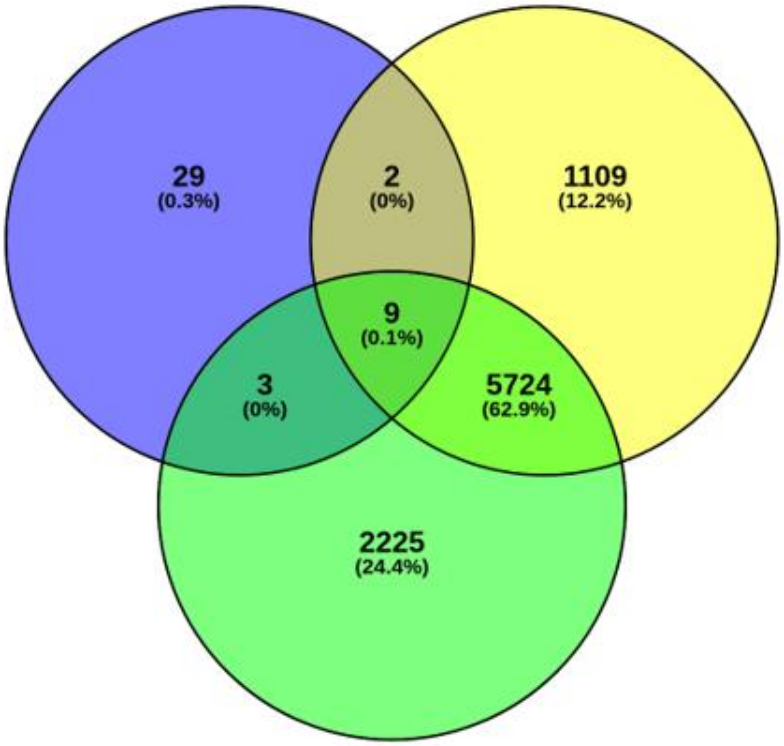


Figure 2. Venn diagram representing the percentage of overlap between significant upregulated (LFC>0) genes in *Actinidia deliciosa* cv. Hayward plants inoculated with *Phytopythium vexans* (Inoculated; blue), flooded for 48 h (Flooded; yellow) and multifactorial (both Inoculated and Flooded; green) at the 96 h timepoint (T96). The diagram was generated through Venny 2.1 (https://bioinfogp.cnb.csic.es/tools/venny/).

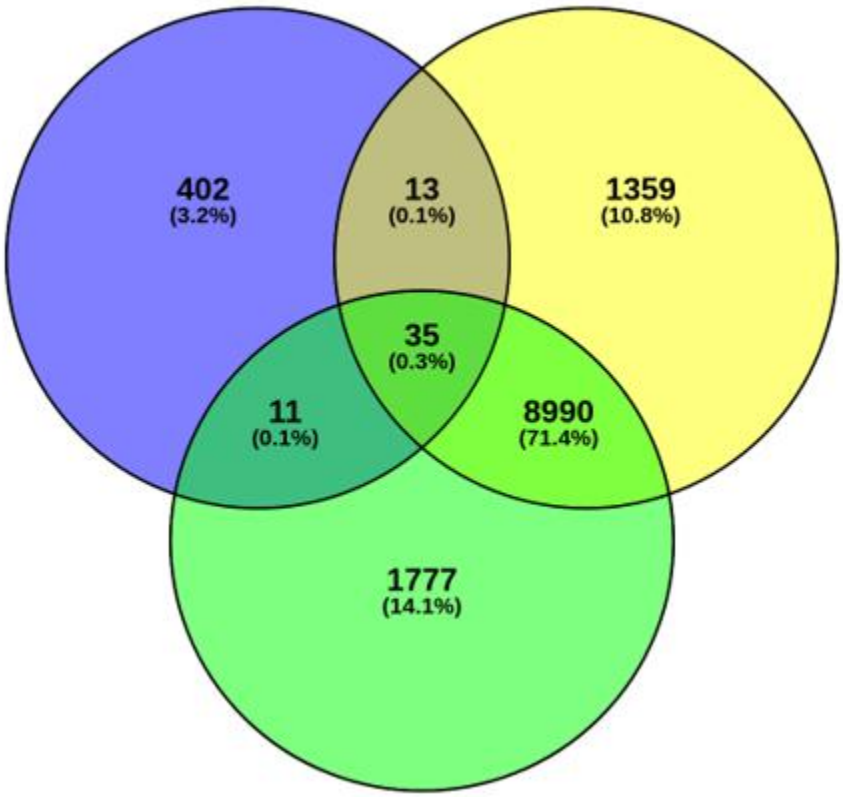


Figure 3. Venn diagram representing the percentage of overlap between significant downregulated genes (LFC < 0) in *Actinidia deliciosa* cv. Hayward plants inoculated with *Phytopythium vexans* (Inoculated; blue), flooded for 48 h (Flooded; yellow) and multifactorial (both inoculated and flooded; green) at the 96 h timepoint (T96). The diagram was generated through Venny 2.1 (https://bioinfogp.cnb.csic.es/tools/venny/).

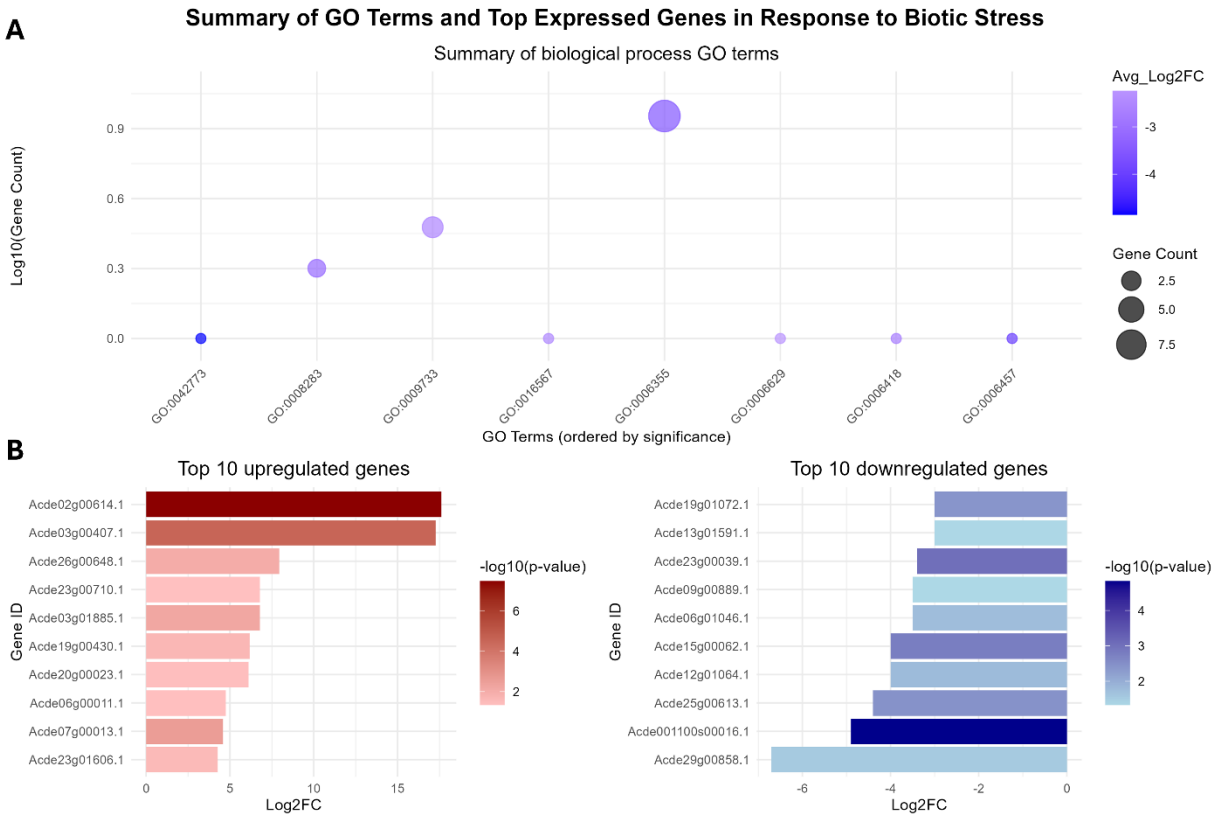


Figure 4. Gene Ontology (GO) enrichment analysis of differentially expressed genes (DEG) in response to biotic stress only (inoculation with *P. vexans*) at T96. (A) Bubble plot representing significantly enriched biological processes (GO terms) for downregulated DEG. GO enrichment analysis could not be performed on upregulated genes due to annotation limitations. The x-axis shows GO terms ordered by statistical significance (most significant on left), while the size of each bubble corresponds to the number of genes associated with the GO term (filtered for Log2FC > 2). The color gradient indicates the average Log2FC of the genes within each GO term, with darker hues representing a greater degree of up- or downregulation. (B) Bar plots of the top 10 up- (left) and downregulated (right) DEG identified. The x-axis represents Log2FC, in which larger values (either positive or negative) indicate greater differential expression between treated vs. no stress control. The color of the bars reflects statistical significance, with darker hues representing more significant associations.

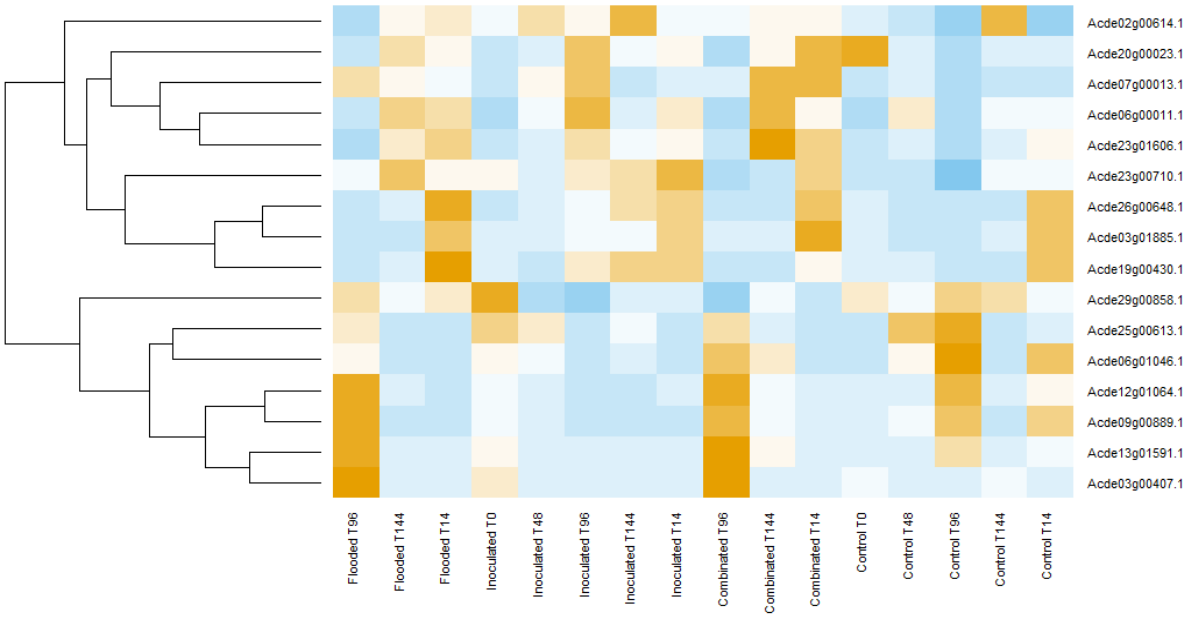


Figure 5. Hierarchical clustering heatmap of the top 10 differentially expressed genes (DEGs) in *Actinidia deliciosa* following inoculation with *Phytopythium vexans* at 96 hours post-treatment (T96). The heatmap was generated using the `pheatmap` package in R, with gene expression values (FPKM) subjected to Z-score normalization. Rows represent individual genes, while columns correspond to experimental conditions (Flooded, Inoculated, Combined, and Control) across multiple time points (T0, T48, T96, T144, and T14). Euclidean distance and average linkage clustering were applied to group genes based on expression patterns. The color scale ranges from blue (low expression) to orange (high expression), with hierarchical clustering displayed for rows. The analysis highlights key transcriptional changes under inoculation stress at T96.

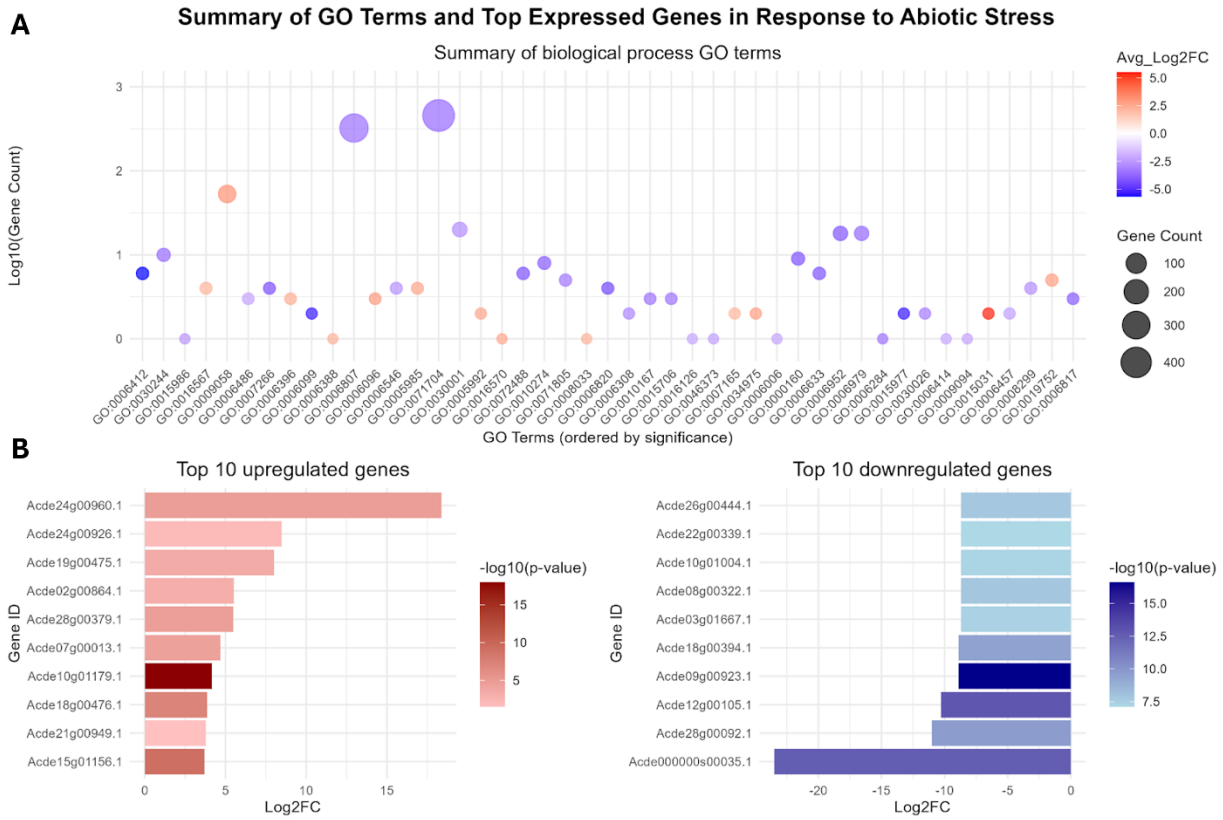


Figure 6 - Gene Ontology (GO) enrichment analysis of differentially expressed genes (DEGs) in response to abiotic stress (root flooding with water) at T96. (A) Bubble plot representing significantly enriched biological processes (GO terms) for up- and downregulated DEG. The x-axis shows GO terms ordered by statistical significance (most significant on left), while the size of each bubble corresponds to the number of genes associated with the GO term (filtered for Log2FC > 2). The color gradient indicates the average Log2FC of the genes within each GO term, with darker hues representing a greater degree of up- or downregulation. (B) Bar plots of the top 10 up- (left) and downregulated (right) DEG identified. The x-axis represents Log2FC, in which larger values (either positive or negative) indicate greater differential expression between treated vs. no stress control. The color of the bars reflects statistical significance, with darker hues representing more significant associations.

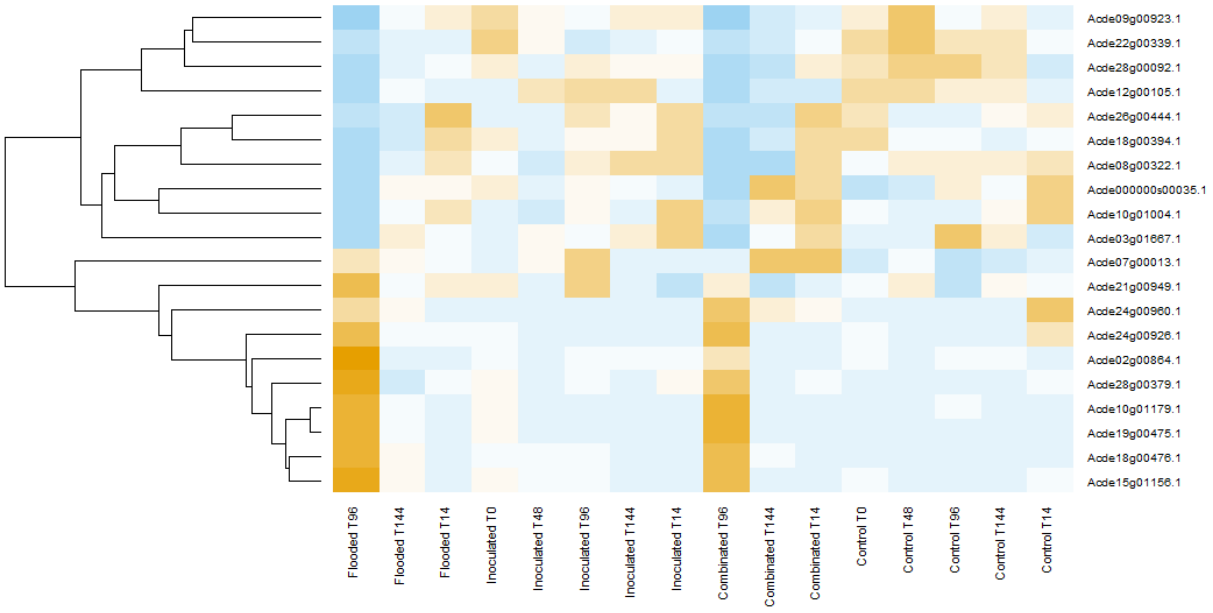


Figure 7. Hierarchical clustering heatmap of the top 10 differentially expressed genes (DEGs) in *Actinidia deliciosa* under flooding at 96 hours post-treatment (T96). The heatmap was generated using the `pheatmap` package in R, with gene expression values (FPKM) subjected to Z-score normalization. Rows represent individual genes, while columns correspond to experimental conditions, including different treatments (Flooded, Inoculated, Combined, and Control) across multiple time points (T0, T48, T96, T144, and T14). Euclidean distance and average linkage clustering were applied to group genes based on expression patterns. The color scale ranges from blue (low expression) to orange (high expression), with hierarchical clustering displayed for rows. The analysis highlights key transcriptional changes under inoculation stress at T96.

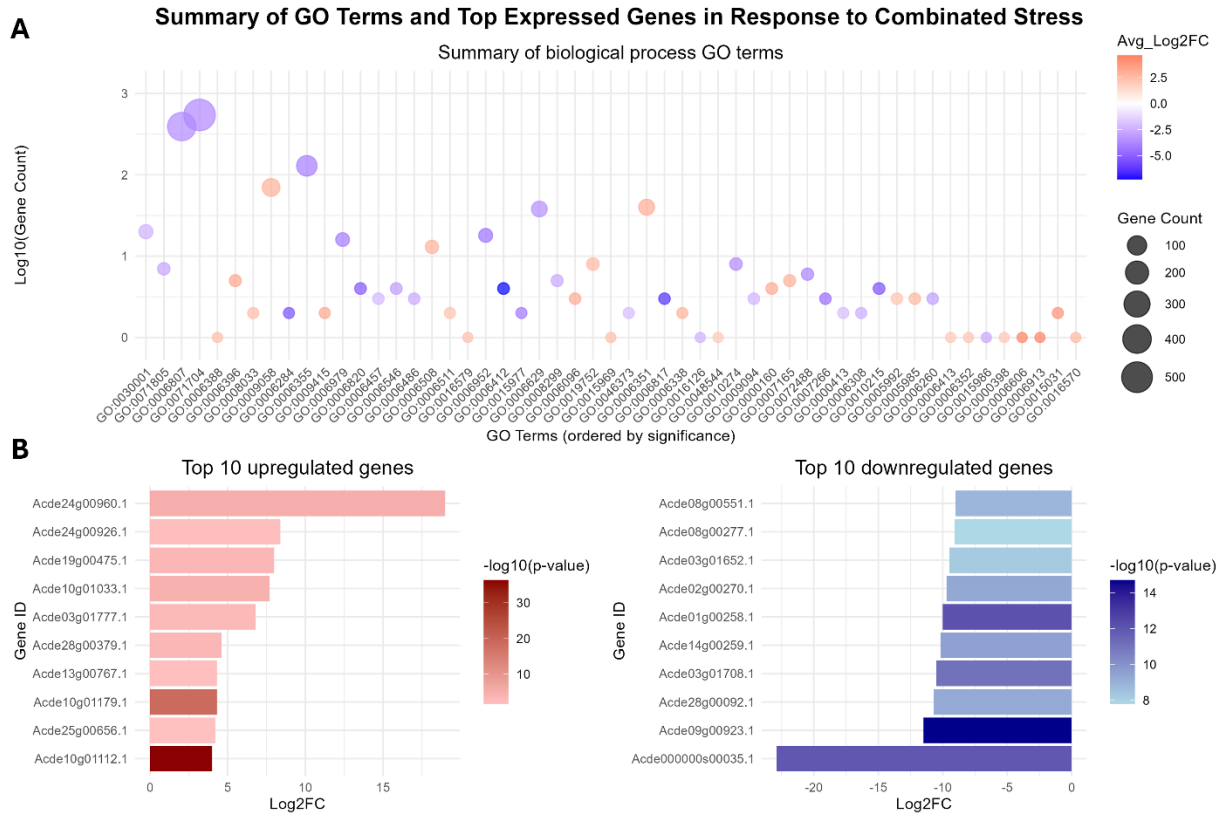


Figure 8. Gene Ontology (GO) enrichment analysis of differentially expressed genes (DEGs) in response to combined stress (inoculation with *P. vexans* followed by root flooding at T96. (A) Bubble plot representing significantly enriched biological processes (GO terms) for up- and downregulated DEG. The x-axis shows GO terms ordered by statistical significance, (most significant on left), while the size of each bubble corresponds to the number of genes associated with the GO term (filtered for Log2FC > 2). The color gradient indicates the average Log2FC of the genes within each GO term, with darker hues representing a greater degree of up- or downregulation. (B) Bar plots of the top 10 up- (left) and downregulated (right) DEG identified. The x-axis represents Log2FC, in which larger values (either positive or negative) indicate greater differential expression between treated vs. no stress control. The color of the bars reflects statistical significance, with darker hues representing more significant associations.

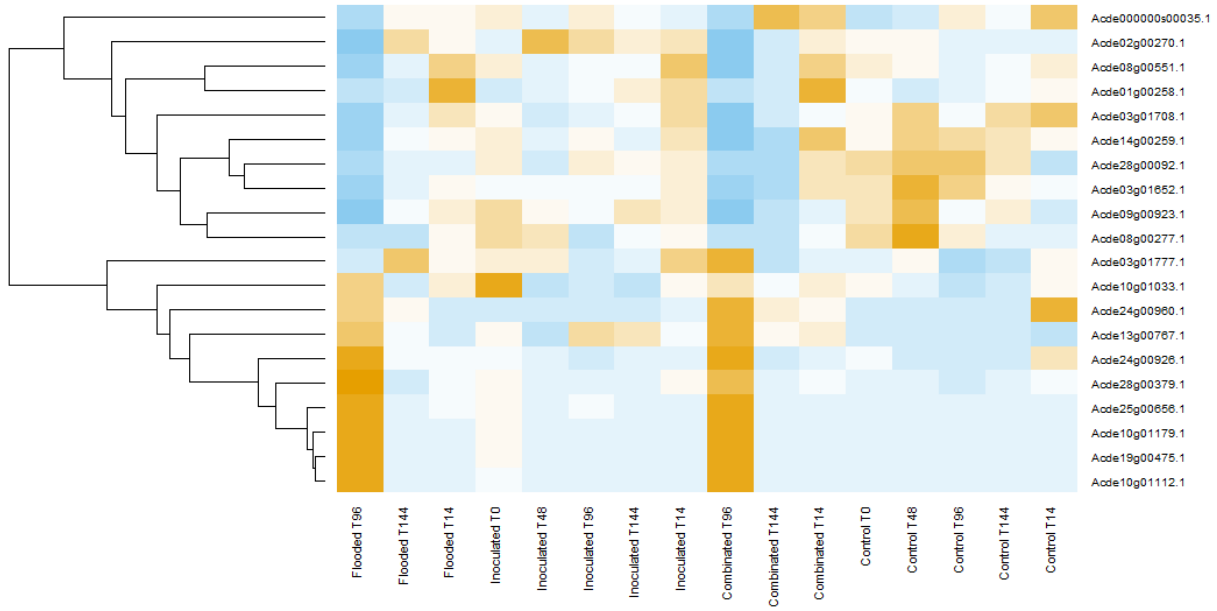


Figure 9. Hierarchical clustering heatmap of the top 10 differentially expressed genes (DEGs) in *Actinidia deliciosa* under combined stress at 96 hours post-treatment (T96). The heatmap was generated using the pheatmap package in R, with gene expression values (FPKM) subjected to Z-score normalization. Rows represent individual genes, while columns correspond to experimental conditions, including different treatments (Flooded, Inoculated, Combined, and Control) across multiple time points (T0, T48, T96, T144, and T14). Euclidean distance and average linkage clustering were applied to group genes based on expression patterns. The color scale ranges from blue (low expression) to orange (high expression), with hierarchical clustering displayed for rows. The analysis highlights key transcriptional changes under inoculation stress at T96.

Supplementary material

Supplementary Table 1 – Details about the evaluated genomes for alignment and their relative BUSCO score (last column).

Full citation	Author	Year	Species and cultivar	Ploidy	Tech	DNA source (Genome)	RNA source (annotation)	Data availability	BUSCO analysis results from dataset eudicots_odb10
Xia, H., Deng, H., Li, M., Xie, Y., Lin, L., Zhang, H., Luo, X., Lv, X., Wang, J. & Liang, D. (2023). Chromosome-scale genome assembly of a natural diploid kiwifruit (Actinidia chinensis var. deliciosa). Scientific Data, 10(1), 92.	Xia et al.	2023	Actinidia chinensis var.deliciosa (from diploid plant)	diploid	ONT + Illumina + HiC	leaves	roots + buds + fruit + leaves + branches	genome sequencing data have been deposited in the NCBI database under the project ID PRJNA85052439 and SRX1746353840	**C:98.7%**[S:66.5%,D:32.2%],F:0.4%,M:0.9%,n:2326; 2296 Complete BUSCOs (C); 1546 Complete and single-copy BUSCOs (S); 750 Complete and duplicated BUSCOs (D); 10 Fragmented BUSCOs (F); 20 Missing BUSCOs (M); 2326 Total BUSCO groups searched
Wu, H., Ma, T., Kang, M., Ai, F., Zhang, J., Dong, G., & Liu, J. (2019). A high-quality Actinidia chinensis (kiwifruit) genome. Horticulture research, 6.	Wu et al.	2019	Actinidia chinensis var chinensis cv HongYang (A. chinensis v3)	diploid	pacbio + HiC	leaves	Rna from based on the RNA-seq data, we downloaded all RNA-seq data from the NCBI database (NCBI SRA accessions: SRR653044, SRR653045, SRR653046.	kiwi genome database	**C:95.4%**[S:75.1%,D:20.3%],F:0.9%,M:3.7%,n:2326; 2219 Complete BUSCOs (C); 1747 Complete and single-copy BUSCOs (S); 472 Complete and duplicated BUSCOs (D); 22 Fragmented BUSCOs (F); 85 Missing BUSCOs (M); 2326 Total BUSCO groups searched
Pilkington, S. M., Crowhurst, R., Hilario, E., Nardozza, S., Fraser, L., Peng, Y., ... & Schaffer, R. J. (2018). A manually annotated Actinidia chinensis var. chinensis (kiwifruit) genome highlights the challenges associated with draft genomes and gene prediction in plants. BMC genomics, 19, 1-19.	Pilkington et al.	2018	Actinidia chinensis var chinensis cv Red5 (A. chinensis v2)	diploid with higher homozygosity than 'Hongyang'	roche 454	leaves	tissue culture whole plant + orchard bud, flower, fruit. Root main, root tip	This Whole Genome Shotgun project has been deposited at DDBJ/ENA/ GenBank (https://www.ncbi.nlm.nih.gov) under the accession NKQK00000000. The version described in this paper is version NKQK01000000. For community contributions please check the list of FASTA gene models available on the Plant and Food GitHub Repository (https://github.com/ PlantandFoodResearch/Red5_WGS_Manual_Annotation) and will be updated as the gene models are further refined.	**C:93.6%**[S:70.6%,D:23.0%],F:2.6%,M:3.8%,n:2326; 2176 Complete BUSCOs (C); 1642 Complete and single-copy BUSCOs (S); 534 Complete and duplicated BUSCOs (D); 61 Fragmented BUSCOs (F); 89 Missing BUSCOs (M); 2326 Total BUSCO groups searched

Supplementary Table 2 - Pairwise comparisons for differential expression analysis of genes

Control Group	Test Group
Control (T0)	Inoculated (T0)
Control (T48)	Inoculated (T48)
Control (T96)	Inoculated (T96) Flooded (T96) Multifactorial (T96)
Control (T144)	Inoculated (T144) Flooded (T144) Multifactorial (T144)
Control (T14d)	Inoculated (T14d) Flooded (T14d) Multifactorial (T14d)

Supplementary Table 3 – Top 10 genes for each treatment based on differential expression analysis.

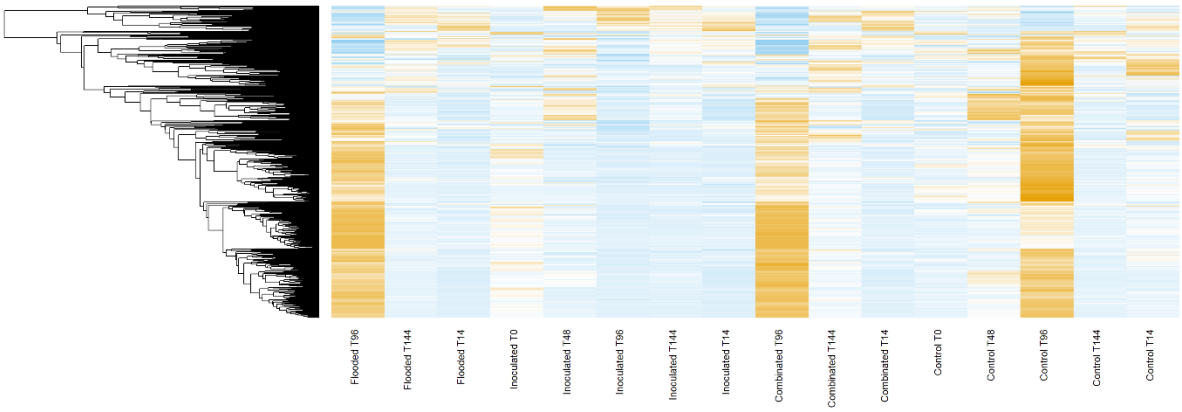
	Biotic Stress, 96hrs		
	Gene ID	log2fc	pvalue
Down Regulated Genes	Acde13g00527.1	-23.03415136	2.50E-12
	Acde000680s00013.1	-23.02704617	4.91E-20
	Acde19g00268.1	-22.74968461	8.32E-12
	Acde000000s00036.1	-22.53240865	8.63E-09
	Acde25g01012.1	-22.50323404	4.87E-09
	Acde06g00561.1	-22.46748764	8.63E-09
	Acde12g01015.1	-22.20380247	0.00019
	Acde09g00778.1	-22.01542757	1.66E-09
	Acde001100s00009.1	-21.78651134	3.74E-07
	Acde001100s00011.1	-21.71929205	0.000119
Up Regulated Genes	Acde02g00614.1	17.62007455	3.24E-08
	Acde03g00407.1	17.2579629	2.56E-05
	Acde26g00648.1	7.937642213	0.009005
	Acde23g00710.1	6.779912422	0.046511
	Acde03g01885.1	6.775823664	0.005886
	Acde19g00430.1	6.178460924	0.022625
	Acde20g00023.1	6.10462702	0.040273
	Acde06g00011.1	4.744797472	0.043397
	Acde07g00013.1	4.585401477	0.002645
	Acde23g01606.1	4.270868126	0.027753
	Abiotic Stress, 96hrs		
Down Regulated Genes	Acde000000s00035.1	-23.48667965	2.77E-13
	Acde09g00248.1	-22.31575239	1.65E-18
	Acde14g01160.1	-21.61585262	0.001346

	Acde13g00918.1	-21.45883261	4.78E-08
	Acde22g00418.1	-12.00759038	2.30E-15
	Acde19g00960.1	-11.66428009	1.30E-15
	Acde27g00969.1	-11.2116716	3.28E-14
	Acde18g00645.1	-11.05905058	1.36E-13
	Acde28g00092.1	-11.03664097	1.82E-10
	Acde05g00672.1	-10.93063863	3.43E-15
Up Regulated Genes	Acde03g00407.1	21.84776244	4.47E-11
	Acde05g01089.1	21.62929565	0.02057
	Acde03g01633.1	20.66159797	0.002306
	Acde24g00960.1	18.37325618	1.63E-05
	Acde02g00614.1	15.6014529	2.27E-08
	Acde25g00666.1	12.11084487	0.003803
	Acde22g00252.1	9.316387055	7.02E-05
	Acde19g00904.1	8.825046407	0.007784
	Acde29g00968.1	8.781253844	0.001556
	Acde07g01292.1	8.742733451	0.00063
	Multifactorial Stress, 96hrs		
Down Regulated Genes	Acde25g00666.1	-26.07707221	2.35E-10
	Acde000000s00035.1	-22.85751245	1.08E-12
	Acde21g00947.1	-21.92697773	0.005135
	Acde09g00248.1	-21.22032601	7.04E-17
	Acde28g00450.1	-21.19972451	9.97E-10
	Acde27g01252.1	-21.01973623	0.023641
	Acde13g00918.1	-20.88569843	9.84E-08
	Acde22g00220.1	-20.81746698	0.003456
	Acde11g00090.1	-20.54787817	0.002731

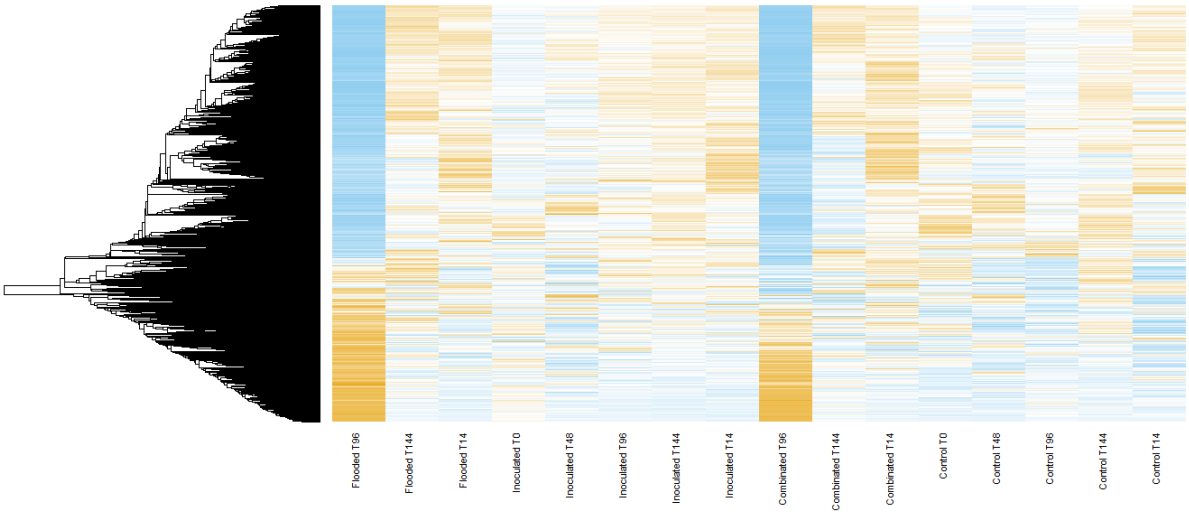
	Acde13g01211.1	-12.27300148	2.53E-18
Up Regulated Genes	Acde03g00407.1	21.42729261	9.64E-11
	Acde03g01633.1	2.08E+01	0.002019
	Acde20g01062.1	19.16651511	0.040792
	Acde24g00960.1	19.05631292	6.53E-06
	Acde02g00614.1	1.78E+01	9.14E-11
	Acde29g00968.1	9.34E+00	0.00066
	Acde22g00252.1	9.34E+00	6.04E-05
	Acde07g01292.1	8.54E+00	0.000787
	Acde24g00926.1	8.399444493	0.007949
	Acde01g00958.1	8.32E+00	0.045921

Supplementary Table 4 - Pathogen load

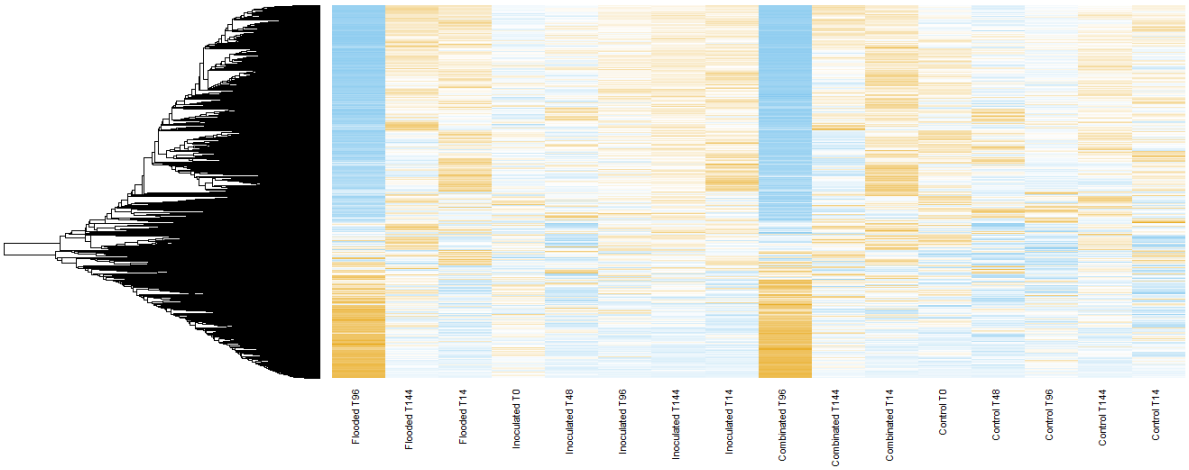
TIME	TREATMENT	AVG Ct	SD	P. vexans quantity (ng)
T 0	NS	0	0.00	0.00
T 0	I	34.12	0.17	7.29
T 48	NS	31.83	0.35	31.30
T 48	I	21.06	0.35	29490.58
T 96	NS	35.94	0.00	2.29
T 96	I	21.82	3.00	18143.27
T 96	IF	24.29	1.74	3780.97
T 96	F	30.49	0.27	73.39
T 144	NS	32.83	4.44	16.51
T 144	I	21.99	2.38	16365.61
T 144	IF	22.33	0.40	13145.95
T 144	F	28.95	1.15	194.79
T 14d	NS	28.05	1.40	345.16
T 14d	I	23.64	0.79	5713.75
T 14d	IF	22.33	0.40	13145.95
T 14d	F	34.33	3.84	6.37



Supplementary Figure 1 – Hierarchical clustering heatmap of all differentially expressed genes (DEGs) in *Actinidia deliciosa* under inoculation at 96 hours post-treatment (T96) compared to the control. The heatmap was generated using the `pheatmap` package in R, with gene expression values (FPKM) subjected to Z-score normalization. Rows represent individual genes, while columns correspond to experimental conditions, including different treatments (Flooded, Inoculated, Combined, and Control) across multiple time points (T0, T48, T96, T144, and T14). Euclidean distance and average linkage clustering were applied to group genes based on expression patterns. The color scale ranges from blue (low expression) to orange (high expression), with hierarchical clustering displayed for rows.



Supplementary Figure 2 – Hierarchical clustering heatmap of all differentially expressed genes (DEGs) in *Actinidia deliciosa* under flooding at 96 hours post-treatment (T96) compared to the control. The heatmap was generated using the `pheatmap` package in R, with gene expression values (FPKM) subjected to Z-score normalization. Rows represent individual genes, while columns correspond to experimental conditions, including different treatments (Flooded, Inoculated, Combined, and Control) across multiple time points (T0, T48, T96, T144, and T14). Euclidean distance and average linkage clustering were applied to group genes based on expression patterns. The color scale ranges from blue (low expression) to orange (high expression), with hierarchical clustering displayed for rows.



Supplementary Figure 3 – Hierarchical clustering heatmap of all differentially expressed genes (DEGs) in *Actinidia deliciosa* under combined stress at 96 hours post-treatment (T96) compared to the control. The heatmap was generated using the `pheatmap` package in R, with gene expression values (FPKM) subjected to Z-score normalization. Rows represent individual genes, while columns correspond to experimental conditions, including different treatments (Flooded, Inoculated, Combined, and Control) across multiple time points (T0, T48, T96, T144, and T14). Euclidean distance and average linkage clustering were applied to group genes based on expression patterns. The color scale ranges from blue (low expression) to orange (high expression), with hierarchical clustering displayed for rows.

Chapter 5 - General discussion and outlooks

This thesis aimed to provide a comprehensive understanding of KVDS as a multifactorial disorder by integrating various perspectives. The study began with a microbiome characterization of KVDS-affected fields in Northwestern Italy, representing the first integrated analysis of oomycetes, fungi, and bacteria in this context. While previous microbiome studies have been conducted in other regions (Savian et al., 2022; Donati et al., 2020), this study focused specifically on Northwestern Italy.

Based on the results from Chapter 2 (Guaschino et al., 2024) communities from northwestern Italy seem to be characterized by a high presence of the soilborne oomycete *P. vexans*. This result was already evidenced by isolation techniques in the same area (Prencipe et al., 2020; Prencipe et al., 2023) and in northeastern Italy (Savian et al., 2020).

This pattern of oomycete dominance aligns with findings from the metabarcoding study of Chapter 2 that reported a highly skewed community structure in KVDS-affected orchards, with *Phytopythium vexans* accounting for over 50% of the oomycete community in the rhizosphere and soil of diseased kiwifruit plants in Northwestern Italy, compared to less than 20% in healthy counterparts. These findings suggest a strong association between oomycete community composition and disease status, with oomycetes—more than fungi or bacteria—emerging as key biotic indicators of KVDS. Notably, *Phytophthora* spp. were consistently rare (<1% relative abundance) across all sample types, challenging previous assumptions about their role in the disease.

The study also aimed to characterize fungal and bacterial compositions: while bacterial genera were diverse, fungal community shifts were more discernible. Although *Fusarium* dominated the rhizosphere regardless of disease status, *Linnemania* and *Dactylonectria* were more prominent in diseased roots, with *Dactylonectria* also detected in healthy roots at lower levels. These shifts align with observations by Savian et al. (2022), supporting the idea that KVDS may involve a transition from a relatively balanced community to one enriched in opportunistic or latent pathogens.

Further supporting a dysbiosis-driven model, is Chapter 2 a β-Nearest Taxon Index (bNTI) metrics was applied to assess community assembly processes. While fungal communities appeared predominantly shaped by stochastic processes, oomycete communities in diseased plants exhibited

a significantly greater influence of deterministic factors. The consistent presence of bNTI values below −2 pointed to the so-called Anti-Anna Karenina Principle (Anti-AKP), whereby deterministic alterations in host biology enable the establishment of novel, potentially pathogenic microbial communities (Arnault et al., 2023).

Similarly, microbiome data from Southern Italy confirmed the presence of *P. vexans* in KVDS-affected fields, strengthening the evidence for its involvement in disease onset (Mosca et al., 2024). Specifically, *P. vexans*-assigned ASVs were enriched in both root and soil samples from symptomatic plants, while asymptomatic plants were associated with higher relative abundances of *Pythium* and other oomycetes—indicating a distinct microbial structure linked to disease symptoms.

A key regional discrepancy concerns the presence of *Phytophthora* spp. In Northeastern Italy, *Phytophthora sojae* has been reported as a major contributor to KVDS, with *P. vexans* also detected (Savian et al., 2022). Other studies have similarly isolated *Phytophthora* species from symptomatic plants in different locations (Donati et al., 2020; Akilli et al., 2011; Kurbetli and Ozan, 2013). However, in our study, *Phytophthora* spp. were not abundant in any sample type, consistently showing less than 1% relative abundance.

Importantly, the pathogenicity of *Ph. sojae* on kiwifruit has yet to be confirmed, whereas several *Phytopythium* species, including *P. chamaehyphon*, *P. litorale*, and *P. helicoides*, have successfully reproduced KVDS symptoms under controlled conditions (Polat et al., 2017; Donati et al., 2020; Savian et al., 2020; Prencipe et al., 2020, 2023). Additionally, *Ph. megasperma* and *Ph. infestans* have been shown to induce KVDS-like symptoms when inoculated on kiwi roots (Donati et al., 2020), and *Ph. citrophthora* has been tested through stem inoculation (Akilli et al., 2011).

In the context of the dysbiosis hypothesis, Chapter 2 examined the role of microbial imbalance using the Anna Karenina Principle (AKP). Our findings indicated that deterministic processes had 2.5 times more influence in diseased communities than in healthy ones. Further analysis of βNTI values suggested the presence of an Anti-AKP scenario, in which deterministic factors—such as changes in host physiology—promote the establishment of pathogenic communities. This contrasts with Mosca et al. (2024), who found only weak support for dysbiosis in KVDS-affected microbiomes. Differences between the two studies may be attributed to variations in sampling timepoints and geographical location.

To reconcile these discrepancies and better understand the biotic drivers of KVDS, future research should adopt a coordinated sampling strategy across seasons and years, encompassing multiple geographic regions and vegetative stages. This would help control for environmental variability, especially weather conditions that can significantly affect oomycete populations.

Our results support the central role of *P. vexans* in KVDS etiology, consistent with findings from both culture-based and sequencing studies. Given KVDS's growing threat to global kiwifruit production, potentially rivaling that of bacterial canker, there is an urgent need to refine our understanding of the disease's causal agents and mechanisms (Mosca et al., 2024). Equally crucial is the development of sustainable, low-impact disease mitigation strategies.

In this regard, the development of molecular diagnostic tools for *P. vexans* is a priority. The diagnostic assay introduced in Chapter 3 was specifically designed for kiwifruit production systems, with an emphasis on avoiding cross-reactivity with host DNA and minimizing false positives. The assay design incorporated comprehensive screening of KVDS-associated oomycetes and fungi during primer design and *in vivo* validation, ensuring robust specificity for both nursery and field applications.

Phytopythium vexans was selected as the assay's primary target due to its consistent association with KVDS across regions and studies. While several DNA-based assays (qPCR and TaqMan) have previously been developed (Spies et al., 2011; Yano et al., 2011; Yang et al., 2012; Wang et al., 2021), they were not tailored for kiwifruit tissues or rhizosphere soils, and lacked validation against complex microbiomes, raising concerns about cross-reactivity. Most of these targets the ITS nuclear region, while others focus on the small subunit rRNA gene (Bent et al., 2009) or a putative inositol polyphosphate 5-phosphatase region (Moein et al., 2019).

Another important consideration is the genetic diversity within *P. vexans* itself; the presence of distinct phylogenetic groups can lead to variable amplification efficiencies, a limitation noted in earlier studies (Spies et al., 2011).

To address these limitations, our assay was optimized specifically for kiwifruit cultivation (Guaschino et al., 2025). Primers were designed to exclude host DNA and non-target microbes, with specificity tested against a panel of common KVDS-associated fungi and oomycetes. The assay also showed successful performance in Apple Replant Disease (ARD)-affected soils from Washington State, demonstrating cross-pathosystem applicability.

Despite the central role of oomycetes, KVDS is increasingly recognized as a multifactorial syndrome involving both biotic and abiotic stressors. Environmental factors, particularly waterlogging and high soil temperatures, reduce host resilience and create favourable conditions for opportunistic pathogens (Martinez-Arias et al., 2022). While flooding impacts on rhizosphere microbiomes have been studied in herbaceous plants (e.g., rice), data for woody species remain limited.

To investigate the interplay between stresses, we conducted a transcriptomic study (Chapter 4) examining kiwifruit gene expression under biotic (*P. vexans* inoculation), abiotic (root flooding), and combined stress.

Prior studies have acknowledged the role of flooding in promoting oomycete-driven decline in woody species, including kiwifruit (Biesbrock et al., 1970; Savian et al., 2020). However, these works lacked molecular resolution or focused primarily on visual symptoms.

Molecular mechanisms underlying root flooding responses in *Actinidia* spp. have been investigated through transcriptomic and RNA-seq approaches before (Gao et al., 2022; Xing et al., 2023; Baldi et al., 2024).

These studies have provided valuable insights into the physiological and transcriptional changes associated with water stress in kiwifruit. Building on this foundation, our study highlights that the plant response to multifactorial stress, specifically the combination of root flooding and *P. vexans* infection, is not merely additive, but involves distinct and complex molecular interactions (Zandalinas et al., 2021). Among the two stressors, flooding emerged as the dominant factor, significantly suppressing immune-related gene expression and thereby increasing host susceptibility to *P. vexans*. This finding is consistent with similar observations in *Persea americana*, where flooding-induced suppression of defense genes heightened vulnerability to *Phytophthora cinnamomi* infection (Reeksting et al., 2016).

In our multifactorial treatment, co-activation of genes such as ADH (alcohol dehydrogenase) and WRKY33 highlighted the disruption of resistance pathways. Specifically, flooding alone triggered ADH expression and a metabolic shift toward anaerobic respiration, while suppressing cell wall biosynthesis—suggesting energy conservation at the expense of growth and immunity.

These findings point to practical interventions. Improving water drainage and root zone aeration in heavy rainfall events could reduce disease onset. Organic soil amendments, proven effective in

systems like ARD involving soilborne oomycetes (Mazzola et al., 2005; 2015)., also warrant exploration.

Another promising strategy is the use of KVDS-tolerant rootstocks. *Actinidia macrosperma* has shown potential (Mian et al., 2022), though further research is needed on its long-term compatibility and productivity. Studies examining associated microbial communities in *A. macrosperma*, *A. polygama*, and *A. arguta* have reinforced *A. macrosperma* as a robust candidate under KVDS-conducive conditions (Mian et al., 2023).

Future efforts may benefit more from selecting rootstocks tolerant to flooding than from attempting to reshape the microbiome directly. A longer-term, though more regulated, solution involves identifying flood susceptibility genes in *Actinidia* and applying gene-editing tools. However, the perennial nature of woody crops presents unique challenges for genome editing in practical breeding programs.

References

Akilli, S., Serçe, Ç. U., Zekaİ Katircioğlu, Y., Karakaya, A., & Maden, S. (2011). Involvement of *Phytophthora citrophthora* in kiwifruit decline in Turkey. *Journal of Phytopathology*, *159*(7-8), 579-581. https://doi.org/10.1111/j.1439-0434.2011.01798.x.

Baldi, E., Pastore, C., Chiarelli, G., Quartieri, M., Spinelli, F., & Toselli, M. (2024). Molecular Responses to Drought and Waterlogging Stresses of Kiwifruit (Actinidia chinensis var. deliciosa) Potted Vines. *Horticulturae*, *10*(8), 834. https://doi.org/10.3390/horticulturae10080834.

Bent, E., Loffredo, A., Yang, J. I., McKenry, M. V., Becker, J. O., & Borneman, J. (2009). Investigations into peach seedling stunting caused by a replant soil. *FEMS Microbiology Ecology*, 68(2), 192-200. doi: 10.1111/j.1574-6941.2009.00668.x.

Biesbrock, J. A., & Hendrix, F. F. (1970). Influence of soil water and temperature on root necrosis of peach caused by Pythium spp. *Phytopathology*, *60*(5), 880-882.

Donati, I., Cellini, A., Sangiorgio, D., Caldera, E., Sorrenti, G., & Spinelli, F. (2020). Pathogens associated to kiwifruit vine decline in Italy. *Agriculture*, 10(4), 119. https://doi.org/10.3390/agriculture10040119.

Gao, Y., jiang, Z., Shi, M., Zhou, Y., Huo, L., Li, X., & Xu, K. (2022). Comparative transcriptome provides insight into responding mechanism of waterlogging stress in *Actinidia valvata* Dunn. *Gene*, *845*, 146843. https://doi.org/10.1016/j.gene.2022.146843.

Guaschino, M., Garello, M., Nari, L., Zhimo, Y. V., Droby, S., & Spadaro, D. (2024). Soil, rhizosphere, and root microbiome in kiwifruit vine decline, an emerging multifactorial disease. *Frontiers in Microbiology*, 15, 1330865. https://doi.org/10.3389/fmicb.2024.1330865.

Guaschino, M., Prencipe, S., Somera, T., Tabone, G., & Spadaro, D. (2025). Development of a qPCR assay for early detection and quantification of Phytopythium vexans in kiwifruit plant and soil affected by Vine Decline Syndrome. *Plant Disease*, (IN PRESS).

Kurbetli, İ., & Ozan, S. (2013). Occurrence of Phytophthora Root and Stem Rot of Kiwifruit in Turkey. *Journal of Phytopathology*, 161(11–12), 887–889. https://doi.org/10.1111/jph.12145.

Martínez-Arias, C., Witzell, J., Solla, A., Martin, J. A., & Rodríguez-Calcerrada, J. (2022). Beneficial and pathogenic plant-microbe interactions during flooding stress. *Plant, Cell & Environment*, *45*(10), 2875-2897. https://doi.org/10.1111/pce.14403.

Mazzola, M., & Mullinix, K. (2005). Comparative field efficacy of management strategies containing Brassica napus seed meal or green manure for the control of apple replant disease. *Plant Disease*, *89*(11), 1207-1213. https://doi.org/10.1094/PD-89-1207.

Mazzola, M., Hewavitharana, S. S., & Strauss, S. L. (2015). Brassica seed meal soil amendments transform the rhizosphere microbiome and improve apple production through resistance to pathogen reinfestation. *Phytopathology*, 105(4), 460-469. https://doi.org/10.1094/PHYTO-09-14-0247-R.

Mian, G., Cipriani, G., Saro, S., Martini, M., & Ermacora, P. (2022). Potential of different Actinidia genotypes as resistant rootstocks for preventing kiwifruit vine decline syndrome. *Horticulturae*, *8*(7), 627. https://doi.org/10.3390/horticulturae8070627.

Mian, G., Cipriani, G., Firrao, G., Martini, M., & Ermacora, P. (2023). Genetic diversity of Actinidia spp. shapes the oomycete pattern associated with Kiwifruit Vine Decline Syndrome (KVDS). *Scientific Reports*, *13*(1), 16449. https://doi.org/10.1038/s41598-023-43754-y.

Moein, S., Mazzola, M., Spies, C. F. J., & McLeod, A. (2019). Evaluating different approaches for the quantification of oomycete apple replant pathogens, and their relationship with seedling growth reductions. *European Journal of Plant Pathology*, 154, 243-257. doi: 10.1007/s10658-018-01652-4.

Mosca, S., Aci, M. M., Procopio, G., Vadalà, V., Vizzari, G., Francomano, E., Mohamed, N. Z., Li Destri Nicosia, M. G., Agosteo, G. E., Spadaro, D., Schena, L., & Malacrinò, A. (2025). Integrated analyses of the plant and soil microbiome identify *Phytopythium vexans* as agent of the Kiwifruit Vine Decline Syndrome. *Plant and Soil*, 509(1), 729–742. https://doi.org/10.1007/s11104-024-06891-5.

Polat, Z., Awan, Q. N., Hussain, M., & Akgül, D. S. (2017). First Report of *Phytopythium vexans* Causing Root and Collar Rot of Kiwifruit in Turkey. *Plant Disease*, 101(6), 1058. https://doi.org/10.1094/PDIS-11-16-1554-PDN.

Prencipe, S., Savian, F., Nari, L., Ermacora, P., Spadaro, D., & Martini, M. (2020). First Report of *Phytopythium vexans* Causing Decline Syndrome of *Actinidia deliciosa* 'Hayward' in Italy. *Plant Disease*, 104(7), 2032. https://doi.org/10.1094/PDIS-10-19-2101-PDN.

Prencipe, S., Schiavon, G., Rosati, M., Nari, L., Schena, L., & Spadaro, D. (2023). Characterization of *Phytopythium* species involved in the establishment and development of kiwifruit vine decline syndrome. *Microorganisms*, *11*(1), 216. https://doi.org/10.3390/microorganisms11010216.

Reeksting, B. J., Olivier, N. A., & Van Den Berg, N. (2016). Transcriptome responses of an ungrafted *Phytophthora* root rot tolerant avocado (*Persea americana*) rootstock to flooding and *Phytophthora cinnamomi*. BMC plant biology, 16, 1-19. doi: 10.1186/s12870-016-0893-2.

Savian, F., Ginaldi, F., Musetti, R., Sandrin, N., Tarquini, G., Pagliari, L., Firrao, G., Martini, M., & Ermacora, P. (2020). Studies on the aetiology of kiwifruit decline: interaction between soil-borne pathogens and waterlogging. *Plant and Soil*, *456*, 113-128. https://doi.org/10.1007/s11104-020-04671-5.

Savian, F., Marroni, F., Ermacora, P., Firrao, G., & Martini, M. (2022). A Metabarcoding Approach to Investigate Fungal and Oomycete Communities Associated with Kiwifruit Vine Decline Syndrome in Italy. *Phytobiomes Journal*, 6(4), 290–304. https://doi.org/10.1094/PBIOMES-03-22-0019-R.

Spies, C. F. J., Mazzola, M., & McLeod, A. (2011). Characterisation and detection of Pythium and Phytophthora species associated with grapevines in South Africa. *European journal of plant pathology*, *131*, 103-119. doi: 10.1007/s10658-011-9791-5.

Wang, T., Ji, H., Yu, Y., Wang, X., Cheng, Y., Li, Z., Chen J., Guo, L., Xu, J., & Gao, C. (2021). Development of a loop-mediated isothermal amplification method for the rapid detection of *Phytopythium vexans*. *Frontiers in Microbiology*, *12*, 720485. https://doi.org/10.3389/fmicb.2021.720485.

Xing, M., Huang, K., Zhang, C., Xi, D., Luo, H., Pei, J., Ruan, R., & Liu, H. (2023). Transcriptome Analysis Reveals the Molecular Mechanism and Responsive Genes of Waterlogging Stress in Actinidia deliciosa Planch Kiwifruit Plants. *International Journal of Molecular Sciences*, *24*(21), Article 21. https://doi.org/10.3390/ijms242115887.

Yang, J. I., Ruegger, P. M., McKenry, M. V., Becker, J. O., & Borneman, J. (2012). Correlations between root-associated microorganisms and peach replant disease symptoms in a California soil. *PLoS ONE*, 7(10): e46420. https://doi.org/10.1371/journal.pone.0046420.

Yano, T., Shimizu, S., Miyoshi, T., Miyata, N., Immon, K., Shinozaki, T., Sawada, H. & Kageyama, K. (2011). Tolerant *Actinidia* species to *Pythium helicoides* and *P.vexans* causing root rot. Acta Horticolture, 913, 517-523. doi: 10.17660/ActaHortic.2011.913.69.

Zandalinas, S. I., Sengupta, S., Fritschi, F. B., Azad, R. K., Nechushtai, R., & Mittler, R. (2021). The impact of multifactorial stress combination on plant growth and survival. *New Phytologist*, *230*(3), 1034-1048. https://doi.org/10.1111/nph.17232.